INVESTIGATIONS INTO RESPONSES OF CYLINDRICAL SHELLS TO RANDOM ACOUSTIC EXCITATION

By

A. V. SWAMY

Submitted In Fulfilment Of The Degree Of

Master Of Science In Mechanical Engineering

Of

The University Of Aston In Birmingham

February 1970

S U M M A R Y.

The response of a structure to random acoustic excitation is dependent on the modal densities, mechanical damping, and radiation efficiency, as well as the acoustic response of the surrounding medium.

This thesis describes the analytical and experimental problems associated with the evaluation of the parameters, and an attempt is made to obtain practical values of these paramters in the particular case of a flanged cylindrical vessel.

The object of the work was to provide accurate basic information which could be used to investigate noise transmission in aircraft structures.

Various methods of measuring and/or calculating the above-mentioned paramters have been investigated and experimental techniques developed which will provide more accurate evaluation of the paramters.

CONTENTS.

Chapter		CONTENTS.	Page

Chapter	CONTENTS.	Page

Appendix.	CONTENTS.	Page

LIST OF SYMBOLS.

As	=	Area of structure.
a	=	Radius of cylinder.
a'	=	Absorption in square meters.
B_{rm}	=	Acoustic structural coupling term.
Co	=	Ambient speed of sound.
C_B	=	Speed of flexural wave.
C_L	=	Speed of longitudinal waves in the panel material.
E	=	Youngs modulus.
E_T	=	Total energy stored in the structure,
E_R	=	Acoustic energy.
f	=	frequency (Hz).
fr	=	Ring frequency (Hz)
fc	=	Critical frequency (Hz)
fm	=	Generalised force on mode m
g_{rm}	=	Coupling constant.
Gr	=	Generalised acoustic source for mode r
g	=	Acceleration due to gravity.
h	=	Material thickness.
J_r	=	Power flow from mode m to mode r /unit mass.
k	=	Wave number
k_s	=	Structural wave number ($2\pi f/C_B$)
k_r	=	Acoustic wave number ($2\pi f/Co$)
L	=	Length of the cylinder
m	=	Structural mode subscript or axial mode number
M	=	Total mass of structure
m_s	=	Mass per unit area of structure
n	=	Circumferential mode numbers

$n_R(\omega)$ = Angular modal density of reverberant field.

$n_s(\omega)$ = Structure modal density.

$Ns(\omega)$ = Number of structure modes in a frequency band. centred on ω.

Nm = Number of well coupled structure modes.

Nrm = Number of well coupled mode pairs in a band.

p = An Integer.

$\langle \bar{p}^2 \rangle$ = Space and time averaged acoustic pressure.

q = An integegr or an acoustic mode velocity potential normal co-ordinate.

$q'(r)$ = Amplitude of the rth acoustic mode.

r = An Integer or acoustic mode subscript.

R_{rad} = Radiation resistance.

R_{mech} = Mechanical resistance.

s = Structure mode displacement normal co-ordinate.

S = Area of panel = ab.

$Sa(\omega)$ = Spectral density of structural acceleration.

$Sp(\omega)$ = Spectral density of acoustic pressure.

T_R = Reverberation time of room.

Ts = Reverberation time of structure.

T = Time average kinetic energy of a mode.

V = Volume of room = abc.

$\langle \bar{V}^2 \rangle$ = Space ahd time averaged vibration velocity.

ρ_o = Ambient density of fluid.

ρ_s = Density of structure.

β_R = Energy decay constant of room.

βs = Energy decay constant of structure.

$\beta(r)$ = Modal damping.

$\beta m, \beta r$ = Half power bandwidth of mode m, mode r $\left(\frac{rad}{sec}\right)$

$\Theta^R(\omega)$ = Average energy per mode.

η = Loss factor = $\beta/2f = \beta/\omega$.

η_{TOT} = Total power loss factor.

Θ = Modal energy/unit mass.

σ = Radiation efficiency.

Λ_{12} = Time average power flow from mode 1 to mode 2.

$\phi . \phi_{12}$ = Panel eigen function, mode coupling factor.

Ψ = Acoustic eigen function.

ω = Circular frequency rad/sec.

ξ_m = $S^{-1} \int_s \phi_m^2 (x)\, dx$, $\xi_r = V^{-1} \int_v \psi_r^2 (x)\, dx$.

λ_B = Bending wavelength in plate.

λs = Coincidence wavelength of structure $\left(\frac{Co}{fc}\right)$

μ = Poissons ratio.

$\mu(\omega)$ = Coupling factor between the acoustic field and the structure.

ζ = Damping ratio c/c_c.

δ = Logarithmic decrement.

Q = Quality factor = $1/2\zeta$

ε = Strain

ν = Normalized frequency

CHAPTER 1.

Introduction.

The problems involved in determining the response of structures subjected to noise (and the subsequent vibration and radiation of this noise) have been of great concern in aeronautics since the early nineteen fifties; the enormous increase in the power of propulsion devices over this period has led to the radiated and transmitted noise being a major social and scientific problem. The Ministry of Technology Research Establishment at Farnborough have taken considerable interest in this subject from its conception, particularly in the area concerning the transmission of noise into aircraft fuselage and its effects on the structure. A long term research programme with a view to solving this problem was then started at this University following a consultation with members of the above establishment.

In order to predict accurately the response of a plate-type structure to a defined noise field, it is essential to have accurate data regarding the primary factors which affect the response. Theoretical analysis of power flow between linearly coupled oscillators has shown that the relationship between acceleration response and sound pressure is a primary function of modal density, mechanical damping and radiation efficiency of the structure as well as the characteristic of the surrounding acoustic medium.

For a thorough study of the general problems related to sound transmission in aircraft structures (which is the primary objective of the work) it was considered to be essential to have accurate knowledge of the paramters and this thesis describes and evaluates various methods of measuring and calculating them.

Experiments have been carried out in a reverberant chamber on a flanged cylindrical vessel, techniques being developed for the measurement of damping, modal density and radiation efficiency of the structure as well as for accurately defining the acoustic response of the test chamber.

A technical survey of some of the more important literature relating to the present work is given which shows that information on structural response in acoustic fields is scarce. The most useful papers in this area have been published in the last ten years; literature on the other topics are readily available.

Because the spectrum of duct noise extends to frequencies well above the fundamental natural frequencies of the complicated mechanical structure, classical vibration analysis is not a very suitable method for estimating response levels. More important, it does not indicate the roles of the various different parameters in a manner which leads to a clear solution for the problem, and hence hinders the generalisation of the results to different system configurations (which is an essential factor in design studies). The development of the statistical energy analysis, with its central concept of power flow between oscillators and its advantage of producing results in terms of the broad paramaters of a system is then discussed and has provided a valuable tool for the solution of this problem.

Chapter 4 contains descriptions of transducers and instrumentation used. An outline of the special instruments built and used are also included. A detailed description of the automatic time and averaging system and its use in conjunction with other instruments for reducing $S_a(\omega)$ / $S_p(\omega)$ and $S_p(\omega)/S_a(\omega)$ data is given. The following chapter reviews the basic theoretical concepts and experimental aspects of room acoustics with particular reference to reverberation, diffusibility and modal density. The practical results of the measurements relating to the room conditions are given.

Accurate calculation of the individual modes and frequencies of vibration are only possible for small homogeneous structures having regular geometry and well defined boundary conditions. In the case of the test specimen, the Arnold and Warburton (11) approach explained in Chapter 6 was used. The techniques used in the solution of the equation on an ICL 1905 computor for determining the modal density is also included.

Chapter 7 deals with two main sections covering damping, firstly in relation to the mechanical damping and its mechanisms and the techniques used in their measurement, and secondly in relation to the radiation damping and the parameters contributing to its response. The use of various experimental techniques and their limitations are also considered.

The expressions for determining the radiation properties of cylinders based on the flat plate formalism devised by Manning and Maidanik (2) are reviewed. The radiation efficiency computed from this method is given and also the experimental results. (This is a well thumbed approximate technique based on numbers of radiating modes being excited in a given frequency band).

The Appendices contain notes on the use of decibels, terminologies used in the thesis, tables of resonant frequencies for the test cylinder and computer programs.

CHAPTER 2.

Technical Survey of Published Literature.

The survey presented in this chapter is of the more important papers relevant to the research work reported in this thesis.

2.1. Room acoustics with particular reference to the reverberation and diffusiblity.

In 1922 W.C. Sabine's collected papers (50) on acoustics were published. With this event the real foundation of modern room acoustics was laid. Sabine had clearly seen that a distinct relation exists between the reverberation of the sound in a room and the sound absorption of the room.

For the reverberation time evaluation one of the first objective recording arrangements using electronic equipment consisted of a microphone, an amplifier and a recording oscillograph. This arrangement was described by E. Mayer (51), but the measured results were difficult to interpret, partly because the reverberation decay was recorded to a linear scale and partly because a "pure" tone was used as a sound source, which resulted in a very irregular decay curve. Considerably smoother decay curves were obtained by Meyer and Just (52) who introduced the warble tone in their experiments but the recordings were still made to a linear scale. A further improvement with respect to smoothness of the recorded reverberation decay curve was introduced by W. Kuntze, who "averaged" the outputs of two different microphones and this method is still very widely used and the averaging of outputs from many microphones is not common.

The determination of reverberation time described so far required a considerable amount of tedious work and therefore a number of experimenters designed various automatic measurement equipment. Around 1930 Meyer, Strutt (53) Mente and Bedell et.al.(54) described a series of such designs. Common to all of them was that as soon as the sound source was shut off an electric timing device was started which was again stopped when the output level from the microphone had fallen by a pre-determined amount. Hunt (55), in 1936, described the method based on a continuous on-and-off switching of a sound source. This method allowed not only an automatic reverberation time measurement to be made but also an automatic averaging of ten measurements and, furthermore, by making the lower switching level adjustable, the complete average reverberation decay curve could be plotted point by point. The averaging procedure used by Hunt, as well as the adjustable lower switching level, offered new possibilities for accuracy in reverberation measurements. In fig. 2.1A is shown a block diagram of the measuring equipment described by Hunt. The operation of the equipment is briefly as follows:-

When a predetermined sound level is attained in the room, the source is turned off and an electric timer is started. As soon as the sound level has fallen to the lower threshold, the timer is stopped and the source is turned on again. The recurrent cycle is stopped after 10 repetitions and the average time for a single decay can be read directly from the timer. Undesired level fluctuations in the reverberation process are minimised by the use of an electric low pass filter at the output of the rectifier and by using a band of noise as sound source.

The reverberation process is assumed to follow an experimental decay function and the use of one of such experimental measuring methods consisted in the charging of a capacitor whereby the potential on the capacitor, under certain predetermined conditions, is a direct measure of the reverberation time. Another method consisted of comparing the discharge of a known R C circuit with the reverberation decay, a method which also led to the development of a reverberation measurement bridge, shown in figure 2.1B. In the bridge circuit, the reverberation process is compensated by a capacitor discharge process and the time constant of the R C circuit is adjusted until the galvanometer deflects equally to the positive and negative side during the reverberation decay.

It was realized that in order to give a satisfactory description of the acoustic of the room the details of the decay trace were also necessary in determining the reverberation time. A great step in the direction of obtaining these details was made by the development of a logarithmic level recording device. Such devices had been developed by Ballantine, Meyer and Keidel, and Van Braunmihl and Weber (56). While Ballantine used a logarithmic amplifier and linear recorder, both Meyer and Keidel and Van Braunmihl and Weber based their instruments on servo principles employing logarithmic input potentiometers. The use of a servo system with the logarithmic input potentiometer has two advantages in comparison with the use of logarithmic amplifiers and linear recorders and they are:

(1) The requirements regarding linear dynamic range of the rectifier are less stringent

(ii) The dynamic recording range of the recorder can be changed simply by changing the input potentiometer.

The modern high speed logarithmic level recorders utilize direct electrodynamic pen drives whereby greater writing speeds can be obtained. By utilizing the high writing speed facility of the recording device, still keeping the writing speed high enough to follow the main decay rate, the fluctuation can be minimised without averaging out the important trends. A new method, Schreeder's integrated impulse method (44) of obtaining reverberation data which, theoretically, should minimise fluctuations and represent the true everage response of an enclosure to interrupted random noise, uses "tone burst" whose spectra cover the desired frequency bands are radiated into the enclosure from loudspeakers. The response of each tone burst is recorded on magnetic tape. The tape recording is then played back in reverse-time direction. The output signal from the tape recorder is squared and integrated and the voltage on the capacitor is then the desired decay curve.

The diffusibility of a room is established by the measurement of correlation coefficients in reverberant sound fields. An instrument for measuring and recording the cross-correlation coefficient R for the sound pressure at two points a distance r apart as a function of time is described by Cook et.al (43). A simple theoretical demonstration of how R varies with wave number k and the distance between the points in a random sound field is also given.

2.2. Vibration of cylindrical shell with particular reference to modal density.

In the theoretical field Rayleigh (29) investigated the extensional vibrations of an infinitely thin cylindrical shell by considering only the potential energy of extension and neglecting the bending effects. Baron and Bleich (45) built up on Rayleigh's theory by first computing the membrane theory frequencies and the displacement ratios corresponding to those frequencies. Using the mode shape from the membrane theory and the strain expression of Flugge (46) they computed the maximum potential energy of bending. To solve for the corrected frequency Baron and Bleich then employed Rayleigh's principle with the combined expressions for the maximum membrane energy and the approximate bending energy.

The general case of flexural vibration of cylinders was later investigated by Love (47). In contrast to Rayleigh, Love worked directly with the equations of motion. In his strain expressions for the cylindrical shell, Love considered the trapezoidal shape of the faces perpendicular to the cylinder axes. His first approximation theory led to an asymmetric frequency determinant because of his elimination of some of the higher order terms. Love started with the effect of transverse normal stress, but eliminated it in his first expression. Flugge (46), by a similar approach, delivered a set of shell equations which included bending effects up to the second order in the thickness. His theory led to a symmetrical set of equations. Flugge then set up the frequency equation for the vibration of a cylinder with freely supported ends.

The problem was further investigated by Arnold and Warburton (14) who considered the vibration of cylindrical shells with freely supported ends both theoretically and experimentally. The boundary value problem they considered was the same as that solved by Flugge which was also mathematically equivalent to the problem considered by Rayleigh and Baron - Bleich. Arnold and Warburton employed the Lagrange equations to set up their frequency equation and the strain expressions they used were those of Timoshenko (39) and neglected the trapezoidal form of the faces perpendicular to the cylinder axes. By using some approximations Heckel (13) derived equations for the number of resonance frequencies and for the point impedance of thin cylinders.

Kenard (87) devised a set of differential equations for the circular cylinder starting with the elasticity equations in three dimensions and using a systematic elimination of higher order terms in the thickness. Junger and Resato (58) have used the Kenard equations to predict the axially symmetric motions of a cylindrical shell and Smith (59) has employed them for the nonaxially symmetric case.

The thin shell theories discussed above take no account of shear deformation and rotatory inertia. All the thin shell theories result in third-order determinants since the three unknowns are the component displacements of the middle surface of the shell. The result is the third order characteristic equation which contains three roots. Thus for each value of the circumferential order n and longitudunal wavelength there are three modes.

The thick shell theories which take account of rotatory inertia and shear contained five unknowns in the nonaxially symmetric case. These unknowns were the three displacements of the middle surface and two rotations of the normal to the middle surface. The first of these theories developed by Mirsky and Herrmann (60) neglected the transverse normal stress effects but still included the rotatory inertia and shear. The nonaxially symmetric theory contained shear deformation constant in the circumferential direction and shear deformation in the axial direction. These shear constants were determined by solving the exact thickness shear vibration problem in the axial and circumferential directions. The asymptotic value of the exact results were then equated to the asymptopic value determined by the shell theory and expressions were then obtained for the sheer constants. Mirsky and Herrmann (66) further developed the second theory and took into account shear deformation, rotatory inertia and transverse normal stress.

Lin and Morgan (61) developed the theory by considering only the axially symmetric case and consequently only one shear constant for deformation in the axial direction was present. Yu (62) started with the equation used by Herrmann and Mirsky, neglecting transverse normal stress effects, and went through a process of differentiation and elimination to derive equations. These equations enabled one to solve for the radial displacement without solving a set of simultaneous differential equations involving the displacement and rotation. The solutions for the remaining displacements and rotations then came about by substituting the value of the radial displacement into the remaining partial differential equations.

Cooper and Naghdi (63, 64) further considered with a variational theorem of Reissner and derived two sets of shell equations which included the effects of rotatory inertia and shear deformations. The values of the shear constants in the theory were obtained as a consequence of the assumptious for stress and displacement in Reissner's variational theorem. In the Herrmann and Mirsky and Lin and Morgan theories the shear stress-strain relations were modified by shear constants which were determined separately.

For shell theories in general, in the membrane and bending theories attention was focussed on the displacement of the middle surface of the shell alone. In the theories which include rotatory inertia and shear the slopes of the shell elements were also considered, in addition to the middle surface displacements. The complete three dimensional theory, on the other hand, considered the most general displacement distribution which satisfied the equations of motion and the surface conditions when the frequencies got so high that the displacement distribution were no longer linear as shown by Greenspon (65) then the shell theories lost their meaning.

For vibration measurement and analysis of complex systems, a technique was given by Kennedy and Pancu (8) for the identification of normal modes on polar plots representing the variation of the response vector with forcing frequency. The basic element was that such a plot for a single mode was a circle, as the vibrator went through a certain resonance, the tip of the total response vector described an arc approaching that of a pure mode response. Identification of those arcs gave the normal modes, which might otherwise be confusingly located or completely hidden in the conventional practice of considering just the amplitude of the forced response.

2.3. Damping properties of materials with particular reference to mechanical damping.

Investigation of the damping properties of material and their engineering significance was started almost two centuries ago. In 1831 Zener (3) showed some interest in this field. Coulomb in his "Memoir on Torsion" not only hypothesized regarding the micro-structural mechanisms of damping but also undertook experiments which proved that the damping of torsional oscillations is not caused by air friction but by the internal losses in the material. He also recognized that the mechanisms operative at low stress may be different from those at high stress. In the nineteenth century the following investigators published on the subject:

Meyers on the friction in liquids, Helmhelz and Sir William Thompson on the "viscosity" of metals in torsion and its nonlinear nature, and Streintz, Klemencic, Grazz, Schmidt, Messer, Wiedmann on the torsional decay of iron, silver and other wires. Klemencic and Schmidt also used the term "internal friction" to describe the phenomenon. Tomlinson carried out a comprehensive study of the decay of torsional vibration of long wires of copper, tin, steel and zinc and investigated such testing variable as stress amplitude, frequency, fluctuating temperature, permanent strain, size of wire, wire drawing effects, heat treatment and many other effects. Erwin worked on hysteretic effects under cyclic tension and Voight did further work on cyclic bending.

The first book which devoted significant space to experimental measurements of hysteretic damping was in the twentieth century and appears to be "Experimental Elasticity" by G.F.C. Scarle. Guillet (1909) investigated possible relationships between internal damping and other properties such as fatigue strength and Barristow carefully studied damping during sustained cyclic stress in the fatigue region. By about 1950 there were somewhat over 1,000 published papers on this subject, but these were mostly concerned with the damping properties of specific materials under specific test conditions.

Energy dissipation mechanisms in the structures, with particular reference to material damping was studied by Lazan (5) who has given a definition of damping and classification and identification of damping mechanisms. The component parts of system and configuration damping were analysed considering certain structural damping mechanisms that were of particular interest. The many units and nomenculture used in material damping were classified in terms of absolute energy units and the relationships among these units were defined. The several types of mechanism involved in material damping were explained and the importance of these mechanisms in various types of material were classified.

The details of mechanical damping measurement methods and the limitations imposed were discussed by Plunkett (4). Various approaches that might be used for different applications were outlined and some of the errors resulting from them were indicated. Further work in that field was done by Kimball (6) who studied the factors controlling internal friction and damping in vibrations.

For the alleviation of vibration and noise, an increasing number of different damping treatments and techniques for their measurement were studied by D.J. Mead and his paper (7) gave details of this, He also described a method for the measurement of modal damping which was developed by Kennedy and Pancuu (8). Johnson and Barr (49) describe the variation of acoustic and internal damping in uniform beams with frequency for the specimen supported in air and vibrating at small amplitude and stress. The experimental results were reported and the approximate theoretical results were also given.

2.4. Radiation properties of structures with particular reference to the cylindrical shells.

Lyon and Maidanik (11) considered the power flow between two randomly excited linear oscillators with a small linear coupling between them. In part one of their paper they considered two oscillator problems, by studying the power flow between the oscillators by evaluating certain second moment of the response directly from the stochastic equations. They also developed an equivalent analogue electrical circuit for the energy flow between the modes. These theories were then applied to a two-mode vibration isolation mount. In part two of their paper the results were modified when two systems each containing many modes interact. A particular application is the power flow which may be thought of as a dense collection of incohent acoustic modes of a large room. Analogue circuits for this problem were also constructed. The equation for the radiation resistance were then formed from the above consideration.

The response to sound and the consequent sound radiation for one linear resonant mode of a part of a large structure were analysed by Smith, Jr.(10) for a general structure. A modal reciprocity relation was established between modal radiation resistance and the transfer function which related incident sound pressure to modal force in the absence of motion. Response and resonant scattering were also analysed for excitation by noise. A further analysis of the response of a specific structure such as a complicated combination of panels and ribs to reverberant sound field was made by Maidanik (9). His analysis was based on the assumption that the noise field was diffuse with equal probability of incident energy in all directions and random enough in time so that its power spectrum was a fairly smooth function of requency.

The practical importance of the radiation resistance of a structure may be appreciated when it is realized that this governs the amount of power radiated from the structure when it is excited by mechanical, fluid or acoustic forces, as well as the amount of power which is absorbed by a structure from a sound field as outlined in references 10 and 11. Below the coincidence frequency the two main sources of radiation resistance were, as shown in reference 9. When the panel dimensions were small compared to an acoustic wavelength, then the pumping of net-volume by the odd-odd modes was dominant. When the panel dimensions were large compared to an acoustic wavelength then the scattering of flexural waves by the supporting edges provided radiating wave numbers in the panel. Lyon (12) explored that latter source of radiation by examining the radiated power from infinite beams in contact with an infinitely extended thin plate.

There were many difficulties involved in the precise analysis of the vibration of complicated structures, but, by applying the statistical approach to vibrating systems, Lyon and Maidanik (48) arrived at a considerable simplification of the analysis at the sacrifice of details which were often not significant. The radiation loss factor, a measure of coupling between the sound and vibration, entered the analysis as a central paramter. The approaches developed for estimating the acoustical properties of complex structures consisting of flat panels have been discussed (see references

9,10,11). There were many structures in practical use that consisted of curved panels and one expected that in some frequency ranges the flat panel analysis might be adequate for such structures but in the other frequency ranges modification of the flat panel analysis might be necessary.

The nature and extent of this modification for thin cylindrical shells was studied by Manning and Maidanik (2) and a theoretical method developed for estimating the radiation efficiency of a cylindrical shell.

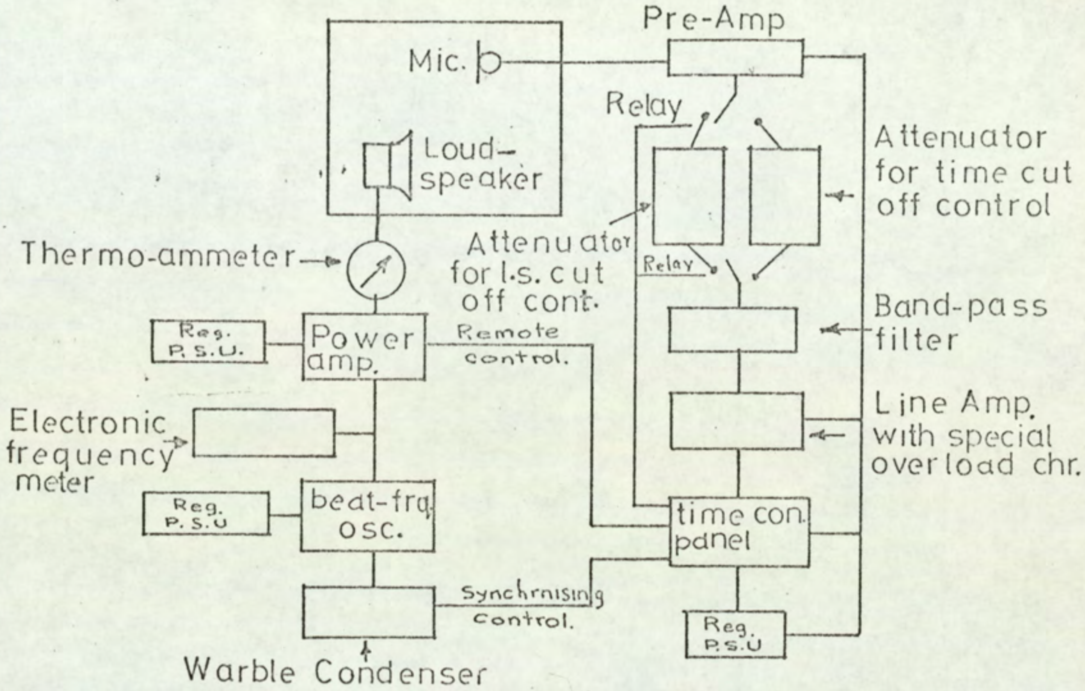

MEASURING ARRANGEMENT FOR CONTINEOUS ON-OFF SWITCHING OF THE SOUND AND AUTOMATIC AVERAGING OVER FEW MEASUREMENTS (F.V. HUNT)

FIG 2·1A

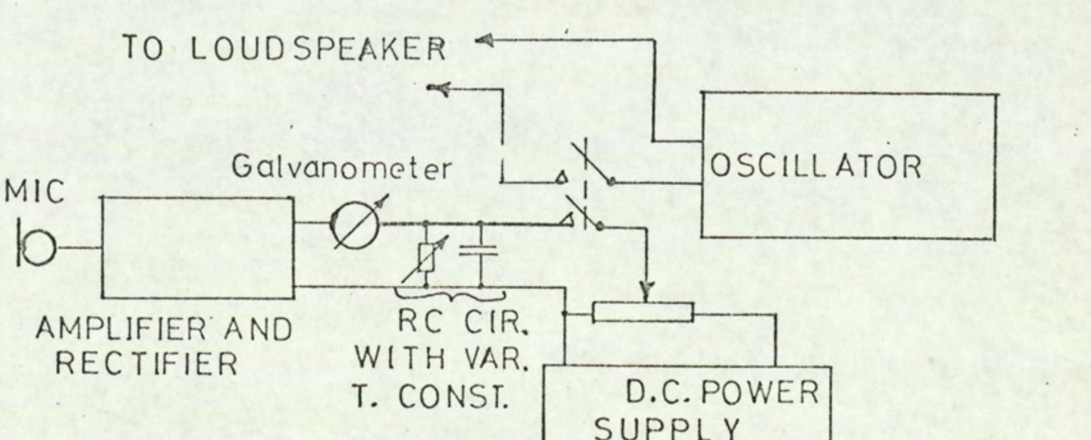

REVERATION MEASUREMENT BRIDGE (Olson and Kreuzer)

FIG 2·1B

Chapter 3.

Structural Response to Reverberant Acoustic Fields

(Basis Theory)

3.1. Introduction.

The energy-flow between two linearly coupled oscillator analogy is extended to the coupling between an ensemble of modes of a structure and a mode or an ensemble of modes of a reverberant sound field. The reverberant field is thought of as constituting a temperature bath in which the structural modes are immersed. The partition of energy between the modes of the acoustic field and the modes of the structure and the parameters which governed this partition is computed using this model.

Application of the results derived in section 3.2. to the cases of the interaction between a single structural mode, a large number of structural modes and a reverberant sound field, which include the assumption that a single structural mode interacts with many acoustic modes, leads to the approximate relationship between average mean square acoustic pressure and average mean square vibration velocity for the multi-mode coupling. These relationships are shown in sections (3.3.) and (3.4) to direct oscillation of the structure with consequent indirect oscilation of the fluid and vice versa.

The basis for the coupled oscillator theory is a paper by R.H. Lyon and G. Maidanik (11) which contains a fundamental formal treatment of the subject. This paper, in an application to the coupling between a sound field and a structure, treats the acoustic field as diffuse and this assumption is common to much of the literature on this subject and, similarly, it is commonly assumed that many acoustic modes couple with any one structural mode. Such assumptions are only justifiable when the acoustic wavelengths are small compared with a typical dimension of the fluid volume. The following theory and the equations derived from it is used as a basis for computing radiation properties of a flanged cylindrical shell.

3.2. Power Flow between structural modes and a reverberant acoustic field.

Lyon and Maidanik considered the power flow between two modes in terms of a difference between their uncoupled energies. This analogy was extended to the coupling between an ensemble of modes of one system and a mode or an ensemble of modes of another system. In the present system it is based on the coupling between a reverberant sound field and a flanged cylindrical shell. The reverberant sound field is thought of as consisting of a temperature bath in which the structural modes are immersed. Using this method, the steady state condition of the two interacting systems are computed by considering the position of energy between the modes of the acoustic field and the modes of the structure and the parameters which govern that partition.

An oscillator in a diffuse sound field which resonates at a frequency, ω, is considered. At this frequency the spectral density of the mean square pressure is,

$$Sp(\omega) = \langle P \rangle / \Delta\omega \qquad 1$$

Since the oscillator senses only the frequency interval given in equation (1), it may be accepted that the second field in this interval has a temperature related to the spectral density and that the oscillator will come to a steady state condition with the field, with an average energy determined by that temperature.

If the reverberant field is contained in a large room of volume V, the acoustic energy in a given interval of frequency is,

$$E_R = \langle p^2 \rangle V / \rho_o c_o^2 \qquad 2$$

This energy is shared by modes in a given bandwidth $(N_R.(\omega)\Delta\omega)$ of the room, where the approximate model density of the room is,

$$N_R(\omega) = \omega^2 V / 2\pi^2 C_o^3 \qquad 3$$

The average energy per mode is the ratio of E_R and $N_R(\omega)\Delta\omega$ and is given by the equation:

$$\theta^R(\omega) = 2\pi^2 \; Co \; \langle p^2 \rangle / \rho o \; \omega^2 \; \Delta\omega \qquad 4$$

It is evident from equation (4) that if all the modes of the room in all frequency intervals were to have the same temperature then the spectrum $Sp(\omega)$, would be fixed in the form $Sp(\omega) \propto \omega^2$. Noise producing devices do not normally have sound level spectra of this form. The various modes in different frequency ranges remain at different temperatures.

If a mechanical oscillator is placed in a steady sound field, it will interact with the oscillators representing the field and power flow between them will result. A steady state will be reached between the reverberant field and the oscillator only if there can be no coupling between different frequencies.

The modes of the structure (flanged cylindrical shell) are considered as constituting an ensemble of oscillators. It may be assumed that they are statistically independent in the sense that their individual energies may be simply added to give the total energy of the system. This assumption requires that the modes be sufficiently separated in frequency space, have fairly high Qs, and be linear.

The formulation of the equation of forced motions of acoustic and structural modes by incorporating the term representing coupling to the other modes is as shown,

$$\ddot{S}_m + \beta_m \dot{S}_m + \omega_n^2 S_m + \sum_r B_{rm} \dot{q}_r = F_m, \qquad 5a$$

$$\ddot{q}_r + \beta_r \dot{q}_r + \omega_r^2 q_r - \sum_m B_{mr} \dot{S}_m = Gr \qquad 5b$$

where, $q_r = (\rho_o V \varepsilon_r / M)^{1/2} q'_r$, 6

$$G_r = (C_o^2 \rho_o / MV\varepsilon_r)^{1/2} \int_V g\psi_r \, dx_q , \qquad 7$$

$$S_m = (M_m/M)^{1/2} S'_m , \qquad 8$$

$$F_m = (M_m M)^{-1/2} \int_S f\phi_m \, dx \qquad 9$$

$$B_{rm} = (C_o^2 \rho_o / V\varepsilon_r M_m)^{1/2} \int_S \psi_r (X) \phi_m (X) \, dx \qquad 10$$

The conservation of energy equation is obtained from equation (5) by multiplying equation (5a) by $\dot{S}m$ and summing over m, multiplying equation (5b) by $\dot{q}r$ and summing over r, averaging the two equations and adding them. The result is,

$$\sum_m \beta_m \langle \dot{S}_m^2 \rangle + \sum_r \beta_r \langle \dot{q}_r^2 \rangle = \sum_m \langle F_m \dot{S}_m \rangle + \sum_r \langle G_r \dot{q}_r \rangle \qquad 11$$

The energy balance equation is thus independent of the coupling and in this sense the coupling is conservative. An exact solution to equation (5) is difficult due to many sound field modes, even in a narrow frequency band, hence, an approximate solution based upon assumptions is derived which will provide most of the important effects of the interaction. It is assumed that Fm and Gr have the properties with respect to the mth and rth modes as do f_1 and f_2 with respect to mode 1 and mode 2 discussed by Lyon and Maidanik in two oscillator problem of reference (11).

With the above mentioned assumptions, equation (5) is written in the following form:

$$\ddot{S}_m + \beta_m \dot{S}_m + \omega_m^2 S_m + B_{rm} \dot{q}_r = F_m - \Sigma_{k \neq r} B_{km} \dot{q}_k \qquad 12a$$

$$\ddot{q}_r + \beta_r \dot{q}_r + \omega_r^2 q_r - B_{mr} \dot{S}_m = G_r - \Sigma_{n \neq m} B_{nr} \dot{S}_n \qquad 12b$$

It is further assumed that q_r's and S_m's are statistically independent and that Σ_r Brm $\dot{q}_r$ has a flat spectrum with respect to the admittance spectrum of the mth mode, and that Σ_r Brm $\dot{S}m$ has a flat spectrum with respect to the admittance spectrum of the Υth mode, and

$$F'_m = F_m - \sum_{k \neq r} B_{km} \dot{q}_k, \qquad 13a$$

$$G'_r = G_r + \sum_{n \neq m} B_{nr} \dot{S}_n \qquad 13b$$

The above assumptions mean that F'_m and G'_r are independent and "White". The equation (12) now represents the coupled motion of only two oscillators, to which the power flow equations derived by Lyon and Maidanik (11) based on power flow between two linearly coupled oscillators apply. The power flow per unit mass from mth to the rth mode is therefore written as,

$$J_{mr} = \varepsilon_{mr} (\theta'_m - \theta'_r), \qquad 14$$

with

$$G_{mr} = \frac{B^2_{mr} (\beta_m \omega_r^2 + \beta_r \omega_m^2)}{(\omega_m^2 - \omega_r^2)^2 + (\beta_m + \beta_r)(\beta_m \omega_r^2 + \beta_r \omega^2_m)} \qquad 15$$

where $\quad \theta'_m = \langle F_m' \dot{S}_m \rangle / \beta_m \qquad 16$

and $\quad \theta'_r = \langle G_r' \dot{q}_r \rangle / \beta_r \qquad 17$

The energy balance equations are,

$$\beta_m \langle \dot{S}_m^2 \rangle + \varepsilon_{mr} (\theta'_m - \theta'_r) = \beta_m \theta'_m \qquad 18a$$

and $\quad \beta_r \langle \dot{q}_r^2 \rangle - \varepsilon_{mr} (\theta'_m - \theta'_r) = \beta_r \theta'_r \qquad 19a$

By multiplying equation 13a by $\dot{S}m$ and equation 13b by $\dot{q}r$ and averaging, the following expressions are obtained,

$$\beta_m \theta'_m = \beta_m \theta_m - \sum_{k \neq r} \varepsilon_{km} (\theta_m' - \theta'_k \qquad 20a$$

and $\quad \beta_r \theta'_r = \beta_r \theta_r + \sum_{n \neq m} \varepsilon_{rn} (\theta'_n \ \theta'_r) \qquad 20b$

Thus the equation 18a and 19a is written in the form,

$$\beta_m \langle \dot{S}_m^2 \rangle + \sum_r \varepsilon_{mr} (\theta'_m - \theta'_r) = \beta_m \theta_m \qquad 18b$$

and $\quad \beta_r \langle \dot{q}_r^2 \rangle - \varepsilon_{mr} (\theta'_m - \theta'_r) = \beta_r \theta_r \qquad 19b$

The field modes which lie in the narrow frequency band will contribute appreciably to the power flow between the acoustic fields and the m^{th} structural mode. In fact the following approximations may be made,

$$g_{rm} \simeq \begin{cases} \beta_{mr}^2 \quad \pi(\beta_m + \beta_r)^{-1} & |\omega_m^2 - \omega_r^2| < (\beta_m + \beta_r)^2 \\ 0 & |\omega_m^2 - \omega_r^2| > (\beta_m + \beta_r)^2 \end{cases} \qquad 20$$

It must be realized that the equations are subjected to the limitation that $\beta_{rm}/\beta_r \ll 1$ and $\beta_{rm}/\beta_m \ll 1$. Thus g_{rm} is second order in B/β.

Since the interaction between the sound field and the structure is confined to modes lying in the same narrow frequency band, it is sufficient to consider the interaction in each frequency band independently. From equation 18b it is noted that the first term on the left hand side is proportional to the power dissipated in the structure, the second term on the left is proportional to the net power radiated by the structure and the terms on the right are proportional to the power supplied by the forces acting on the structure, the constant of proportionality being M. By definition then,

$$\sum_m \varepsilon_m \langle \dot{S}'^2_m \rangle R_{mech} = M \sum_m \beta_m \langle \dot{S}^2_m \rangle \qquad 21a$$

and
$$\sum_m \varepsilon_m \langle \dot{S}'^2_m \rangle R_{rad} = M \sum_{m,r} g_{mr} (\Theta'_m - \Theta'_r), \qquad 21b$$

where $\sum_m \varepsilon_m \langle \dot{S}^2_m \rangle$ is the mean square surface velocity of the structure.

The radiation and mechanical resistance is defined by equation (21) will be dependent on the modal energy distribution which would present a severelimitation on their usefulness. If consideration is given to one structural mode or to a reverberant structural vibration field, it will be seen that R_{rad} and R_{mech} will achieve values indepently of the energy distribution.

3.3. Single structural modes.

Consider the case where the structure is driven by external random forces and the acoustic field is generated by the structure only. From equations (13b and (17) it was found that $\theta_r = \theta_r = 0$ for all r, and from equation (18a) $\langle \dot{S}_m^2 \rangle \simeq \theta'_m$. Equations (21a) and (21b) reduce to,

$$R\ mech = \beta_m M \qquad 22$$

and

$$R\ rad = M \sum_r g_{mr}, \qquad 23$$

respectively. From equations (18b) and using equations,

$$\sum_r \varepsilon_{(r)} \langle \dot{q}^2_{(r)} \rangle = \frac{S_p(\omega)\ \Delta\omega}{\rho_o^2 C_o^2} \qquad \text{and} \qquad \sum_{(m)} E_{(m)}\ \dot{S}^2_{(m)} = \frac{S_a(\omega)\ \Delta\omega}{\omega^2}$$

$$\frac{S_{p(\omega)}}{S_{a(\omega)}} = (\rho_o/C_o)\left(\frac{R rad}{\beta r}\right)\left(2\pi^2\, n_R(\omega)\right)^{-1} \qquad 24$$

where

$$\beta_r = \beta_k = \beta_R \qquad 25$$

In considering the reciprocal case where the acoustic field is generated by external random forces, but no external forces are acting on the structure, although $\theta_m = 0$, θ'_m is finite. Since there are very many acoustic modes even in a narrow frequency band, it is seen from equation (20a) that

$$\beta_m\ \theta'_m \gg rm\ (\theta'_r - \theta'_m), \qquad 26$$

and thus $\langle \dot{S}_m^2 \rangle \simeq \theta'_m$ (see equations (18a) and (20a).

In accordance with the above considerations, $\theta_r^R \simeq \theta_k^R \simeq \theta^R$

may be set. With this approximation the following equations are obtained.

$$\frac{S_a(\omega)}{S_p(\omega)} = \Gamma(\omega)\ \mu(\omega) \qquad 27$$

where $\mu(\omega) = \text{Rrad}\ (\text{R mech} + \text{Rrad})^{-1}$ 28

and $\Gamma(\omega) = 2\pi^2\ C_o/M\rho o$ 29

$$\therefore \quad \frac{S_a(\omega)}{S_p(\omega)} = (\ 2\pi^2\ C_o\ /M\rho o\ )\ \frac{\text{R rad}}{\text{R rad} + \text{R mech}} \qquad 30$$

3.4. Reverberant Field of Structural Vibration.

The properties of the vibrational field and the structure is assumed to satisfy

$$\beta_m \simeq \beta_h \simeq \beta_s \qquad 31$$

and $\Theta_m{}^s \simeq \Theta_h^s \simeq \Theta^s$ 32

Since in usual cases $n_s(\omega) \ll n_R(\omega)$, by the similar argument as for the single structural mode,

$$\text{R mech} = \beta_s\ M \qquad 33$$

and $\text{R rad} = M \sum_{r,m} g\text{mr}/N_s(\omega)$ 34

with the approximation given by equations (31) and (32) it follows that where the structure alone is directly excited.

$$S_p(w)\ /S_a(\omega) = (\ \rho o/C_o\ )\ (\text{R rad}/\beta_R)\ \ (2\pi^2\ n_R(\omega))^{-1} \qquad 35$$

and $\text{R rad} = \left(\frac{S_p(\omega)}{S_a(\omega)}\right)(2\pi^2\ n_R(\omega)\ \beta_R)\left(\frac{Co}{\rho o}\right)$ 36

and when the acoustic field is excited

$$S_a(\omega)\ /\ S_p(W) = \Gamma(\omega)\mu(\omega). \qquad 37$$

where $$\Gamma = \frac{2\pi^2}{1} \left(\frac{n_s(\omega)}{M}\right) \left(\frac{C_o}{\rho_o}\right) \qquad 38$$

and $$R\ rad = \left(\frac{S_a(\omega)}{S_p(\omega)}\right) \left(\frac{M\rho_o}{2\pi^2\ C_o}\right) \left(\frac{R\ rad + Rmch}{n_s(\omega)}\right) \qquad 39$$

The steady-state relation between the modal temperature of the structure and the modal temperature of the acoustic field is thus established. When Rrad$\gg$Rmech, the modal energy of the structure becomes equal to the modal energy of the sound field if the reverberant sound field is behaving as a temperature bath. When the above inequality does not hold, then the temperature of the structural mode assumes a value, a fraction $\mu(\omega)$ less than the equilibrium value.

Chapter 4.

Use of Instruments in the Measurement and Analysis of the Structural Response to Narrow Band Excitation.

4.1. Introduction.

In this Chapter a brief description is given of some of the main instruments employed in the present research. Also discussed is the building of any special instruments needed for this work. No attempt has been made to include every minor detail, only the information relevant relating to the present work is included.

A full description of the measurement and analysis systems is given in section 4.7 (i, ii and iii).

4.2. Transducers.

(i) Microphones.

The B & K Condenser microphones designed for precision sound pressure measurements were used for all the noise measurements. Their range of application covered the audio frequencies from 20 Hz to 40kHz and of pressure levels of 32 dB to 160 dB. When these microphones were exposed to a sound pressure, the diaphragm was submitted to an alternating force proportional to the pressure and the diaphragm area. The consequent movement of the diaphragm varied the capacity, and these variations were transduced into an AC voltage component when a constant charge obtained by means of a stabilised DC polarised voltage was present between the electrodes.

The microphones were calibrated using a B & K Pistonphone Type 4220 which is a small portable battery driven unit. When fitted to the microphone a sound pressure level of 124 dB was obtained at 250 Hz with less than 3% distortion. Ambient pressure corrections were done by taking a reading from the barometer.

When more than one microphone was used for the same sound pressure level measurements, the output response of each microphone was normalised at the calibration stage. This was achieved by passing the output via either a variable attenuator or an amplifier with variable gain control and by adjusting the gains as necessary, the sensitivities of the microphones were thus normalised.

(ii) Accelerometes.

All vibration measurements were made by using Piezo-electric compression mode accelerometers. These were light and had a natural frequency greater than 100 k Hz. The accelerometers were of the conventional design and the DJB Model A/04 was used normally. The charge sensitivitt of this model was around 3 PC/g with a wide flat frequency range.

The accelerometers were fixed to the surface of the structure using a thin film of special wax. When more than one accelerometer was used for the same measurements, the output response was normalised during the calibration stage using a vibration amplifier with variable gain control potentiometer.

The calibration was made using a small B & K Type 4290 electrodynamic vibrator with an accurately calibrated control accelerometer built in. Using the control accelerometer in the feed back loop with a B & K feed back controlled sweep oscillation, the vibration of the table was held constant in the frequency range 100 Hz to 20 k Hz, and the accelerometer was fixed onto the vibrator table and its frequency response and output sensitivity were measured.

(iii) Loudspeakers.

Sound radiation into the room was via 'Goodmans' Axiam 10" high fidelity loudspeakers. These loudspeakers were installed in accurately designed boxes in order to maintain their frequency response characteristics. Six loudspeakers connected in parallel were placed in positions such that their sound radiation would maintain approximately a diffused field condition in the enclosure. All the speakers used had a frequency response from 40 to 15 k Hz and a power handling capacity of 10 watts with input impedence of 15/16 OHMS.

(iv) Mechanical Vibtator

The structure was mechanically excited with a 'Goodmans' vibrator which was enclosed in a sound proof box. The vibrator was of robust construction and was driven from an oscillator amplifier. The frequency response of the vibrator was limited to 15 k Hz and the power required for its operation was 5 VA.

4.3. Amplifiers

(i) Charge Amplifiers

The piezo-electric transducers were used with the very high input and low output impedance, resistance in parallel with a capacitor feed back 'charge' amplifier. These amplifiers produce voltage outputs proportional to the electrical charge present at their inputs and hence proportional to the quantity being measured. The charge amplifiers normally used were a six and four channel unit manufactured by Environmental Equipment Ltd., Type CVA6 and CVA2. These had a variable response on each between 0 and 30 mv/pc. The flat frequency response characteristic of the amplifier was between 2 Hz to 15 K Hz.

(ii) Power Amplifiers

'Series 3' Radford amplifiers, designed for high quality sound reproduction, were used for radiating sound into the enclosure. The 'MA 25' amplifier of 25 watts output rating had a flat frequency response characteristic from 20 Hz to 20 K Hz at a very low distortion and maintained stability under all conditions of output leading and input waveform.

(iii) Vibration Amplifiers

A 24 channel amplifier was designed especially for the measurement of vibration responses from piezo-electric transducers. Every channel was equipped with a variable gain potentiometer. The outstanding characteristic of the amplifiers were a very high input impedance in the order of 50 M ohms and a flat frequency response characteristic to well above 20 K Hz.

(iv) A.C. Amplifiers

Quite often it became necessary to amplify very low level A.C. signals in the feedback circuit, especially when a compressor was used. A Levall Transistor A.C. Amplifier Type TA 40 was very useful for this, since it had a high input impedance and a very low noise-to-signal ratio, the frequency characteristic of which was 4 Hz to 400 Hz within ± 3 dB.

4.4. Data Recording

(i) Magnetic Tape Recorder

To record data on site and whenever it was not possible to do an on-line analysis, an Ampex FR 1300 transportable tape recorder was used. This was a high quality recorder designed for use with a one inch magnetic tape on which fourteen channels of information could be recorded simultaneously. A frequency modulation recorder per replay system was used on this particular instrument so that high quality recordings down to zero frequency (D.C.) were possible with very little dependence on the properties of the tape itself.

The FR 1300 tape recorder operated with a 108 K Hz carrier frequency at a tape speed of 60 ins/sec and was normally adjusted such that either a 1v r.m.s. or 0.5v r.m.s. signal produced a 40% frequency deviation. Built-in filtering limited the maximum recording frequency to 20 k Hz at a tape speed of 60 ins/sec. Topespeeds of 30, 15, $7\frac{1}{2}$, $3\frac{3}{4}$ and $1\frac{7}{8}$ ins/sec. with the appropriate filters were also available. With the standard 1100M reels of tape, recording times from 12 to 384 minutes were obtainable at the fastest and lowest speeds respectively.

(ii) Level and x-y Chart Recorders

The B & K level recorder type 2305 and Hewlett Packard, Moseley x-y chart recorder were mostly used for the accurate recording of signal levels in the frequency range 10 Hz to 20kHz.

(iii) Oscilloscope and Camera

The storage oscilloscope was a special purpose instrument designed to store and display on the cathode-ray tube, the input signal for viewing and photographing. This facility was extensively used and with the aid of a polarised camera the information was photographed for later analysis.

4.5. Signal Generators and Wave Analyses

(i) Sine Random Noise Generators

This instrument covered a frequency range from 20 Hz to 20 k Hz and consisted of a wideband noise generator, a beat frequency oscillator, several filters and amplifiers and an automatic output regulator (compressor). At the output terminals the following three types of singal were obtained:

1) sine wave;
2) narrow band random noise;
3) wide band random noise.

The basic principle of operation of the Sine-Random Generator is shown in fig. 4A. In position for sine-wave and narrow bands of random noise the generator worked on the heterodyne principle using two mixers, and in position for wide band random noise the signal from the noise generator was fed via a low-pass filter directly to the output amplifier. The compressor circuit could be controlled from an external voltage, whereby it was possible to keep the vibration or sound pressure level constant during measurement.

The main operating principles of the generator were as follows:

a) Sinusoidal

A 3 k Hz oscillator modulated a 123 k Hz carrier signal. The lower sideband (120 k Hz) of the modulated signal was separated in an intermediate frequency amplifier which, incidently, acted simultaneously as a regulation amplifier. After the lower side-band had been selected, the signal was mixed with a signal of a frequency of between 100 k Hz and 120 k Hz originating in a variable oscillator. A low-pass filter (cut off, 20 k Hz) selected the difference frequency which was amplified in the output amplifier before being passed onto the output and meter circuit.

b) Narrow Band Noise

The sequence was as above, except that instead of modulating the 123 k Hz with 3 k Hz sine wave, a 3 k Hz signal of randomly varying amplitude was used. This was achieved by filtering and amplifying a wide-band noise signal.

c) Wide Band Random Noise Generator

The signal from the noise generator was set, via a low-pass filter the cut-off frequency of which was 20 k Hz, to the output amplifier. The wide-band noise generator supplied a signal with constant power spectral density in the frequency range 20 Hz to 20 k Hz with a truly Gaussian instantaneous voltage distribution up to 4σ (four times the r.m.s. value).

A B & K sine random generator type 1024 was used throughout the present experimental work.

(ii) Quantech 304 Wave Analyser

This instrument was widely employed in obtaining modal densities of the cylindrical shell from the amplitude and phase response tests. The instrument's three constant bandwidth filters of the heterodyne receiver type were operated in the tracking or fixed modes. The filter bandwidths were 1, 10 and 100 Hz at 3 dB points.

Referring to the block diagram in fig. 4B, at input signal having a frequency component within the range 0 to 5 k Hz could be analysed, either by manual tuning or by an automatic linear sweep. The incoming signal from the transducer was first used to modulate the output of a variable frequency voltage-controlled sweep oscillator whose output was between 10 and 15 k Hz. The first intermediate frequency stage allowed only the lower sideband of the modulated signal to pass and the resulting output was then split into two separate channels. The signal in each channel was subsequently used to modulate, respectively, the quatrature-phase outputs (r and j) of a fixed 10 k Hz oscillator. Thus, providing the original input signal was in the range of 0 to 5 k Hz, the lower sideband resulting from this second stage of modulation could be made of zero frequency by adjusting the variable frequency oscillator.

After passing through the constant bandwidth filters, the r and j channels were then chopped and summed to give a meter indication of the amplitude of the data signal within the effective passband.

A pure, sinusiodal signal at the tuning frequency was available from the instrument. This was obtained by amplitude modulation of the 10 to 15 k Hz sweep oscillator signal with that from the 10 k Hz fixed oscillator and low-pass filtering the result to obtain the lower side- band. By using this output to drive either the vibrator or loudspeakers, the response analogue from the transducer of the system under test could be fed back to the analyser. The centre frequency of the analyser was then always identical to the excitation frequency and therefore the analyser functioned in the tracking mode.

The linear D.C. voltage analogues of both the meter deflection and the swept frequency were also provided. These were used to drive an x-y chart recorder to obtain a trace of the input signal response within the passband against filter centre frequency.

For the phase measurement, the D.C. voltage analogue output of both, the real (r) and imaginary (j) portions of the input signal were simultaneously plotted on an x-y chart recorder against one another, a polar diagram resulted, from which the phase response characteristic of the specimen was determined.

(iii) Spectral Dynamics SD 101A Tracking Filters

Two Spectral Dynamics data analysis systems were used in the experimental work discussed in sections 4.7 (i) and 4.7 (ii). Both these systems employed the above filters.

The tracking filters had a useful frequency range of 2 Hz to 25 k Hz and used a hetodyning frequency of 100 k Hz. A choice of plug-in crystal, lattice-type filters were available having -3db bandwidth of 1.5, 5, 10, 20 and 50 Hz respectively. All these filters had shape factors of 4, indicating that their bandwidth at the 60 db attenuation points were four times that at the 3 db points. An internal, mains frequency calibration signal could be switched to the input of the crystal filters to check that their gain was unity within the passband. The SD 101 A could be tuned directly by an external sinusoid without the need for a frequency to voltage converter.

A simplified block diagram of fig. 4C shows the principle of operation.

4.6. Special Purpose Instrument

(i) Automatic Space and Time Averaging System.

This instrument was designed and built in the Department of Mechanical Engineering to determine the mean square of the measured response at several stations of a continuous system both with respect to time and to the number of stations in the system. Thus, if the acceleration response to random excitation at the Ƴth station in the system is (A_r(r = 1....n) at any instant, then the mean square acceleration $\bar{a}^2$ was given by

$$\bar{a}^2 = \frac{1}{Tn}\int_0^T\left[\sum_{r=1}^n a_r^2\right] dt \quad \text{or} \quad \frac{1}{Tn}\sum_{r=1}^n\left[\int_0^T a_r^2\, dt\right]$$

Thermal converters were used in this instrument to perform the squaring and integration with respect to time. A thermal converter is shown in fig. 4.D and consists of a heater and thermocouple junction in an evacuated glass bulb. The thermocouple junction measured the temperature of the heater wire so that the voltage output was proportional to temperature. The temperature of the heater wire was proportional to the input power, making the output voltage proportional to the input power.

$$\text{Input Power} = \frac{1}{T}\int_0^T RI_{in}^2 \, dt$$

where I_{in} is a function of time.

The integration and division by time was caused by the long time constant of the thermal converter so that the converter was time averaging

$$\text{Hence, } V_{out} \propto \frac{1}{T} \int_0^T I_{in}^2 \, dt.$$

A block diagram of the instrument under discussion is shown in fig. 4E. Preceding each thermal converter was a driver amplifier so that

$$V_{out} \propto \frac{1}{T} \int_0^T V_{in}^2 \, dt$$

where V_{in} is the input voltage to the driven amplifier.

Since the input voltage to the instrument and the output voltage from the thermal converters were not connected electrically, but only thermally, summation of the thermal converter outputs could be achieved by connecting the converter outputs in series, i.e. each converter acted as a voltage generator as shown in fig. 4E.

The maximum output from each converter was about 6 mv making it necessary to add an output stage amplifier to give an adequate voltage output for recording and detection. In this particular instrument there were two chains of series connected converter outputs, each chain consisting of twelve converters. The two chains could be used independently or connected together to form one chain of twenty four converters i.e. two mean square values may be obtained simultaneously from up to twelve inputs each or one mean square value from up to twenty four inputs signals.

The total number of inputs to the instrument was 24 in two groups of 12. The flat frequency response was from 200 Hz to 5 k Hz, $\pm$ 1/2 db (mean square) or $\pm$ 1/4 db (r.m.s.) from 60 Hz to 15 k Hz and $\pm$ 1 db (mean square) or $\pm$ 3/4 db (r.m.s.) from 40 Hz to greater than 20 k Hz. The input impedance was 10 K ohms. A meter analogue output of 0-600 mv d.c. for under F.S.D. was available from the instrument for calibration purposes.

The automatic Space and Time Averaging instrument together with other instruments were employed to obtain the sound pressure and acceleration ratio, hence the overall system calibration (Transducer through to plotter) was performed as deacribed below.

One side of the instrument (12 microphone inputs) was used to measure the mean square sound pressure level and the other side (12 accelerometer inputs) to measure the mean square acceleration. The relation between mean square pressure and acceleration were as follows:

(a) Sound Pressure Level

The 124 db sound pressure level generated by the pistonphone gave 2.5v r.m.s., being the normalised sensitivity of the microphones.

$$124 \text{ db (re } .0002 \ \mu\text{Bar)} = 31.6 \ N/M^2 \equiv 2.5\text{v}$$

The maximum signal level for the particular test was not expected to exceed 0.3v and therefore this range was selected.

$$0.3\text{v} \equiv \frac{0.3}{2.5} \times 31.6 \ \frac{N}{M^2} = 3.8 \ \frac{N}{M^2}$$

Meter Full Scale Deflection = $(0.3v)^2 \equiv 3.8^2 \ \frac{N^2}{M^4}$

600 mV analogue output = $(0.3v)^2 = 0.09v^2 = 14.44 \ \frac{N^2}{M^4}$

which determined the plotter scale in $\frac{N^2}{M^2}$

(b) Acceleration

100 mV = 1g was the normalised sensitivity of the accelerometer at calibration. The maximum input voltage was expected to be 100 mV hence 0.1 V range was chosen.

$0.1V \equiv 1g \equiv 9.81 \ \frac{M}{sec^2}$

Meter Full Scale Deflection = $(0.1V)^2 \equiv 9.8^2 \ \frac{M^2}{sec^4}$

600 mV Ahalogue Output = $0.01V^2 \equiv 9.6 \ \frac{M}{sec^4}$

which determines the plotter scale in $\frac{M^2}{sec^4}$

Since the ratio of $\frac{(\text{Acceleration})^2}{(\text{Sound Pressure level})^2} \left(\frac{\bar{a}^2}{\bar{p}^2} \right)$

then, $\left(\frac{\bar{a}^2}{\bar{p}^2} \right) = \frac{\text{Acceleration meter F.S.D.}}{\text{S.P.L. meter F.S.D.}} = 96 \ \frac{M^2}{sec^4} \times \frac{M^4}{14.4 \ N^2}$

$\left(\frac{\bar{a}^2}{\bar{p}^2} \right)$ (both meters F.S.D.) $= 6.66 \left(\frac{M}{N \ sec^2} \right)^2$

Thus when both meters indicated F.S.D. the plotter read 6.66

$\left(\frac{M^3}{N \ Sec^2} \right)^2$ and fixed a point on its axis.

For the (sound pressure level) ^{2}/ (acceleration)^2 ratio, the system 'calibration' was carried out as follows:

c. Sound Pressure Level

124 db S.P.L. (re 0.0002μBar = 31.6 $\frac{N}{M^2}$ $\equiv$ 2.5V

.03v range was selected for full scale deflection.

$$0.03V = \left(\frac{0.03}{2.5}\right) \times 31.6 \ \frac{N}{M^2} = 0.38 \ N/_{M^2}$$

$$\text{Meter F.S.D.} = (0.03V)^2 \equiv 0.38^2 \ \frac{N^2}{M^4}$$

$$\text{600 mV analogue output} = (0.03v)^2 \equiv 0.144 \ \frac{N^2}{M^4}$$

d. Accelerometer

100 mV = 1g

0.3v range was selected for full scale deflection

$$0.3v \equiv 3g \equiv 29.43 \ \frac{M}{sec^2}$$

$$\text{Meter F.S.D.} = (0.3V)^2 \equiv 29.43^2 \ \frac{M^2}{sec^4}$$

$$\text{600 mV analogue output} = (.3V)^2 \equiv 866 \ \frac{M^2}{sec^4}$$

$$\text{The ratio } \frac{\bar{p}^2}{\bar{a}^2} \frac{(F.S.D.)}{(F.S.D.)} = \frac{.144}{866} \left(\frac{sec^4}{M^2} \times \frac{N^2}{M^4}\right)$$

Thus a point on the plotter axis was fixed.

4.6. (ii) Electrical Network used in the Measurement of Reverberation Time.

In the practical method of obtaining the squared and integrated impulse response for determining the reverberation time, some of the electrical networks suggested in the B & K Technical Review No.4.1966 were assembled in the Department of Mechanical Engineering with a few modifications and used for this purpose. The block diagram of the set-up is shown in fig. 5·3B and descriptions of the specially designed circuits are given below.

a. Squaring Circuit

The circuit using its recommended values shown in fig. 4G was built for a maximum input voltage of 10 volts r.m.s. The input signal s(t) was rectified and the squaring was obtained by applying three different bias voltages to the diodes so that they started conducting at different input levels.

b. Integrating Network

In order to avoid using a D.C. amplifier with matching impedance in the system to avoid any loading the integrating circuit was patched using a Burr-Brown Amplifier as shown in fig. 4H. The ± 15 V power supply to this was obtained from a Burr-Brown power supply unit. This modification to the recommended circuit did not alter the integration characteristics.

c. A.C. Amplifier

An A.C. amplifier with a maximum of 26 as shown in fig. 4J was also built and used in the system.

4.7. Typical Data Reducing And Analysis Systems.

The layout of the measuring and analysis systems in fig. 4.7 (i,ii,iii,) is self explanatory. The calibration of the individual instruments were made in accordance with the instructions given in the manuals and where ever necessary the system calibration were also carried out before every experiment.

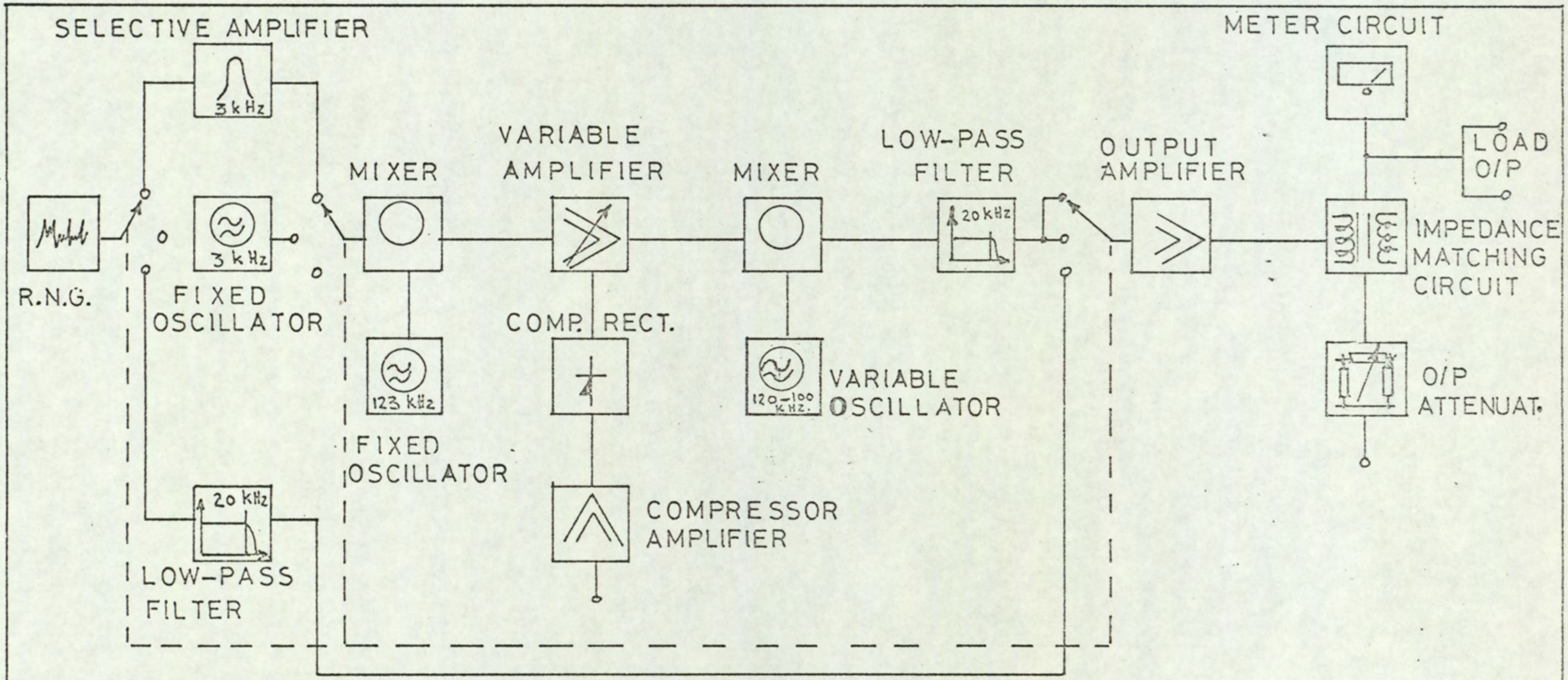

FIG.4A

BLOCK DIAGRAM OF THE SINE-RANDOM GENERATOR

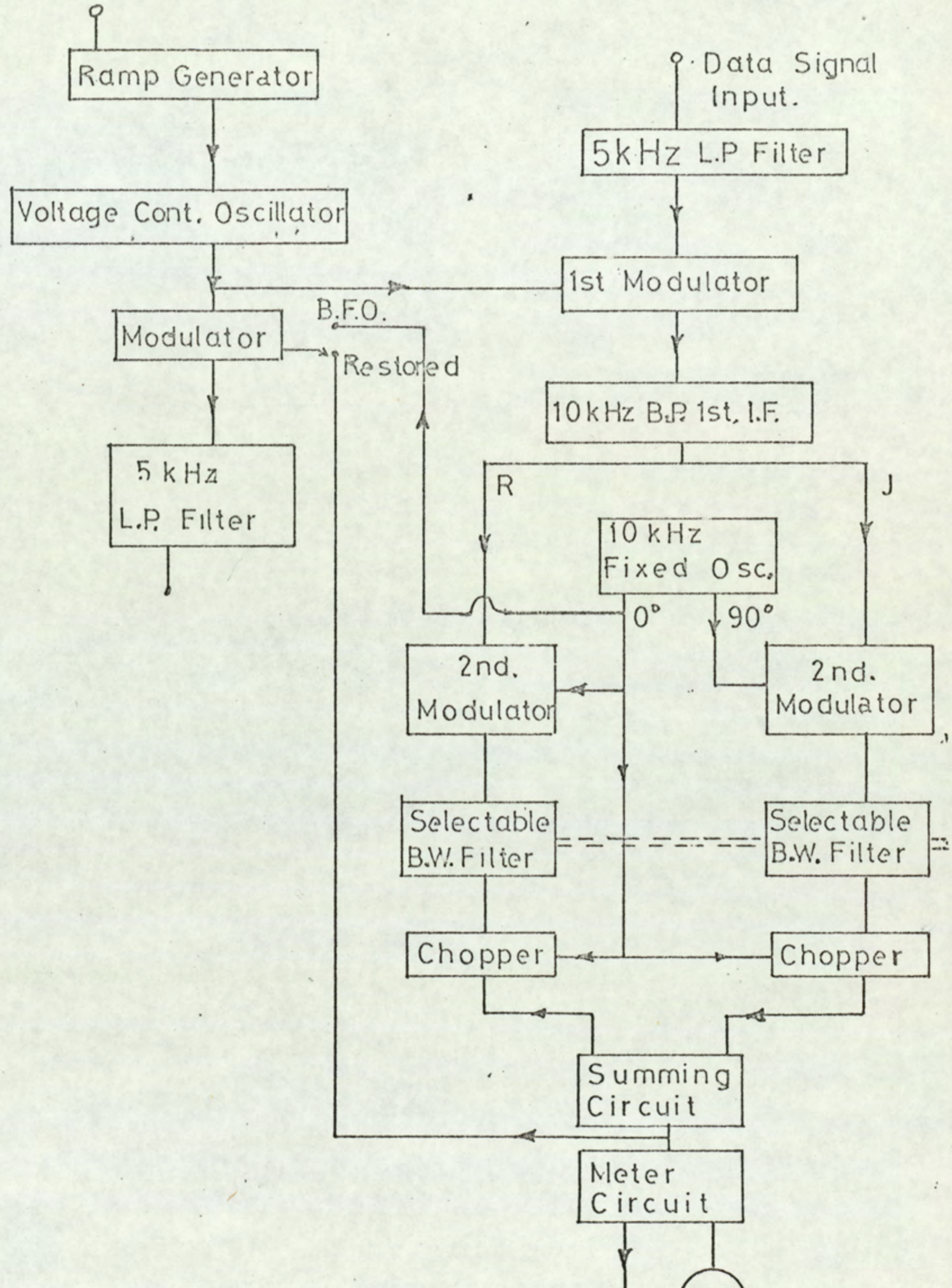

QUANTECH 304 WAVE ANALYSER FACILITIES

FIG. 4B

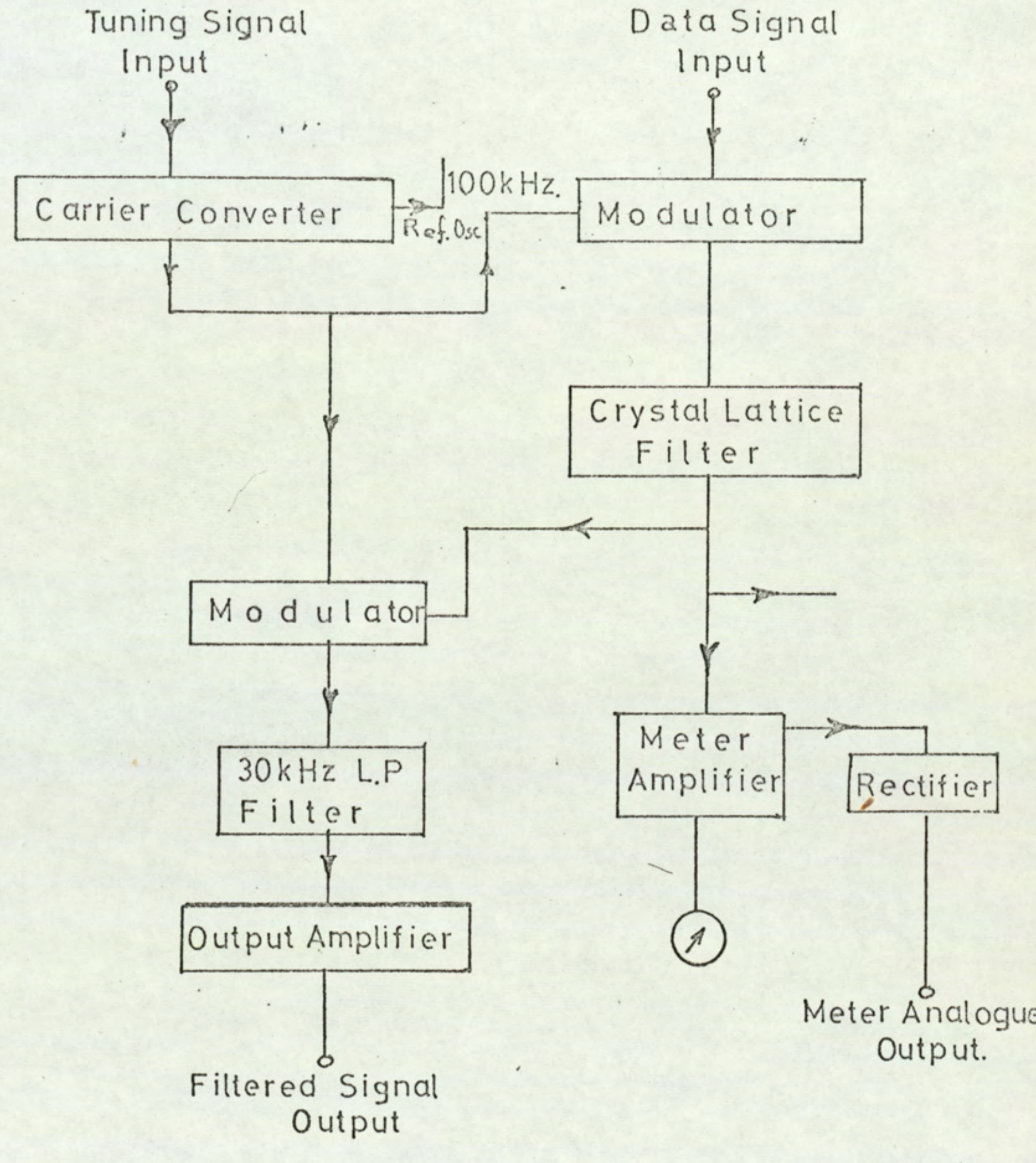

SPECTRAL DYNAMICS SD101A
TRACKING FACILITIES.

FIG 4C

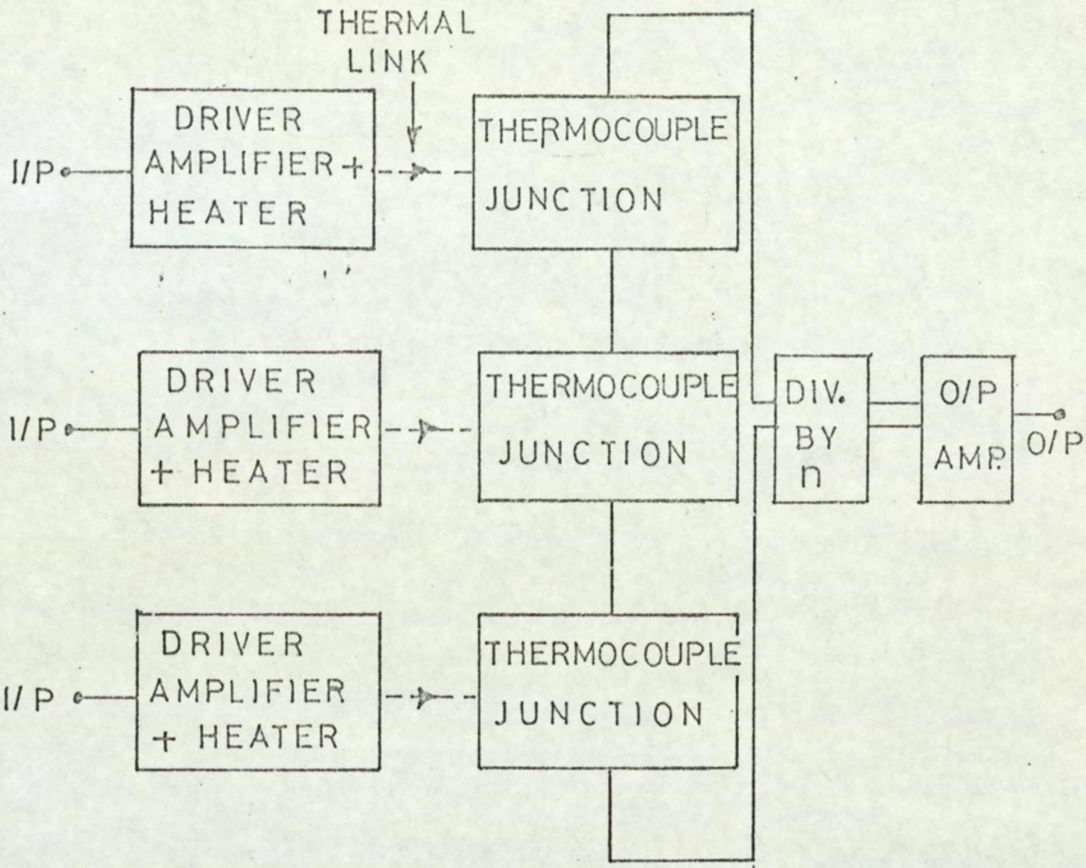

SCHEMATIC DIAGRAM OF INSTRUMENT FUNCTION

FIG. 4E

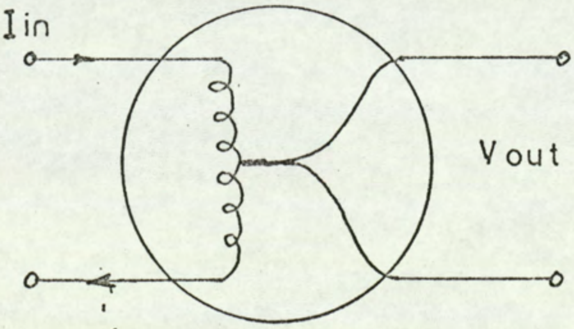

$$V_{out} \propto \frac{1}{T}\int_0^T I_{in}^2\, dt$$

THERMAL CONVERTER

FIG.4D

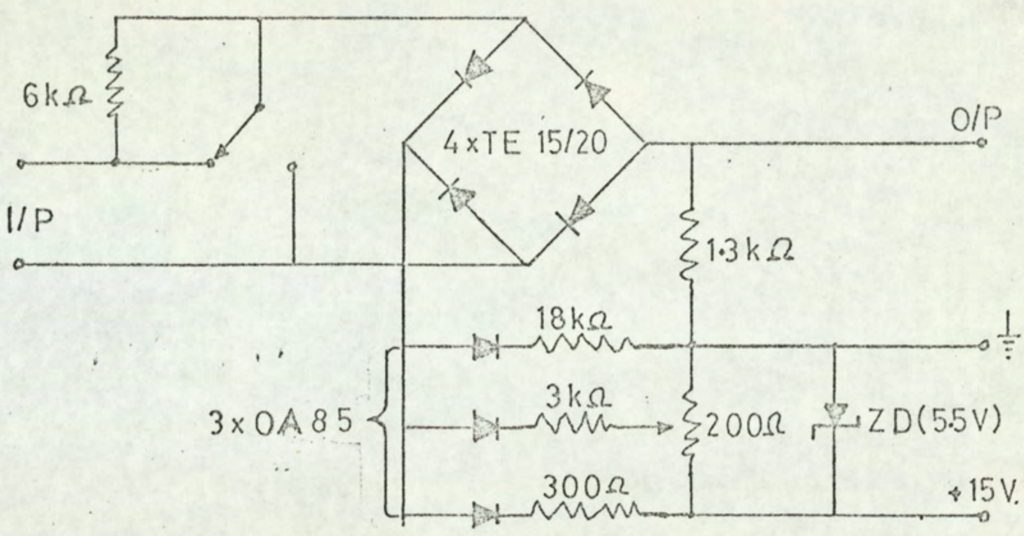

SCHEMATIC DIAGRAM OF THE SQUARING CIRCUIT

FIG.4G

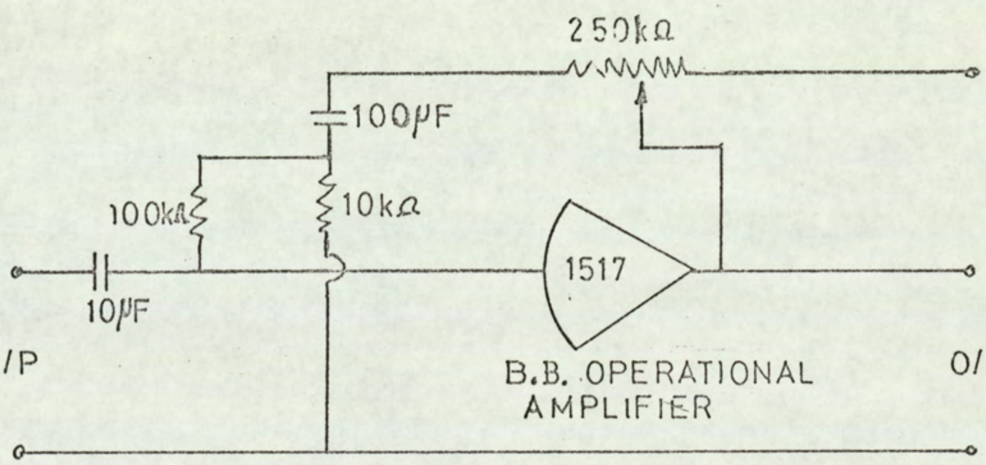

SCHEMATIC DIAGRAM OF THE AMPLIFIER CIRCUIT

FIG.4J

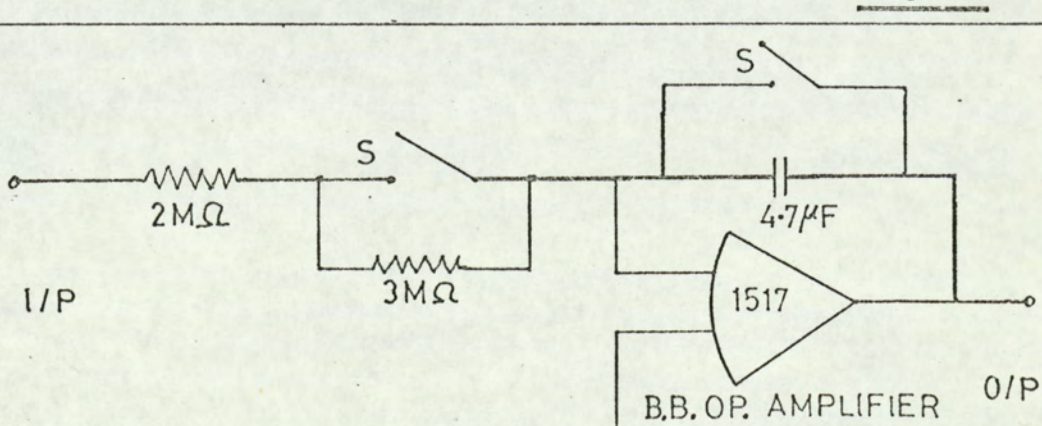

SCHEMATIC DIAGRAM OF THE INTEGRATING CIRCUIT

FIG. 4H

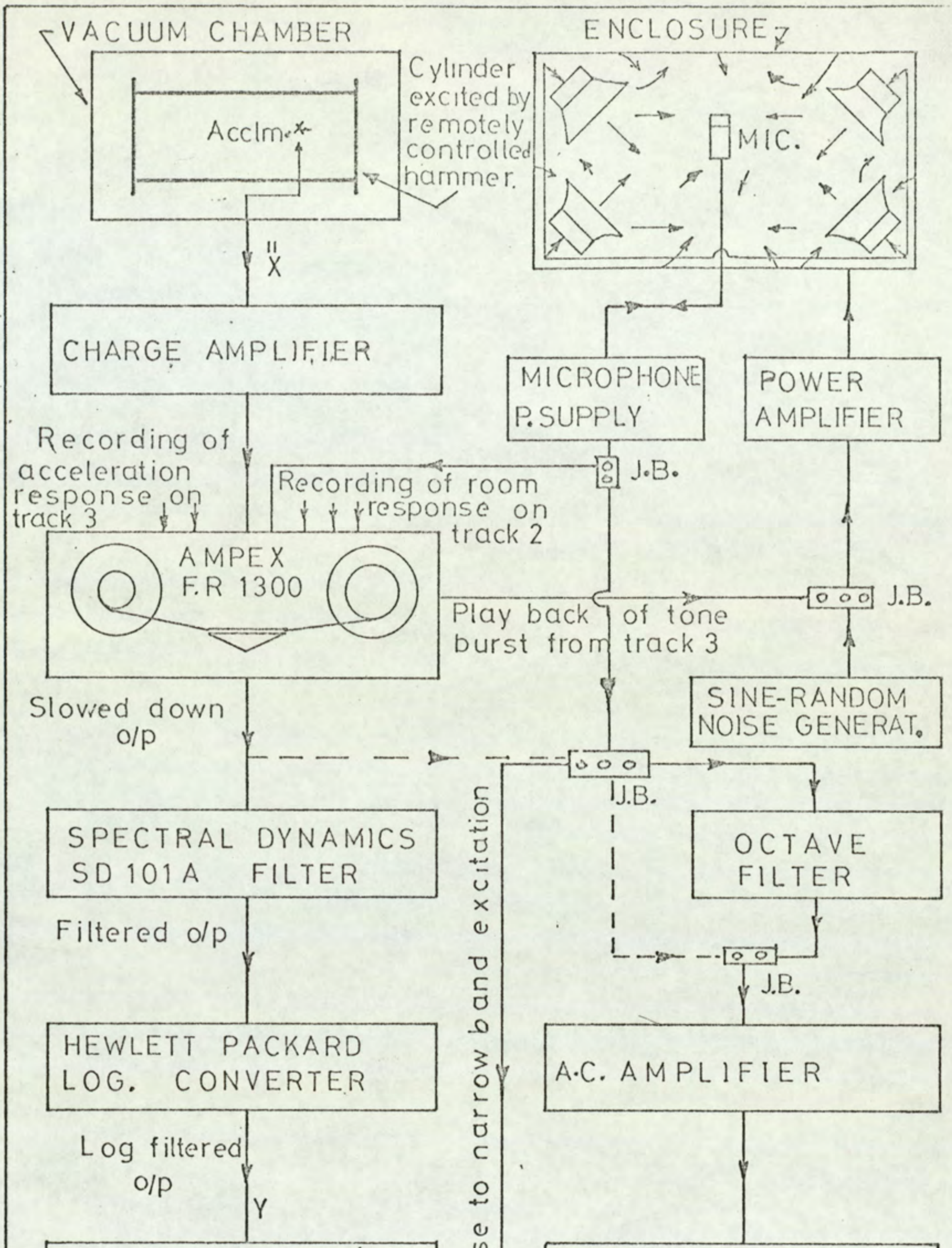

INSTRUMENTS USED IN MEASURING STRUCTURAL AND ROOM DAMPING

FIG 4.7(i)

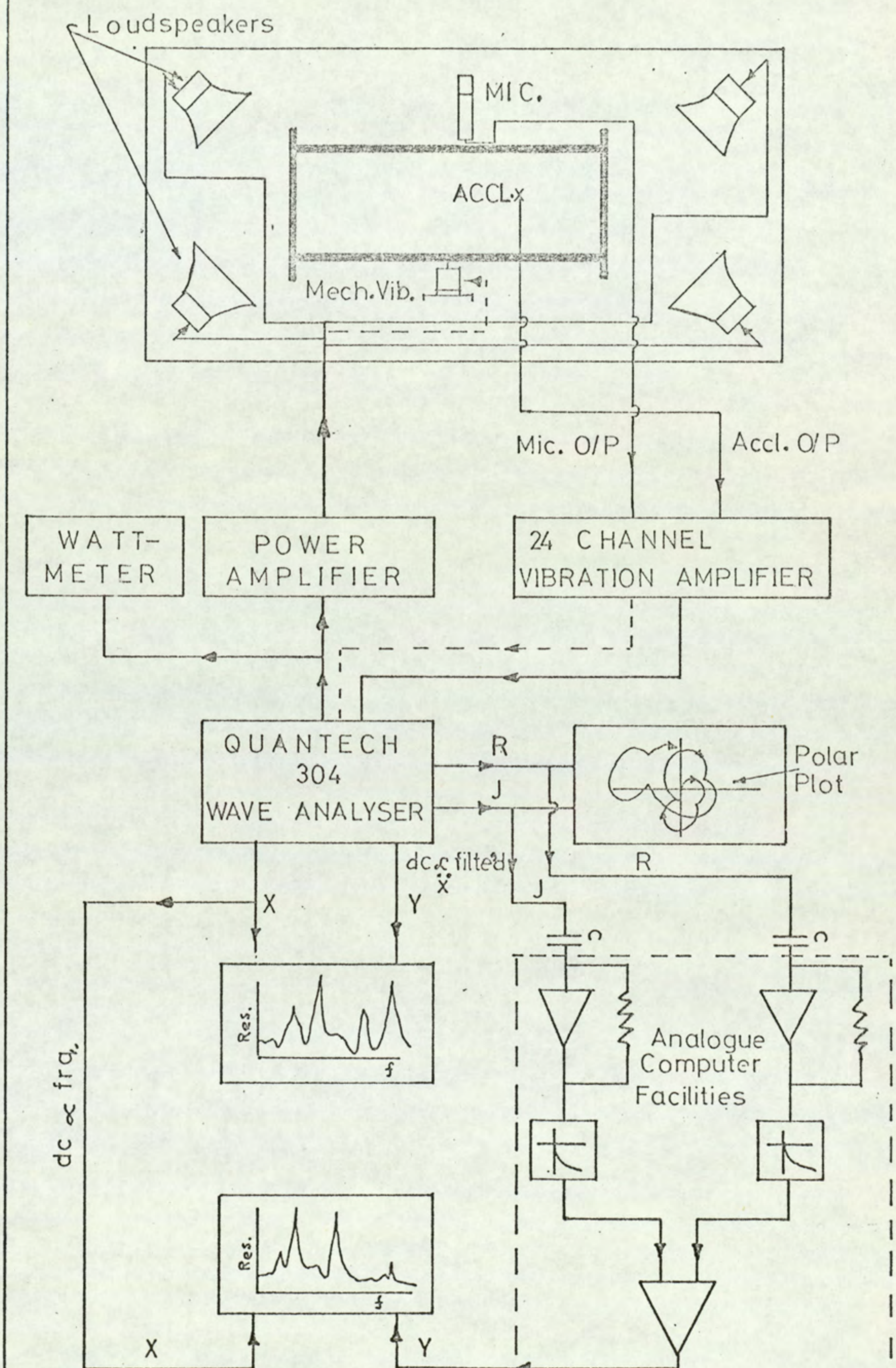

INSTRUMENTS USED IN MEASURING AND SEPARATING STRUCTURAL MODES

FIG 4.7(ii)

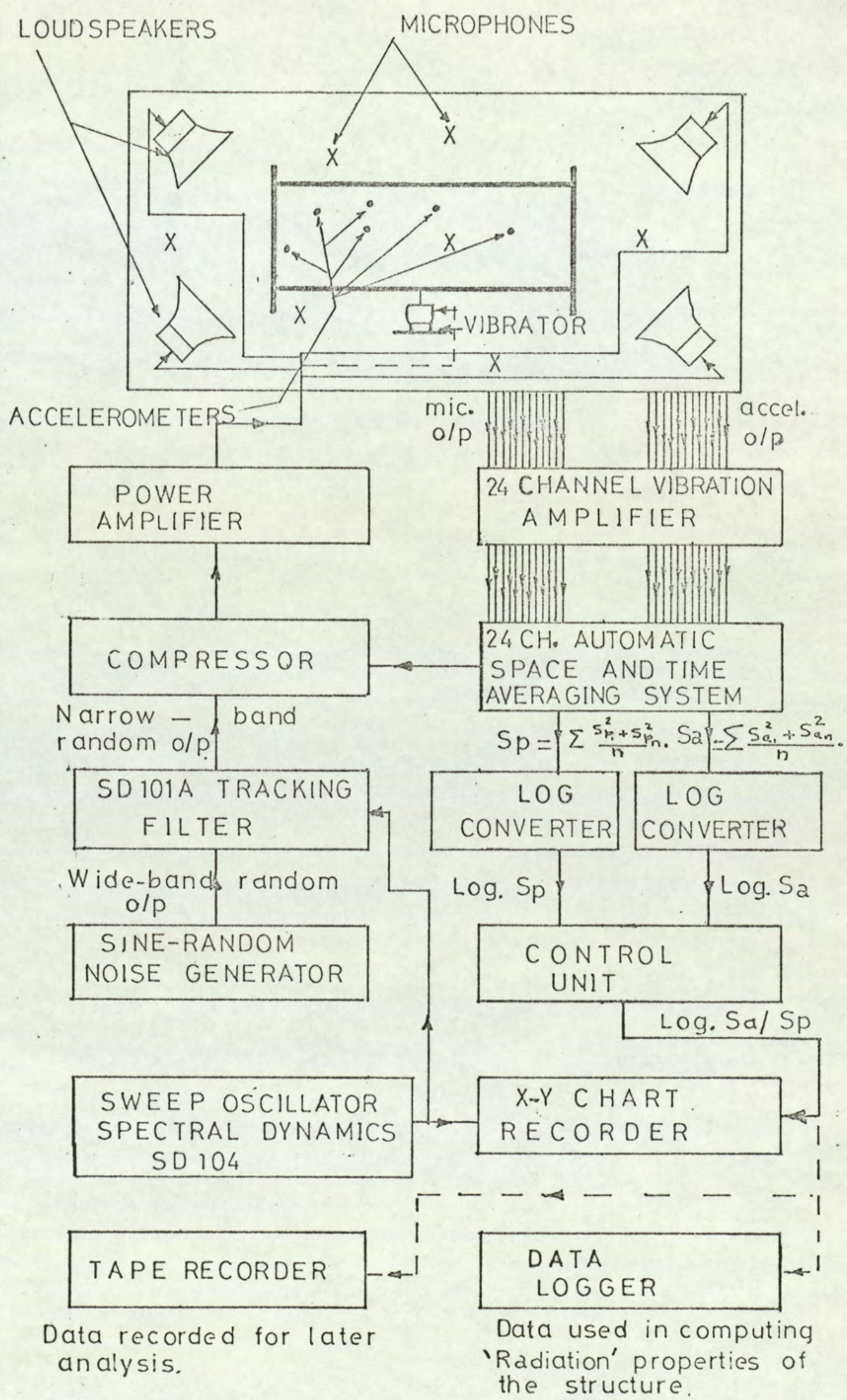

INSTRUMENTS USED IN MEASURING $S_a(\omega)/S_a(\omega)$ AND $S_a(\omega)/S_a(\omega)$

FIG 4.7(iii)

Chapter 5. Room Acoustics

5.1. Introduction

In determining the acoustic qualities of a room, one of the important factors is the measurement of its reverberation time. The accuracy with which it can be determined from the decay curve is limited by random fluctuations in it. A method to minimize the effects of the fluctuations in decay response on the measured reverberation-time value is to repeat the reverberation experiment many times and to average the data obtained from the individual responses. This method takes quite a lengthy analysis time and often fails to reveal a true nature of the decay, especially when the response is subject to a multiple decay rate as can be seen in the curves of fig. 5.21A.

The high initial decay value containing much of the valuable information persists only for a few decibels and if the data is not carefully reduced much of the information can be lost. Decays with multiple slopes, point to a lack of sound diffusion in the room. In some reverberant rooms the diffusion decreases during the decay and therefore it is the initial decay rate that is important for the determination of the statistical absorption. To extract all the useful information from the decay curves, many such curves obtained under identical physical conditions should be averaged and not just the decay rates or reverberation times obtained from individual decay curves.

A new method for measuring reverberation time is described by Schroeder (14), which, in a single measurement, yields the decay curves that are identical to the average over infinitely many decay curves that would be obtained from exciting the enclosure with band pass-filtered noise. Thus, the difficulties mentioned in the conventional methods of determining the reverberation times are reduced to some extent.

Rooms in which random sound fields can be established are important tools in applied acoustics. Two outstanding problems are the production of random sound fields and the determination of whether or not a given sound field is random. This can be determined approximately from the point measurements in the room and from the method developed by Cook and associates (43) who consider a cross-correlation coefficient, R, the sound pressure at two different points in the sound field and from these the acoustic qualities of a closed room is determined more closely.

The modal density is another parameterthat also determines the acoustic quality of a room. It is not very easy to measure this parameter experimentally, but from the theoretical approximations based on the enclosure dimensions and ambient speed of sound, the modal density can be predicted to a reasonable accuracy.

The work reported in this chapter is based on the basic assumption described and the measurements are made to obtain the best technique in the determination of reverberation time and to establish the acoustic quality of the room in which most of the tests for the measurement of various paramters including noise transmission will be made.

5.2. Measurement of Reverberation.

5.21. Basic Concepts.

Basic consideration in the aspects of the reverberation process, and of room acoustic problems in general, can be understood by taking into account the wave nature of sound. It was shown experimentally by Knudsen (57) that reverberant sound has characteristic frequencies which are properties of the room and not necessarily only of the source which initiates the reverberations. These characteristic frequencies can be found by solving the three-dimensional wave equation governing the sound propagation in the room and are commonly termed room resonances. They set-up a complicated scheme of standing wave pattern, which changes completely as the frequency of the sound changes. The abrupt change in the sound level when the source is turned off can be represented by a complex frequency spectrum and the reverberation process contains signals with more than one frequency even if the steady state sound source consists of a pure tune only. If these signal frequencies coincide with some of the room resonances beat will occur and the reverberation decay curve will show a number of fluctuations. The less damped the room resonances are, and the "purer" the tone of the sound source, the greater will be the fluctuation in the reverberation process. It has, therefore become a common practice to use a "band of frequencies" as the sound source, centred around that particular frequency the reverberation of which it is desired to study. In this way the number of room resonances taking part in the decay will be so great that the fluctuations in the decay curve will, more or less, average out. The "band of frequencies", may concist of a band of random noise, a warbled tone, a number of closely spaced pure tone or simply a tone burst. To assume the excitation of as great a number of room resonances as possible within the frequency band produced by the sound source, the position of the source in the room must also be considered.

The accuracy with which reverberation times can be determined from the decay curves is limited by random fluctuations in the decay curves. These random fluctuations result from the mutual beating of normal modes of different natural frequencies. The exact form of the random fluctuation depends on, among other factors, the central amplitudes and phase angles of the normal modes at the moment that the excitation signal is turned off. If the excitation signal is a band pass filtered noise, the initial amplitudes and phase angles are different from trial to trial. Thus, for the same enclosure, and identical transmitting and receiving positions within the enclosure, different decay curves are obtained, shown in fig. 5.21A, the difference being a result of the randomness of the excitation not of any changes in the characteristics of the enclosure.

5.22. Methods of Reverberation Time Evaluation.

(i) From the measurement of the decaying response.

The two most commonly used methods in the measurement of reverberation time are outlined in this section. Common to both methods are the use of a sound source, a microphone, an amplifier and a recorder capable of responding to a quickly decaying output. By using a 'Sine Random Noise Generator', random or pure tone sound can be produced in the enclosure. The decaying output from the microphone may be filtered in the desired frequency band before recording. An example of such a measuring arrangement is shown in fig. 5.22A where a small gun is used to produce a sound source instead of a noise generator. When the gun is fired, the sound level in the room will first rapidly increase and then decrease according to the reverberant properties of the room. The output from the microphone placed in the enclosure is filtered and then recorded. The reverberation time is measured from the initial portion of the recorded decay curve.

This method is convenient when only a limited number of reverberation curves are to be measured. When a great number of curves are to be recorded over a wide frequency range, the use of a gun as a sound source is unsatisfactory as it would require one shot for every curve. It is then advantageous to employ the method where the sound source consists of a noise generator and one or more loudspeakers in the room, as shown in fig. 5.22B. When a steady noise field in the enclosure is obtained, the noise is cut off and the output is recorded as before and the reverberation time obtained from it.

(ii) <u>From the Measurement of the Integral of the Squared Impulses of the decaying response.</u>

The basis of Schroeden's (44) "Integrated impulse method" is that the ensemble average of the square of the reverberation noise decay in an enclosure equals the time integral of the enclosure squared impulse response. To arrive at this result, it is considered that the room is excited by "stationary white noise" which is suddenly shut off. If the noise is stationary and white this can be mathematically stated by the equation,

$$\langle n(t_1) \times n(t_2)\rangle = N \times \delta(t_2 - t_1) \qquad 1.$$

where

t_1 and t_2 are two arbitrary chosen instants of time

$(t_2 - t_1)$ is the Dirac δ function

$\langle n(t_1) \times n(t_2)\rangle$ is the autocovariance function of the noise.

N is the noise power per unit bandwidth

The response of any linear network to our arbitrary time function $n(\tau)$ is considered next;

$$s(t) = \int_{-\infty}^{t} n(\tau) \times r(t) - \tau)\, d\tau \qquad 2.$$

Here $r(t-\tau)$ is the impulse response of the network at the time t, to a unit impulse occurring at time τ

By considering the room a linear acoustic network and squaring equation (2) the double integral is obtained and shown as follows:

$$s^2(t) = \int_{-\infty}^{\tau=t} d\tau \int_{-\infty}^{\Theta=t} d\Theta \times n(\tau) \times n(\Theta) \times r(t-\tau) \times r(t-\Theta) \qquad 3.$$

The upper limit of integration should be taken to be 0, if this is chosen as the instant of time when the noise is shut off.

Averaging the above expression over the emsemble of noise signals and utilizing equation (1).

$$\langle n(\tau) \times n(\Theta)\rangle = N \times \delta(\Theta - t)$$

the equation below is obtained:

$$\langle S^2\ (t)\rangle = \int_{-\infty}^{0}\int N \times \delta(\Theta-\tau) \times r(t-\tau) \times r(t-\Theta)\, d\Theta\, \delta\tau \qquad 4$$

As $\delta(\Theta-\tau)$ is zero except when $\Theta = \tau$ and as the integral over the delta function equals unity, equation (4) finally becomes

$$\langle S^2\ (t)\rangle = N \times \int_{-\infty}^{0} r^2\ (t - \tau)\ d\tau \qquad 5.$$

From $\tau = 0$, the function $\langle S^2\ (t)\rangle$ represents the ensemble average of the squared reverberation process. To obtain the function an "infinite" number of measurements would be necessary and the reverberation time determined according to normal procedure would be half the actual reverberation time due to the squaring.

On the other hand, the time integral $\int_{-\infty}^{0} r^2(t - \tau)\delta\tau$ represents basically, a single measurement of the squared impulse response of the linear network integrated over an infinite time.

By definition $r(t - \tau)$ is the unit impulse response of the system under consideration. If such an impulse occurred at $\tau = -\infty$ then the above integration merely states that the squared response has to be theoretically considered and integrated over an infinite period of time. In practice, the response to unit impulse is only measurable over a certain, very finite, period of time. The meaning of integral is thus to consider the integration as long as the response of the system to a unit impulse can be determined in practice, and the limits of integration are chosen accordingly.

The "unit impulse" is in practice often obtained by means of a pistol shot, a tone burst or other short lasting sound phenomena.

Normally band-limited noise is used, to be able to determine the reverberation as a function of frequency. As soon as the noise is band-limited, equation (1) does not hold in a strict mathematical sense, because a certain time correlation is imposed upon the noise. If the effective correlation interval is small compared with any part of interest in the reverberation decay process, equation (1) is still valid in a practical sense.

To obtain the true impulse response the length of the impulse used to determine the filtered response of the room should be short compared to the period of the filter centre frequency.

5.3. Techniques Used in the Measurement of the Reverberation Time of the Room.

The first part of this experiment was made to compare the results from the "Interrupted Noise Method" with the "Integrated Impulse Method" when the measurements were made under the same experimental conditions. This was performed with a view to finding out the most reasonable method that can be used for the measurement of reverberation time in the narrow frequency band.

The practical method of obtaining the squared and integrated impulse response was from the tape recorded tone burst whose spectra covered the wide frequency bands which were radiated into the room from the loudspeakers. The response of the enclosure to each tone burst was picked up by microphone whose output was recorded and then played back in reverse-time direction. The output signal from the tape recorder was squared and integrated by means of RC network and then recorded. The description of the measuring circuits are given in Chapter (4). The experiment was then repeated and the output from the microphone filtered in the narrow frequency band during play back of the tape for evaluation. Some of the decay curves are given in fig. 5.3A. The arrangements of the measuring instruments are given in fig. 5.3B.

For the purpose of interrupted noise experiment, the wideband random noise having the same spectra as in the previous experiment was radiated into the enclosure from the loudspeakers. When the noise level in the room attained a steady intensity, it was cut off and the decaying output picked up by the microphone was recorded using the level recorder. This was again repeated and the microphone output filtered in the required frequency band and the response recorded as before. The results of some of the decay curves are given in fig. 5.3C. In fig. 5.22B is shown the experimental flow diagram.

From the data obtained it was observed that no immediate advantage is gained by using the "Integrated Impulse Method" as the spread in the determined values was so small that it could be dismissed as being due to evaluation error. The laboratory made circuits used in the "Integrated Impulse Method" were seen to carry a spurious signal although great care was taken to eliminate much of it and this could have been one of the reasons for the spread in the data obtained by the two methods.

In the final evaluation of the reverberation time in the 50 Hz frequency band, the wide band random response from a noise generator was radiated into the room from the loudspeakers. The noise level distribution in the room was detected by the microphone placed at various positions in the room. When the noise level had reached a steady condition, the input to the loudspeakers was cut off and the decaying response picked up by a microphone placed in the centre of the room was recorded on the magnetic tape recorder. The tape was then slowed down and the response filtered in the 50 Hz band filter and recorded on the x-y chart recorder. The time to decay over 10 db from the initial portion of the decaying response curve was measured and then a decay time over 60 dB was computed. The reason for slowing down the tape was so that the chart recorder would respond to the actual decay response signal to be measured and not the x-y chart recorder decay time. This was repeated for various filter band centre frequencies and the result is given in fig. 5.3E. The experimental flow diagram is as shown in fig. 5.3D.

The damping of the room was then computed from the reverberation time and the equation:

$$10 \log_{10} \left(\frac{13.8}{T_{60}} \right) \text{dB}$$

and the result is given in fig. 5.3F.

The reverberation contributes to the total amount of noise existing in a room over a period of time, since it produces audible prolongation of noise during these intervals in which no noise is actually being emitted by the source. The reverberation time, t_{60}, depends only on the volume of the room and the total room absorption, according to the formula:

$$t_{60} = 0.161 \frac{V}{a'} \quad \text{sec} \qquad 1$$

$$a' = \frac{0.161 \ V}{t_{60}} \qquad 2$$

where V = Volume of enclosure in cubic meters

a' = Absorption in square meters (Sabine units)

The room absorption is computed from the decay time measurement and the result is given in fig. 5.3G.

5.4. Determination of diffusibility of the reverberant sound field.

5.41. Basic consideration.

Reverberation chambers used for acoustical measurements should have completely random sound fields. In an ordinary room a great deal of sound is reflected from the walls. Thus, the sound at a given position in the room is made up of that which travels directly from the source plus the sound that comes from other directions as a result of reflection. Under such circumstances the sound pressure does not decrease so rapidly. Non uniformity of absorption and of shape of the room surfaces tend to increase the scattering of sound within the room. When the conditions are such that the sound waves are travelling equally in all directions and the sound pressure is everywhere the same within the room then the sound field is perfectly diffuse. As a consequence of reflection from the boundaries of a room the sound persists for some time after the source has stopped.

Two outstanding problems in applied acoustics are the production of random sound fields in reverberant rooms and the determination of whether or not a given sound field once established, is random. A completely random sound field is defined such that at every point within the enclosure, plane waves near a particular frequency, having the same average intensity for all directions and phases, will have passed by after a sufficiently long time.

5.42. Technique Used in the Determination of Diffusibility of the Reverberant Room.

A reference microphone was placed in the centre of the room. Wide band random noise then radiated into the enclosure from the loudspeakers placed randomly near the walls. Another microphone having the same sensitivity as the reference microphone was rotated round while point measurements were taken and compared with the outputs from the reference microphone. This experiment was repeated with the narrow band noise radiated into the enclosure at different filter centre frequencies. Where the variations in the noise level was too large, the reflector and the loudspeaker positions were altered to improve the distribution.

It was found that when the enclosure was excited with the wideband random noise the variation in the noise level was $\pm$ 1.5 dB. With the room excited in the narrow band, the fluctuation in the noise level depended very much on the frequency bandwidth and its centre frequency. The narrower the bandwidth of excitation, the greater were the fluctuations that were observed. On an average the variation in the narrow band was $\pm$ 4 dB.

The diffusibility of reverberant sound field can also be determined from consideration of a cross-correlation coefficient, R, as discussed in the paper (43) by Cook and associates, for the sound pressure at two different points in a sound field and a theoretical demonstration of how R varies with wave numbers, k. ($k = 2\pi/$the wavelength (λ)) and the distance r between the points in a random sound field is given. The measured variation of R as a function of k, and r in a reverberant room is a useful criterion for helping to determine whether or not a random sound field is present. It is claimed that the cross-correlation coefficient defines the acoustic quality of a closed room more completely than the reverberation time does.

Some preliminary investigation has been made, to date, using this technique and work is in progress to further refine experimental methods so that the data can be resolved more accurately.

5.5. Modal Density of the Room.

An attempt was made to determine the modal density of the room experimentally, but because of very high concentration of resonances it was almost impossible to count the peaks. Therefore the approximate theoretical equation given in reference (1) was used. The modal density of the room is given by:

$$\frac{dn}{df} = \left[\left(\frac{4\pi^2 f^2 V}{C_a^3}\right) + \frac{\pi f A}{2 C_a^2} + \frac{L}{8 C_a}\right]$$

where $V = l_x \times l_y \times l_z$.

$$L = 4(l_x + l_y + l_z)$$

$$A = 2(l_x l_y + l_x l_z + l_y l_z)$$

C_a = Ambient speed of sound

The equation was solved on a ICL 1905 computer. The results are shown in fig. 5.6A.

5.6. Discussion of the Results and Conclusions.

The traces displayed in fig. 5.3C clearly show a multiple rate of decay and the best reverberation time shown in fig. 5.3E reduced for the reverberant room from the initial portion of the traces sampled at different centre frequencies of a 50 Hz filter band indicate that above 7k Hz much of the acoustic energy is either absorbed by the walls or transmitted through. A confirmation of this observation is given in fig. 5.3G. The experimental results in fig. 5.3E also show that the reverberation time is dependent upon the frequency hence the diffusibility of the room is affected by this condition. Point by point measurement in the room showed this characteristic when the room was subjected to a narrow band excitation. This condition was very much improved when the room was excited with wide band random source.

For this particular size of the reverberant room and the wall conditions, which were not specislly prepared, it seems that a reasonable reverberant condition can only be created in the frequencies quoted above. This situation could be improved if the walls are prepared so that much of the energy is not absorbed.

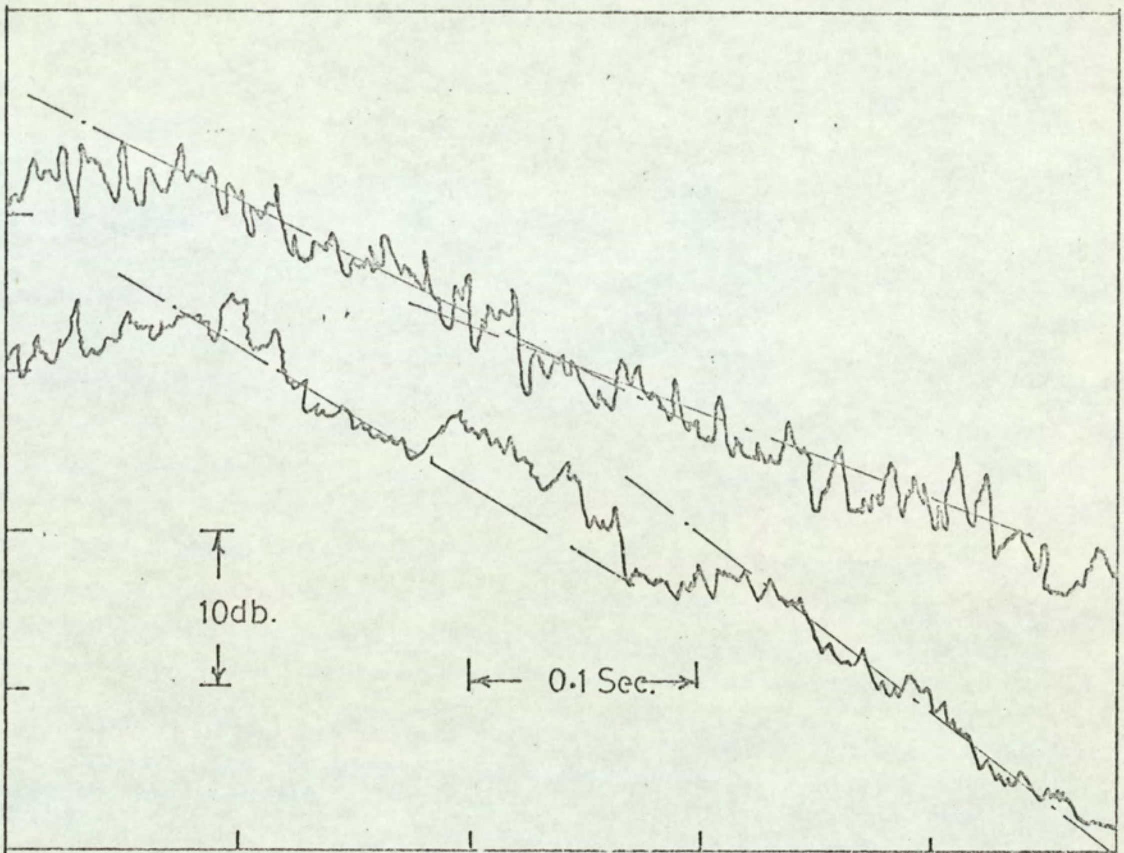

NOISE DECAY CURVES OBTAINED UNDER IDENTICAL TEST CONDITION.

FIG 5.21A

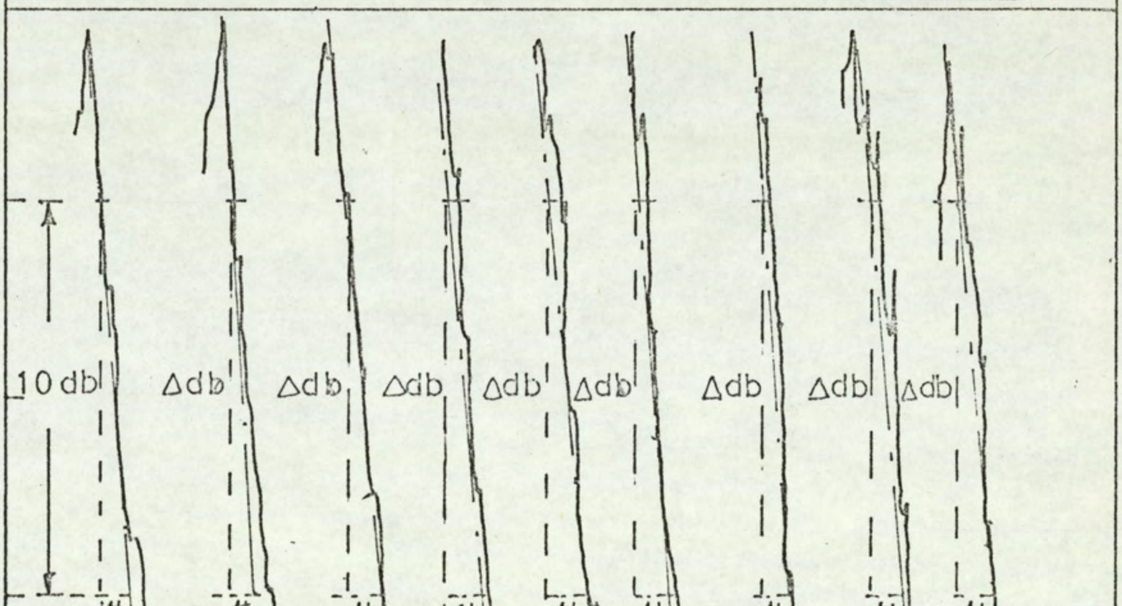

FILTERED RESPONSE OF NOISE DECAY CURVES AT DIFFERENT FILTER BAND CENTRE FREQUENCIES.

FIG 5.3C

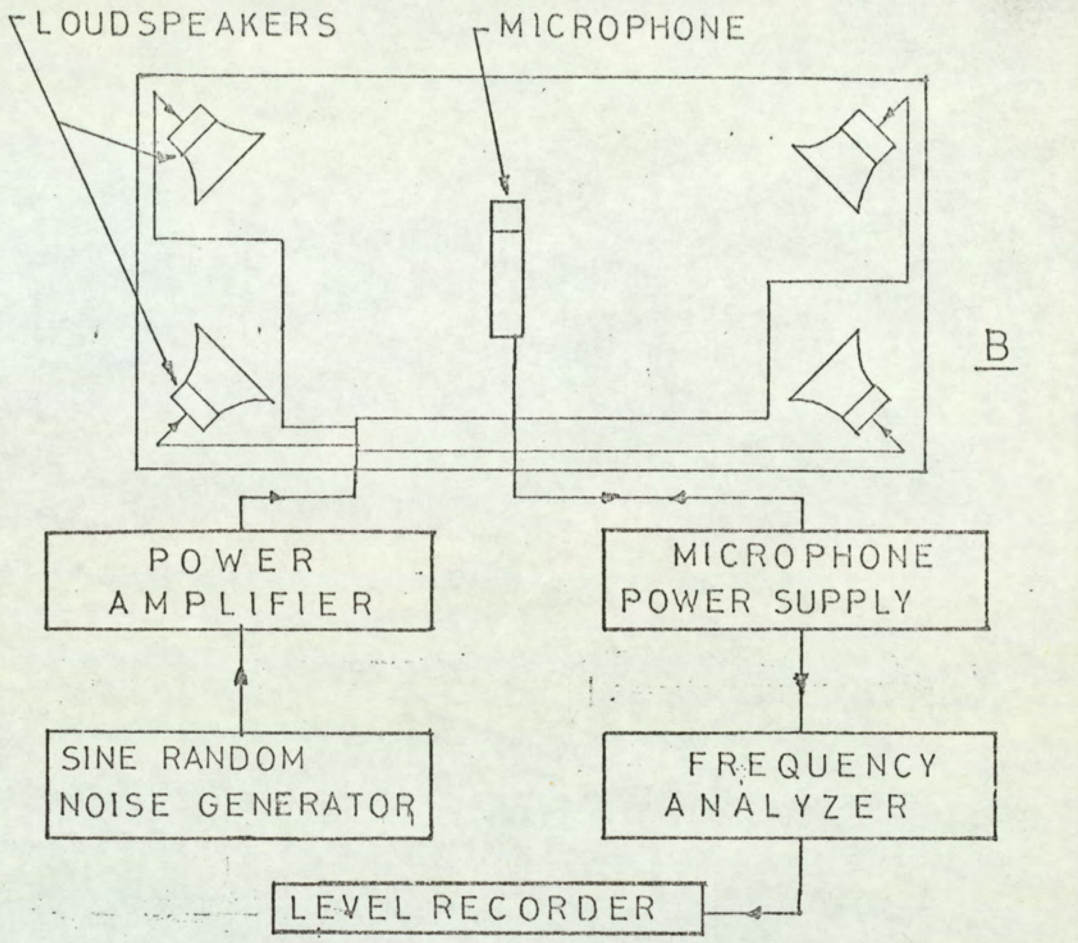

MEASUREMENT OF REVERBERATION TIME USING LOUDSPEAKERS AND SINE RANDOM NOISE GENERATOR.

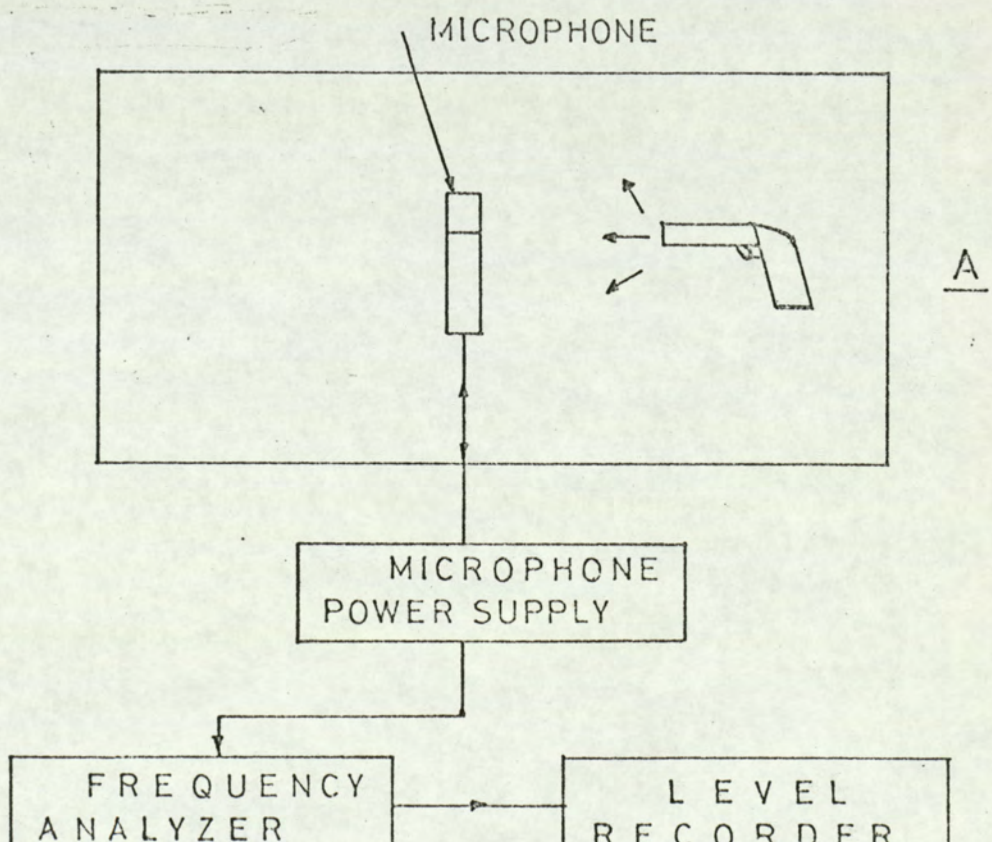

MEASUREMENT OF REVERBERATION TIME USING A GUN AS SOUND SOURCE.

FIG 5·22

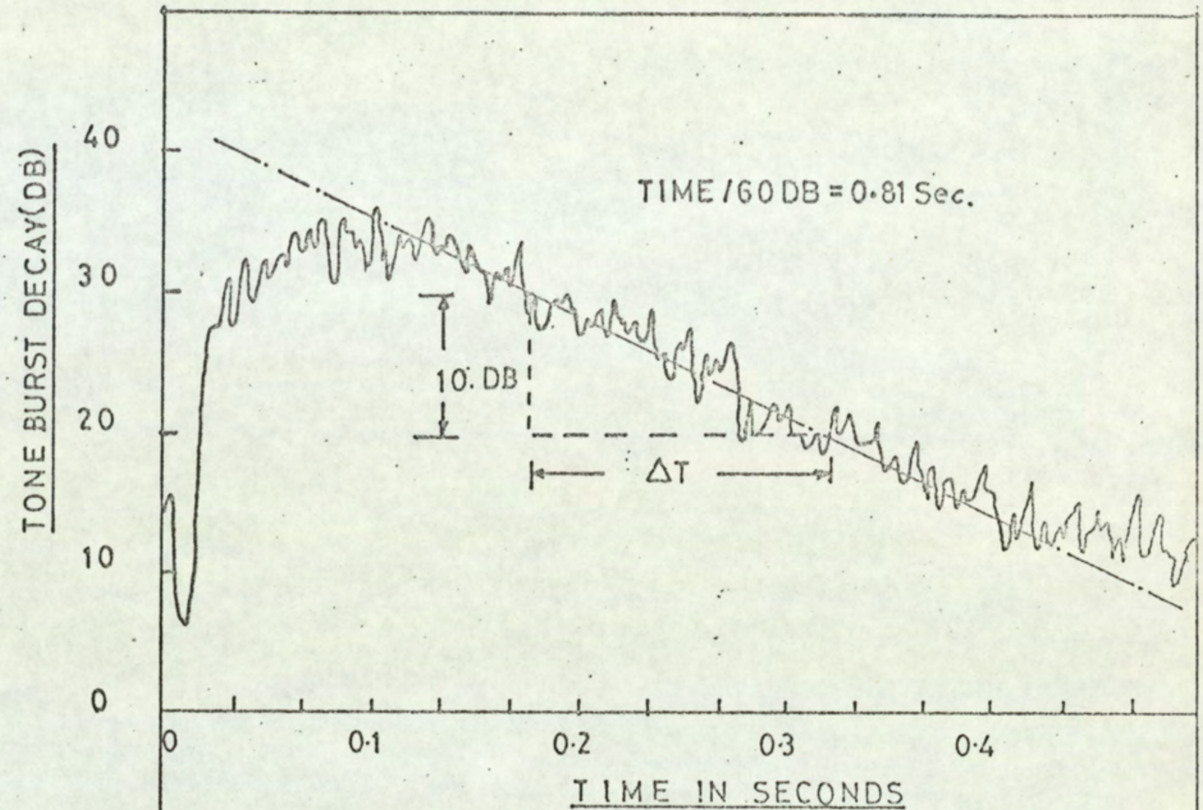

TONE BURST RESPONSE OF THE DECAY TIME.

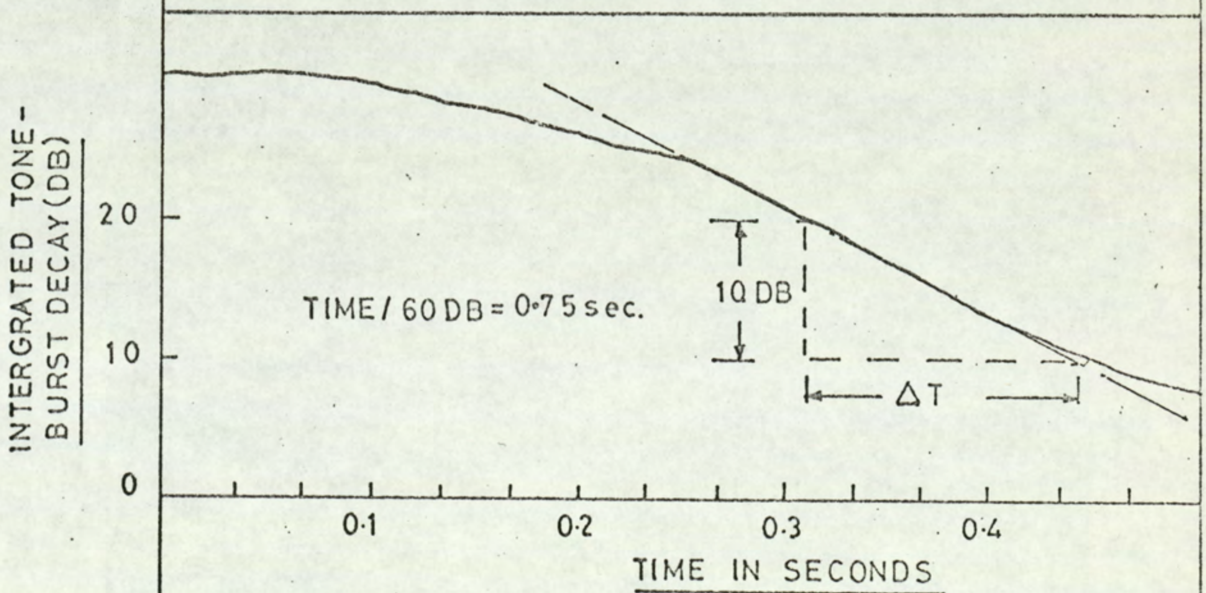

EXAMPLES OF TONE BURST DECAYS. REVERBERATION TIME IS OBTAINED BY FITTING THE BEST STRAIGHT LINE TO 1st. 10 DB AND THE REMAINDER OF DECAY CURVE, RESPECTIVELY.

FIG 5·3A

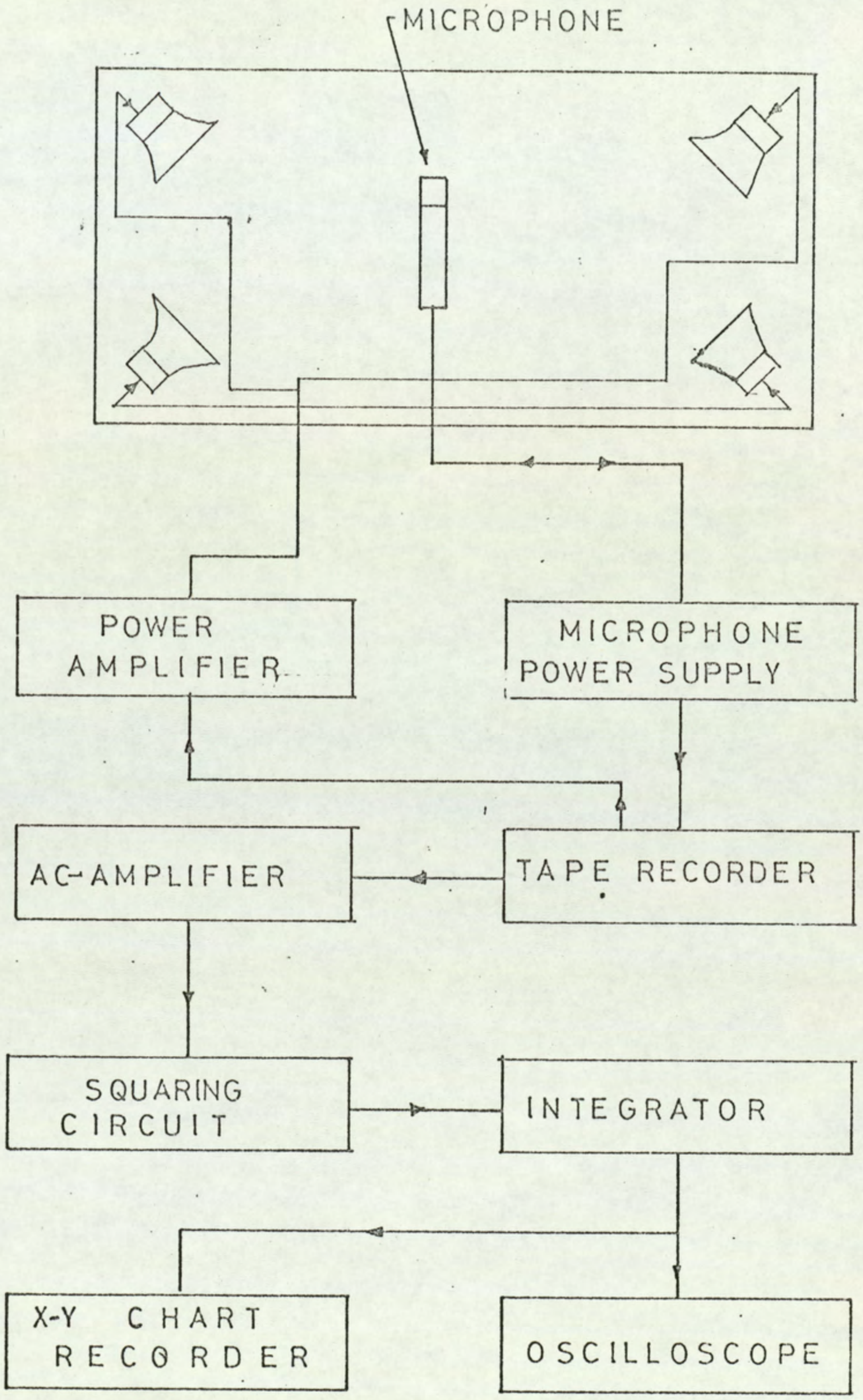

BLOCK DIAGRAM OF THE INSTRUMENTATION FOR THE MEASUREMENT OF REVERBERATION TIME ACCORDING TO THE "INTEGRATED IMPULSE METHOD"

FIG 5.3B

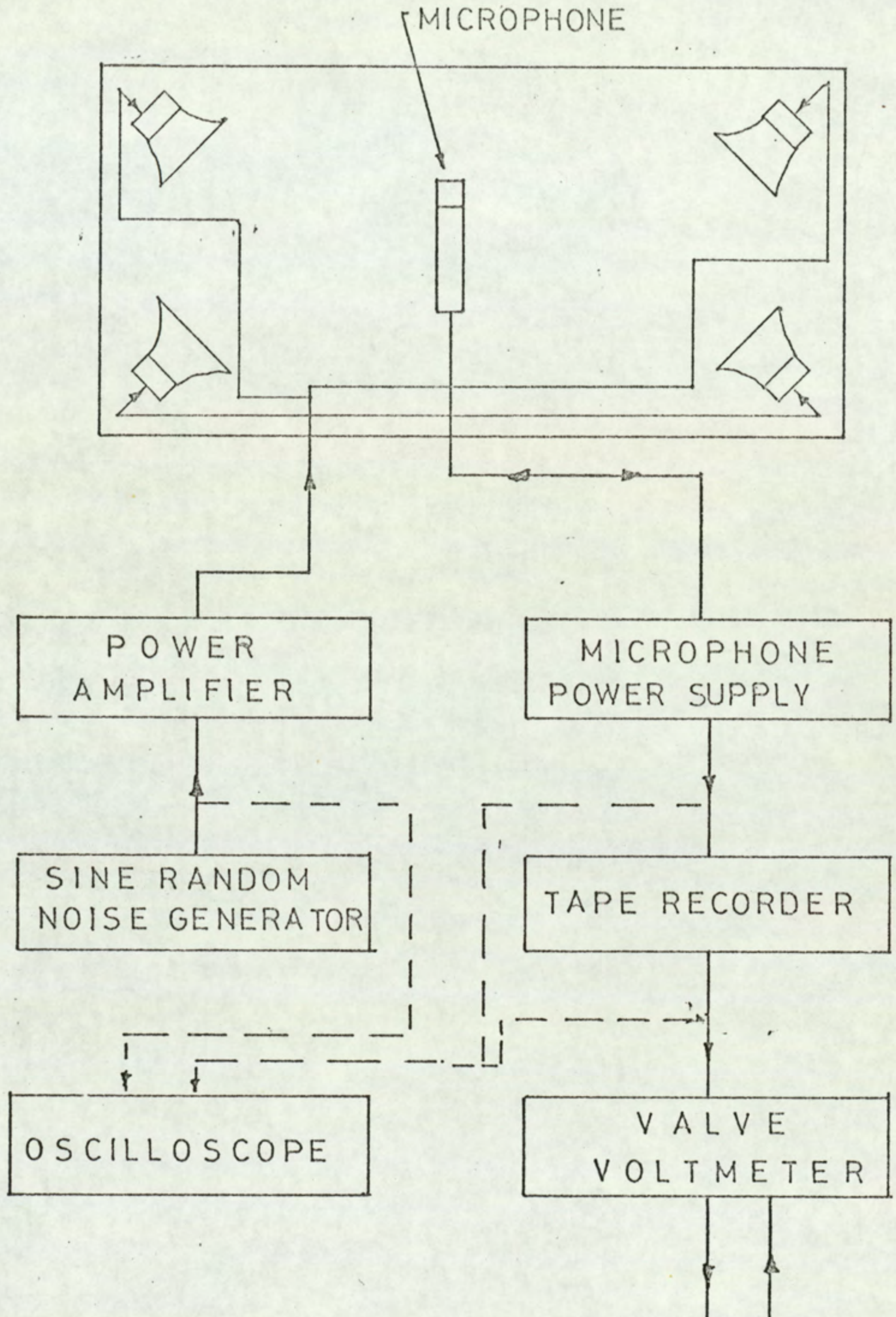

BLOCK DIAGRAM OF THE INSTRUMENTATION USED FOR THE MEASUREMENT OF THE REVERBERATION TIME.

FIG 5.3D

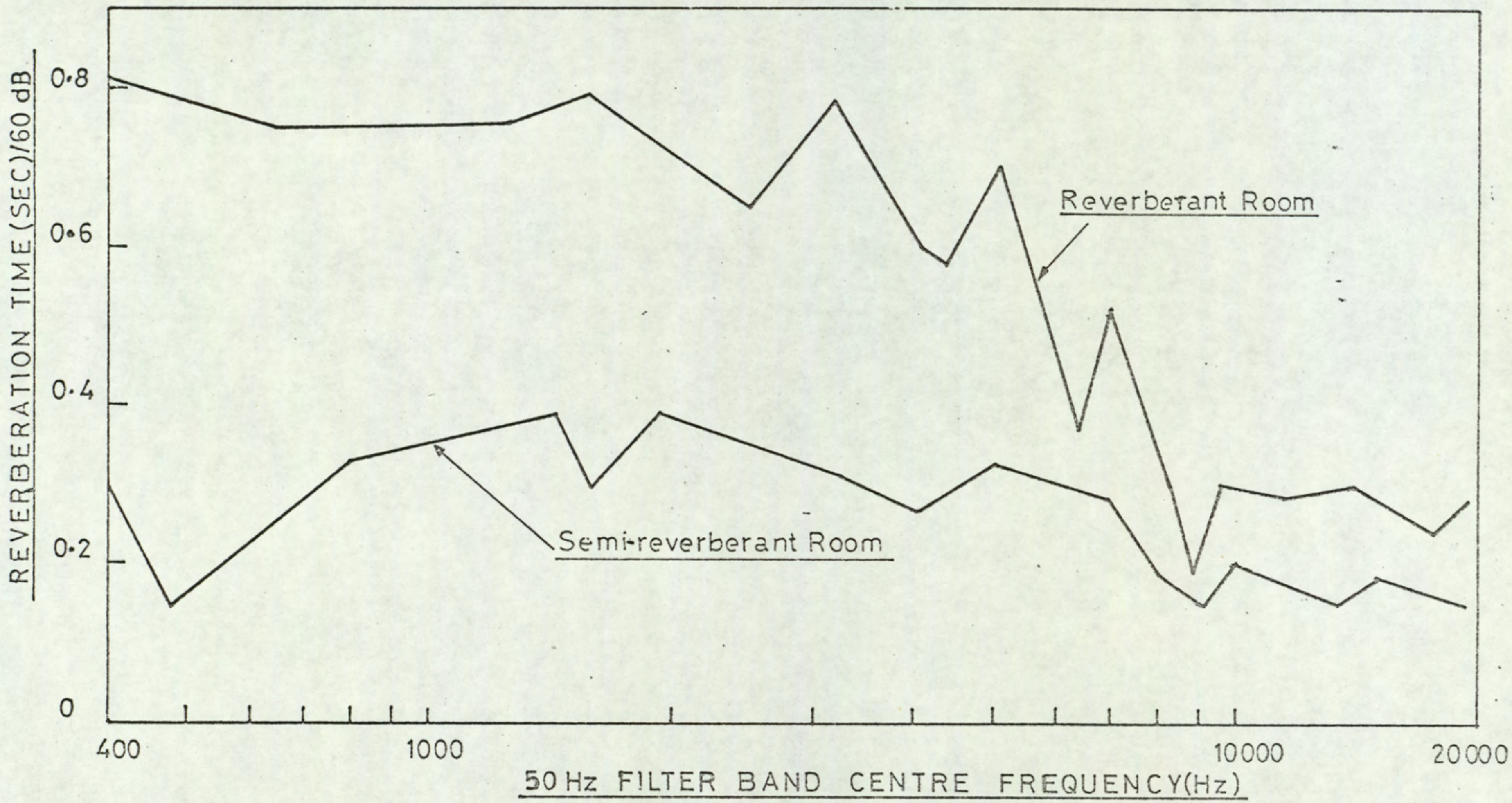

REVERBERATION CHARACTERISTC OF THE ACOUSTIC LABOROTORIES

FIG 5.3E

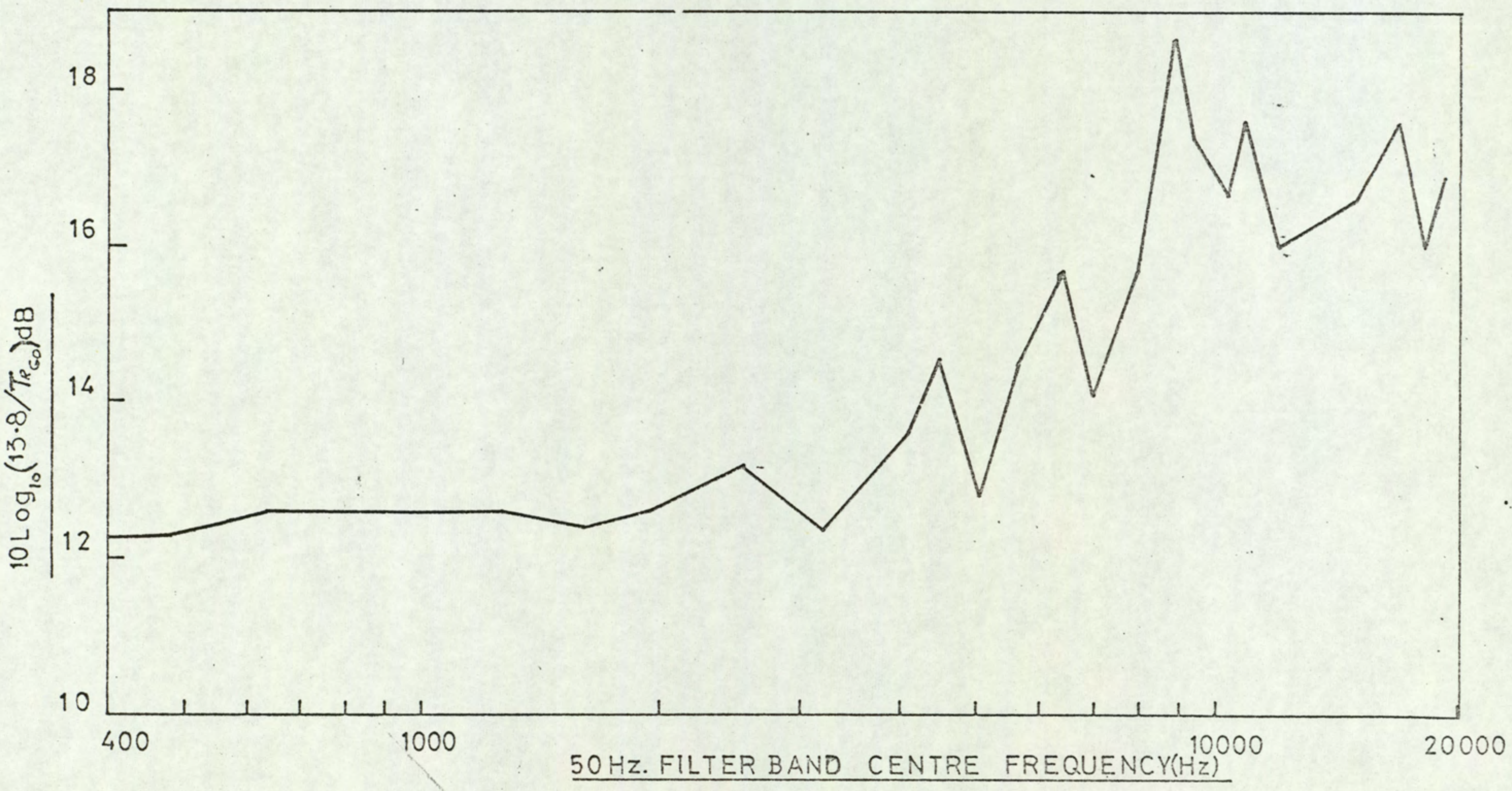

DAMPING OF THE REVERBERANT ROOM MODES FIG 5·3F

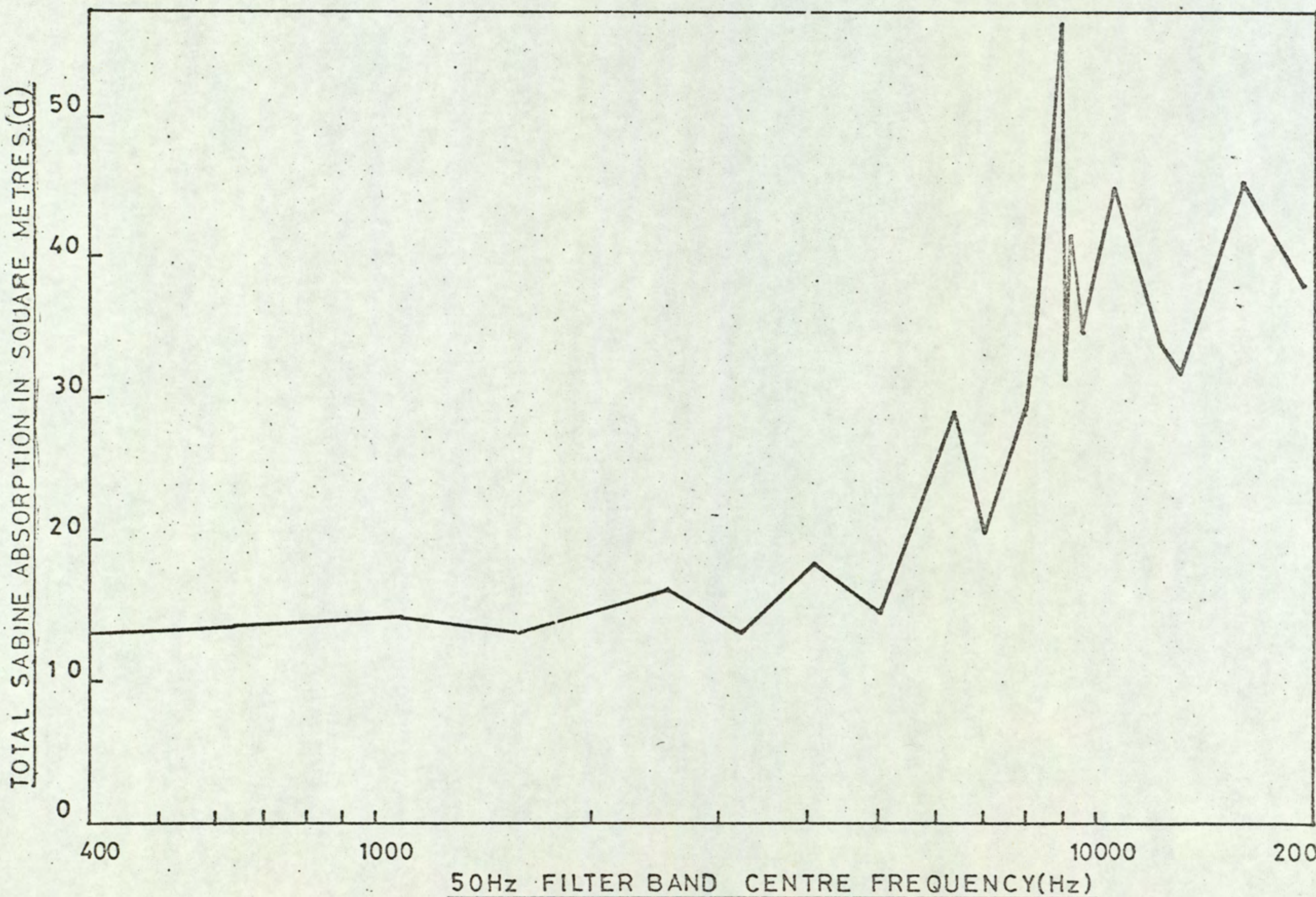

ABSORPTION CHARACTERISTIC OF THE REVEBERANT ROOM FIG 5·3G

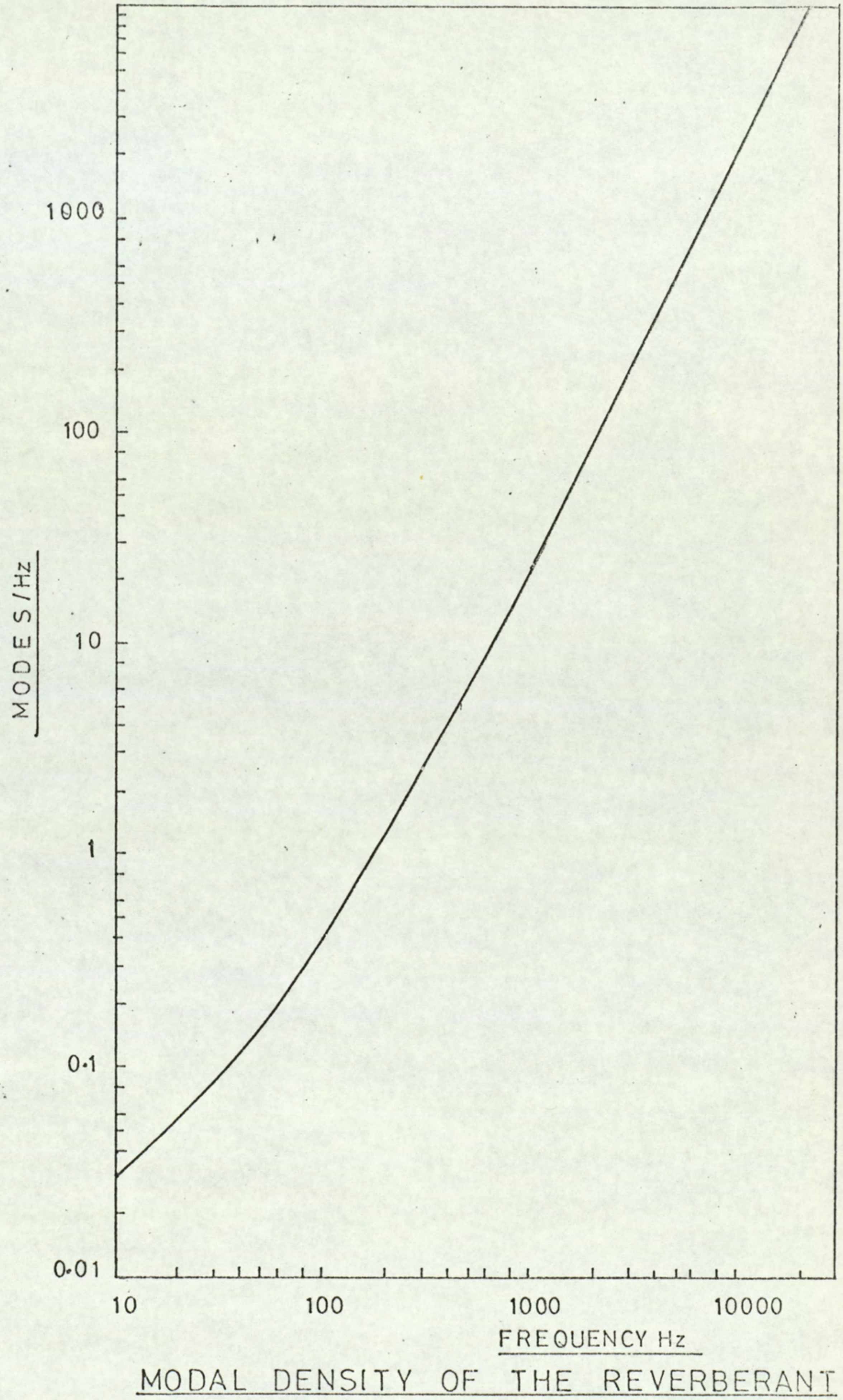

MODAL DENSITY OF THE REVERBERANT ROOM

FIG 5.6A

CHAPTER 6.

Modal density of flanged cylindrical shell

6.1 Introduction

Structures having cylindrical shapes have wide industrial application, but the variety of ways in which they can vibrate presents a complex problem. In view of the possibility of resonance, a knowledge of the natural frequencies of such structures is of immense value in design procedure. It has been noted that certain types of vibration are more easily stimulated than others and the response is a strong function of frequency and damping.

The main actions involved during vibration are distortion of the whole cross-section and the length of the structure. The distortion is periodic around the circumference and along the length, as shown in fig. 6.1A and denoted by N and M. The intersection of a constant N line with its vertical M line gave the corresponding natural frequency. In fig. 6.32A is shown some of the frequencies at which they occur for the flanged cylindrical shell, 72 ins long, 18 ins in diameter and 0.048 ins thick when the effect of acoustic media were neglected.

For the response to forced vibration, an investigation by Warburton (40) of an infinitely long thin cylindrical shell showed that when the fluid is air, there were resonant frequencies very close to the shell in a vacuum and to the natural frequencies of the internal column of fluid. In order to simplify the present analysis considerably, it was assumed that the effect of fluid on the structure is negligible.

The experiments conducted on the cylindrical shell were intended to determine the number of modes in a frequency band when excited mechanically and acoustically. Where these modes were found close together, two different methods were used to separate them.

6.2 Theoretical Considerations

6.21 Frequency Equations for Cylindrical shell with freely supported ends without the effect of acoustic medium.

Mathematical expressions for the flexural vibrations of freely supported cylinders having a wall thickness of the shell much smaller than the shortest wavelength are derived by Arnold and Warburton (14). The expressions are first derived for the component strains of an element of the cylinder situated at the middle surface, (an imaginary surface situated at mid-thickness) in terms of its rectangular displacements u, v and w in directions X, Y and Z as shown in fig. 6.21A. These relations define the possible ways in which an element may deform elastically. Thereafter an attempt is made to find expressions for u, v and w which are not only compatible with elastic strain but also satisfy the specific end conditions.

After the desired wave-forms have been obtained, the strain energy and kinetic energy of the cylinder are derived respectively in terms of displacement and rate of change of displacement, the latter involving the unknown frequency. Lagrange's equations are then written for the three independent displacements u, v and w, and after elimination of the arbitrary amplitude constants, a cubic equation is eventually obtained. The roots of this equation define the frequencies associated with a given nodal arrangement.

For freely supported cylinders, neglecting the effect of acoustic media the expressions for the displacement were assumed for the component directions, X, Y and Z as shown in fig. 6.21A and given by the following equations:

$$
\begin{aligned}
u &= A \operatorname{Cos} \frac{m\pi x}{\ell} \cos n\phi \cos\omega t \\
v &= B \operatorname{Sin} \frac{m\pi x}{\ell} \sin n\phi \cos\omega t \\
w &= C \operatorname{Sin} \frac{m\pi x}{\ell} \cos n\phi \cos\omega t
\end{aligned}
\qquad 6.1
$$

Here A, B and C are amplitude constants, M and N define the nodal arrangement in directions X and ϕ, and $\frac{\omega}{2\pi}$ is the frequency of vibration. As an example, if N = 2 and M = 1, the form of the radial displacement, ω, is represented in the diagram of fig. 6.21B and 6.21C.

The above expressions satisfy the end conditions and are compatible with the strain relations. By application of the Lagrange equations to the derived expressions for strain energy and kinetic energy, constants A, B and C may be eliminated to form the cubic equation:

$$\Delta^3 - k_2\Delta^2 + k_1\Delta - k_o = 0 \qquad 6.2$$

where the coefficients k_o, k_1 and k_2 are constants for a given cylinder under a given nodal configuration and the vibration frequency is given by

$$f = \frac{1}{2\pi a}\left[\frac{E\, g\, \Delta}{\rho_s\,(1-\mu^2)}\right]^{1/2} \qquad 6.3$$

Expressions for the coefficients k in terms of the cylinder dimensions, elastic constants and mode of vibration are as follows:

$$
\left.
\begin{aligned}
k_o &= \tfrac{1}{2}(1-\mu)^2(1+\mu)\lambda^4 + \tfrac{1}{2}(1-\mu)\beta\Big[(\lambda^2+n^2)^4 - 2(4-\mu^2)\lambda^4 n^2 - 8\lambda^2 n^4 - 2n^6 \\
&\quad + 4(1-\mu^2)\lambda^4 + 4\lambda^2 n^2 + n^4\Big] \\
k_1 &= \tfrac{1}{2}(1-\mu)(\lambda^2+n^2)^2 + \tfrac{1}{2}(3-\mu-2\mu^2)\lambda^2 + \tfrac{1}{2}(1-\mu)n^2 + \beta\Big[\tfrac{1}{2}(3-\mu)(\lambda^2+n^2)^3 \\
&\quad + 2(1-\mu)\lambda^4 - (2-\mu^2)\lambda^2 n^2 - \tfrac{1}{2}(3+\mu)n^4 + 2(1-\mu)\lambda^2 + n^2\Big]
\end{aligned}
\right] \; 6.4
$$

$$\left.\begin{aligned} k_2 &= 1+\tfrac{1}{2}(3-\mu)(\lambda^2+n^2)+\beta\left[(\lambda^2+n^2)^2+2(1-\mu)\lambda^2+n^2\right] \\ \text{where}\quad \beta &= \frac{h}{12a^2}\ , \qquad \Delta = \frac{\rho_o\, a^2(1-\mu^2)\, 4\pi^2 f^2}{E g} \end{aligned}\right] \qquad 6.4$$

Equation 6.2 gives three real positive roots for, Δ, and thus three frequencies for any specific nodal pattern. In practice, only the lowest of these frequencies need be considered since the others are well above the aural range.

As some terms in the above expressions are small compared with others and, moreover, Δ^3 and $k_2\Delta^2$ are small compared with the other terms of the cubic equation, the following linear equations may give good approximations:

$$\Delta = \frac{k_o}{k_1} + \frac{k_2}{k_1}\left(\frac{k_o}{k_1}\right)^2$$

where

$$k_o = \tfrac{1}{2}(1-\mu)^2(1+\mu)\lambda^4 + \tfrac{1}{2}(1-\mu)\,\beta\left[(\lambda^2+n^2)^4 - 8\lambda^2 n^4 - 2n^6 + n^4\right]$$

$$\begin{aligned} k_1 &= \tfrac{1}{2}(1-\mu)(\lambda^2-n^2)^2 + \tfrac{1}{2}(3-\mu-2\mu^2)\lambda^2 + \tfrac{1}{2}(1-\mu)n^2 \\ &\quad + \tfrac{1}{2}(3-\mu)\,\beta(\lambda^2+n^2)^3 \end{aligned}$$

$$k_2 = 1+\tfrac{1}{2}(3-\mu)(\lambda^2+n^2)$$

6.211 Effect of Flanged Ends on Frequency.

The relation between the fixing influence of the flanges of fig. 6.21D and the solid of fig. 6.21E is required so that the wave length factor of the latter may be used for frequency calculations. The assumption is made that equivalence will exist when an equal bending moment per unit slope is produced by each at the external radius a_1.

For a thin circular plate of radius a_1 and thickness H, the slope at the edges, owing to a moment M per unit length of the periphery is, (39):

$$\psi = \frac{Ma_1}{D(1 + \mu)} \qquad 6.6$$

where $D = \dfrac{EH^3}{12(1 - \mu^2)}$

When a circular plate of radius a_2 with a central hole of radius a_1 and a thickness H_1 is considered, the slope, ψ, at the inner boundary owing to an applied moment M per unit length is given by (39):

$$\psi = \frac{Ma_1\left[a_1^{\,2}(1 - \mu) + a_2^{\,2}(1 - \mu)\right]}{D_1\,(1 - \mu^2)(a_2^{\,2} - a_1^{\,2})} \qquad 6.7$$

where $D_1 = \dfrac{E\,H_1^{\,3}}{12(1 - \mu^2)}$

Equating equations 6.6 and 6.7 leads to

$$H = H_1\left[\frac{\eta^2 - 1}{\left(\frac{1 + \mu}{1 - \mu}\right)\eta^2 + 1}\right]^{\frac{1}{3}} \qquad 6.8$$

where $\eta = \left(\dfrac{a_2}{a_1}\right)$

6.12 Equivalent wavelength factor.

A knowledge of the way in which the equivalent wavelength for a cylinder with fixed ends varies with the wavelength of a freely supported cylinder of similar simensions, when each vibrates with the same number of nodes. Level variation of equivalent wavelength, λe, with wavelength, λ, is required. For a given cylinder of length, ℓ, under a particular mode of vibrations, there can exist a freely supported cylinder of similar cross-section having an identical frequency. If the length of the latter be $\ell - \ell'$, then $\lambda_e = \frac{m\pi a}{\ell - \ell'}$ and $\lambda = \frac{m\pi a}{\ell}$. This leads to the relation,

$$\lambda_e = \left(\frac{m + c}{m}\right)\lambda = (m + c)\frac{\pi a}{\ell}. \qquad 6.9$$

where $c = m\left(\frac{\ell'}{\ell - \ell'}\right)$, c is a function of m, n and cylinder dimensions.

For a cylinder with solid ends, if the factor, c, is expressed as a function of thickness ratio, $\frac{h}{H}$, it should be zero when H is small and 0.3 when H is large. An empirical expression to satisfy this condition derived by Arnold and Warburton is:

$$\lambda_e = \left[m + 0.3e^{-q\,(h/H)}\right]\frac{\pi a}{l} \qquad 6.10$$

where a suitable value for, q, is determined from experiment.

6.22 Frequency equation for cylindrical shell in an acoustic medium.

For the vibration of a cylindrical shell without the effect of the acoustic medium, three equations of motion were obtained in terms of the axial tangential and radial components of displacement. When the effects of the acoustic media are included in the response to vibration of an infinitely long thin cylindrical shell, Warburton (40) has shown that the equation is obtained by considering the components of force in the radial direction acting on an element of the shell will have additional terms due to the pressure acting on it. The other two equations, corresponding to components of force in the axial and tangential directions, are unchanged by the pressure of fluid media.

The resonant frequencies of a cylindrical shell in acoustic media are given by:

$$\Delta^3 - k_2\Delta^2 + k_1\Delta - k_o + \Delta(\Delta^2 - C_1\Delta + C_o)\mathrm{Re}\left(f(x)\right) = 0 \qquad 6.11$$

The expressions for the coefficients in terms of the cylinder dimensions, elastic constants and mode of vibration are as follows:

$$\left.\begin{aligned}
k_o &= \tfrac{1}{2}(1-\mu)^2(1+\mu)\lambda^4 + \tfrac{1}{2}(1-\mu)\beta\Big[(\lambda^2+n^2)^4 - 2(4-\mu^2)\lambda^4 n^2 - 8\lambda^2 n^4 - 2n^6 \\
&\quad + 4(1-\mu^2)\lambda^4 + 4\lambda^2 n^2 + n^4\Big] \\
k_1 &= \tfrac{1}{2}(1-\mu)(\lambda^2+n^2)^2 + \tfrac{1}{2}(3-\mu-2\mu^2)\lambda^2 + \tfrac{1}{2}(1-\mu)n^2 + \beta\Big[\tfrac{1}{2}(3-\mu)(\lambda^2+n^2)^3 + 2(1-\mu)\lambda^4 \\
&\quad - (2-\mu^2)\lambda^2 n^2 - \tfrac{1}{2}(3+\mu)n^4 + 2(1-\mu)\lambda^2 + n^2\Big] \\
k_2 &= \tfrac{1}{2}(3-\mu)(\lambda^2+n^2) + 1 + \beta\Big[(\lambda^2+n^2) + 2(1-\mu)\lambda^2 + n^2\Big] \\
C_o &= \tfrac{1}{2}(1-\mu)(\lambda^2+n^2)^2 + \beta\Big[2(1-\mu)\lambda^4 + \tfrac{1}{2}(1-\mu)n^4 + (2-2\mu+\mu^4)\lambda^4 n^2\Big] \\
C_1 &= \tfrac{1}{2}(3-\mu)(\lambda^2+n^2) + \beta\Big[2(1-\mu)\lambda^2 + n^2\Big]
\end{aligned}\right\} \quad 6.12$$

and

$$\text{Re } f(x) = \frac{\rho_o}{\rho_s}\frac{a}{h}\frac{2}{\pi}\frac{1}{x^2}\frac{Y_n'(x)}{J_n'(x)}\frac{1}{\left[J_n'(x)\right]^2+\left[Y_n'(x)\right]^2} \qquad 6.13$$

$$\text{Im } f(x) = \frac{\rho_o}{\rho_s}\frac{a}{h}\frac{2}{\pi}\frac{1}{x^2}\frac{1}{\left[Y_n'(x)\right]^2+\left[J_n'(x)\right]^2} \qquad 6.14$$

where $Jn(X)$, $Yn(X)$ = Bessel functions of first and second kinds

$$x \equiv k\,a \equiv \left[\left(\frac{\Omega a}{c}\right)^2 - \lambda^2\right]^{1/2}, \qquad \Omega\frac{a}{c} > \lambda$$

$$\beta = \frac{h^2}{12\,a^2}$$

6.23 The effects of surrounding medium on the modes of vibration.

The displacement patterns of the natural modes are generally assumed unaffacted by the surrounding and enclosed media. It has been shown by Richard and Mead (31) that the mechanical impedances of the modes can be drastically changed. If the enclosed region contains a great deal of sound absorbing material, then the effect of the enclosed medium will be primarily resistive and as a result damping of the modes is increased. If there is no sound absorption, however, the medium will add to the stiffness or mass of the modes.

It is possible that the additional stiffness will be infinite at frequencies where certain standing waves occur in the enclosure. These standing wave patterns have modes at the structural surface. If they are excited acoustically from the outside under harmonic conditions, the acoustic pressure on the inside surface of the structure is the same as on the outside surface, but, acting in the opposite direction, effectively cancels the effect of the external pressure and no structural motion results. The additional stiffness may also be zero. Under these conditionsthe standing wave excited within the enclosure has velocity anti-modes and pressure modes at the structural internal surface. The acoustic pressure at some other points inside the enclosures will certainly be very high. Such cavity resonances can occur within cylinders. There exist standing waves within the structure which will cause high internal noise levels at certain frequencies. There are also other standing waves with modes at the surfaces which will inhibit the skin motion at other frequencies, yet still cause large sound pressure to exist within the structure. Under some conditions the cavity resonance effect can cause the modal frequency to be considerably different from that of the structural mode in vacuo as described by Warburton (40).

Outside the structure, the vibrating motion causes sound waves to be radiated away from the surface. Since, in general, these waves are not plane waves, the pressure at the skin surface due to this radiation has components in phase with the velocity, and also in quadrature with the velocity. The former components constitute the acoustic damping pressure.

The latter components are in anti-phase with the structural acceleration, and constitute the 'virtual inertia' of the medium in conjunction with the structure.

6.24 <u>Effect of structure on the sound field</u>.

When sound waves impinge on the surface of cylindrical shell, the effective exciting pressure on the surface is twice that of the incident field due to the effect of total reflection of the wave. The pressure components having wavelengths less than the characteristic dimensions of the body are effectively doubled by the reflection effects. If the wavelength is much greater than these dimensions, "scattering" of the incident wave occurs due to non-uniform reflections. The effective pressure is still increased, but not by as much as a factor of two. The wavelength of the frequency components of greatest interest are usually much shorter than the structural dimensions. The noise pressures used for response calculations should therefore be twice those measured free field conditions.

6.3 Numerical Computation for resonant frequencies.

6.31 Comparison of natural frequencies derived for the two conditions.

The resonant frequencies for a cylindrical shell in a fluid medium determined by Warburton (40) were found to be very close to the natural frequencies of the shell without the effect of fluid medium derived by Arnold and Warburton (14). These frequencies were also very close to the natural frequencies of the internal column of fluid. With water as the fluid, the resonant frequencies showed a considerable divergence from the natural frequencies of the shell in a vacuum.

For the purpose and accuracy required in the present work, it was assumed that the resonant frequencies are unaffected by the presence of the fluid media and solution for the frequency equation developed by Arnold and Warburton (14) is used.

6.32 Solution of Frequency Equation for freely Vibrating cylindrical shell.

The numerical computations were done on an ICL 1905 computer for the following standard parameters:

(i) Cylinder diameter = 18 ins. (0.4572M)

(ii) Cylinder Length = 72 ins. (1.8288M)

(iii) Material thickness = 0.048 ins. (1.2192×10^{-3}M)

(iv) Poisson's Ratio = 0.29

(v) Young's Modulus = $30 \times 10^6 \frac{lb}{in^2}$ ($2.092 \times 10^6 \frac{kg}{M^2}$)

(vi) Density of material = $0.284 \frac{lb}{in^3}$ ($7861 \times \frac{kg}{M^3}$)

(vii) Acceleration due to gravity = $386.088 \frac{in}{sec^2}$ ($9.80665 \frac{M}{sec^2}$)

(viii) Number of axial half waves = 1-160.

(ix) Number of circumferential waves = 2-59.

The roots of the cubic equation 6.3, were computed from the above values. The frequency equation 6.4, was then calculated from the result of the lowest positive real root of the cubic equation. The results are shown in fig. 6.32A.

Further computation was carried out to search for all N and M crossings and to identify the frequency at which they occured. These crossings of N and M lines gave the resonant frequencies of the cylindrical shell. The computer program and the table of resonant frequencies are given in Appendix 3.

From the table of resonant frequencies, the modal density in the 50 Hz band was computed and the results are shown in fig. 6.32B.

6.4 Techniques used in the measurement of modal density of flanged cylindrical shell.

6.41 Amplitude response measurement.

The enclosed cylinder was placed freely on point contacts approximately in the centre of the reververant room. The pure tone excitation to the mechanical vibrator attached to the centre of the cylinder was from a Quantech Analyser. The test was carried out within the flat frequency response range of the vibrator. The output to pure tone excitation from an accelerometer placed on the skin of the cylinder was filtered in narrow band and recorded on the x-y chart recorder by sweeping the frequency through a frequency range of 100 Hz at a time. The test was then repeated for the other accelerometer positions randomly placed on the skin of the cylinder. The test was also carried out on open cylindrical shell freely supported on point contacts.

During the course of the preliminary investigation it was felt that perhaps all the structural modes were not being excited by the vibrator and therefore the above experiment was repeated with the structure being excited by sweeping a pure tone sound through the same frequency whilst the same accelerometer outputs were recorded. The results are shown in figs. 6.41A, 6.41B and 6.41C. The experimental flow diagram is shown in fig. 6.41D.

The modal density was obtained by counting the number of peaks from the recordings and dividing by the frequency bandwidth. This test procedure was continued for frequencies up to 1500 Hz and above, in which there were signs of overlapping modes and the mode counting became difficult.

6.42 Vector analysis method for the determination of closely spaced modes of vibrations.

The methods of analysis and mode determination discussed in Section 6.41 are valid in cases where at any one frequency only one mode contributes to the predominant part of theresponse. Where modes having significant response are close together in frequency the results of the mode determination can be misleading, as in the case of the flanged cylindrical shell as shown in fig. 6.42A. The response test on the cylinder shown in fig. 6.42B shows that in between predominant modes there are many intermediate modes all very close together in frequency. In such a situation, amplitude response measurements are not adequate to identify the intermediate modes because the responses in the modes overlap in frequency. This can be observed from the theoretical results in fig. 6.32A and from the tables of resonant frequencies. It is possible that one might excite one of the intermediate modes at resonance, but at this frequency other modes may have significant response.

To separate the components of individual modes, the vector analysis method suggested by Kennedy and Purcu (8) was used. The basis of the method is the polar plot of the response vector relative to the vector of the forcing pressure. For a lightly damped single mode this polar plot is a complete circle whose diameter is inversely proportional to the damping of the mode. In the case of the cylindrical shell being considered, the damping is reasonably low and therefore the circumference is traversed in a relatively small frequency interval. As the frequency of the forcing pressure is increased through one resonance the tip of the response vector describes an arc approximating to part of the circle of the single mode response. Identification of the arcs gives the normal modes which might be hidden if the amplitude response only were measured.

An example of a polar diagram for one response vector is shown in fig. 6.42C, while the instrumentation flow diagram is shown in fig. 6.41D.

From fig. 6.42C it can be seen that further complication arises when modes are very close together in frequency such that their arcs join together giving the appearance of a single mode. In this case it is necessary to go one step further to isolate the two modes. In the simple single degree of freedom case, the tip of the response vector travels the greatest distance per cycle per second at resonance. Therefore, the rate of change of arc length with frequency, $\frac{ds}{df}$, was plotted against frequency and maximum occured at resonance. This experiment was carried out with the aid of an analogue computer and from the result of fig. 6.42E it was possible to identify two very closely spaced resonances even when the peak on the amplitude response diagram shows a continuous curve. The experimental flow diagram and instrumentation is shown in fig. 6.42F.

For the purpose of the two experiments in this section, the structure was mechanically excited from the sinusoidal input to the vibrator. The output from the Quantech Analyser was used for this purpose. The cylinder was placed approximately in the centre of the room, freely supported on point contacts. The response from an accelerometer placed on the skin of the structure was amplified, filtered in the narrow band and then recorded on an x-y chart recorder. The experiment was repeated with the structure being excited acoustically and for different accelerometer positioned on the skin of the cylinder.

6.5 Results and Discussions

The accuracy of the theoretical results computed depended upon the assumption made in the derivation of the equation for thin cylindrical shells with freely supported ends. Lagrange equations were used to set up the frequency equation. The strain expressions used were those of Timoshenko (42) and neglected the trapezoidal form of the forces perpendicular to the cylinder axis. The membrane and bending effects contained in the theory were quite adequate for thin cylinders. The coefficients of the cubic equation were functions of Poisson's ratio, diameter to length ratio and thickness to length ratio, and so the accuracy of the roots of the equation relied on these parameters. The frequency equation, on the other hand, has further parameters, namely Young's modulus, the material density and the acceleration due to gravity and the accuracy depended on the square root of these values. A change of Poisson's ratio by $\pm$ 0.01 gave a frequency variation of $\pm$ 23 Hz at 13 Hz and this variation diminished at the lower frequency end but increased at higher frequencies. This variation is quite small for the kind of accuracy that is expected, especially when the equation is based upon many approximations.

A comparison of this theory with many others was made by Greenspan (40), who found that it is adequate for a thickness ratio of 0.9 and for modes up to M = 38; above this the accuracy does not hold too well. This has put a limitation on the validity of the equation. For M equals 38 and N equals 46, the frequency computed for the cylindrical shell is 13.451 kHz and is shown by broken lines in fig. 6.32A.

The tables of resonant frequencies shown in Appendix 3 are for all the values up to 20 kHz and the accuracy above 13.4 kHz may not be all that good as indicated by Greenspan. From the computed resonant frequencies it can be seen that there are modes very close together in some frequency bands above 1.5 kHz which confirm the results found by experiments.

Since the derivation of the equation is based on many assumptions and approximations, it would be necessary to use as exact values as possible for the structure parameters then only reasonable accuracy can be placed on the computed results. The results given in this chapter are therefore valid only for the stated values. With the aid of the computer and the program given in Appendix 3 it would not be a difficult problem to compute resonant frequencies for the other paramater if required.

From the results shown in figs. 6.41 snd 6.41B of amplitude against frequency for the cases when the cylinder was mechanically and acoustically excited, it can be seen that the number of resonant peaks in each case were different , usually less when mechanically excited. When the same cylinder ends were opened and subjected to similar excitation, the level of the peaks were different as can be seen from fig. 6.41C.

It is very likely that all the modes were not excited well enough to be detected. This could have been due to the location of the vibrator at the point of excitation or perhaps the size of the model was too large. When the structure was acoustically excited, however, pressures of approximately equal intensity came from all the directions in the room, thereby exciting the whole range of modes high enough to be detected. The reason for the resonant peaks being higher in the case of the open cylinder is due to the fact that the structure was subjected to exciting pressure energy from both sides which acted in phase at some frequencies displaying higher level of peaks and in anti-phase when the modal energies were subtracted displaying peaks of low level. The room condition, the size of the model and the method of excitation are some of the most important factors governing the accuracy of the experimental results.

The closely spaced modes were separated successfully in the lower frequency ranges only ($\leq$ 1500 Hz) but further refinements to the instrumentation and experimental techniques were needed for better accuracy giving scope for further work in this region.

The Kennedy and Pancu method (8), as outlined in Section 6.42, relates to discrete frequency tests only. Similar information can be obtained to discrete frequency tests only. Similar information can be obtained in the case of random excitation from the cross power spectrum of the strain and the pressure excitation as measured by a microphone. The real part of cross spectral density gives the real component of the response vector and the imaginary part of the cross power spectrum gives the imaginary component of the response vector. This method is recommended for future work and is given in reference (42).

Different methods used for the measurement of modal density are given in fig. 6.5A.

6.6 Conclusions

From the theoretical and the experimental results the following conclusions are made:

(i) Above 1.5 kHz the modes lie very close together in some frequency bands, but below 1.5 kHz they are irregularly spaced.

(ii) The source and the point of excitation are some of the most important factors governing the accuracy of experimental results.

(iii) The theory used for the solution of frequency equation showed good comparison with the experimental results for the parameters tested.

(iv) The concentration of resonant frequencies are between 3.4 kHz and 3.8 kHz.

(v) Above the ring frequency (3778 Hz), the modal density as shown in fig. 6.32B is very nearly constant. This is in agreement with the theory that the cylinder vibrates as if it was a flat plate, the modal density of which is constant.

m = number of half-waves along the length
n = number of full waves around the circumference

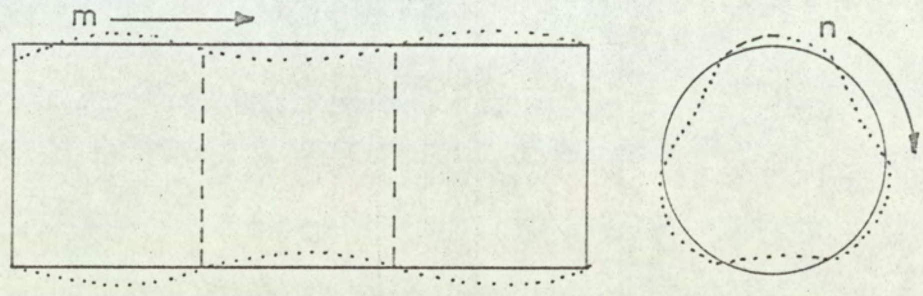

ILLUSTRATION OF AN 'OVERALL' MODE OF VIBRATION OF A CYLINDER

FIG 6.1A

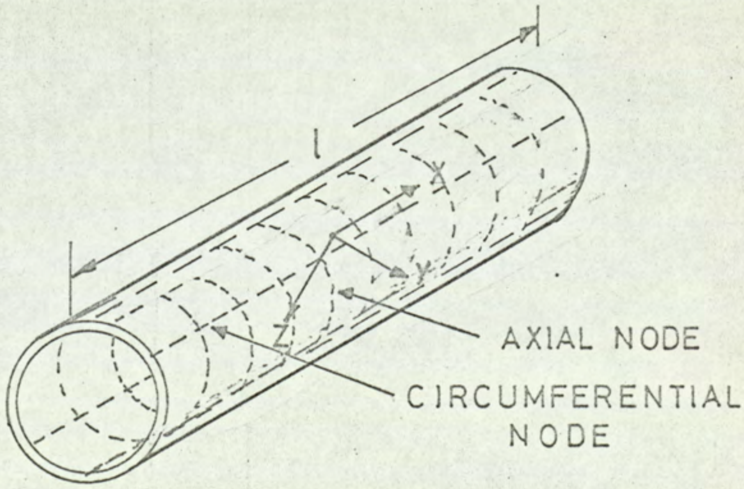

FORMS OF VIBRATION OF THIN CYLINDERS

FIG 6.21A

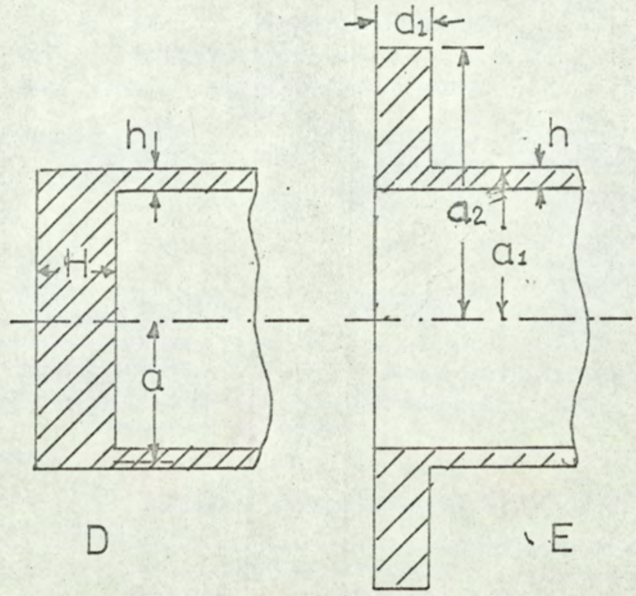

TYPES OF CYLINDER ENDS

FIG 6·21

CIRCUMFERENTIAL VIBRATION FORMS

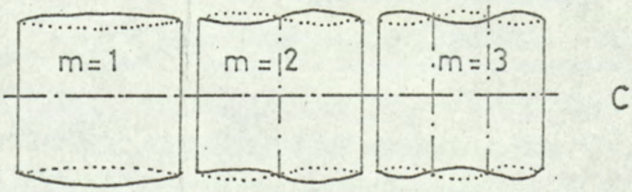

AXIAL VIBRATION FORMS

FIG 6·21

THEORETICAL FREQUENCY CURVES

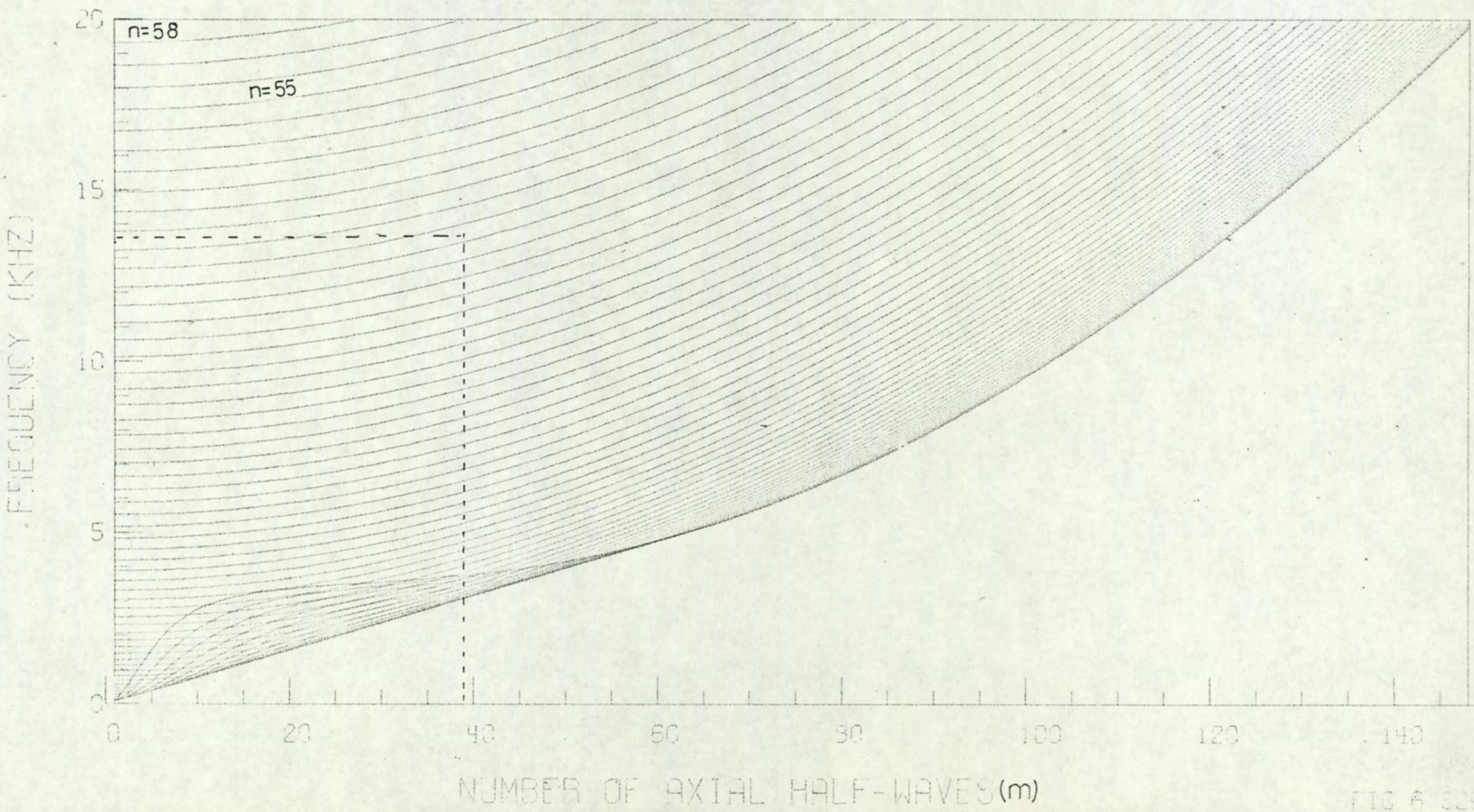

FIG 6.32A

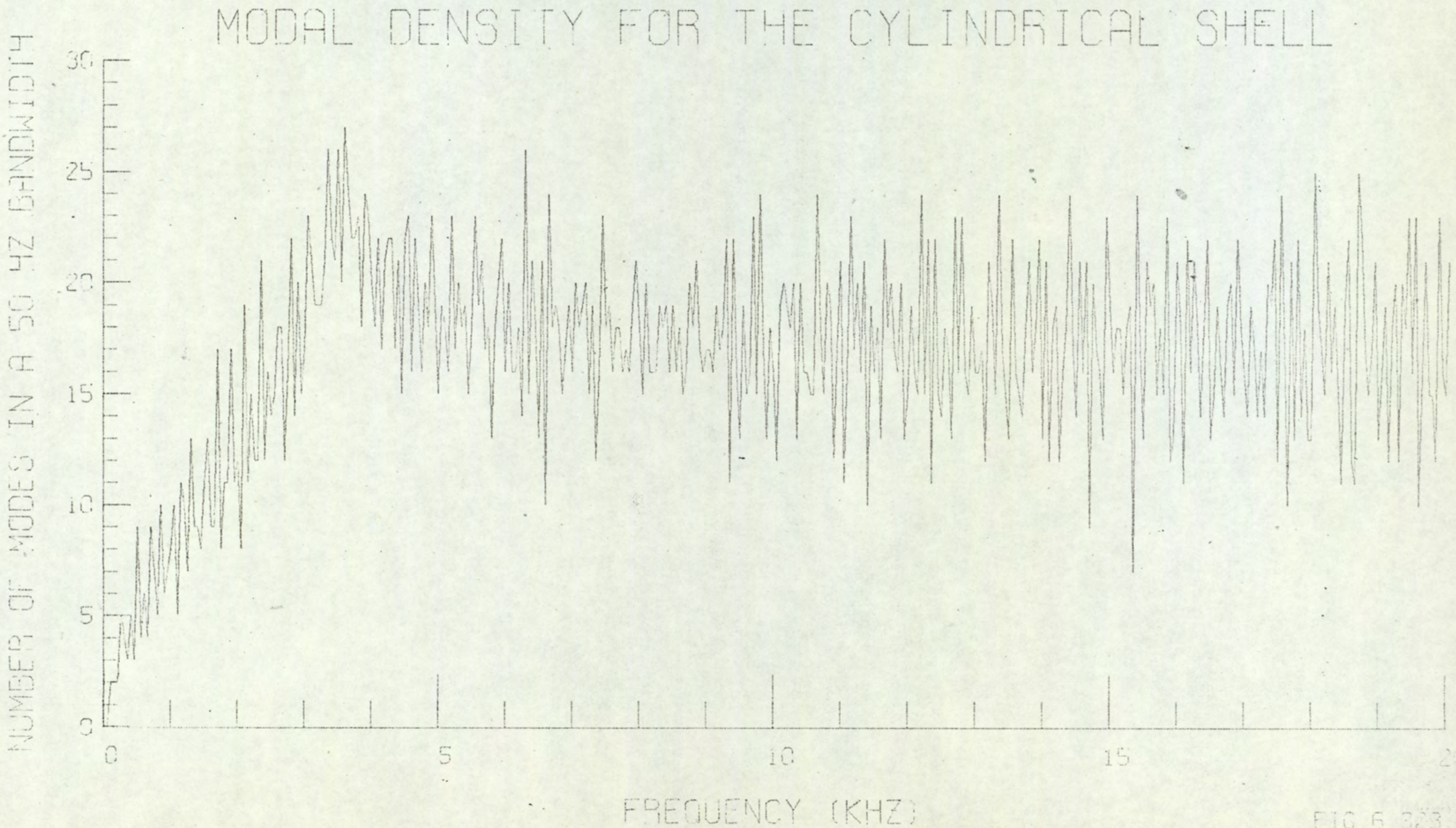
MODAL DENSITY FOR THE CYLINDRICAL SHELL
NUMBER OF MODES IN A 50 HZ BANDWIDTH
0
5
10
15
20
25
30
FREQUENCY (KHZ)

FIG 6 323

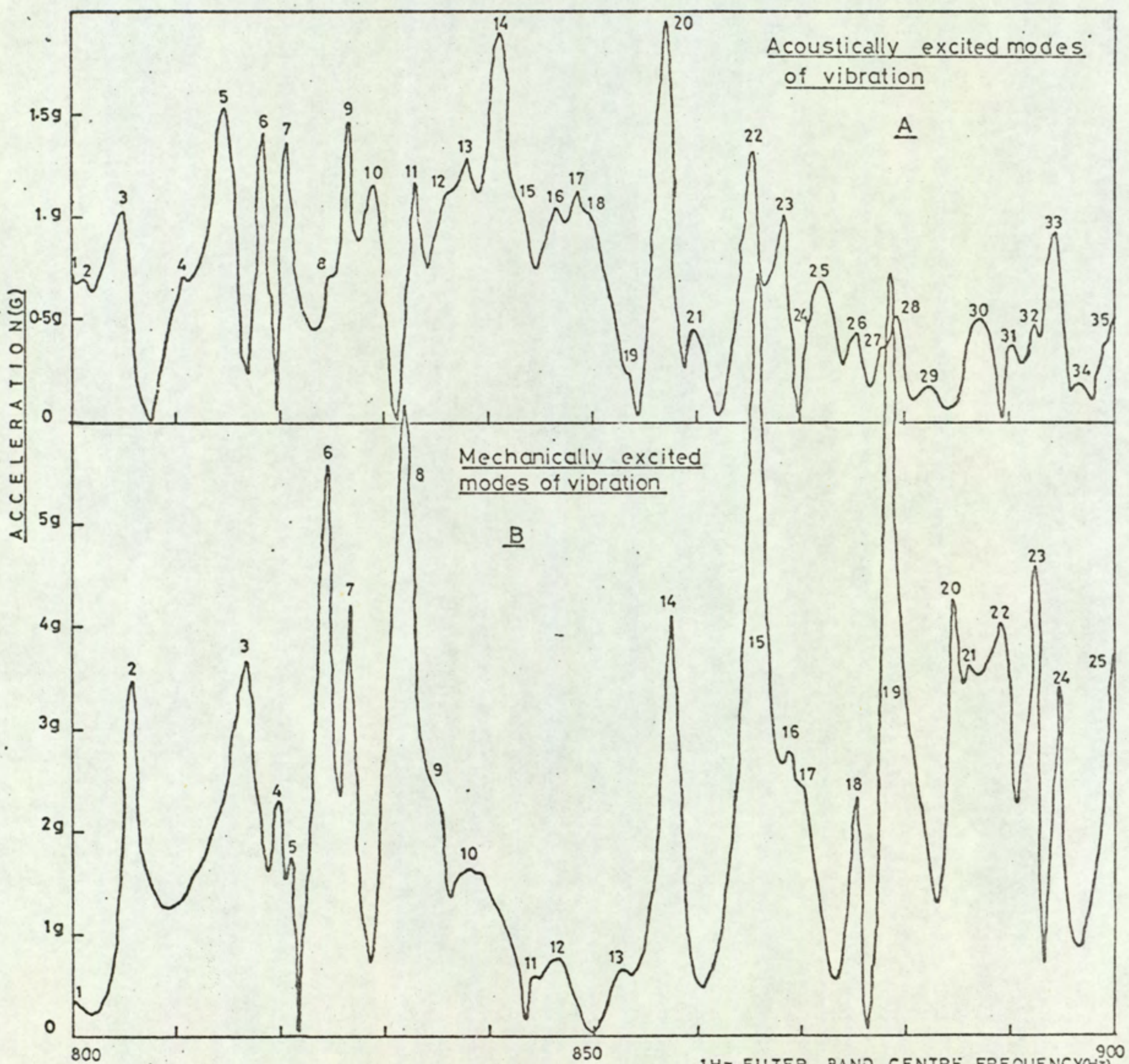

MODES OF VIBRATION OF FREELY SUPPORTED FLANGED CYLINDRICAL SHELL (enclosed)

FIG 6.41

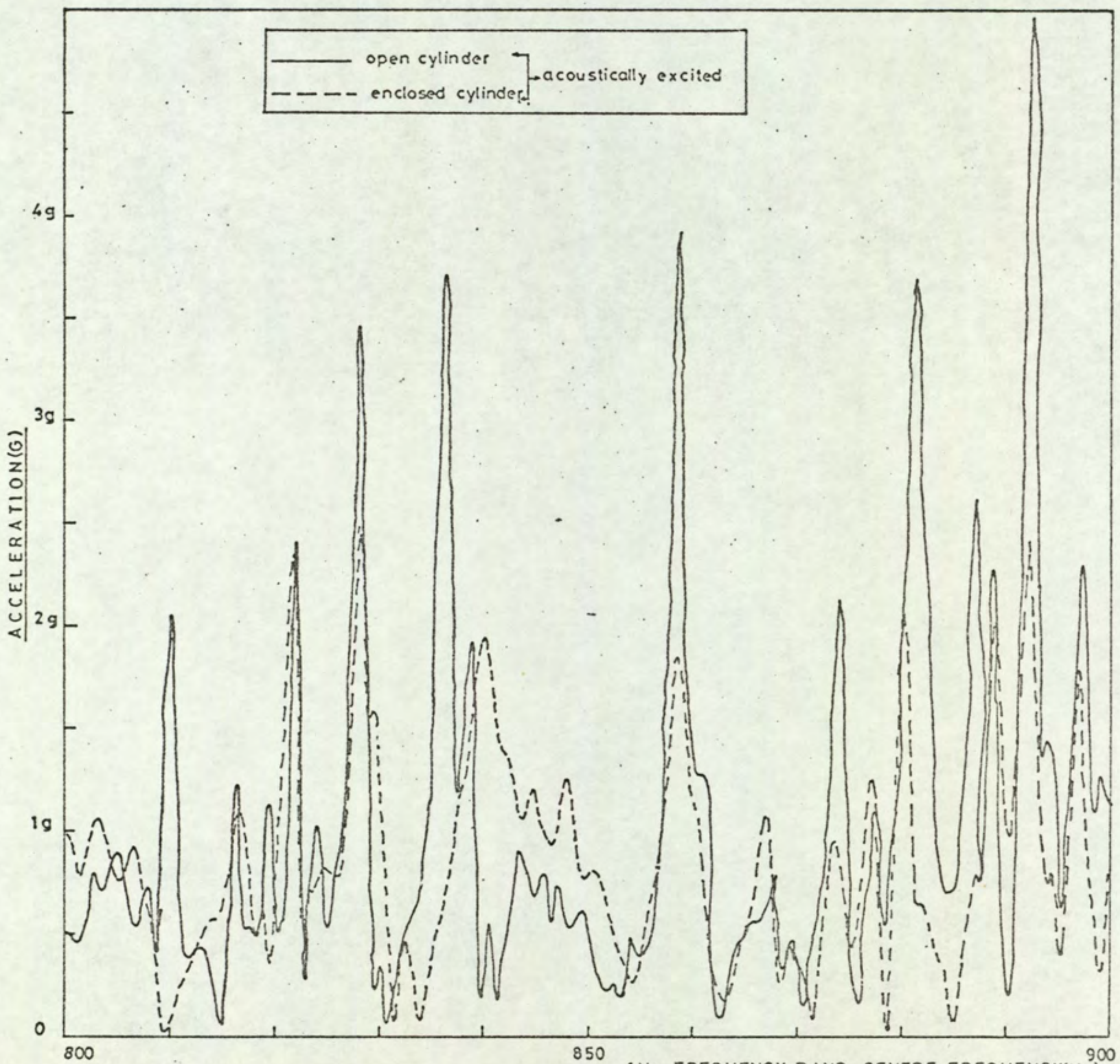

MODAL DENSITY OF FREELY SUPPORTED FLANGED CYLINDRICAL SHELL FIG 6·41C

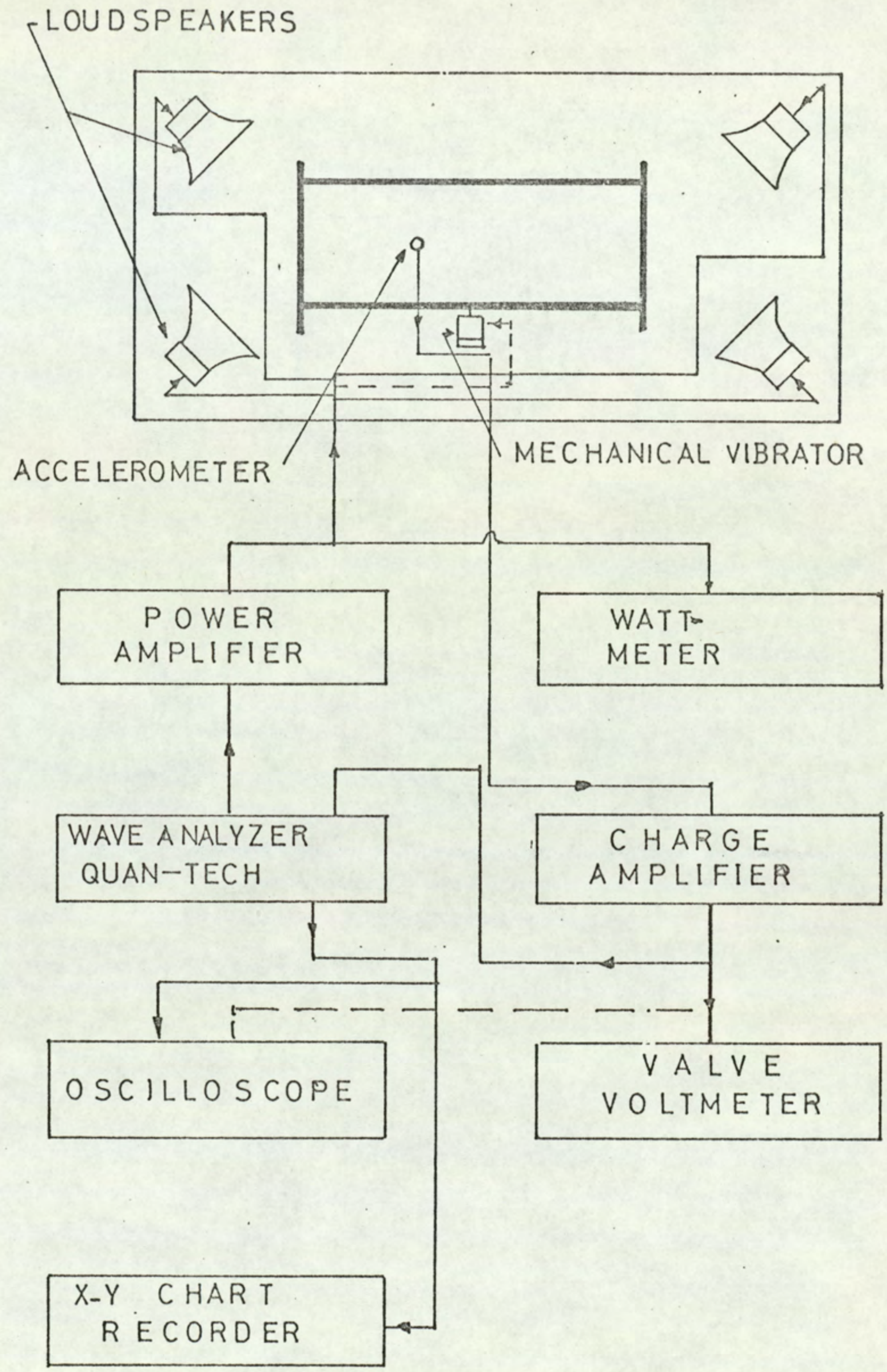

BLOCK DIAGRAM OF THE INSTRUMENTATION

FIG 6.41D

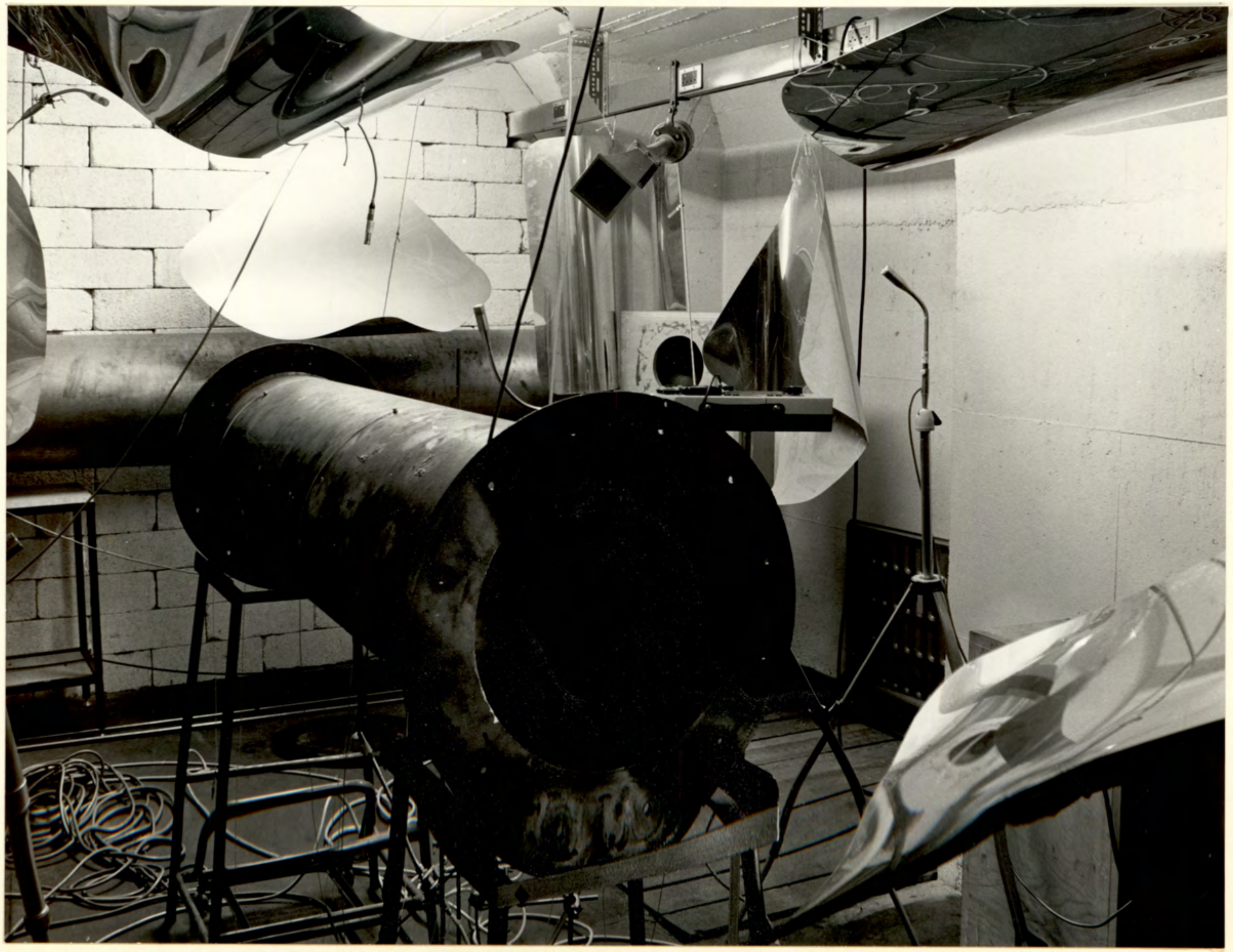

FIG 6·42A

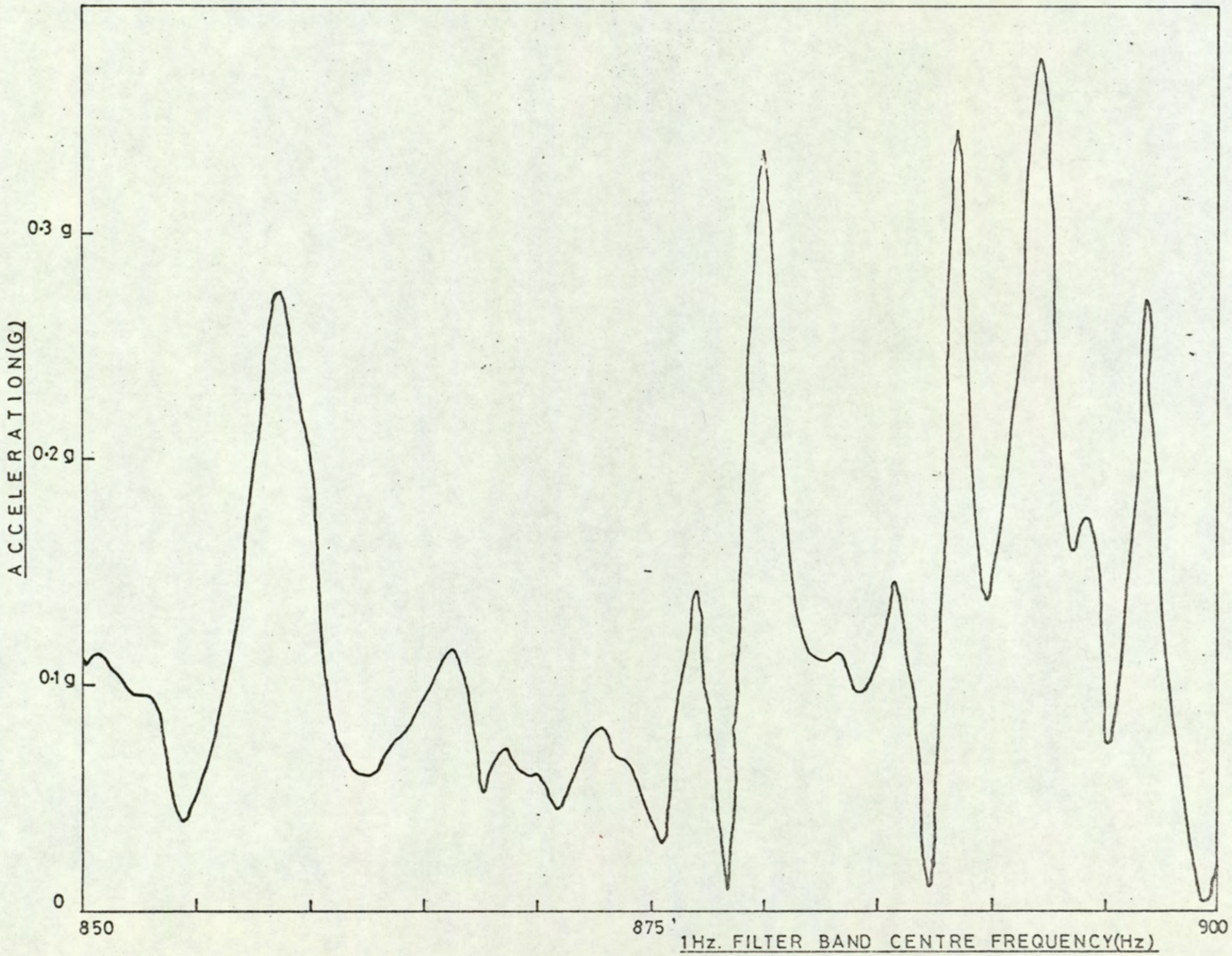

MODES OF VIBRATION OF FREELY SUPPORTED FLANGED ENCLOSED CYLINDRICAL SHELL

FIG 6·42B

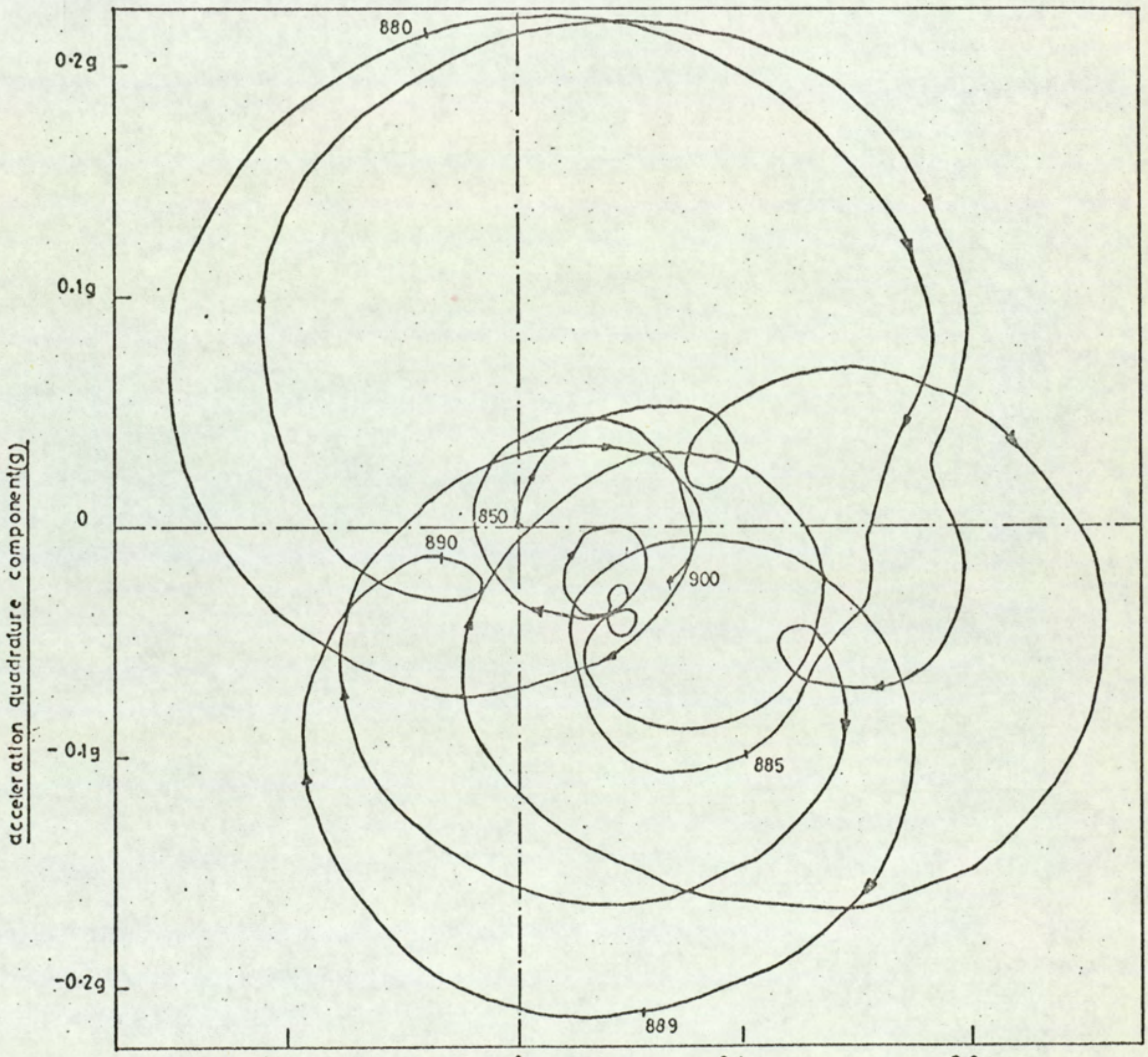

VECTOR RESPONSE DIAGRAM FROM ACCELEROMETER ON ENCLOSED CYLINDRICAL SHELL FIG 6·42C

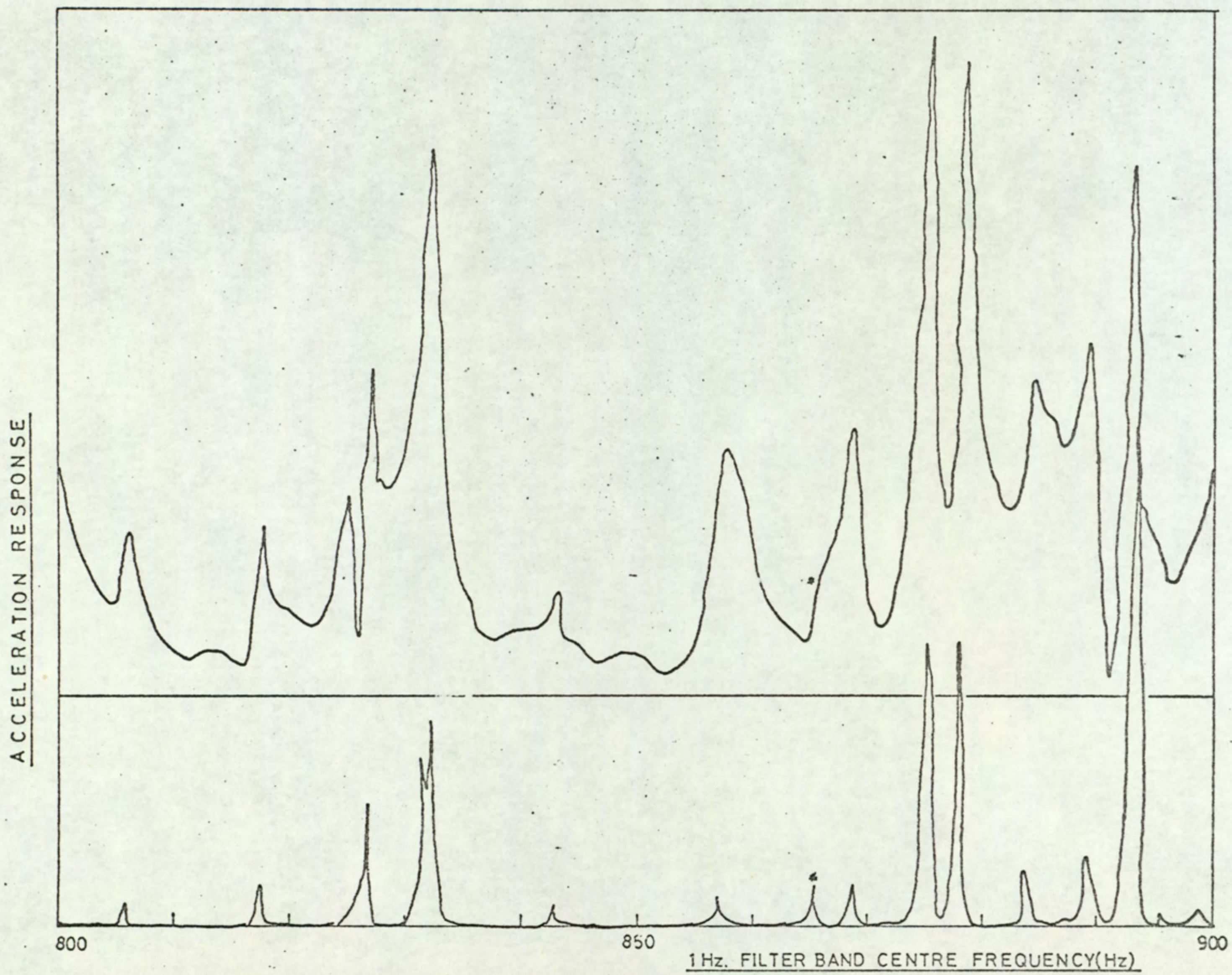

SEPARATION OF CLOSELY SPACED MODES IN FLANGED ENCLOSED CYLINDRICAL SHELL FIG 6.42E

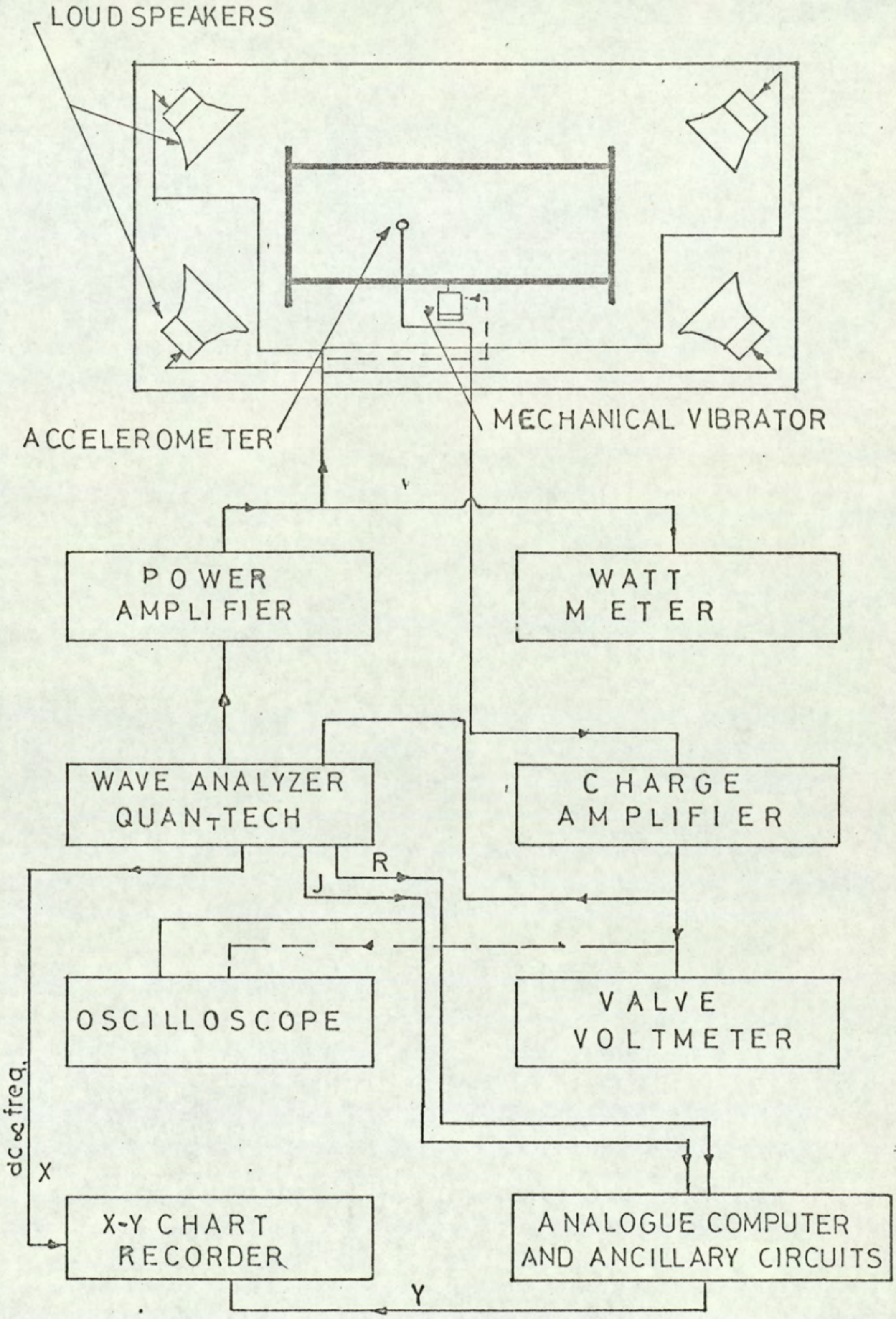

BLOCK DIAGRAM OF INSTRUMENTATION

FIG 6.42F

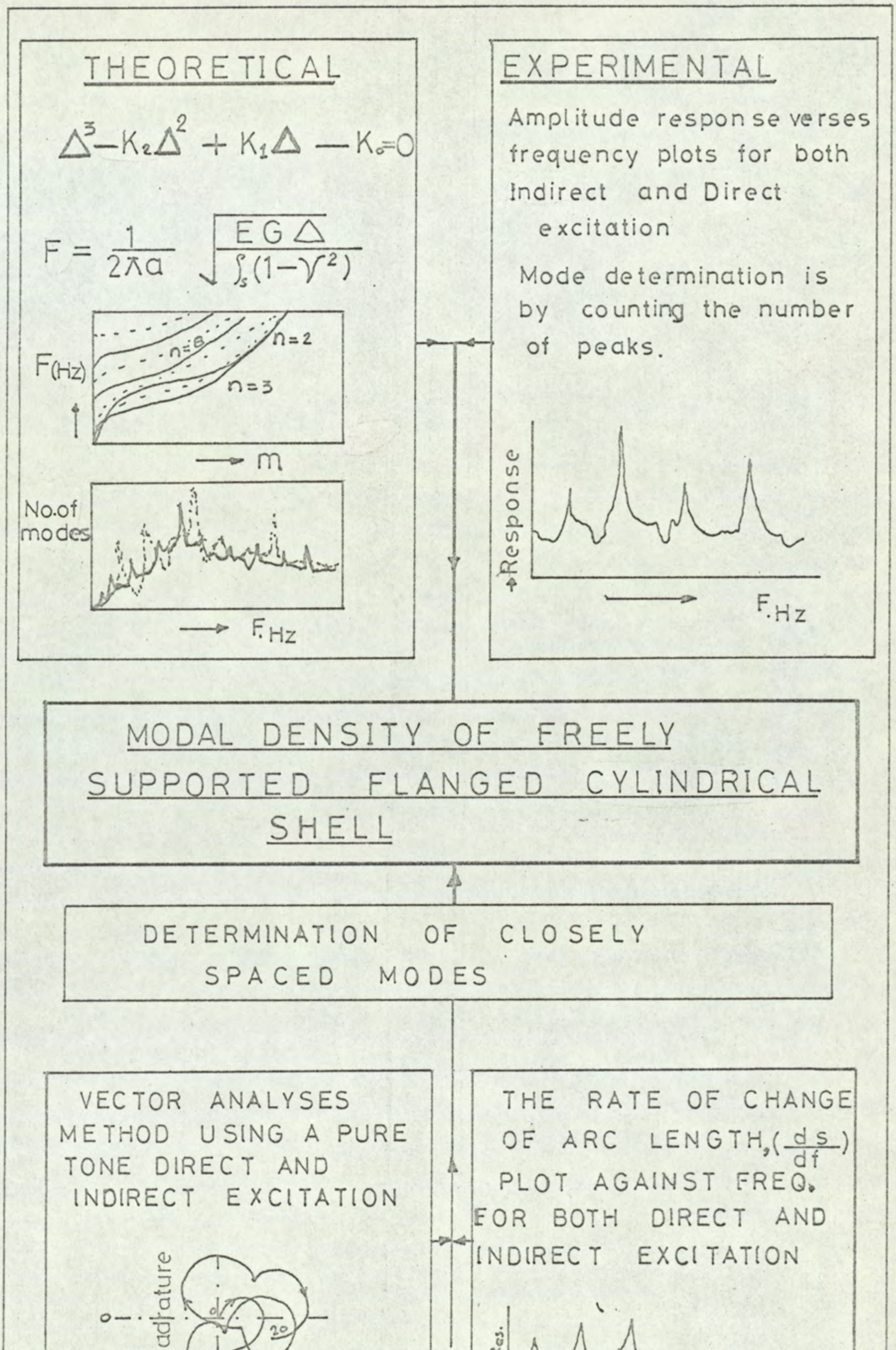
THEORETICAL
$\Delta^3 - K_2\Delta^2 + K_1\Delta - K_0 = 0$
$F = \frac{1}{2\pi a}\sqrt{\frac{EG\Delta}{\int_s(1-\nu^2)}}$
F(Hz)
n=8
n=2
n=3
m
No.of modes
F.Hz
EXPERIMENTAL
Amplitude response verses frequency plots for both Indirect and Direct excitation
Mode determination is by counting the number of peaks.
Response
F.Hz
MODAL DENSITY OF FREELY SUPPORTED FLANGED CYLINDRICAL SHELL
DETERMINATION OF CLOSELY SPACED MODES
VECTOR ANALYSES METHOD USING A PURE TONE DIRECT AND INDIRECT EXCITATION
quadrature
in phase
20
10
THE RATE OF CHANGE OF ARC LENGTH, ($\frac{ds}{df}$) PLOT AGAINST FREQ. FOR BOTH DIRECT AND INDIRECT EXCITATION
Res.
f_{Hz}
CORRELATION TECHNIQUE

FIG 6.5A

CHAPTER 7.

Part 1 - Mechanical damping in flanged cylindrical shell.

7.1. Introduction

The damping is one of the most important properties in a structure when it undergoes vibrations of resonant character and its behaviour is considered under two sub-divisions, internal and external dissipation of energy. The internal dissipation is related to a number of factors which include among others, the material, the stress amplitude, the stress distribution and the frequency of oscillation. External dissipation of energy, on the other hand, is dependent on the system's external mountings, joints and the associated connections, and on the external medium within which the system is subjected to vibration. If it is a simple linear system and excited harmonically at its resonant frequency, the damping is the only system characteristic which will control the response of vibrations. When the same system is excited in random manner, however, the mean square value of the displacement is inversely proportional to the product of damping and stiffness.

The capacity of a structure to dissipate vibratory energy plays an important role in establishing the levels of the structures responses to excitation such as jet noise, the spectra of which extends over wide frequency bands. In order to obtain a realistic value of the magnitude of this energy dissipation, it is desirable to understand the mechanisms responsible for this phenomena so that the analyst and the designers of structures can combine the knowledge favourably at the initial stages.

The increased emphasis in recent years on acoustical treatment and the growing importance of near resonance effects in the analysis of structural systems have accentuated damping capacity as an important engineering design property. Although the damping properties of a structural system might provide valuable information for analysing the general internal mechanisms of structure, (analogous in some respects to using the material as a microstructural research tool), this has not been a principal reason for understanding the present work. Rather, the main reason for interest in the damping properties of the structure has been to provide data required for determining the dynamic response of the structure to random excitation.

There is a variety of motivations in damping research. The wide scope of damping applications in engineering and the wide range of materials and test conditions studied by Lazan and Plunkett (4.5) led to the development of several experimental techniques. A description and comparison of the different methods for measuring damping is given in Section 7.3. The damping behaviour of structural materials has not, by contrast, been brought to a comparable mathematical level. Many of the procedures and assumptions which have proved so successful for poly-metric materials are generally unrealistic for structural materials, particularly at stress levels of engineering interest. It has been necessary to describe the damping properties of structural materials at engineering stress levels in terms which involve energy dissipation. The damping energy units used for structural materials specify the area within which lies a stress-strain hysteresis loop, and not its shape, as shown in fig. 7.1A. In the analysis of the dynamic response of systems which include highly nonlinear damping for example, it would be necessary to know not only the area within the hysteresis loop but also its shape.

The work reported in this chapter is particularly concerned with the variation of internal damping with frequency of a flanged cylindrical shell, freely supported in air and vacuum, vibrating at small amplitude and stress. Much useful work (6,30) has already been carried out on the frequency dependency of internal dissipation of solids but this has generally been confined to relatively low frequencies. With the higher operating speeds and the associated frequencies now current in modern technology, it was felt that extension of such experimental work to higher frequencies and modes is necessary with systems for which vibration frequencies up to 20k HZ and even above may be important. The work, to date, was carried out for only one structural geometry as a part of experimental data required to compute radiation properties and therefore the results shown are confined to this model. The experimental techniques developed can be applied to structures with any configurations, provided care is exercised in the analysis of the results.

In the experiments, care was taken to eliminate support damping. This was largely accomplished by careful positioning of the thin wires from which the specimen was suspended. Thus the only effective external dissipating influence remaining was that due to the air when the test was performed under normal room conditions. Some of the experiments described in this chapter were carried out in a pressure vessel having evacuation facilities to create a vacuum so that mechanical damping was measured without the influence of air damping. This facility was made available to the University of Aston by Dr. Yeh, Head of the Vibration Section, English Electric Research Laboratory, Whetstone.

In what follows are descriptions of damping mechanisms, measurement techniques and experimental results obtained in different room and structure conditions.

7.2 Basic Concepts and theoretical considerations in structural damping.

7.21 Mechanical damping.

The term damping has been defined by Lazan (5) as the energy dissipation properties of a material or system under cyclic stress. In most cases a conversion of mechanical energy to heat is involved. Within the context of this definition, energy must be absorbed and dissipated within the specific system before the term damping is applicable. Once the energy has been accepted by the structure in its modes of vibration, it will either be dissipated internally or re-radiated back into the space. The former is the internal damping and latter the radiation damping. Material damping, sometimes called internal friction, internal damping or hysteretic damping, is related to the energy dissipation in a volume of macro-continuous media. In general, material damping is associated with the energy dissipation which takes place when a more or less homogeneous volume is subjected to cyclic stress and the damping mechanisms are associated with the internal micro- and macro-structure of the material. Whereas material damping occurs in a volume of a macro-continuous medium, system damping involves configuration of parts or inter-action among the various phenomena.

Among the types of system in which damping under cyclic stress may be important are:

(i) Structural systems in which energy is dissipated in various types of joints, interfaces or fasteners.

(ii) Hydro-mechanical and acoustical systems in which damping occurs through fluid flow. Acoustical damping and radiation, oil flow through orifices, and dashpot effects are examples of this type of damping.

(iii) Electro-mechanical systems in which energy conversion and dissipation may take place through the interaction between electrical or electro-magnetic phenomena and physical bodies. An example of this type of energy loss is the system damping associated with magnetic hysteresis and eddy current.

Beyond the damping energy dissipated internally by the material of the structural members, the joints and fixings also dissipate energy. The relative shear motion which can take place between mating surfaces of joints offers the greatest potential for dissipating this energy. In the case of a dry interface, coulomb friction provides the mechanism for dissipating energy under cyclic shear displacement.

Materials are not perfectly elastic even at very low stress levels. In-elasticity in materials manifests itself in a variety of different ways. Under cyclic stress, for example, in-elastic behaviour takes the form of a stress-strain hysteretic loop as illustrated in fig. 7.1A. Although such loops are always present at stress, they are often too narrow to be observed by conventional methods. The shape of the loop depends on the damping mechanism operative.

7.22 Methods of Increasing Damping

It is unlikely that an increase in the friction damping of structural joints can be obtained without an increase in fretting fatigue troubles. By careful structural design, it might be possible to optimize the acoustic damping by ensuring that the natural frequencies of the important modes occur in the region of the peaks but when this happens, the modes will be found to be good acceptors of acoustic energy as well as good radiators.

The most promising method, (31), of increasing damping is to add certain anti-vibration materials to the structure. These are usually high-polymers and have very high material damping properties. When damping materials are added to plate-like structures they may be added in the form of unconstrained or constrained layers. An unconstrained layer has one surface which is perfectly free and is obtained when the treatment is sprayed or trowelled on to the surface where it dries and hardens. Alternatively, a pre-formed layer of the material may be stuck straight on to the surface to be damped. When the composite plate undergoes flexural vibration there is a linear variation of direct bending strain across the section of the plate. Energy is dissipated as the damping material undergoes this oscillating direct strain, illustrated in fig. 7.22A.

An unconstrained layer, on the other hand, has no free surface but is sandwiched between two stiff layers, one of which is the basic plate to be damped. The other may be a thin metallic foil, which together with the damping constitutes, "damping tape". Both, the foil and the damping layer may be very thin and yet give quite good damping properties. The principal damping mechanism here is the shearing of the damping layer which dissipates energy by virtue of the shear strain it undergoes when the composite plate vibrates, see fig. 7.22B. The same shearing mechanism applies to the double-skin sandwich configuration shown in fig. 7.22C. The two skins are bound together with a visco-elastic material having high damping properties. If the skin-stringer construction is to be retained, the structural damping may also be increased by including visco-elastic layers at the interfaces of the rivetted joints in the structure. The layers help to transmit the load and, furthermore, prevents fretting between the joint plates around the rivets. A cross-sectional view of the damped cylindrical shell using visco-elastic material is shown in fig. 7.22D.

An increasing number of different damping treatments and techniques are becoming available for the alleviation of vibration and noise. In assessing which of these is likely to be the most beneficial to a particular situation, several different factors may have to be considered. Foremost amongst these is the ultimate affectiveness of the treatment on the system response as to which of the treatments gives the greatest alternatives of vibration, stress or noise. Mead, (7), discusses the problems involved in assessing damping. Sometimes the factors of weight and bulk of the treatments, their sensitivities to changes of environment, the cost and the ease of application, fabrication or removal are of comparable importance. For example, if a damping treatment on a surface absorbs moisture and so promotes corrosion fatigue of the surface it is of no real value, even if it is by far the best means of preventing sonic fatigue. Factors such as these and many others must be considered in the general assessment before damping treatment may be applied.

7.23 Measurement of mechanical damping.

Various methods (4) of measuring damping that appear to have some application to engineering needs are described in this section. Nearly all descriptions of damping are derived from the linear single degree of freedom systems with a viscous damper in parallel with the spring as shown in fig. 7.23A. The main descriptions are given under the following headings:

7.231 Logarithmic decrement

7.232 Amplification factor

7.233 Equivalent viscous damping

7.234 Quality factor

7.235 Complex Spring Constant

7.236 Bandwidth, $(\frac{\Delta f}{f})$

7.237 Energy loss factor

7.231 Logarithmic decrement.

The decay rate of damping is based on the concept of energy dissipation per cycle of vibration. If this energy loss is small compared to the stored energy then the amplitude of oscillation will not decrease very much in one cycle of free vibration and the motion will be very close to being sinusoidal. This phenomena was proved from tests performed on a mild steel cantilever beam and the result is shown in fig. 7.231A. For a system vibrating in a single mode shape, the frequency is a defined quantity and the energy loss per cycle is therefore a function only of amplitude.

A system in which the energy loss per cycle is proportional to the square of the amplitude, has linear damping. In this case, the relative decrease in amplitude is constant and Dan Hartong (32) showed that,

$$1 - \frac{\Delta x}{x} = e^{-2\pi\xi} \qquad 7.1$$

where Δx is the amplitude loss per cycle and ξ is the ratio of equivalent damping constant, $C_{equiv.}$ to critical damping value C_o. Then the logarithmic decrement is given by,

$$\delta = -\ln(1 - \frac{\Delta x}{x} = 2\pi\xi \qquad 7.2$$

If the logarithmic decrement, (δ) is independent of amplitude then,

$$\delta = \frac{-1}{n} \ln \frac{x_n}{x_o} \qquad 7.3$$

where n is the number of cycles between x_n and x_o, shown in fig. 7.231B.

By counting the number of cyles, N_e, for the amplitude to decay to $\frac{x_o}{e}$, logarithmic decrement is given by

$$\delta = \frac{1}{N_e} \log_e \frac{1}{e} = \frac{1}{N_e} = \frac{1}{f_n} t_e \qquad 7.4.$$

where t_e is the time to decay to $\frac{x_o}{e}$.

If one takes the envelope, X(t), of the x curve, which is approximately a damped sinusiod,

$$\delta = \frac{1}{f_n X} \frac{dx}{dt} = - \frac{1}{f_n} \frac{d \ln x}{dt} = - \frac{2.302}{f_n} \frac{d \log_{10} x}{dt} \qquad 7.5.$$

Expressing the amplitude on a decibel (Appendix 1), Scale

$$Y_{dB} = 20 \log_{10} x$$

$$\therefore \quad \delta = (- 0.115/f_n) \frac{dy}{dt} \qquad 7.6.$$

7.232. <u>Amplification factor.</u>

In a linear single degree of freedon system, if a constant sinusoidal excitation force is applied with gradually increasing frequency, it is found that the amplitude of vibration steadily increases to a maximum and then decreases as the frequency is further increased. It is found that near where the amplitude is a maximum, there is only one value of frequency, at which the applied force is exactly in phase with the vibratory velocity. At this frequency the applied force is completely dissipated in damping at the resulting amplitude and this amplitude is a measure of damping. The definition of a linear system is that the amplitude of vibration is proportional to the exciting force and the ratio between vibration amplitude at resonance and that at zero frequency is a true and dimensionless measure of damping as shown in (33) for example $\frac{X_{res}}{X_{st}} = A =$ amplification factor.

7.233. Equivalent Viscous Damping.

If it is desired to find the amplitude of a damped forced vibration in the neighbourhood of resonance, the concept of an equivalent viscous damping is used. The equivalent viscous damping is the amount of viscous damping that would give the same amplitude as the damping force in question and is given by the expression,

$$(ED)_{Viscous} = \pi C \omega X^2 = 2\pi \xi k \frac{\omega}{\omega_n} X^2 \qquad 7.7.$$

and $$\left(\frac{Work}{cycle}\right)_n = \pi F X_n \qquad 7.8.$$

For the case $\frac{\omega}{\omega_n} = 1$, the amplitude of a viscously damped single degree of freedom system is,

$$X_n = \frac{F}{C\omega_n} \qquad 7.9.$$

It can then be defined,

$$C_{equiv.} = \frac{F}{\omega X_n} \qquad 7.10.$$

For any damped system, even those which are not viscously damped, the damping factor, ξ, may also be expressed in terms of critical damping where,

$$C_c = 2\sqrt{km} = 2\omega_n M_{equiv.}$$

$$\xi = \frac{C_{equiv.}}{C_c} \qquad 7.11.$$

7.234. Quality factor.

The qualifactor of a system is defined in terms of the ratio of the energy dissipated to the energy stored. If the amplitude is constant, the sum of the kinetic and potential energies is almost constant, and the energy stored may be measured by the maximum value of either one. It was shown by Kimball (2.) that

$$\text{Quality factor } (Q) = \frac{\pi}{\delta} = \frac{2\pi W}{\Delta W} \qquad 7.12.$$

where W is the stored energy and ΔW is the dissipated energy per cycle. W is equally the energy supplied to the system per cycle by the external force F, since the definition is only valid for a steady state condition

7.235 Complex Spring Constant.

The complex spring constant is defined in terms of the steady state response to forced vibration (37). The real part, k, is that portion of the spring force in phase with the displacement divided by the resulting displacement, and the imaginary part, ηk, is that part in the quadrature divided by the displacement shown in fig. (7.235A). Since real and imaginary refer to the components of the phasor, this approach only has direct meaning for sinusiodal motion. The real and imaginary portions of the elastic modulus, (34) (E' and E'' respectively) are derived from the corresponding parts of the spring constant in a standard fashion.

The modulus of elasticity, E', may be defined in terms of the stored energy per unit volume:

$$W = \frac{1}{2}\frac{\sigma^2}{E'} = \frac{1}{2} C^2 E' \qquad 7.13.$$

The imaginary component, E'', may be related to the specific damping energy, as used, for example by Lazan, in a similar way for small damping.

$$D = \pi \epsilon^2 E'' = 2\pi \frac{E''}{E'} \cdot \frac{1}{2}\frac{\sigma^2}{E'} = 2\pi \frac{E''}{E'} W \qquad 7.14.$$

7.236. Bandwidth.

The method is based upon the difference in the two frequencies at which the amplitude is the same if the exciting force is the same. For a linear viscously damped system, Foster (35) has shown that

$$2\zeta = \frac{\Delta f}{f_o}\left[\frac{x^2}{x_{max}^{\;2} - x^2}\right]^{1/2} \qquad 7.15.$$

where Δf is the difference between the two frequencies at which the amplitude is x_1, f_o is the undamped natural frequency, x_{max} is the amplitude at f_o and ζ is the damping ratio $\frac{c}{c_c}$ as shown in fig. 7.236A. A commonly used criterion is $x_{max} = \sqrt{2}\,x$, or:

$$2\zeta = \left(\frac{\Delta f}{f_o}\right)_{3dB} \qquad 7.16.$$

Relationships Among Definitions.

Definite relationships among the various definitions of damping may be established only for a linear single degree of freedom system. Comparing the various dimensionless ratios:-

$$\zeta = \frac{1}{2Q} = \frac{1}{2}\left(\frac{\Delta f}{f_o}\right)_{3dB} = \frac{\delta}{2} = \frac{E^{11}}{2E^{1}} = \frac{\eta}{2} = \frac{1}{2A}.$$

Then $\quad D = \pi\epsilon^2 E^{11} = 2\pi \frac{E^{11}}{E^{1}} \cdot \frac{1}{2}\frac{\sigma^2}{E^{1}}$

$$\zeta = \frac{C_{equiv.}}{c_c}\,, \quad c_c = \sqrt{km}\cdot 2 = \frac{2k}{\omega_n} = 2\,m_{equiv.}\omega_n$$

The above relationships are only valid for a linear single degree of freedom system with linear viscous damping though most of them are approximately so far non-linear damping.

7.237. Energy loss factor.

The loss factor is a commonly employed dimensional measure of structural damping. For a structure vibrating in steady state, it is usually defined as the ratio between the energy dissipated per cycle and 2 times the (time-wise) maximum total strain energy stored in the structure. For damping that is not too high, say $\eta < 0.2$ (a condition that is met in nearly all practical structures) the ratio is approximately, $\eta \simeq 2c/_{c_c}$, where c denotes an equivalent viscous damping coefficient for the structure and frequency of interest, and c_c represents the corresponding critical viscous damping coefficient. The structural decay time over 60 dB can readily be shown to be related to the loss factor, η, as

$$\eta \simeq 2.2 \left(T_{60\,sec} \cdot f_{Hz} \right)^{-1}$$

where f denotes the centre frequency of the band in which measurements are being taken.

7.3 Damping Measurement Techniques

7.31 Decay Rate

This method is used for special tests in engineering, but is also the approach favoured by physicists interested in low stress level effects. The technique (36) is to suspend a disc from a wire, twist through a small angle, release and record the amplitude compared against time. The logarithmic decrement may be calculated from the amplitude ratio, a known number of full cycles apart, fig. 7.231B.

$$\delta = \frac{1}{n} \ln \frac{x_o}{x_n}$$

Many methods have been used to measure the angular amplitudes, but the most satisfactory, for simplicity, accuracy and lack of external loading, is a plane mirror mounted on the torsional mass. For low frequency work, measurements may be made by projecting a beam from the mirror on a scale, while for faster decay rates the beam is projected on to slow moving film and the results measured after developing the film.

The main drawbacks of this method are the possible energy loss at the fixing and the limitation in the range of frequency and the specimen sizes that may practically be studied. Various ingenious schemes have been used to decrease the energy loss at the ends but these are always open to question.

In making these measurements, the transducers used must not influence the results; this is not a serious limitation in decay measurements since absolute values are not required, all that is needed is linearity. The weight of a standard vibration pickup such as an accelerometer or velocity pickup is usually a fraction of that of the specimen being measured, depending upon the specimen size. Electric wire strain gauges have been successfully used, but are a bit of a nuisance to fasten on, capacitance or variable reluctance devices do not have this drawback but usually have more complex electronics, making them expensive and less readily available.

A linear recording of amplitude will seldom allow a dynamic range of more than 10 to 1 (20dB). The standard level recorder, used in acoustic work, has a logarithmic potentiometer with a range of 300 to 1 (50dB). In addition, the problem of replotting the cycle amplitude to form a smooth curve is avoided, taking the small difference between large numbers and resmoothing, since the logarithmic decrement is directly related to the time slope of the dB curve, fig. 7.31A.

$$\delta = - \frac{0.115}{f_n} \frac{d(dB)}{dt}$$

The type of damping may be deduced from the decibel curve. Viscous damping gives a straight line; the curve of coulomb, or friction, damping is convex upward (negative second derivative), material damping in which the damping constant increases with amplitude gives a curve which is concave upward.

7.32 Bandwidth.

This technique is widely used since it only uses the same equipment used for forced vibration driving to determine mode shapes and frequencies. It is important to maintain a constant evaluation force by using a feed-back system with the aid of compressor. The frequency is then changed until the amplitude is a maximum and the two frequencies, lower and higher, at which the amplitude is a given fraction of the maximum are found. The damping is then found from

$$Q = \frac{f_o}{\Delta f}\left[\frac{x_{max}^2 - x_1^2}{x_1^2}\right]^{1/2}$$

and Δf, should be kept as small as possible to minimize interference from other resonances of the specimen.

7.33 Energy Measurements.

There are a number of different measurement schemes which are based upon a comparison of dissipated energy with stored energy in off-resonance measurements. One of these methods is the rotating beam. If the end of a cantilever beam is weighted it will deflect vertically, X_v; if it is now rotated with the weight on, it will have a small horizontal deflection, x_H, and, for small values of δ

$$\delta = \pi \frac{x_H}{x_v}$$

This method lends itself well to the determination of δ, as a function of frequency and stress level and for finding the effect of stress history on damping. For plastics and rubber where the damping is high and very frequency dependent, the damping is measured by taking the ratio of the stress to the quadrature and in phase components of strain. The dissipative elastic modulus is also found by measuring the area in the hysteresis loop, see fig. 7.1A, on a stress-strain or force deflection curve during cyclic loading.

Similar results are obtained from the phase angle of impedance rather than resonant frequencies, but in this case the primary measurement is the ratio

$$\tan\theta = \frac{E^{11}}{E} = \eta = 2\xi$$

At resonant frequency one may find the energy input from force and velocity measurements. In this case the energy input per cycle is,

$$\Delta W = \frac{\pi F \mathcal{V}}{\omega_n}$$

since F and $\mathcal{V}$ are in phase. The stored energy is found from the effective mass, which in turn may be found from the shape of the impedance curve, from frequency change due to added mass, or by computation.

$$W = \tfrac{1}{2}\, m_{eff.} \mathcal{V}^2$$

Thus

$$\delta = \frac{\Delta\omega}{W} = \frac{2\pi F \mathcal{V}}{\omega_n m_{eff} \mathcal{V}^2} = \frac{2\pi F}{\omega_n m_{eff} \mathcal{V}} = 2\pi \frac{Z}{Z_0}$$

$$\therefore Q = \frac{Z_0}{Z}$$

where Z is the (minimum) impedance at resonance (zero phase-angle) and Z_0 is the specific impedance, $\omega_n\ m_{eff.}$

7.34 Amplification factor.

Amplification factor measurements are difficult to use for absolute measurement of damping, since the reference level may be hard to find. If the driving force, geometric configuration and boundary condition is unchanged and the resonant frequency does not change much, the ratio of the amplitudes at resonance is inversely proportional to the ratio of the damping constants. Such a measurement is a rapid way of finding the effects of changes in damping methods or materials, provided the damping is not large enough to affect the vibration shape appreciably.

7.35 Low-Stress Methods.

A number of low-stress devices are in use to investigate the physical characteristics of various material (38). Since these appear to have fundamental limitations which restrict them to low stress levels or high damping value, they do not give information of direct value for engineering design. Among these (36) are standing wave measurements in travelling wave systems, mechanical impedance bridges and axial rod resonance excited by electro-static or electro-magnetic devices.

7.4 Technique used for the measurement of damping in the flanged cylindrical shell.

7.41 Direct measurement of structural damping.

7.411 From the measurement of logarithmic decrement.

The damping ratio of the flanged cylindrical shell was measured by shock exciting the specimen and storing the record on the oscilloscope of the filtered response from a piezo-electric strain gauge fixed to the skin of the cylinder. An example of such a record is shown in fig. 7.51A. The value of the logarithmic decrement was then calculated from the measurement of amplitude of the decaying curve. An average of twelve readings were taken to arrive at a figure of 0.1390 for logarithmic decrement. It was ensured that each time the test was repeated, the exciting force and the point of impact were identical. The damping was computed from the equation,

$$\zeta = \delta \Big/ \left[4\pi^2 + \delta^2\right]^{\frac{1}{2}} \tag{1'}$$

where δ is the logarithmic decrement given by the equation,

$$\delta = \ln \frac{x_0}{x_1} = \frac{2\pi\zeta}{(1-\zeta^2)^{\frac{1}{2}}} \tag{2'}$$

The value obtained for the damping ratio is 0.0197. For the purpose of this test, the cylinder was placed on point contacts at the flanges approximately in the centre of a room lined with sound absorbing material that gave reasonably free field conditions, See Appendix 22.

The damping ratio obtained from this experiment is the result of one particular point on the skin of the specimen. Since many coupled modes are associated with the vibration of cylindrical shell structures, it would not be simple to deal with them just in a general form. For practical purposes it may be convenient to consider the principal uncoupled modes only, five of which are shown in fig. 7.51B, because in many cases only one or two modes are dominantly excited, depending on the shape of the shell. The logarithmic decrement for such a mode can give a very misleading result; even at such a resonance, a large portion of the amplitude may be due to the reactive components of other modes very close to it. For the specimen tested, a combination of resonant frequencies were obtained as shown in fig. 7.51C, and it was not found possible to separate these closely coupled modes to apply the logarithmic decrement method of analysis successfully. For a good assessment of damping to be made using this method, one would have had to sample quite a number of positions on the structure resulting in lengthy analysis time. The limitation of this method was also noticed at higher frequencies where many very closely linked modes are excited. For detailed investigation of damping, the method outlined in Section 7.52 is used.

7.412 From the measurement of bandwidth of the resonant peak.

The linear damping of a mode widely separated from its neighbours can be readily measured from the width of the frequency curve. In making detailed measurements of the damping of the modes, the main difficulty arose when the modes of the flanged cylindrical shell were found to occur close together in the frequency spectrum of interest and their resonant peaks tended to overlap. As an example, consider the frequency-response curve measured from an accelerometer placed on the skin of the specimen excited by harmonic plane sound waves. The response curve is shown in figure 7.512A. It will be noticed that the width of the peak for some of the modes cannot be measured readily, if at all. Furthermore, some resonances are lost in the troughs between the peaks. For this particular structure it was not found possible to obtain a reasonable value for the damping ratio, for the frequency range of interest from the measurement of the bandwidth and applying the equation

$$\zeta = \left(\frac{\Delta f}{2f_o}\right)_{3dB}$$

An attempt was made to separate the modes by plotting the response components in phase with, and in quadrature with, the acoustic exciting pressure. The vector response diagram so obtained is shown in fig.7.512B and this covers the same frequency range as the response curve of fig. 7.512A.

The response of a single isolated mode, when plotted in this way, gives a pure circle, centered on the in-phase axis. Several modes of different frequencies combine to give the complex system of loops, curves and knots of figure 7.512B. Once a resonant frequency has been established, the arc is completed to give the single degree of freedom resonant circle and the resonant diameter drawn. The origin of this diameter represents the displaced origin of the single degree of freedom system, the length represents the response of the mode and the argument represents the phase relative to the exciting pressure. The damping in the mode is determined from the resonant circle by measuring the phase angle at two frequencies close to resonance, (8).

The damping ratio, ζ, is given by

$$\zeta = \left(\frac{\omega_2 - \omega_1}{\omega_n}\right) \left(\frac{1}{\theta_2 - \theta_1}\right) \qquad 7.17$$

as illustrated in fig. 7.512B.

The damping ratio of one of the modes shown here is approximately 0.0004.

It was found that the plotting of the vector response is an extremely tedious business and at higher frequencies of interest, it was not possible to separate the modes successfully. The limitations of this method to discrete frequency response test, and the impossibility of separating the modes at higher frequencies, led to other methods where the measurement of damping is obtained from the average number of modes being excited in a frequency band.

7.42 Measurement of decay time and damping of the structure in a pressure vessel.

The method used in the analysis of the loss factor - a commonly employed dimensionless measure of structural damping - was from the assessment of mechanical decay times. It was assumed that when the source of vibration is removed from the structure, the energy content can only be dissipated in two ways.

(a) By mechanical structural losses.

(b) By radiating the energy in the form of sound.

If all the sound energy radiated is dissipated in the far field, one can relate the total loss factor to the structural decay time (Appendix 2.1), defined as the interval within which the signal power decays by a factor of 60 dB, by:

$$\eta_{TOT} = \frac{2.2}{T_{s\,60}\, f} = \eta_{rad} + \eta_{m} \qquad 7.18$$

where f is the centre frequency of the band in which measurements are taken and $T_{s\,60}$ is the structural decay time over sixty decibels.

In a vacuum, the energy radiated in the form of sound is zero, thus,

$$\eta_{m} = \frac{2.2}{T_{v\,60}\, f} \qquad 7.19$$

where $T_{v\,60}$ is the structural decay time in vacuum.

This experiment was carried out in a pressure vessel, 3 feet in diameter and 8 feet long, which was lined with one inch thick polyurethane foam to ensure the absorption of the radiated sound energy. The structure used for the experiment was a flanged cylindrical shell, 72 inches long, 18 inches in diameter and 0.048 inches thick. The cylinder was enclosed by two end plates having the same thickness as the shell. The end plates were bolted to the flanges and rubber packings were used between the end plates and the flanges to prevent fluid leakage. Since internal and radiation damping were the subjects of study, the suspension of the specimen had to be such as to introduce as little damping as possible. The specimen was, therefore, suspended by means of two thin wires attached to the flanges.

For the measurement of structural decay times, the vessel shown in fig. 7.52A containing the specimen was filled with air at ambient pressure and temperature. The structure was then struck approximately in the middle by means of a remotely controlled hammer. The transient output of eight accelerometers randomly placed on the skin of the cylinder was recorded on magnetic tape. The experimental flow diagram is shown in fig. 7.52B.

The pressure vessel was then evacuated by pumping the air out to a vacuum of 736 mm of mercury. The whole operation was then repeated and the results recorded as before.

The rate of decay of accelerometer signals recorded on magnetic tape was slowed down and recorded on an x,y chart recorder through a 50 HZ bandwidth filter. The arrangement of the equipment is shown in fig. 7.52C.

In the process of filtering the decaying signal, one second averaging time was applied to average some of the detailed fluctuations as much as possible so as to obtain clear trends in the curve. Steps were taken to ensure that the averaging was within reason so that the important trends were not averaged out and that the actual signal output to the filter was recorded and not the filter characteristic.

This analysis procedure was repeated with various centre frequencies. The decay time over 10 dB was measured from the initial portion of the decay curves which contains much of the valuable information. An average decay over 60 dB was then computed, the results of which are shown in fig. 7.52D. The total and mechanical loss factors were computed from the results of decay times using equations 7.18 and 7.19 and the results are shown in fig. 7.52E.

7.43 Measurement of decay time and damping of the structure in the semi-reverberant room.

This experiment was carried out in a room which was lined with sound absorption material and the room when tested had reasonable free field conditions,(Appendix 2.2.) The model was suspended from wires approximately in the centre of the room, to ensure a balanced distribution of any radiated energy.

For the first test, the excitation, signal recording and analysis techniques used were the same as described in Section 7.52. The results were computed as before and are shown in figs. 7.52D and 7.53A.

In the second case the structure was excited with a wide-band random noise level of approximately 100 dB which was continued for a period of time to ensure even energy distribution in the room before cut off. Four loud speakers, having a frequency from 40 HZ to 15k HZ, were placed in the room at positions such that a steady sound energy distribution around the specimen was maintained. When the sound source was cut off, the decay output of the accelerometer placed on the skin of the specimen was recorded on magnetic tape and analysed as before. The experimental and analysis flow diagram is shown in fig. 7.53B. The decay times and loss factors were then computed for enclosed and open cylinder, the results of which are shown in figs. 7.53C and 7.53D.

7.5 Results and Discussion

7.51 Measurement of damping ratio by Logarithmic decrement and bandwidth methods.

The values of the damping ratio(ζ) measured in the cylindrical shell by the two methods are not the same.

In the first case, although the freely decaying output from the transducer was filtered in a narrow band before recording, the results obtained from the repeat of identical tests showed a wide variation in the value of the damping ratio. It seems that a varying number of modes were being excited each time the test was repeated and the results were being influenced by the number of interacting modes occuring close to each other in the frequency band. It is quite likely that the structure, when transiently excited, vibrated in many uncoupled modes and the only reasonable estimate of damping would have been to make measurements in every mode separately and add the values averaged over at least twelve tests. The accuracy of the result is therefore based on some of the following:

(a) The number of modes being excited.

(b) The measurement of amplitude ratio from the freely decaying trace.

(c) The amount of energy losses at the fixings and to the environment.

(d) The linearity of the system.

In the second case, extreme care had to be taken to separate the modes before measurements were made. The result is for one particular mode only and the accuracy relied on the following:

(a) The measurement of frequency at either side of the resonant frequency $\frac{\omega_2 - \omega_1}{\omega_n}$

(b) The accuracy by which the modes were separated.

(c) The linearity of the system.

The results from the two methods can only be compared when the number of modes in the frequency band contributing to the energy level in the logarithmic decrement is known.

7.52 Measurement of decay time.

The results of decay time measurements shown in figs. 7.52A, 7.52D and 7.53C for various room and structure conditions is very nearly the same above 8.5K Hz. Even in the lower frequency ranges, the difference is not so high as expected. From the individual decay traces shown in fig. 7.62B, it can be seen that, in vacuum, the energy decay shows a smooth trace, while, in the air, the trace is subject to many bumps, but the decay rate appears to be the same. This seems to be due to the reflecting energy being in the form of an echo from inside the cylindrical structure or from the walls of the compartment in which the test was carried out. Although the test compartment walls were lined with sound absorbing material to reduce reflection of sound energy, it seems that at some frequencies this did not make much effect. Results of the tests carried out in a larger room of semi-reverberant nature show that above 1 K Hz the decay time is very nearly the same as for the structure tested in vacuum. The comparison between open and closed ended cylinders also do not show much difference in their decay times above 5 k Hz. Some interesting results might have been obtained if the same structure was tested in an anechoic chamber and a comparison made with the present test. On the whole it seems that at higher frequencies, which is the range of interest in the present work, there is not a great deal of difference in the decay time. Since the structural decay time was required as a datum for radiation properties of structure, the test carried out in the vacuum was sufficient for the present time.

The accuracy of the result is therefore based on the following:

(a) The energy losses at the fixings.

(b) The instrumentation and method of analysis.

(c) The linearity of the system.

(d) The room conditions, freefield or otherwise.

7.53 <u>Mechanical Loss factor</u>.

The mechanical loss factors for different room and structure conditions were calculated from the mechanical and total decay times of the flanged cylindrical shell. This was based on the concept that the energy, E, with which a structure of total mass, M, vibrates is expressed as $E = M\bar{V}^2$, in terms of mean square velocity $\bar{V}^2$ of the structure. When the power supply to the structure is "turned off", the energy is assumed to decay as $e^{-\delta t}$, where t denotes the time, then the power is $-dE/dt = \delta E$. In the steady state the power input, P, must equal the power loss so that,

$$P = M\bar{V}^2 = \frac{13.8}{T} \; M\bar{V}^2$$

The structural decay time (Appendix 2.1) $T = \frac{13.8}{\delta}$ is a quantity which lends itself well to experimental determinations.

At frequency, ω, the power loss factor in the system is given by,

$$\eta = \frac{13.8}{T\,\omega}$$

The assumptions underlying the above derivations are:

(a) The energy is uniformly distributed over the structure.

(b) Exponential decay of energy with time.

(c) Linear boundary and fluid absorption conditions.

The results are discussed as follows:

(i) Effects of different room conditions

It can be seen from fig. 7.52E that different room conditions do have effects on the total damping in the structure. From the results of the test carried out in the vessel, it can be seen that the energy losses to the surroundings are higher on either side of the ring, (3778 Hz) and coincidence (9159 Hz) frequencies. Further, the result of the test in the semi-reverberant room shows a clear increase in the radiation damping beyond 1.6k Hz. Greater radiation losses are due to good coupling between the sound field and the structure. Below 1.7k Hz the mechanical losses are greater ($\eta_m > \eta_{rad}$), hence poor coupling.

(ii) Effects of different cylinder and room conditions.

Fig. 7.53 shows the results of the effects of different cylinder and room conditions from which it can be seen that the fluctuation of the total energy losses, ($\eta_m + \eta_{rad}$) is considerable. For the enclosed cylinder, radiation losses are higher above 1.7k Hz, while for the open cylinder the fluctuation is not so much, though a marked increase in radiation damping is seen between 2.5k Hz to 4.5k Hz and 7.5k Hz to 10k Hz. The enclosed cylinder is seen to be heavily damped when compared with the open cylinder except at and on either side of the critical (Appendix 2.6) frequency (9159 Hz).

The total energy losses are higher than when the structure was excited by an impact, when perhaps only a limited number of modes were excited. In the case of the structure being excited acoustically, a fair distribution of acoustic energy is applied all over the structure, hence, as a large number of modes are excited as a result, energy flow is high.

A comparison between the mechanical loss factors obtained by the two methods is shown in fig. 7.63A. The difference in the results is due to the limitation in the assumption and inaccuracies in the equation used for calculating the radiation loss factor based on the acceleration and pressure spectral densities, the modal density and the reverberation time of the room.

7.6. Comparative Results.

If different methods are used to measure damping, one may well expect to get different values, all seemingly correct. The relationship among the various methods have been based on linear, single degree of freedom systems with linear viscous damping. If more than one normal mode is involved in the measurement, the effective damping is apt to increase. Most types of damping are amplitude dependent; a method of measurement which depends on measurements at different amplitudes, such as bandwidth, must give different results from one made at a single amplitude, such as energy input. A decay rate measurement determined from the slope of the logarithmic amplitude curve should be different from one based on the number of cycles required to decay to 1/e. A discrepancy based on non-linearities would seem to obviate the results since the fundamental assumptions are violated. With a difference which is based on torsional stress in one case and bending stress in another, or on solid versus hollow specimens, one would get different results for different problems which were not capable of comparison. For these reasons one must take the measurements under circumstances which closely resemble those for which the information is needed.

The simplest way to find the energy loss in a complex structure is by means of decay rate. These values may then be used for design purposes or to predict the effects of other kinds of energy dissipation. The raw data so obtained, such as a logarithmic decrement, can not be used directly to give resonant amplitude without a great deal more analysis, although it may be useful, as it is, for comparison.

For multi-degree of freedom systems, the energy dissipation above, or alternatively the logarithmic decrement of a particular mode, may give a very misleading picture of the amplitude to be expected for a resonant peak associated with one of the higher modes. This is because, even at such a resonance, a large fraction of the amplitude may be due to reactive components of mode shapes with natural frequencies close to the exciting frequency. These, of course, will be very little effected by changes in damping. In a similar fashion, as estimate of damping based on the ratio of the resonant peak to the average response, or based on the ratio of resonant response to anti-resonant response, will over-estimate the damping, often by large ratios. A reasonable estimate of damping may be possible if care is taken not to violate the assumptions too drastically. For greater usefulness to other engineers, the size, shape and frequency of the specimen should be reported. It seems that the simplest form of measurement is decay rate and it should give reliable results if the data is carefully reduced.

CHAPTER 7

Part 2 - Radiation damping in flanged cylindrical shell.

7.7 Introduction

The radiation loss factor, a dimensionless measurement of damping, is defined as the coupling between the sound and vibrations. Its value is estimated from a close study of the energy exchange between the structure and the sound field.

The manner in which the vibrating structures radiate noise is an important subject in noise control. It governs such effects as the radiation from machine housings, air and space-craft panels, submarine hull structures, building walls and many such structures subjected to mechanical or sound field excitation. The parameters that govern the sound radiation are the power flow linkage between the structural vibration and the sound pressures that are transmitted to the environment.

In the work at present considered, the structure is a flanged cylindrical shell subjected to narrow band excitation in the frequency ranges where very many modes of vibration are contributing to the response, or where the appropriate wavelength are small compared to the dimensions of the structure. This has resulted in a very complicated pattern of vibration and for this reason, the statistical theory of room acoustics developed by Lyon and Maidanik (11) is used for the analysis.

7.8 Theoretical Considerations

If a structure is immersed in a reverberant sound field, the amount of energy which will flow into it is based upon the degree of coupling between the structure and the sound field, an example of which is shown in fig. 7.9A. Its value is determined by the thickness of the material, the geometry and the method of construction. The amount of energy which the structure will accept in any particular frequency band depends on how many modes will resonate in that particular frequency band and accept energy from the sound field. Once the energy has been accepted by the structure in its modes of vibration, it will either be dissipated internally or be re-radiated back into the space. The loss of energy is expressed through a total damping which has contributions from radiation and from internal dissipation.

The modal energy of a damped resonant mode at equilibrium was derived by Smith (10). His equation is,

$$MV^2 = \left(\frac{2 \pi^2 c_o}{\rho_o \omega_o^2} \right) \left(\frac{Sp(\omega)}{1} \cdot \frac{\eta_{rad}}{\eta_{rad} + \eta_m} \right) \tag{7.31}$$

Lyon and Maidanik (11), show that where a structure contains several modes of vibration in the frequency bandwidth in which measurements are taken, the corresponding response equation may be obtained from equation (7.31), by multiplying it by the number of modes in that frequency band then,

$$\frac{S_a(\omega)}{S_p(\omega)} = \left(\frac{2 \pi^2 n_s(\omega)}{M \rho_o} \right) \left(\frac{\eta_{rad}}{\eta_{rad} + \eta_m} \right) \tag{7.32}$$

In equation (7.32), η_{rad} and η_m are averaged over the frequency band.

7.9. Measurement of radiation loss factor in flanged cylinderical shell

7.91 Direct determination of radiation loss factor

It was shown by Lyon and Maidanik (11) that the acceleration spectral density on a structure vibrated mechanically is related to the pressure spectral density it produces in the room for curved or flat panels by,

$$\eta_{rad} = \rho_o C_o \sigma / \omega M_s = R_{rad} / \omega M \tag{7.33}$$

and

$$R_{rad} = \left[\frac{S_p'(\omega)}{S_a(\omega)}\right] \left[\frac{27.6 \pi^2 n_R(\omega) C_o}{T_R \quad \rho_o}\right] \tag{7.34}$$

$$\therefore \quad \eta_{rad} = \left[\frac{S_p(\omega)}{S_a(\omega)}\right] \left[\frac{27.6 \pi^2 n_R(\omega) C_o}{M T_R \quad \rho_o \quad \omega}\right] \tag{7.35}$$

The reverberant time and the modal density of the room were obtained as described in Chapter 5.

For this experiment the cylinder was placed on point contacts at the flanges approximately in the centre of the reverberant room. The structure was mechanically excited with the driving mechanism being fed with white-noise source filtered in 50 HZ bands. The acceleration and sound pressure levels so produced were measured at twelve random positions from which the mean square values of pressure and acceleration spectral density were computed by the automatic space and time averaging system described in Chapter 4. The experimental flow diagram is shown in fig. 7.10A and in fig. 7.10B is shown the result of radiation loss factor.

7.92 Indirect determination of radiation loss factor.

For the purpose of this test the experimental set-up was the same as in section 7.9. except the structure was acoustically excited, as shown in fig. 7.10A. The acceleration spectral density of a structure vibrated acoustically is related to the pressure spectral density it produces in the room by,

$$\eta_{rad} = \left[\frac{S_a(\omega)}{S_p(\omega)}\right]\left[\frac{13.8}{T_S}\ \frac{M}{\omega}\right]\left[\frac{\rho_o}{C_o\ 2\pi^2 n_s(\omega)}\right] \tag{7.36}$$

Since $$R_{rad} = \left[\frac{S_a(\omega)}{S_p(\omega)}\right]\left[\frac{13.8}{T_S}\right]\left[\frac{M^2}{2\pi^2 n_s(\omega)}\right]\left[\frac{\rho_o}{C_o}\right] \tag{7.37}$$

and from equation 7.32,

$$\eta_{rad} = \left[\frac{S_a(\omega)}{S_p(\omega)}\right]\left[\frac{M\ \rho_o}{2\pi^2\ n_s(\omega)\ C_o}\right]\frac{\eta_{rad} + \eta_m}{1} \tag{7.38}$$

where $\eta_{rad} + \eta_m = \frac{13.8}{T_s\,\omega}$

The results of the above calculations are shown in fig. 7.102A.

7.93. <u>Determination of radiation loss factor, from the measurement of structural decay time.</u>

The total damping, η_{tot}, was found from structural decay time measurements, the relation being

$$\eta_{rad} + \eta_m = 13.8/\omega\, T_{s\ 60} = \eta_{tot} \tag{7.39}$$

In a vacuum the energy radiated in the form of sound is zero, thus

$$\eta_m = \frac{13.8}{\omega\, T_{V.\ 60}} \tag{7.40}$$

$$\therefore\ \eta_{rad} = \frac{13.8}{T_{S\ 60}\,\omega} - \frac{13.8}{T_{V.60}\,\omega}$$

$$= \frac{13.8}{\omega}\left[\frac{1}{T_S} - \frac{1}{T_V}\right]_{60} \tag{7.41}$$

The result of this computation is shown in fig. 7.103A.

7.10. Estimation of Coupling factor between reverberant acoustic field and the structure.

The coupling factors were estimated in two ways, by a method suggested in (11), and from the measurement of structural decay times.

The expression for the coupling factor was derived by Lyon and Maidanik (11).

$$\frac{S_a(\omega)}{S_p(\omega)} = \Gamma(\omega)\ \mu(\omega) \tag{7.42}$$

$$\Gamma(\omega) = 2\pi^2 \left[\frac{n_s(\omega)}{M}\right] \frac{c_o}{\rho_o} \tag{7.43}$$

$$\mu(\omega) = \frac{\eta_{rad}}{\eta_{rad} + \eta_m} \tag{7.44}$$

and
$$\frac{S_a(\omega)}{S_p(\omega)} = 2\pi^2 \left[\frac{s(\omega)}{M}\ \frac{c_o}{\rho_o}\right] \frac{\eta_{rad}}{\eta_{rad} + \eta_m} \tag{7.45}$$

$$\mu(\omega) = \frac{S_a(\omega)}{S_p(\omega)} \quad \frac{M\ \rho_o}{2\pi^2\ n_s(\omega)\ c_o} \tag{7.46}$$

The values of $S_p(\omega)$ and $S_a(\omega)$ were measured as described in Section 7.92 and the modal density was measured as explained in Chapter 6.

The second method used for the estimation of the coupling factor was from the measurement computer of the radiation and total loss factors and equation 7.44. The results obtained from this calculation are shown in fig. 7.11B.

The results of some of the tests carried out to examine the coupling between the acoustic and the structural modes are shown in fig.7.12A and 7.12B. For the specimen tested, many interacting modes were excited and for this reason it was only possible to observe the coupling clearly in the lower frequency ranges.

7.11. Coupling between a reverberant acoustic field and the end plate of flanged cylindrical shell.

The equation 7.45 shows that the total radiation loss factor is a function of pressure and acceleration spectral density, the structure constant and the radiation loss factor of the structure. The expression for the radiation loss factor will depend on the geometry and the method of excitation. From the expression 7.44, the coupling factor is seen to be dependent on the ratio of acceleration and pressure spectral density, the modal density and the structure constants. In order to examine the parameters,the structure was excited by pure tone and the results of some of the measurements are shown in fig.7.12A and 7.12B. It was observed that at the lower frequencies, the end plate modes coupled well with the acoustic modes while around and above the ring frequencies the end plates did not seem to matter very much. The experimental flow diagram for this test is shown in fig. 7.12C.

7.12. Results and Discussion.

7.121 Radiation loss factor derived directly.

From the results shown in fig. 7.103B, it is seen that above the ring frequency (Appendix 2.5), (3778 Hz), the internal dissipation in the structure becomes smaller compared with radiation damping. This means that there was an equilibrium between the modal energies of sound field and the structure, and hence a stronger coupling and larger exchange of energy between the sound field and the structure. Below the ring frequency this coupling is seen to be very poor and much energy is dissipated internally as is obvious from the experimental result in a vacuum.

The accuracy of radiation loss factor calculation is based on the assumptions made in the derivation of the equation and the following are some of the important ones:

(a) Diffused field around the structure.

(b) The modal density and the decay time of the structure, the accuracy of which are discussed in Chapter 5.

(c) Even distribution of energy over the structure.

In fig. 7.13A are shown the results of total loss factor derived by two methods. The difference is due to the error involved in calculating the radiation damping, the reason for which are described above.

7.122 Radiation loss factor derived Indirectly.

In fig. 7.102A are shown the results of the measurement derived by two methods, both of which have a close comparison. The level of energy losses are higher when compared with that derived indirectly. This clearly indicates that the energy flow is a strong function of the number of modes being excited in a frequency band and their coupling with the sound field modes. There is a good coupling around the ring frequency (3778 Hz). The level of the energy losses are very low above 4k Hz and this is due to the limitations in the loudspeakers when excited in the narrow band (50 Hz).

7.123 Radiation loss factor derived from the measurement.

The accuracy of this result depends on the measurement of decay times and the constant 13.8, described previously. A clear indication of higher radiation losses around the ring frequency and critical (Appendix 2.6) frequency is seen.

7.124 Coupling between the reverberant acoustic field and the structure.

Coupling factor derived by the two methods are very nearly the same as shown in fig. 7.11B. There is a very good coupling around the ring frequency as expected. The response above 4k Hz is rather low and this is due to the limitation in the loud speakers to narrow band excitation, but from the shape of the trace it can be seen that there is a good coupling around the coincidence frequency.

From the direct experimental results shown in fig. 7.9A, 7.12A and 7.12B, it is quite clear that the coupling is dependent upon some of the following:

(a) Geometrical shape of the structure.

(b) The end conditions.

(c) The diffusibility of room.

7.13. CONCLUSIONS.

The main findings discussed in this chapter are for a flanged cylindrical shell undergoing vibration of small amplitude.

Mechanical damping is found to be higher below the ring frequency and around 6.5k Hz.

Radiation damping is quite high at and either side of the ring and critical frequencies, hence, there is a good coupling between the structure and the sound field.

Both the mechanical and radiation damping measurements are dependent on the structural geometry and for complex structures, measurements must be taken on either a scaled model or a full-size structure.

Different methods used for the measurement of damping ratio and damping (loss factor) in the speciment are given in fig. 7.7A.

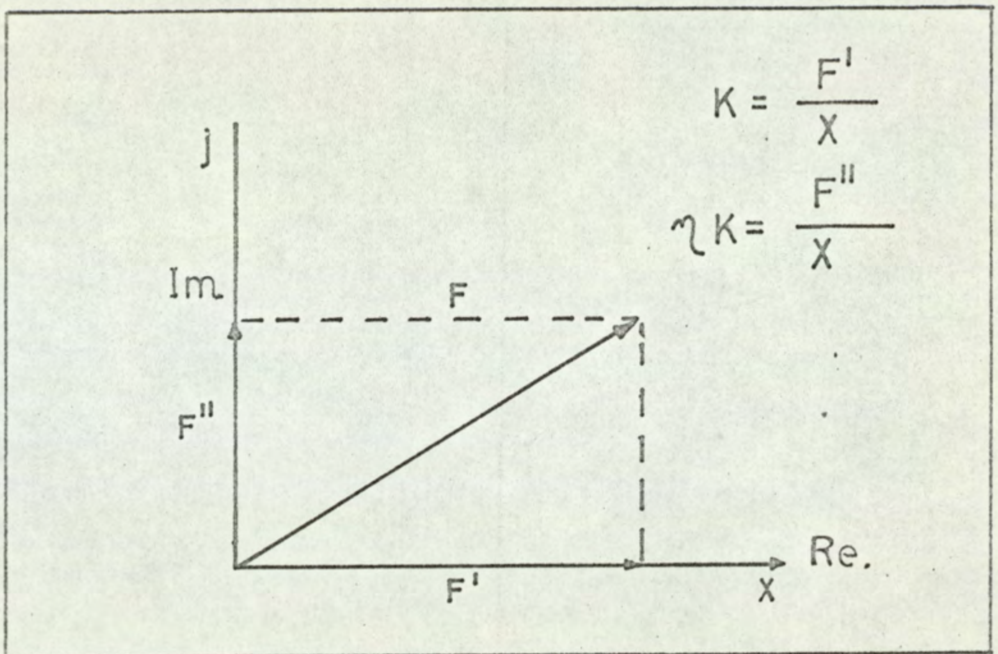

PHASOR DIAGRAM OF DAMPED FORCED VIBRATIONS.

FIG 7.23 5A

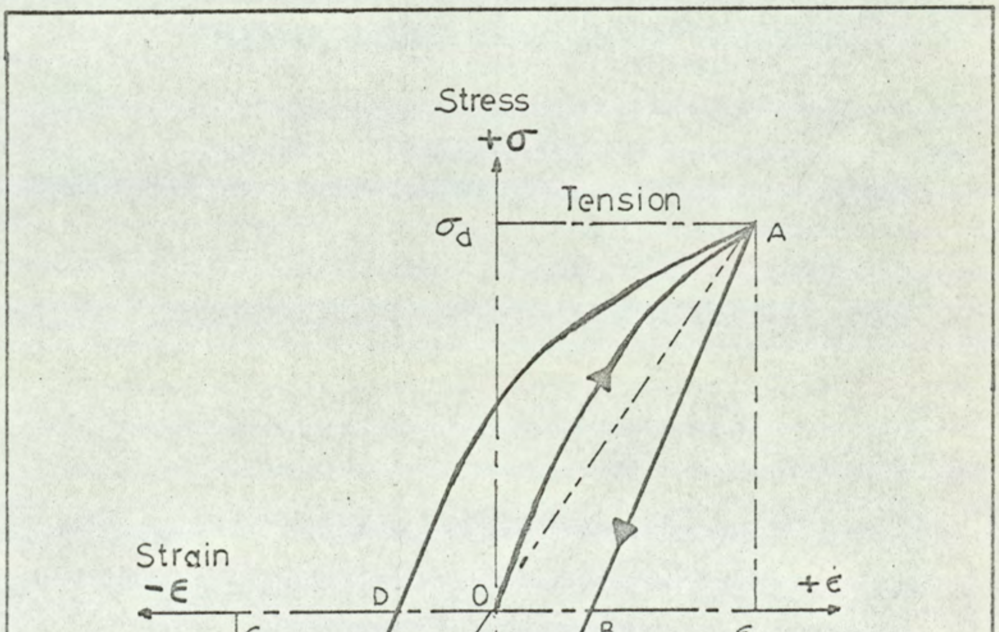

TYPICAL STRESS-STRAIN HYSTERESIS LOOP FOR MATERIAL UNDER CYCLIC STRESS.

FIG. 7.1A

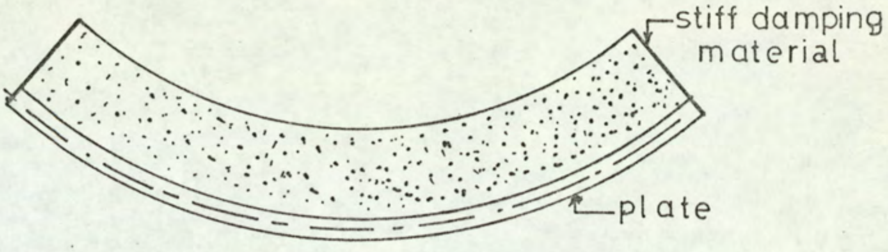

'UNCONSTRAINED LAYER' CONFIGURATION

FIG. 7.22A

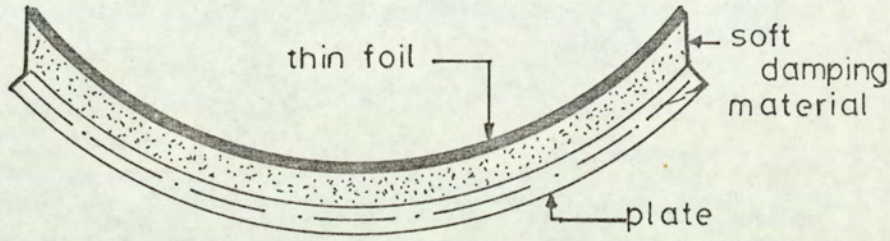

'DAMPING TAPE' CONFIGURATION

FIG. 7.22B

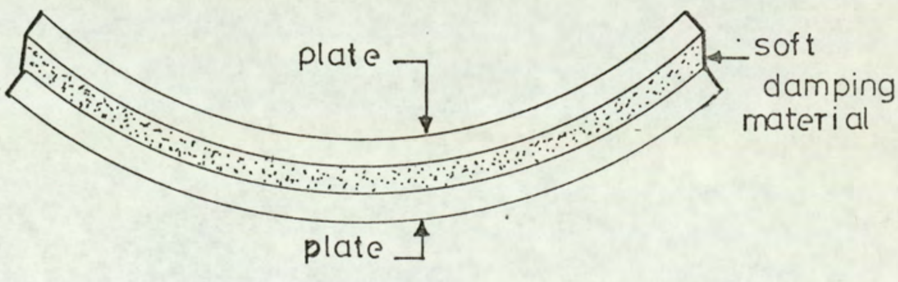

'DOUBLE-SKIN' CONFIGURATION

FIG. 7.22C

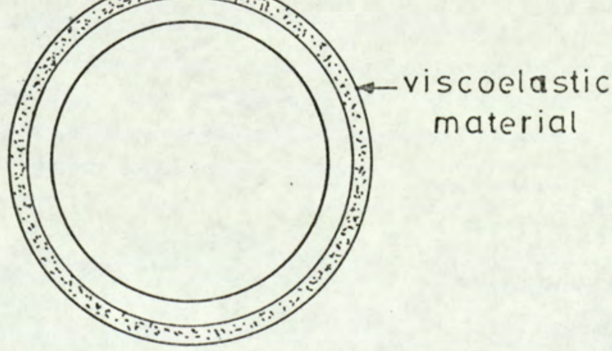

CROSS-SECTIONAL VIEW OF A TWO-LAYERED CYLINDRICAL SHELL FIG 7.22D

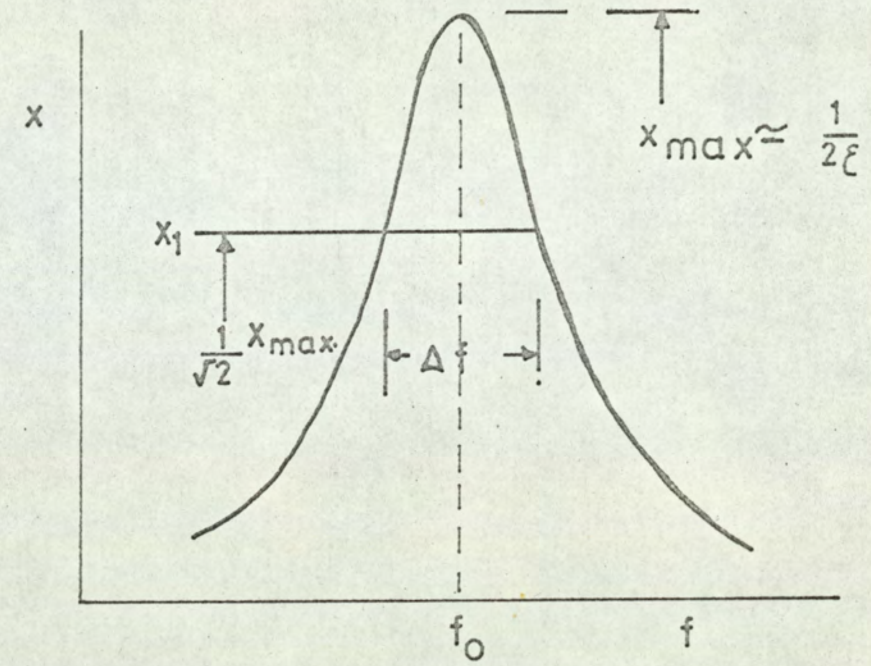

BAND-WITH OF RESPONSE CURVE

FIG.7.23.6A

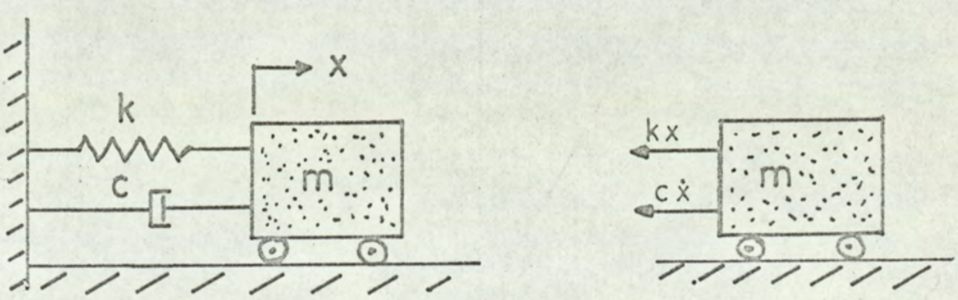

FREE VIBRATION WITH VISCOUS DAMPING

FIG 7.231A

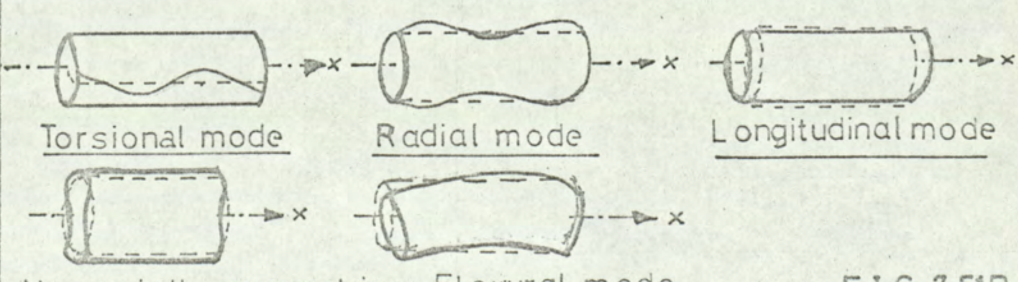

FIG 7.51B

FIVE TYPES OF MODES.

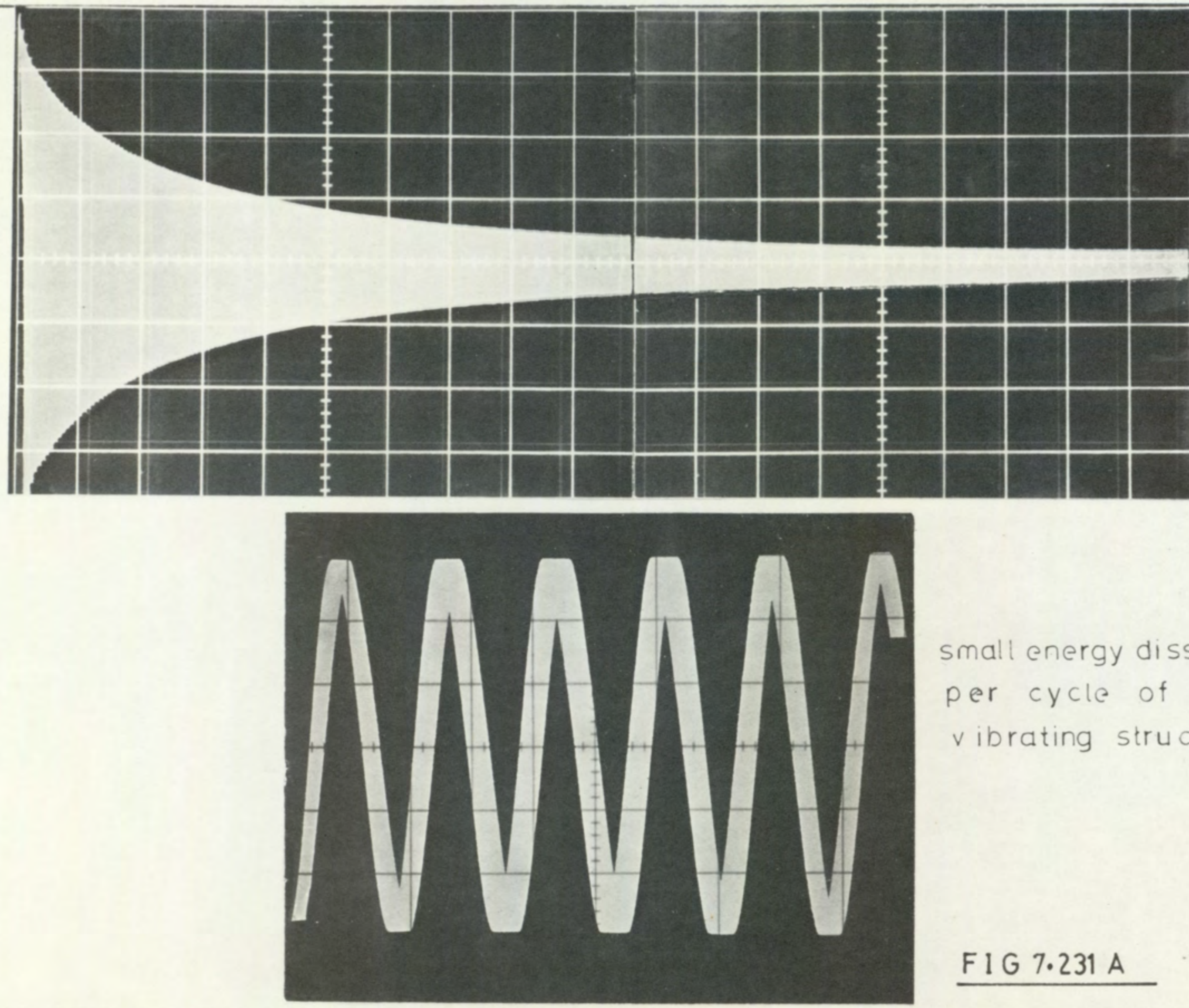

small energy dissipation per cycle of damped vibrating structure.

FIG 7·231 A

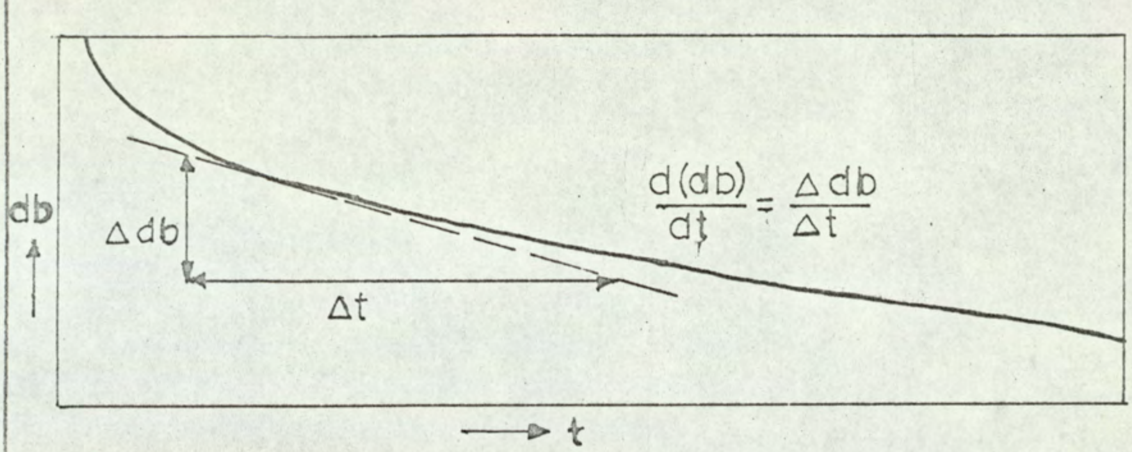

LOGARITHMIC DECAY CURVE

FIG 7.31A

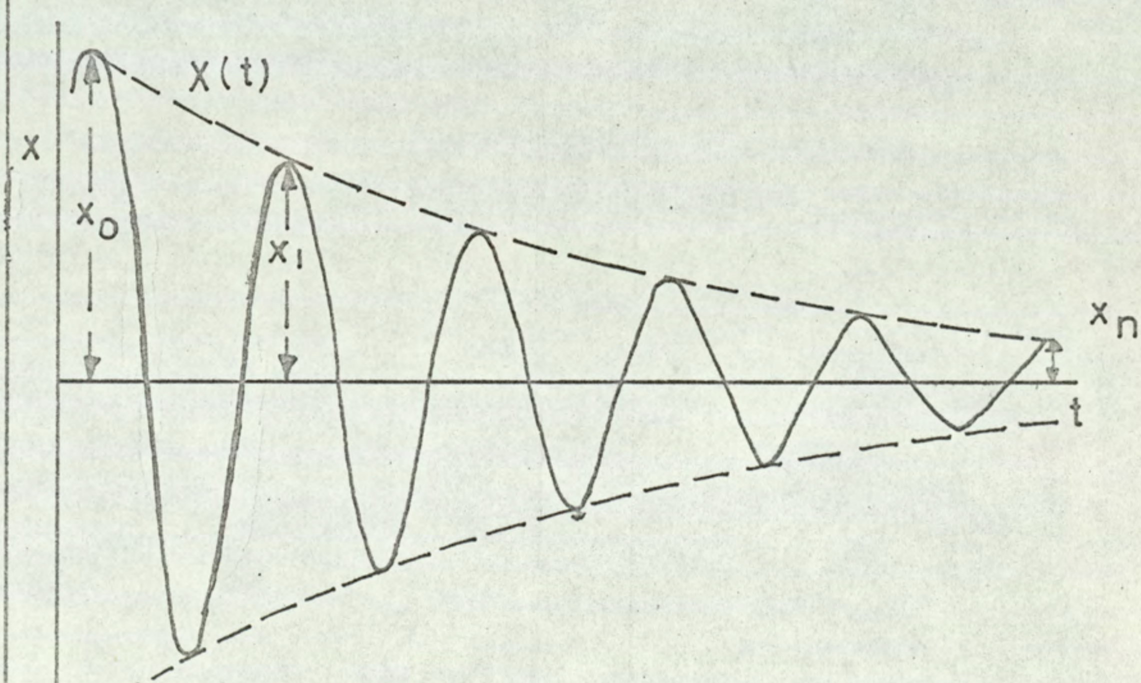

DECAY OF A DAMPED VIBRATING SYSTEM

FIG.7.231 B

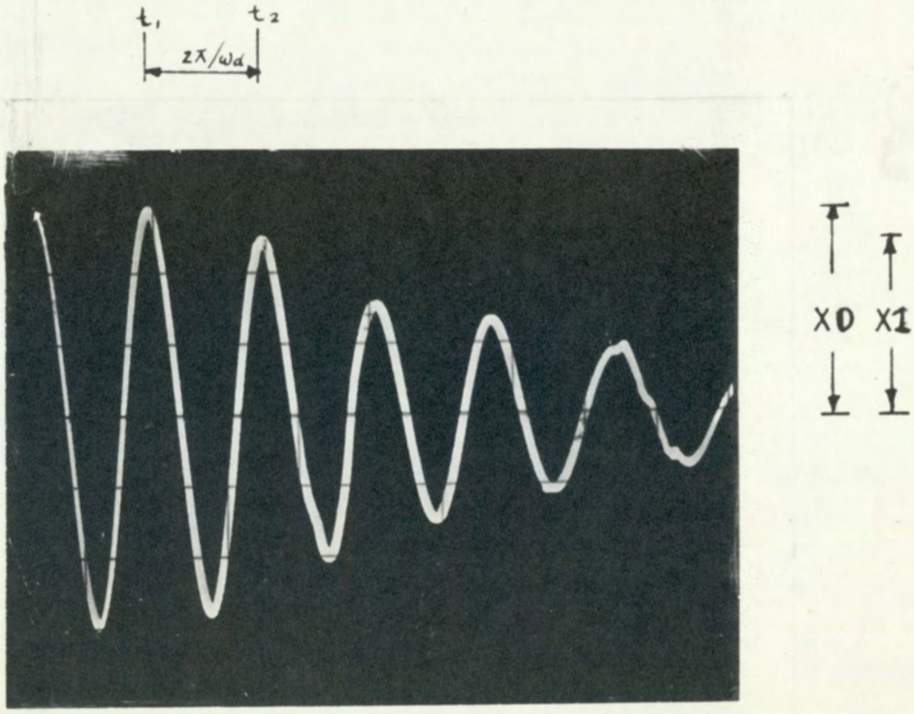

EXPERIMENTAL DECAY TRACE OF DAMPED VIBRATION.

FIG.7.51A

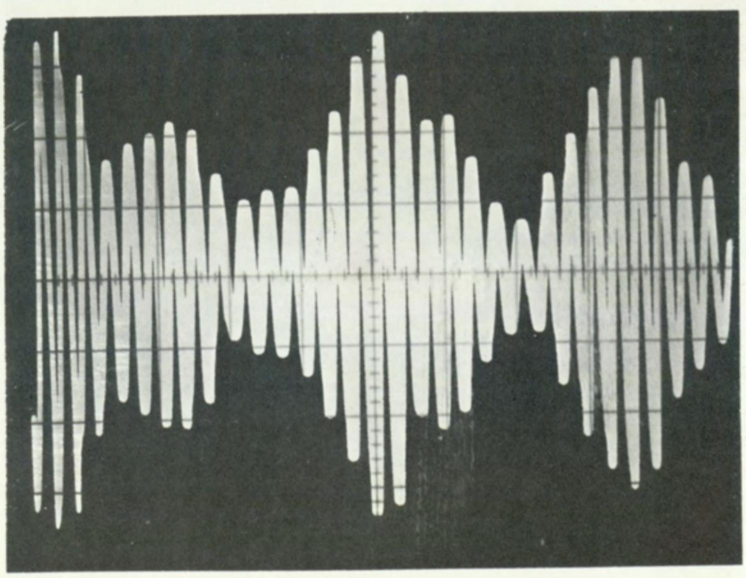

INTER-ACTING RESONANT FREQUENCIES

FIG.7.51C

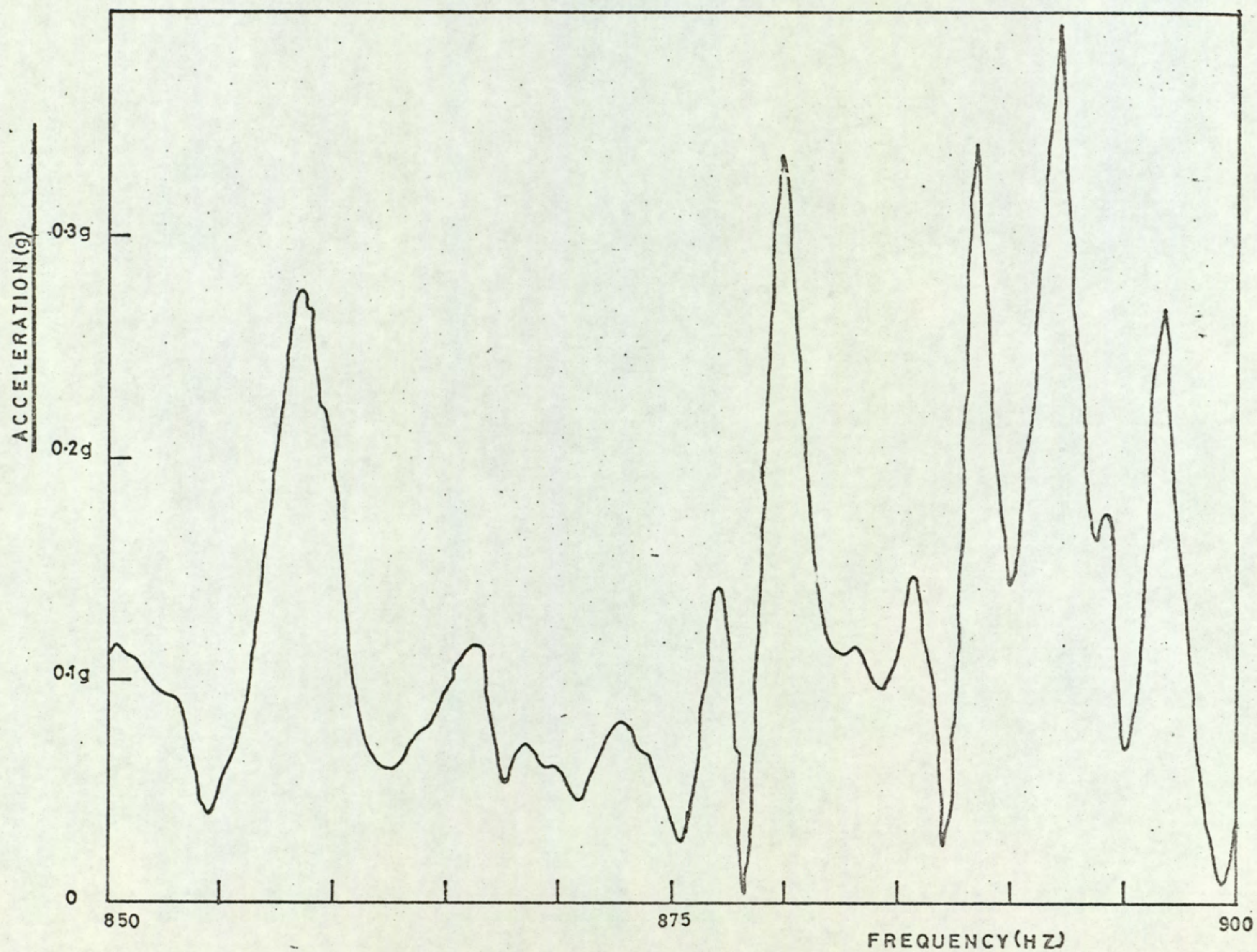

NUMBER OF MODES AS A FUNCTION OF FREQUENCY (HZ)

FIG 7·512A

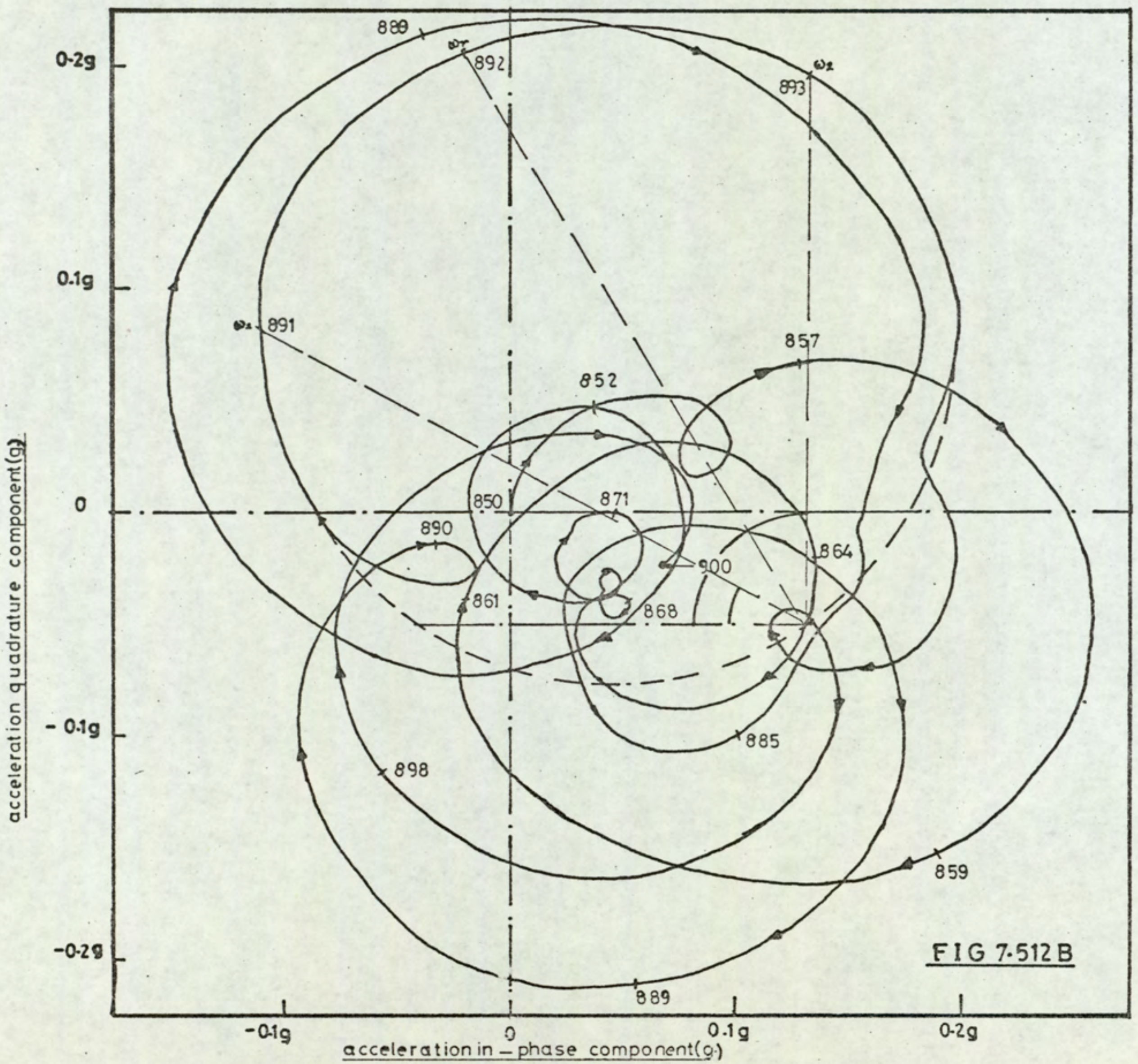

FIG 7·512 B

VECTOR RESPONSE DIAGRAM FROM ACCELEROMETER ON ENCLOSED CYL. SHELL

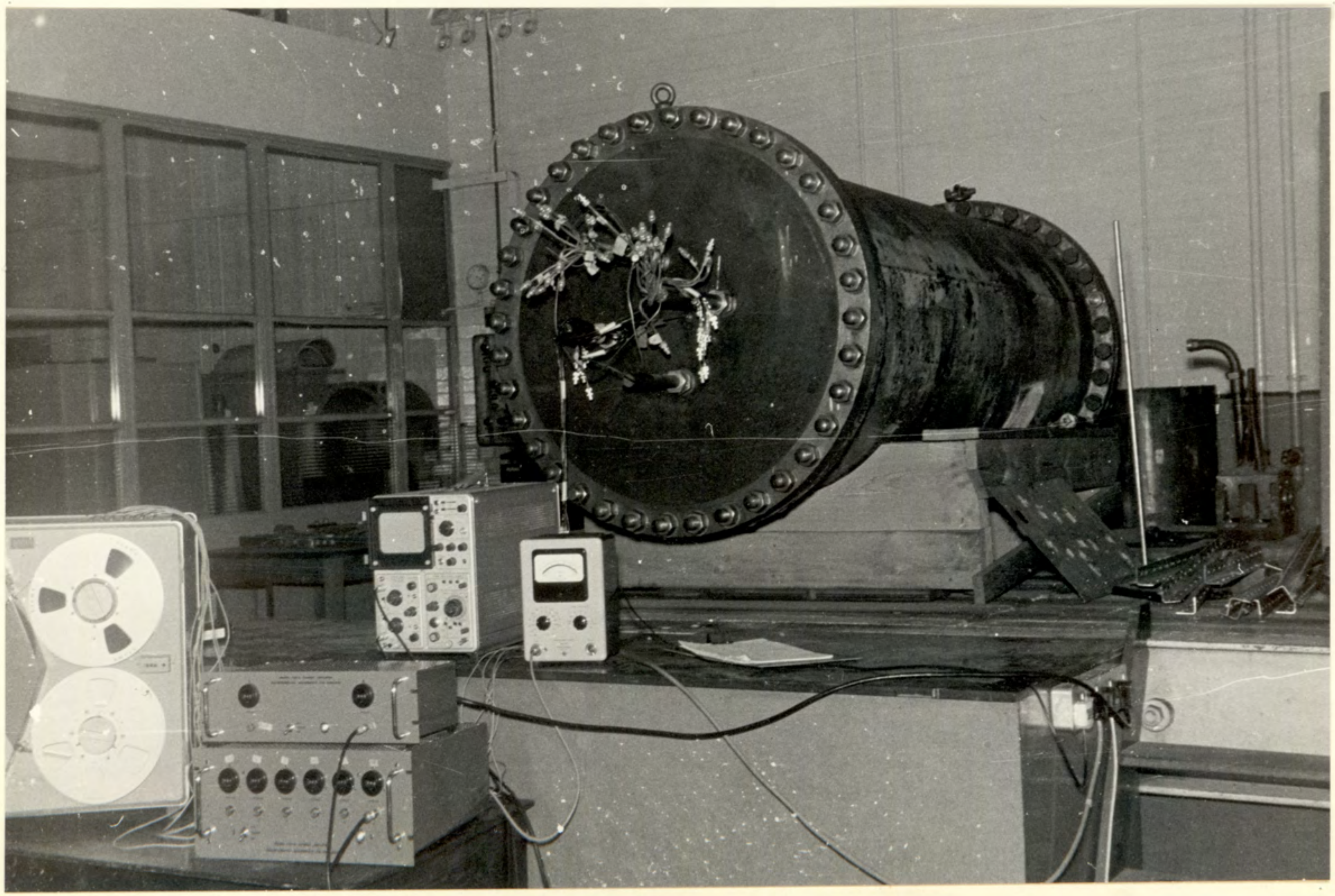

FIG 7.52A

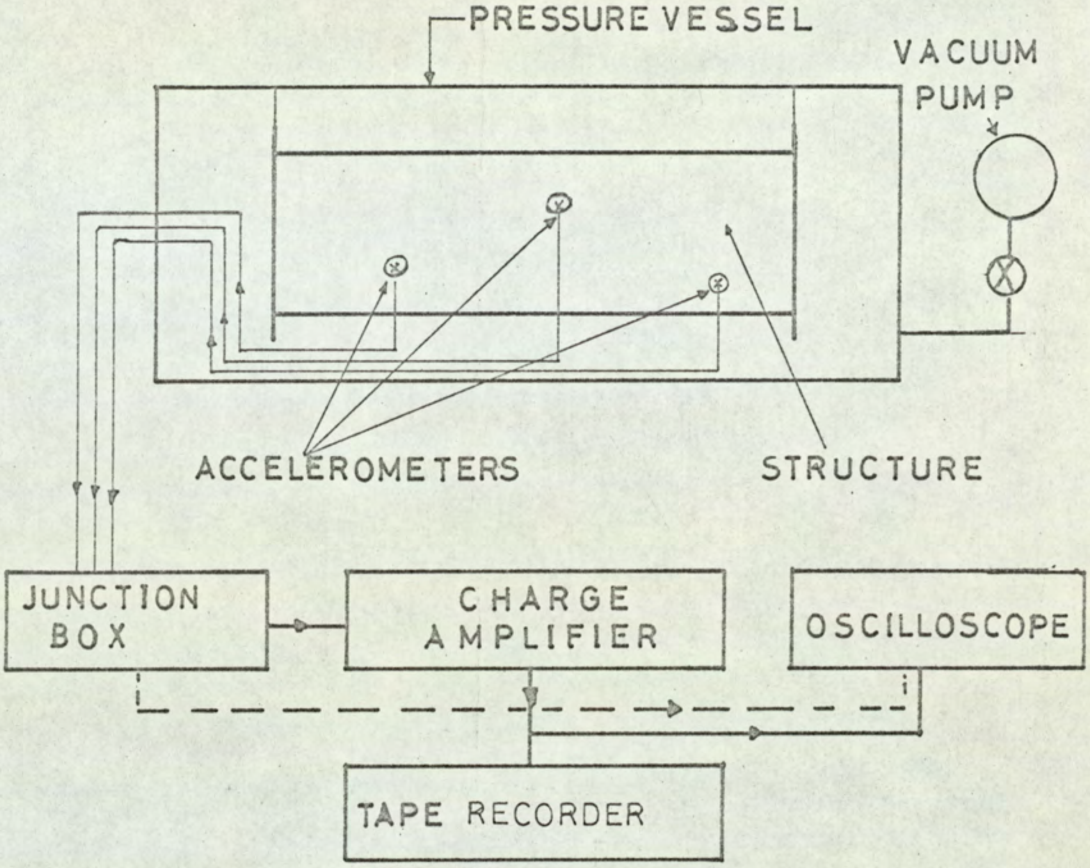

EXPERIMENTAL FLOW DIAGRAM

FIG 7.52B

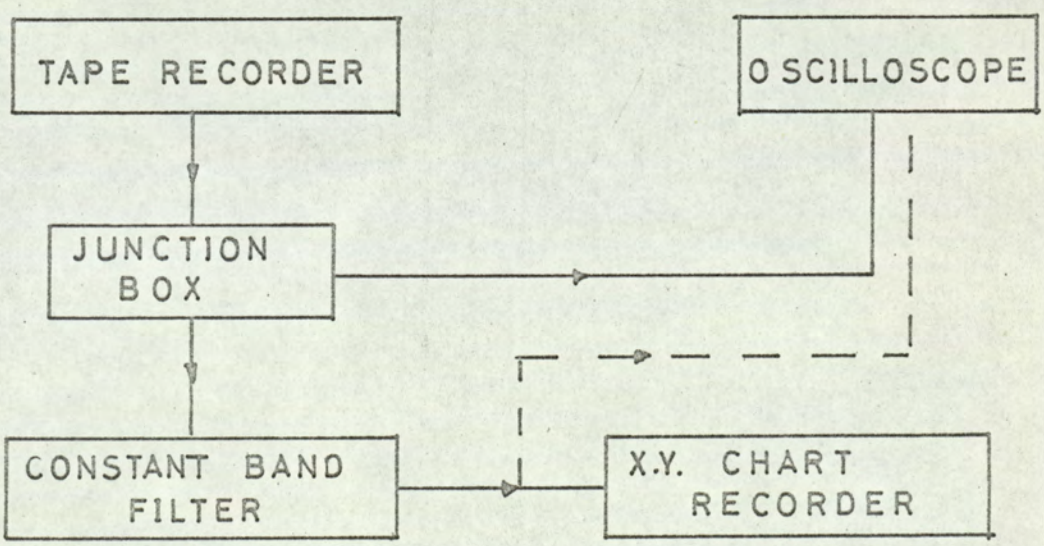

ANALYSIS FLOW DIAGRAM

FIG 7.52C

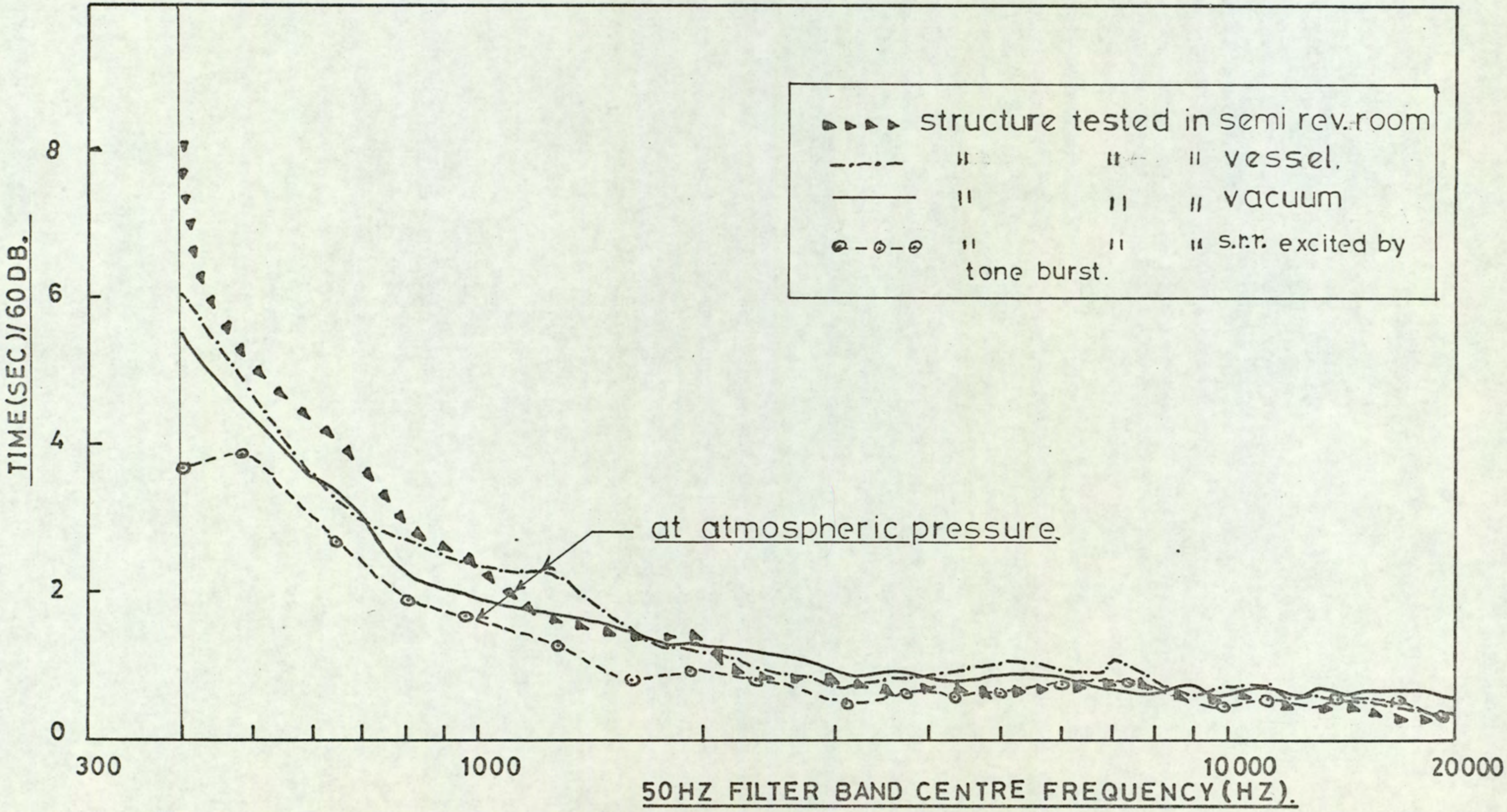

DECAY TIME OF ENCLOSED FLANGED CYLINDRICAL SHELL. FIG. 7.52D

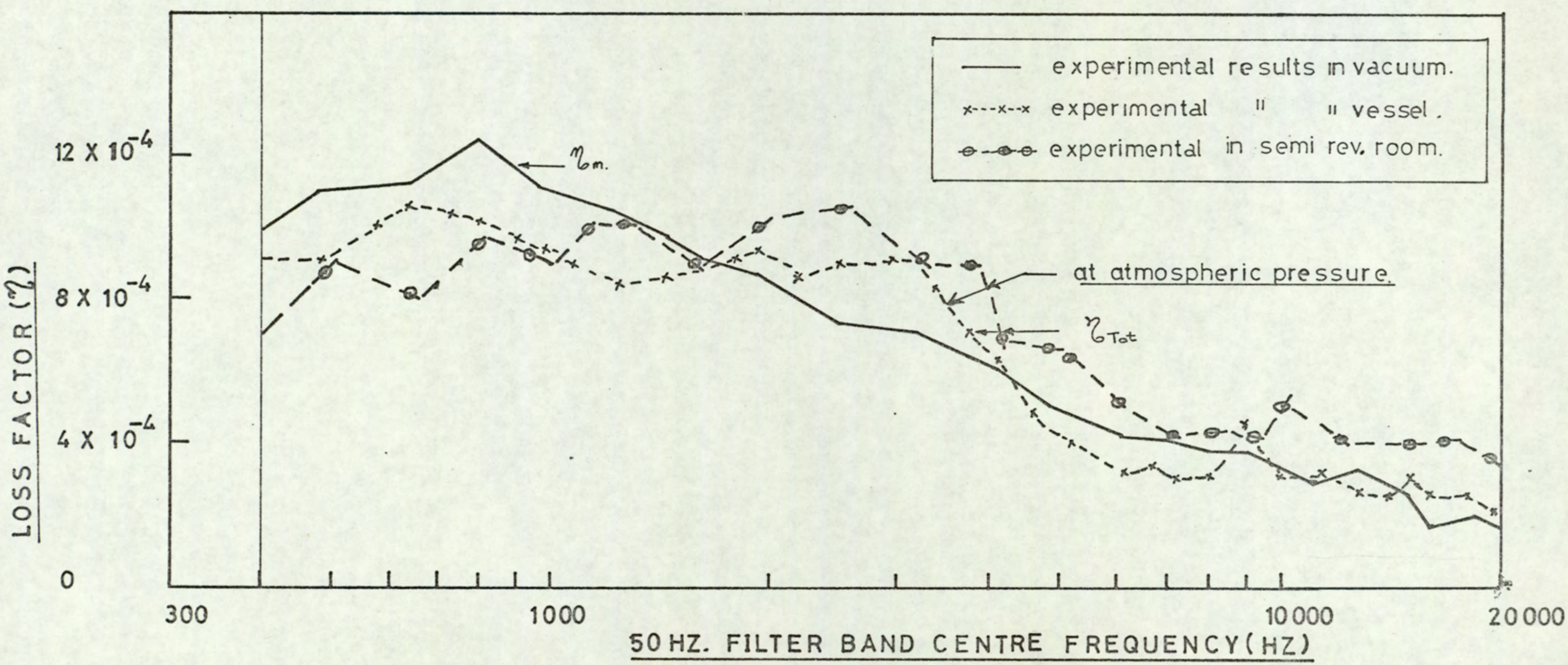

EFFECT OF DIFFERENT ROOM CONDITIONS ON CONTRIBUTION TO STRUCTURAL LOSS-FACTOR (enclosed cyl. shell)

FIG 7.52E

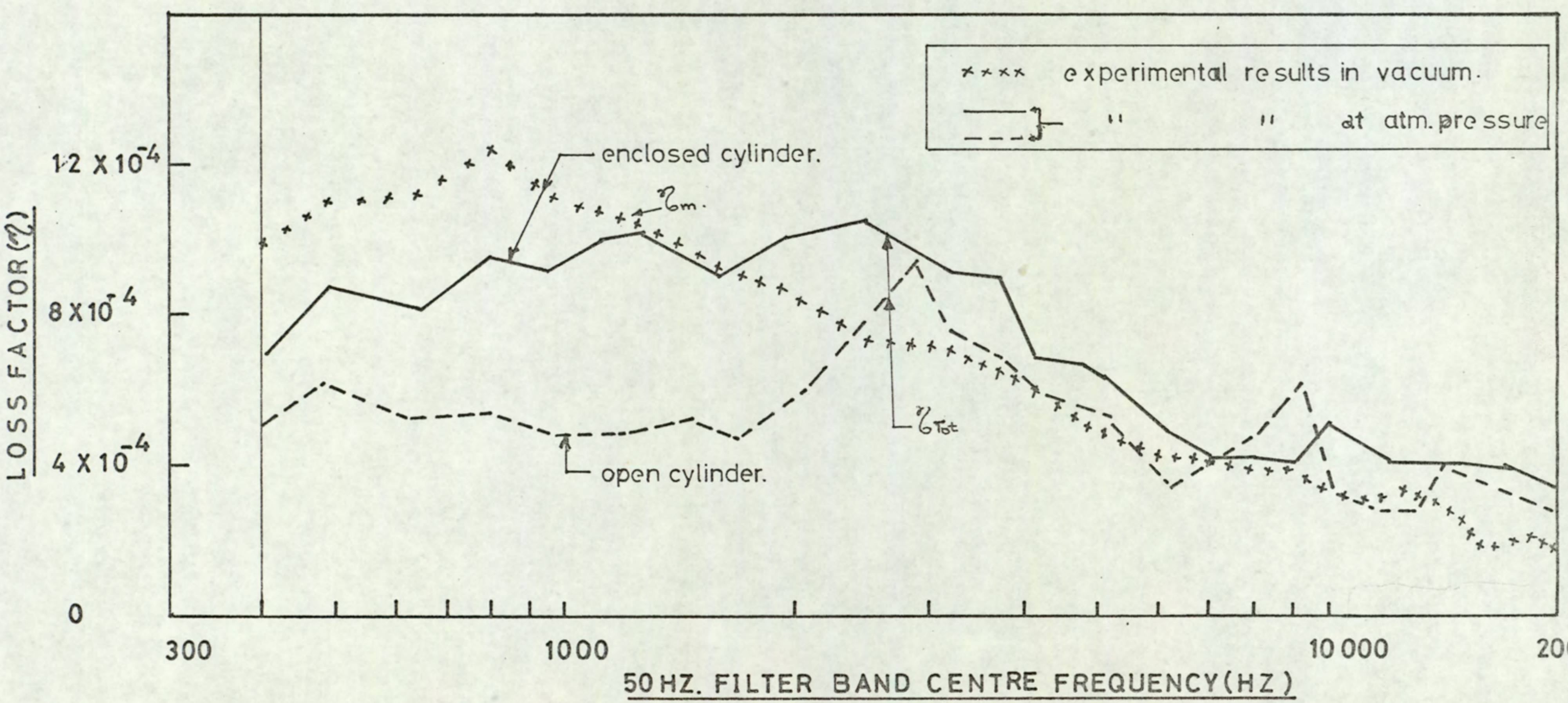

EFFECT OF DIFFERENT ROOM AND CYLINDER CONDITIONS ON CONTRIBUTION TO STRUCTURAL LOSS-FACTOR

FIG. 7·53A

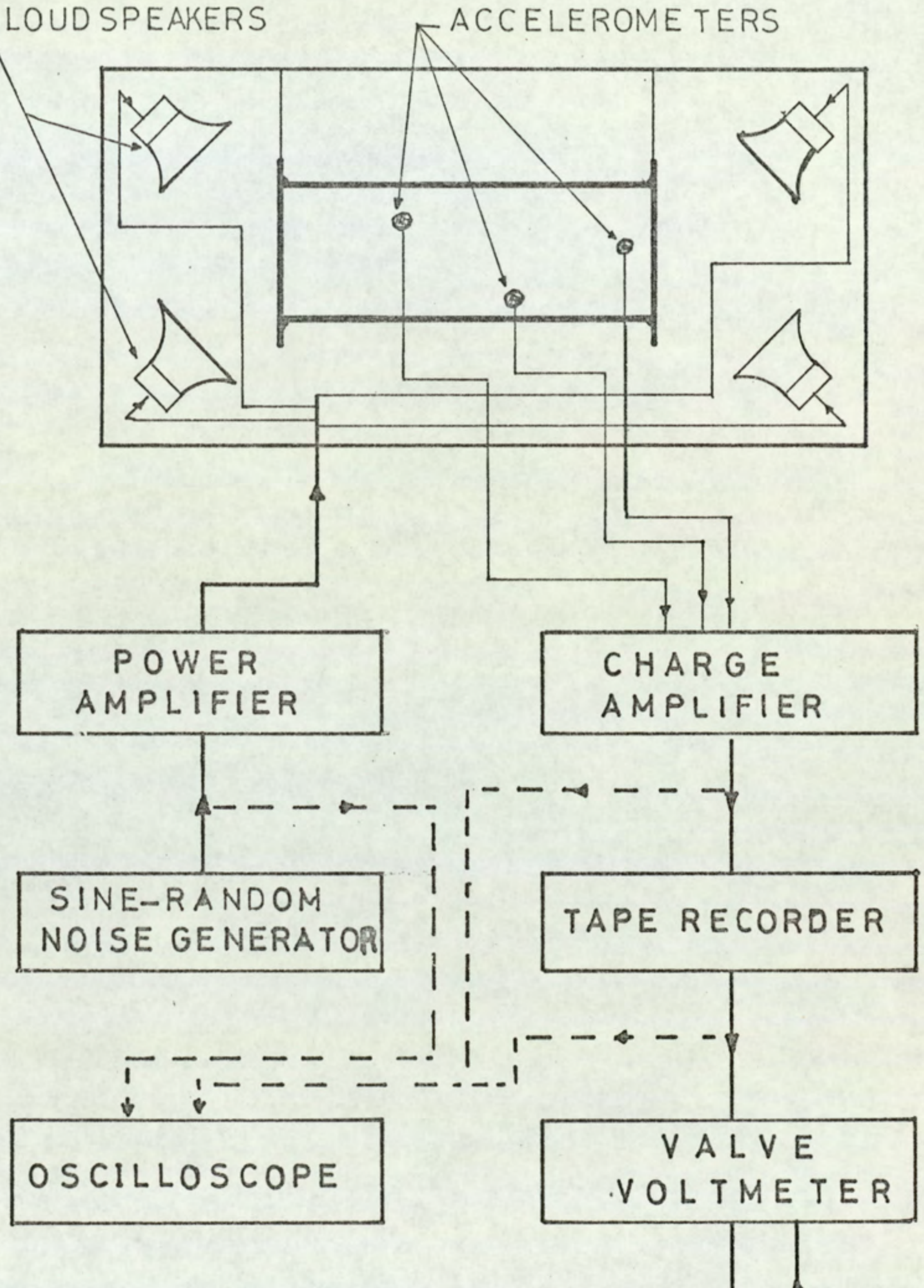

BLOCK DIAGRAM OF THE INSTRUMENTATION

FIG 7·53B

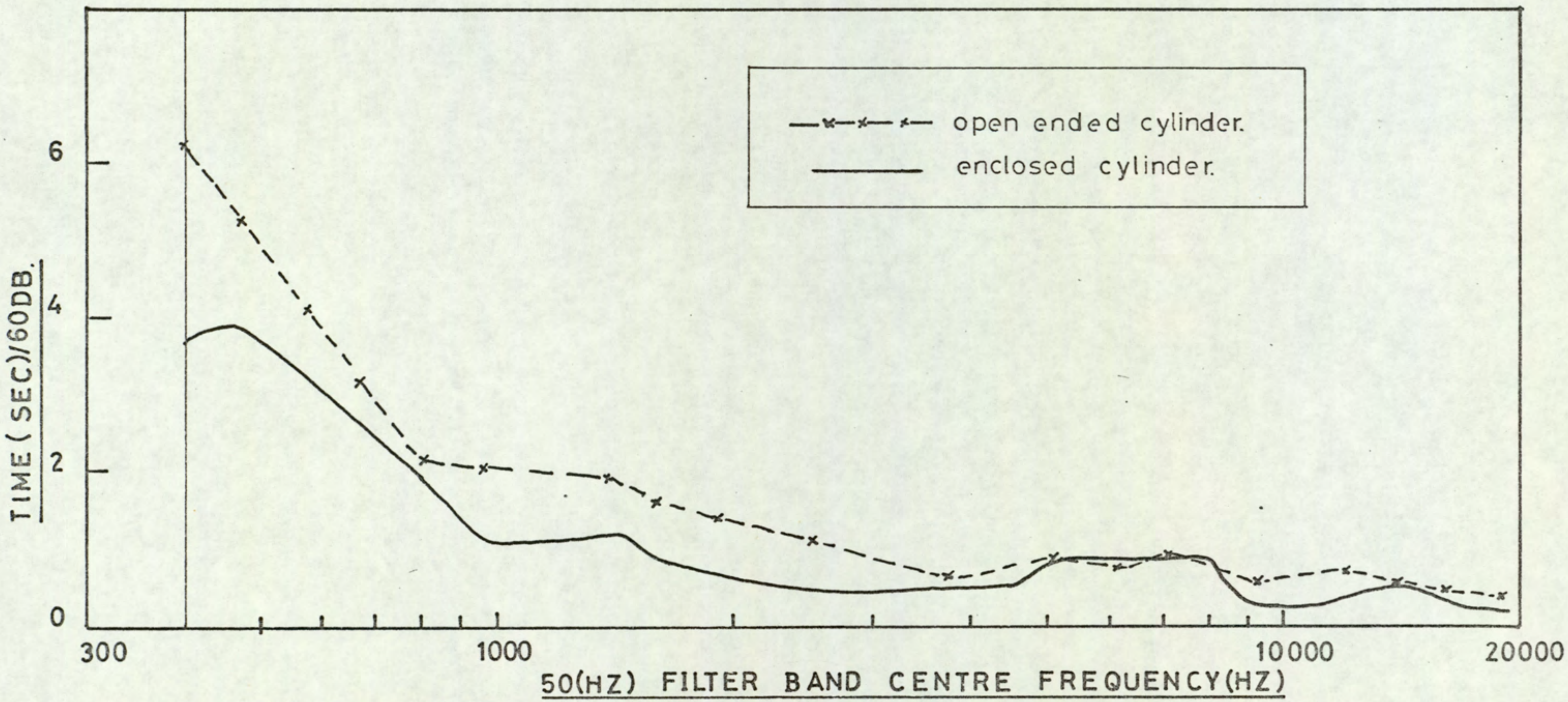

EFFECT OF DIFFERENT CYLINDER CONDITIONS ON CONTRIBUTION TO DECAY TIME WHEN ACOUSTICALLY EXCITED

FIG 7.53 C

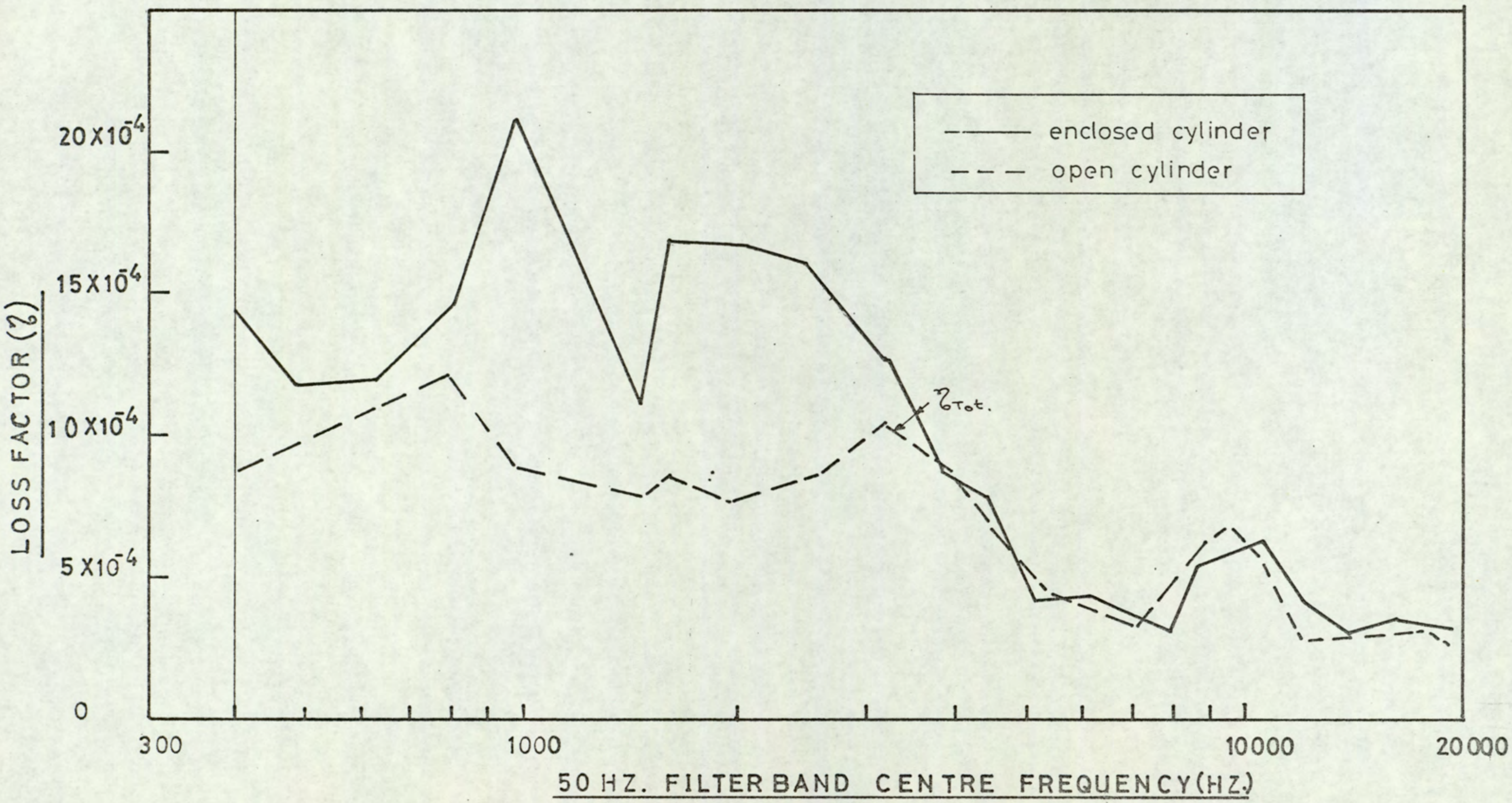

EFFECT OF DIFFERENT CYLINDER CONDITIONS ON CONTRIBUTION TO STRUCTURAL LOSS-FACTOR WHEN ACOUSTICALLY EXCITED

FIG 7.53D

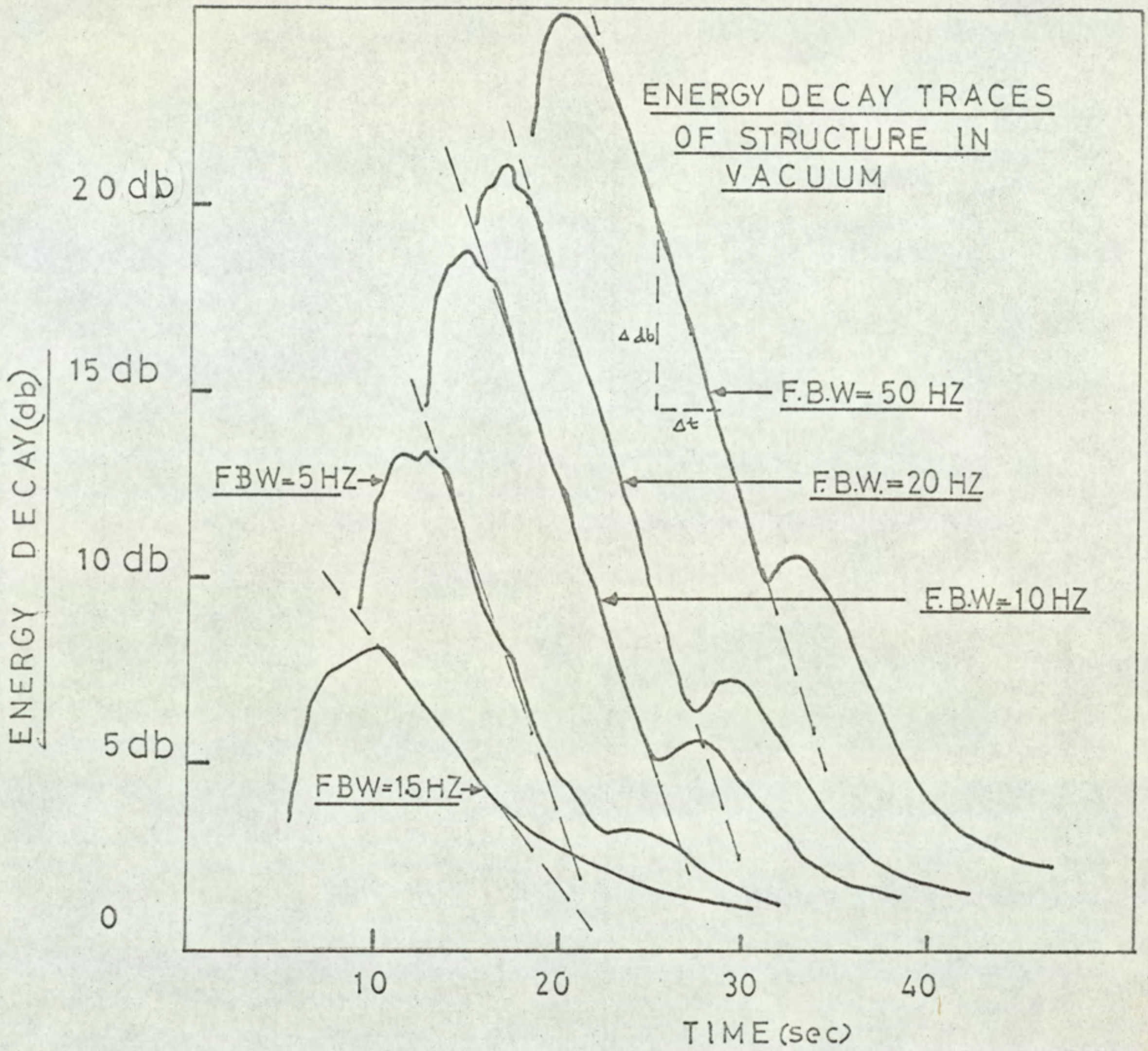
ENERGY DECAY TRACES
OF STRUCTURE IN
VACUUM
20 db
15 db
10 db
5 db
0
ENERGY DECAY (db)
F.B.W= 50 HZ
F.B.W.= 20 HZ
F.B.W= 10 HZ
FBW= 5 HZ
FBW=1.5 HZ
Δdb
Δt
10
20
30
40
TIME (sec)

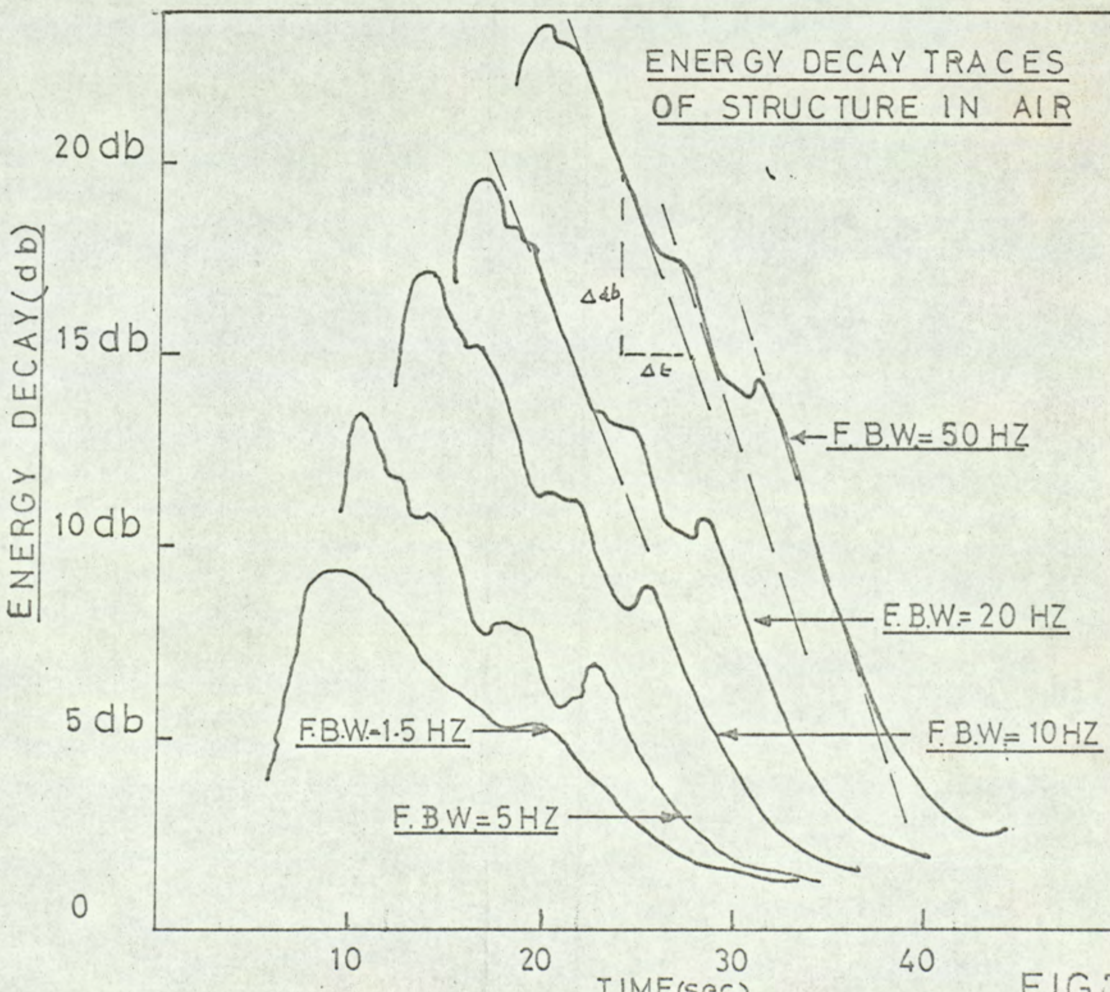
ENERGY DECAY TRACES
OF STRUCTURE IN AIR
20 db
15 db
10 db
5 db
0
ENERGY DECAY (db)
F. B.W= 50 HZ
F. B.W= 20 HZ
F. B.W= 10 HZ
F.B.W-1.5 HZ
F. B.W= 5 HZ
Δdb
Δt
10
20
30
40
TIME (sec)

FIG 7.62B

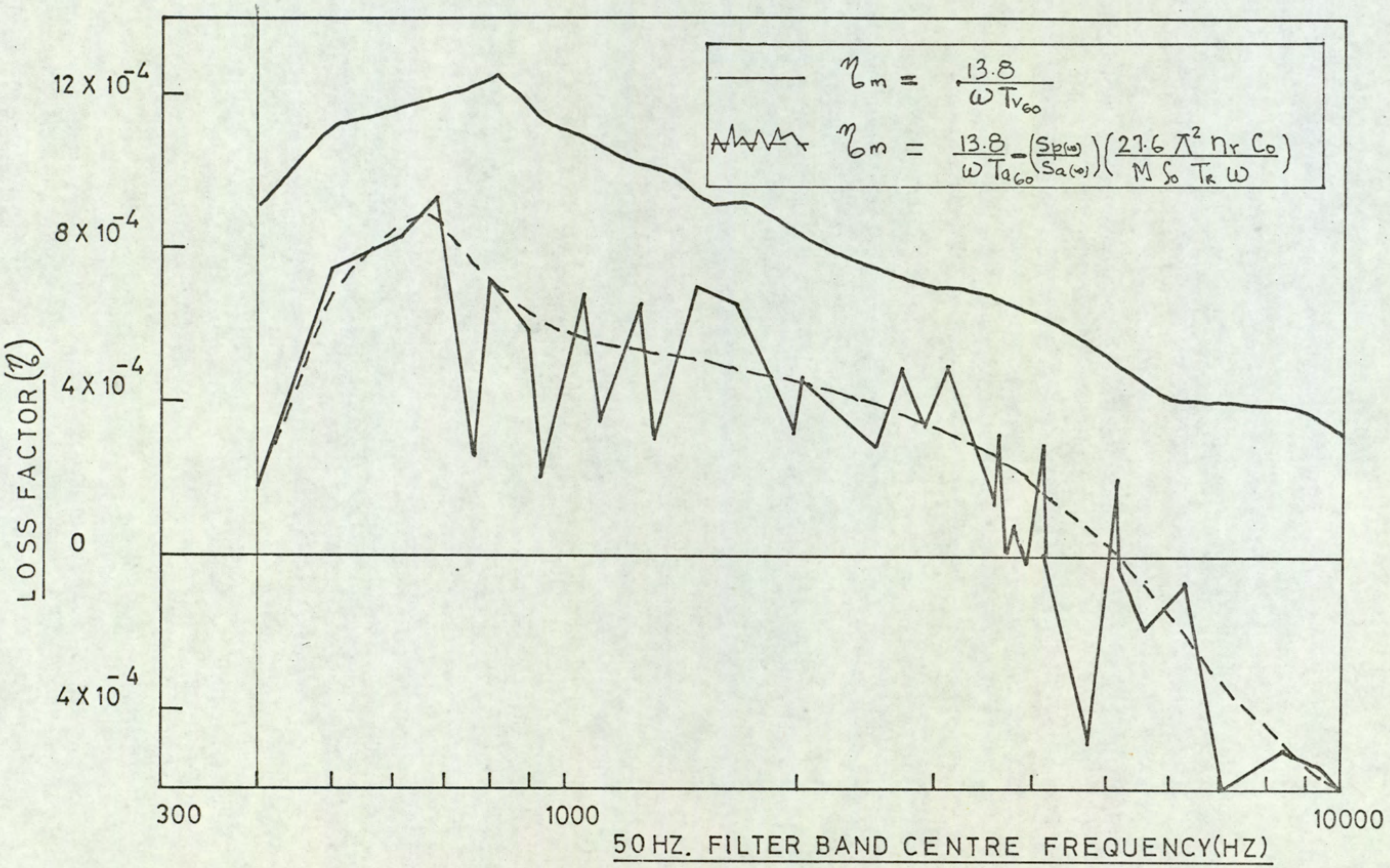

MECHANICAL LOSS FACTOR

FIG 7.63A

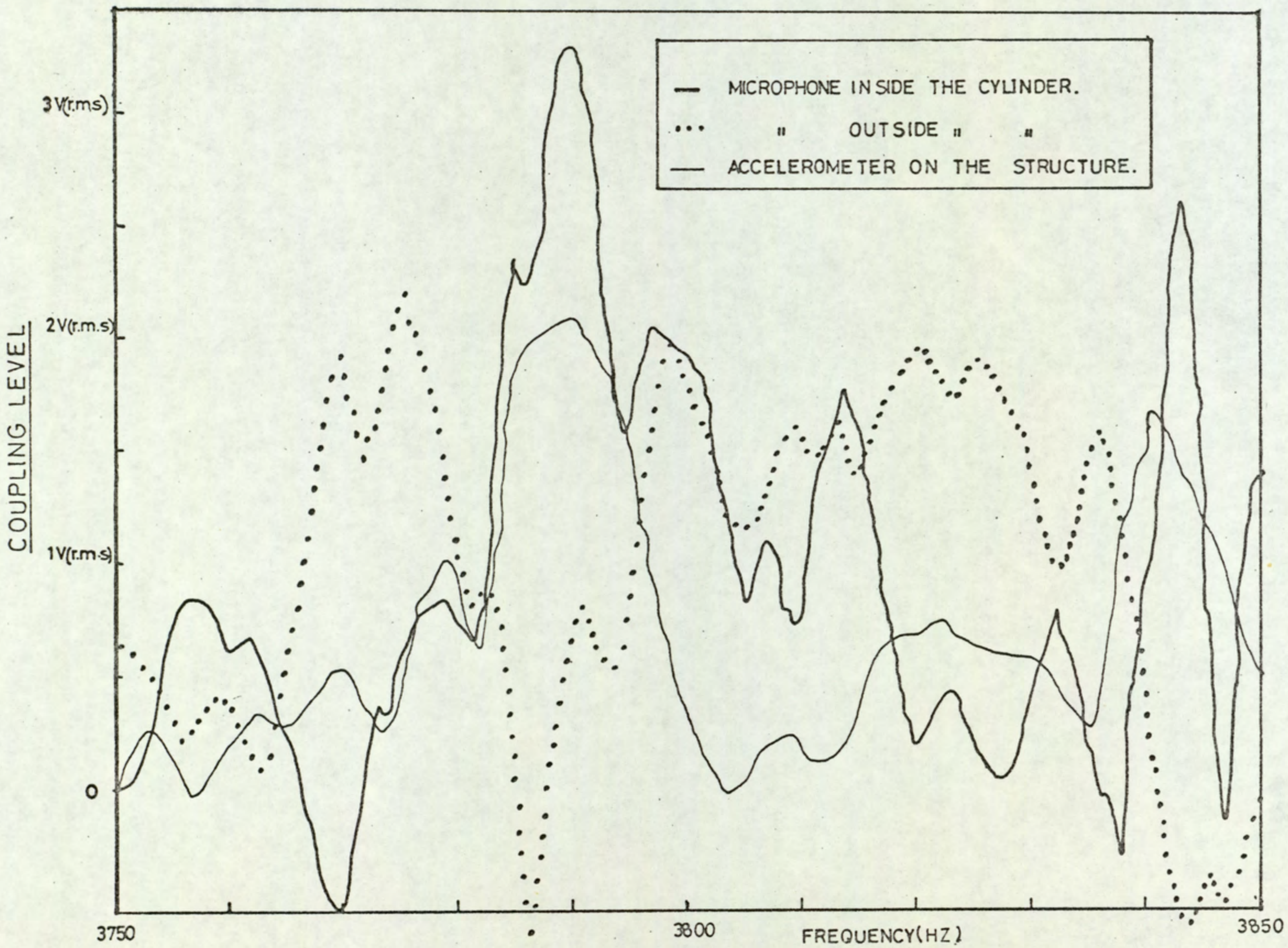

COUPLING BETWEEN ACOUSTIC AND STRUCTURAL MODES FIG 7.9A

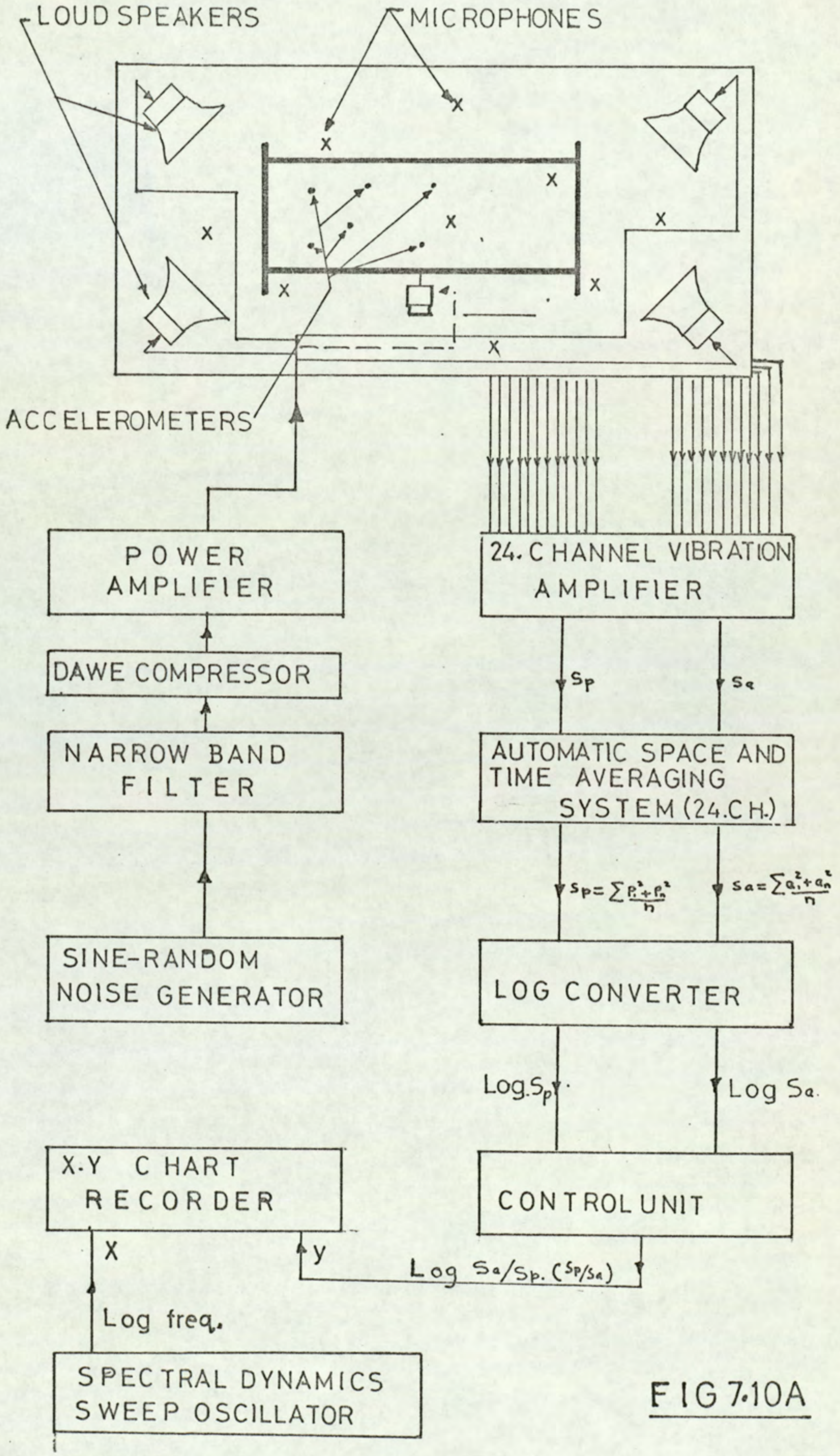

FIG 7.10A

BLOCK DIAGRAM OF THE INSTRUMENTATION

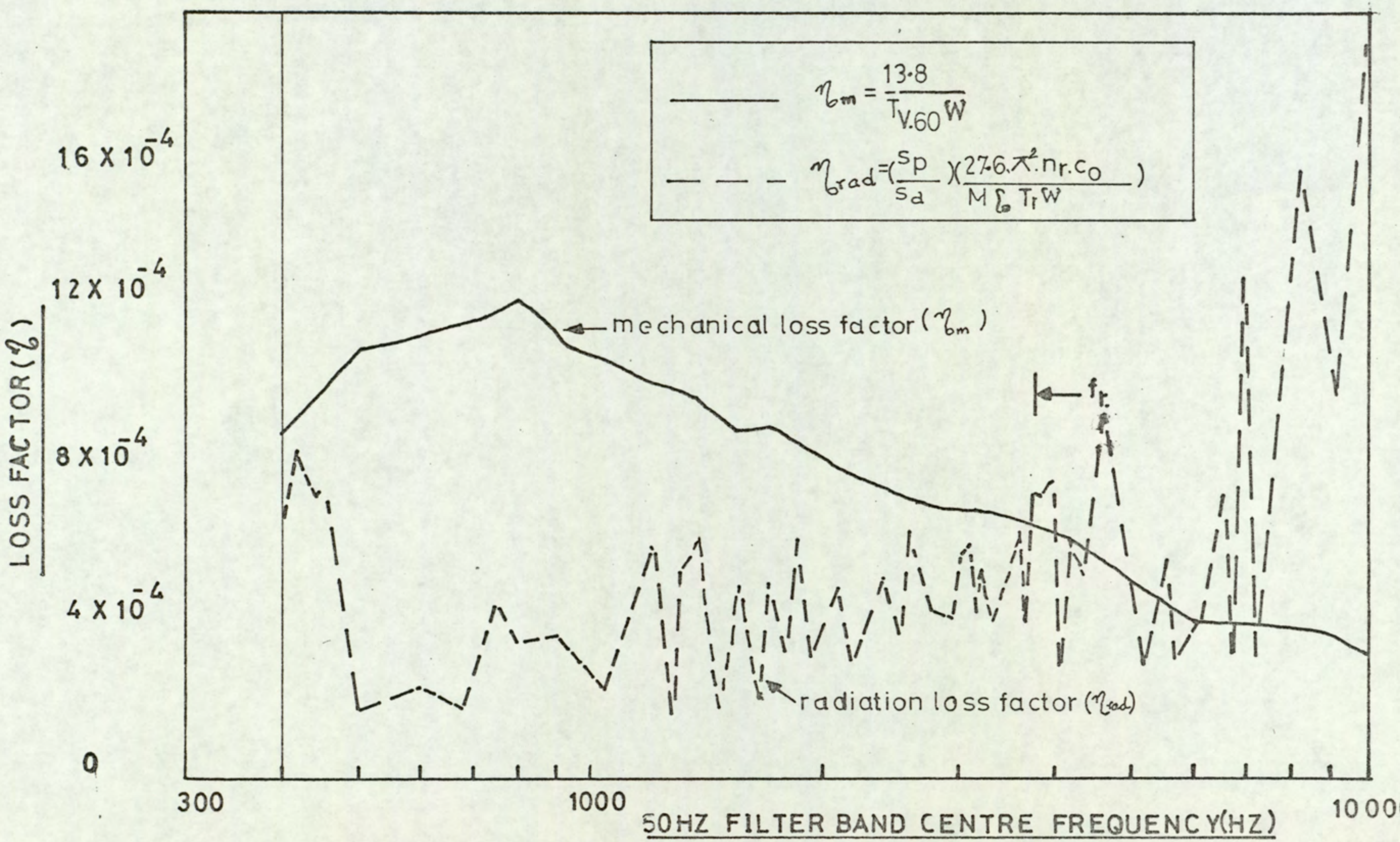

MECHANICAL AND RADIATION LOSS FACTORS IN FLANGED CYLINDRICAL SHELL

FIG 7.10B

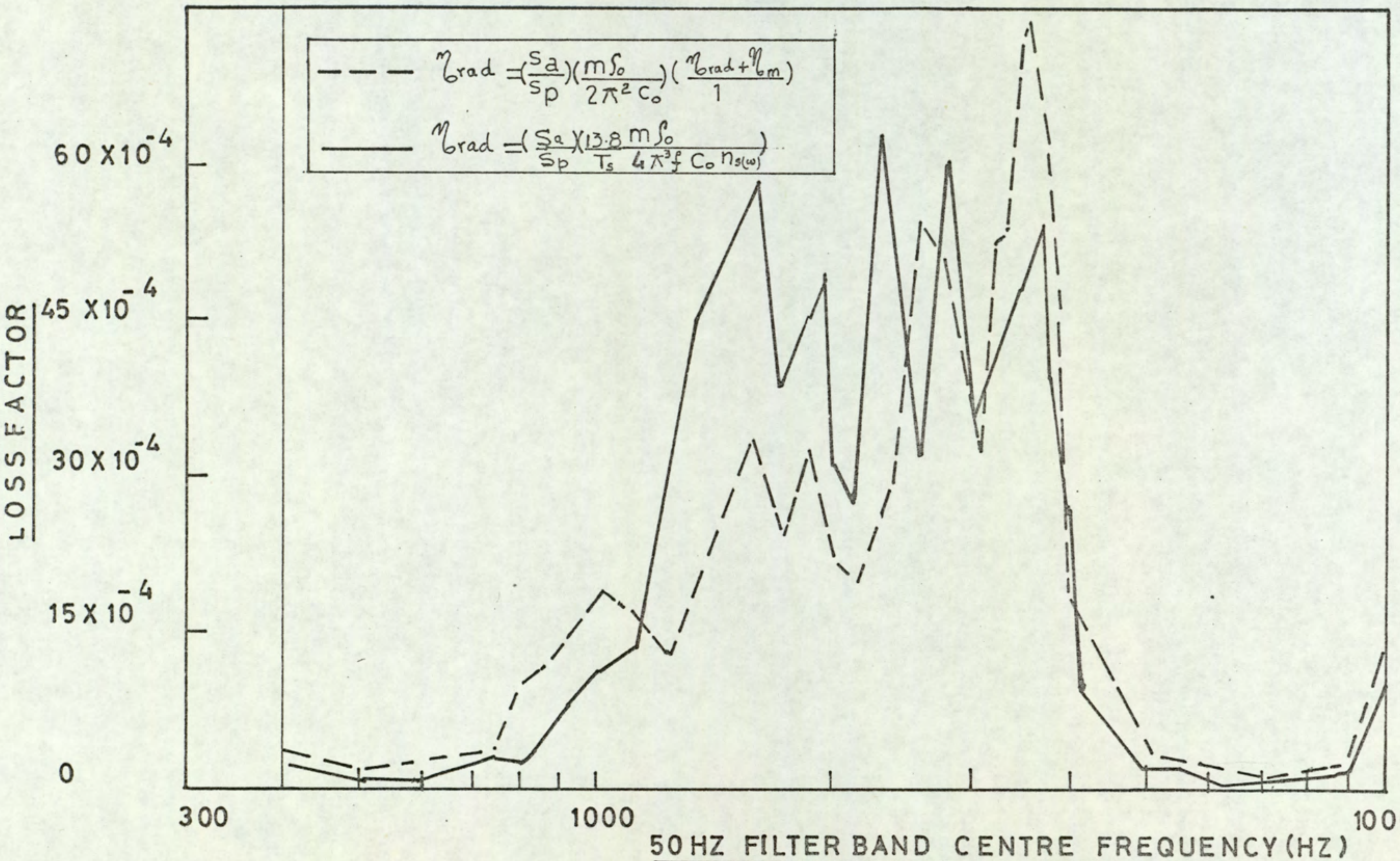

RADIATION LOSS FACTOR IN FLANGED ENCLOSED CYL. SHELL WHEN ACOUSTICALLY EXCITED

FIG 7.102A

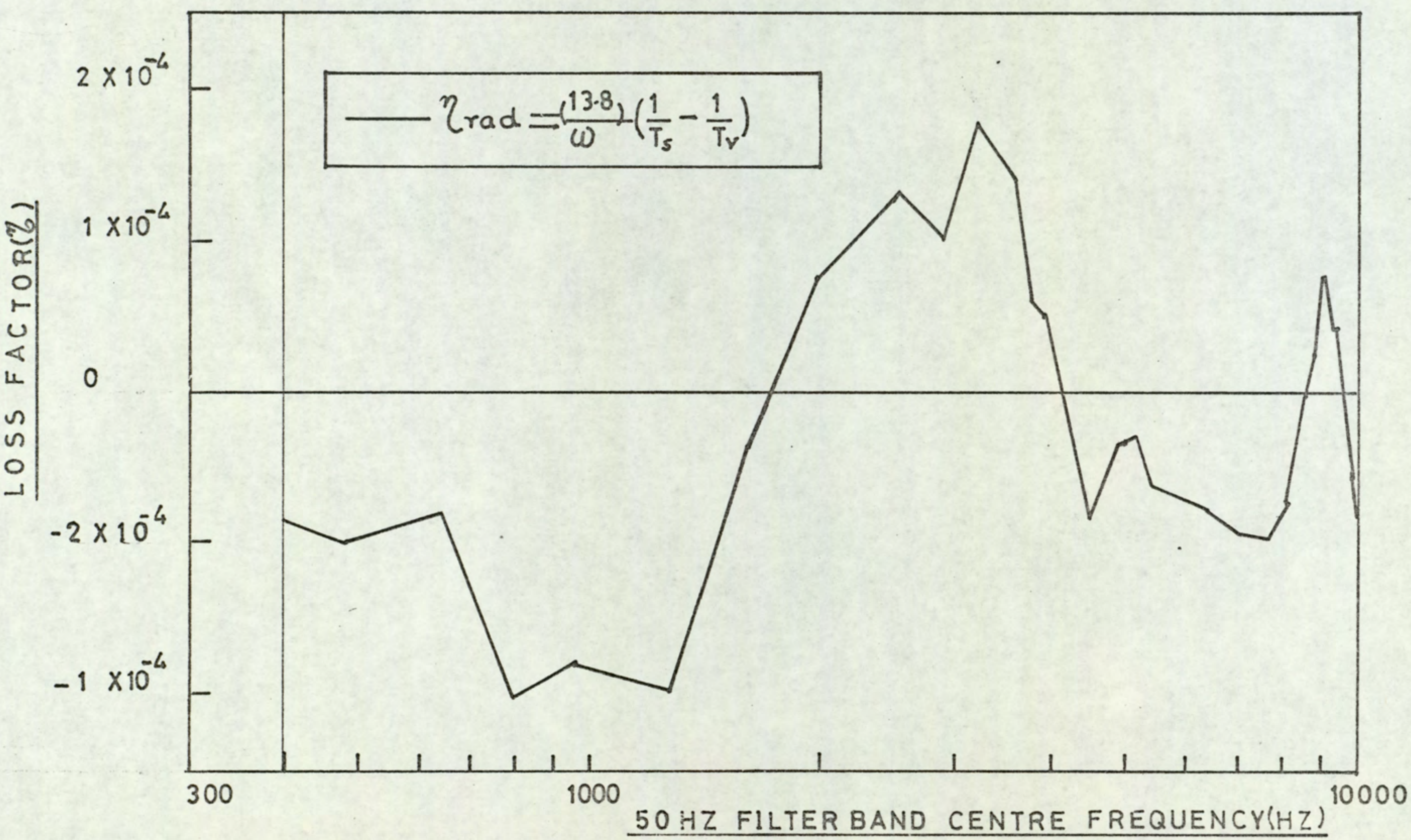

RADIATION LOSS FACTOR IN FLANGED ENCLOSED CYLINDRICAL SHELL FIG 7.103A

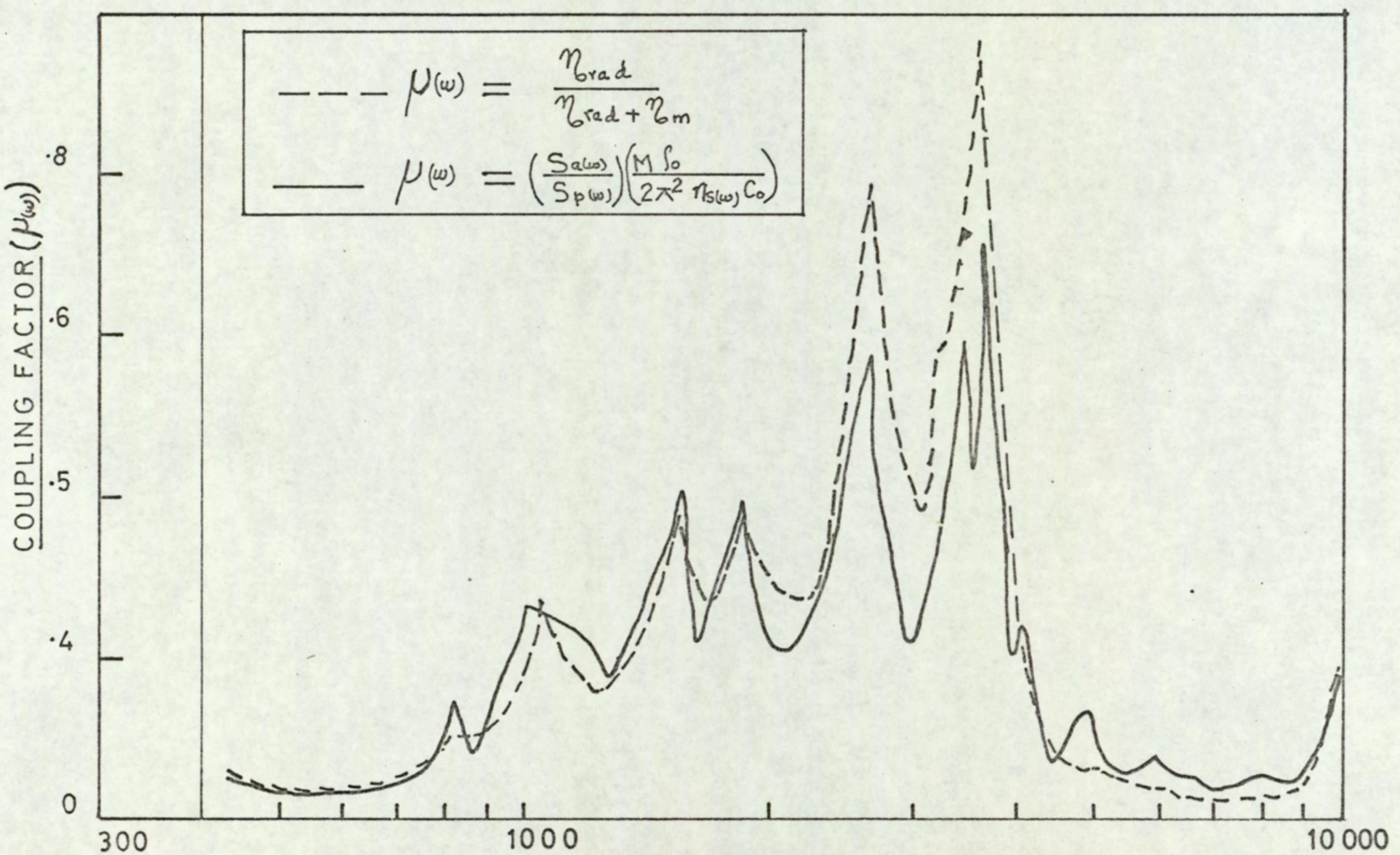

COUPLING FACTORS FOR FLANGED ENCLOSED CYLINDRICAL SHELL FIG 7.11B

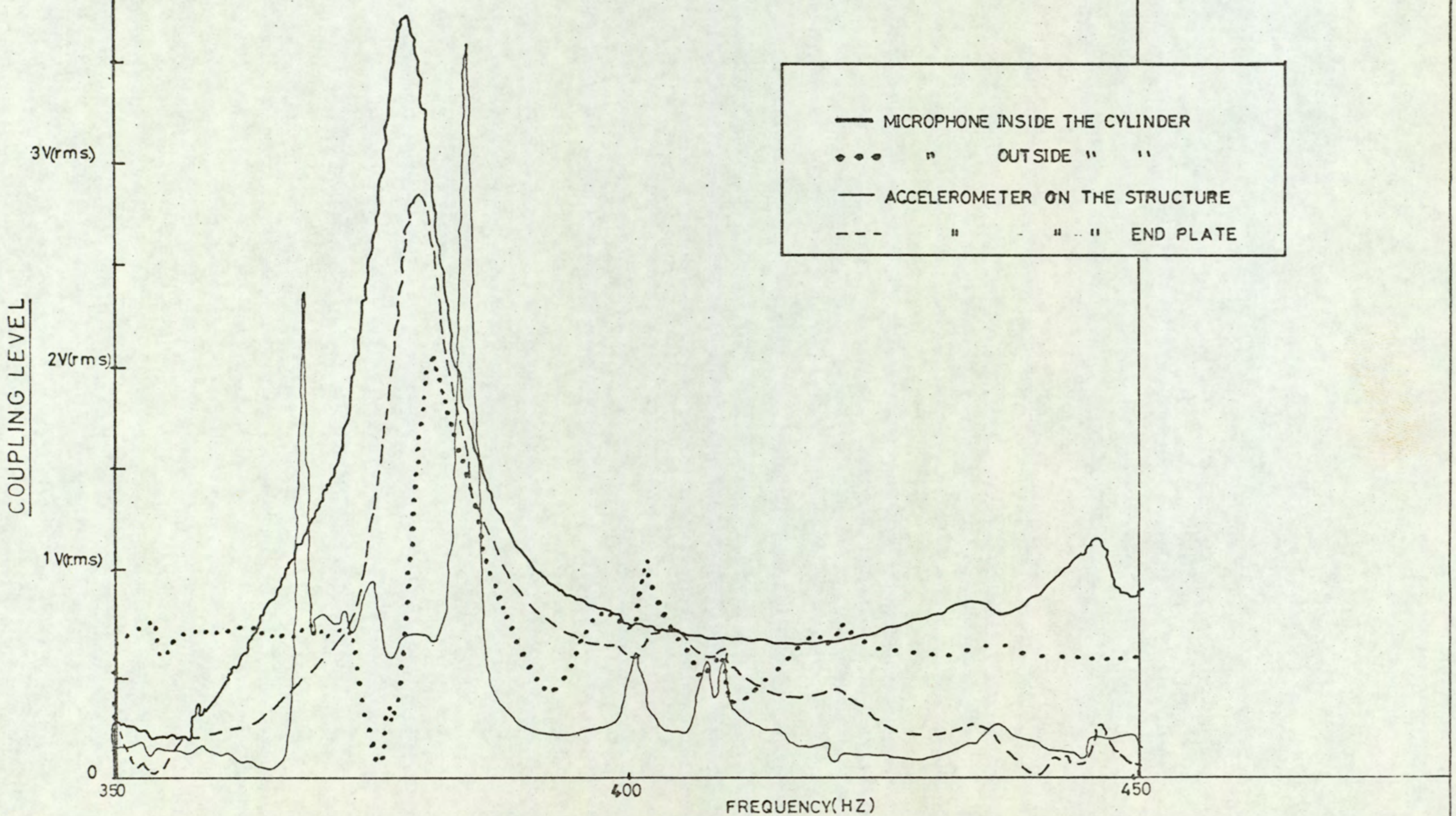

COUPLING BETWEEN ACOUSTIC, STRUCTURAL AND ENDPLATE MODES FIG 7.12A

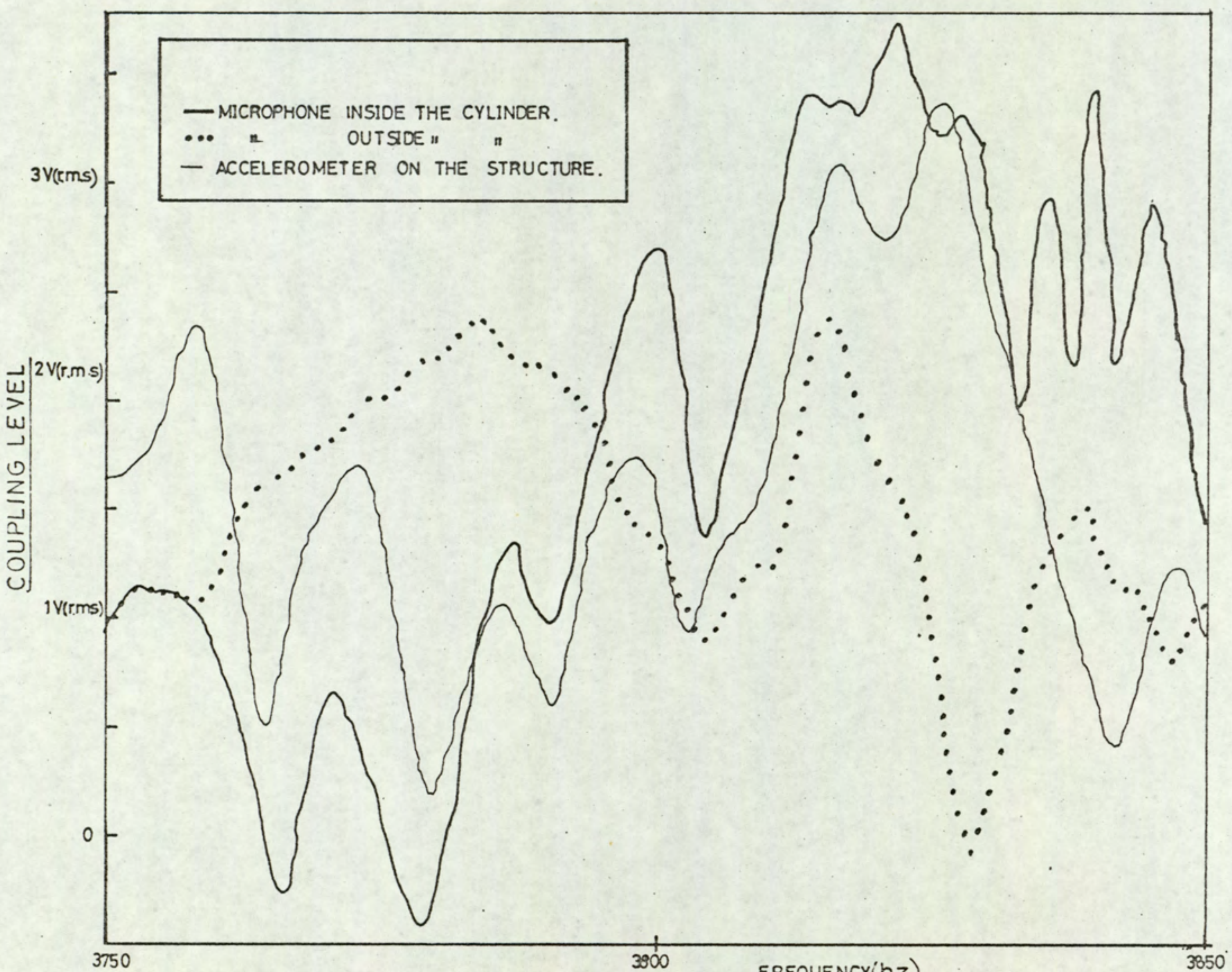

COUPLING BETWEEN ACOUSTIC AND STRUCTURAL MODES WITH NON-REVERBERANT END CONDITION.

FIG 7.12B

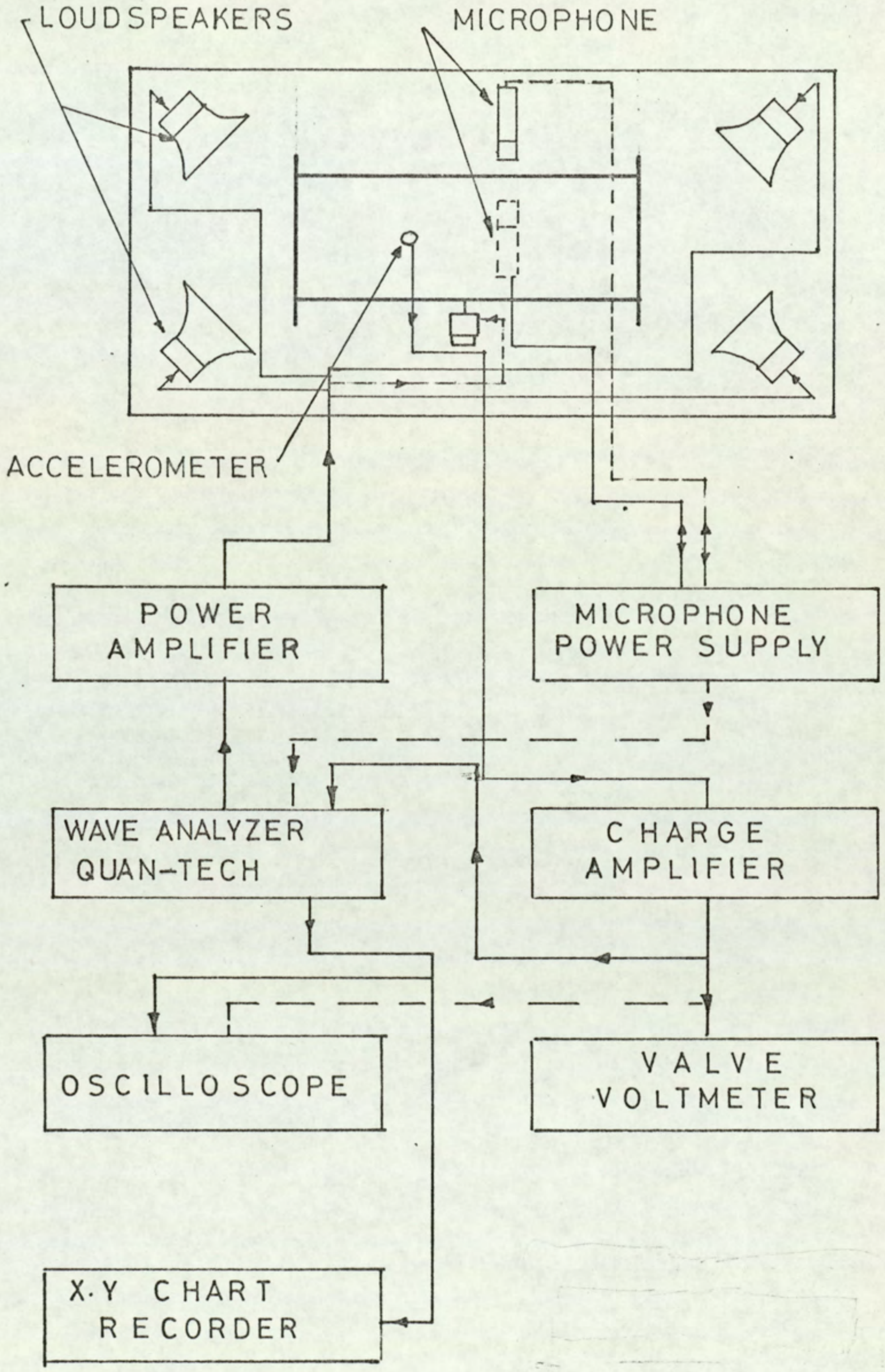

BLOCK DIAGRAM OF THE INSTRUMENTATION

FIG 7.12C

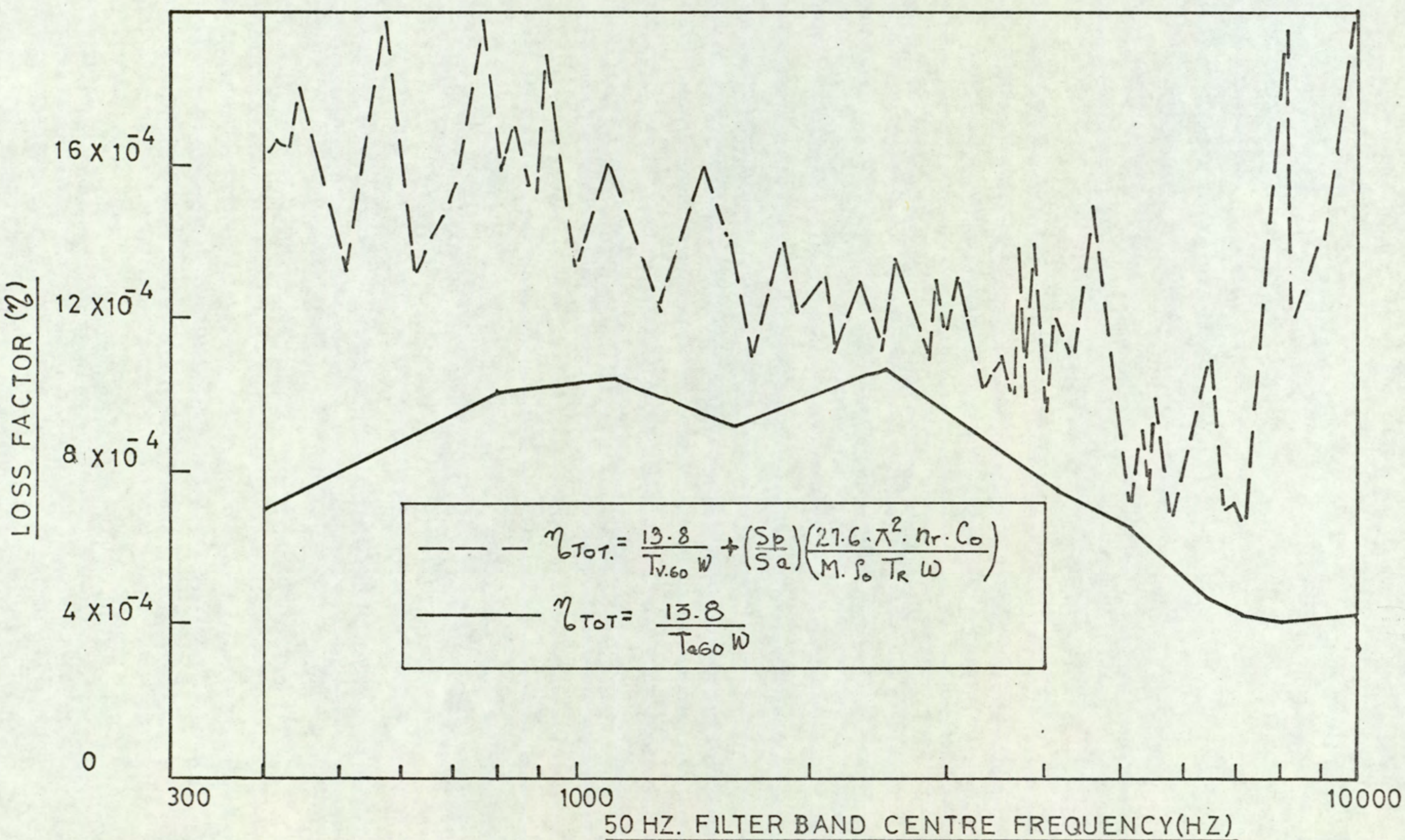

TOTAL LOSS-FACTORS IN FLANGED CYLINDRICAL SHELL

FIG 7.13A

$$\eta_m = \frac{13.8}{T_v\,\omega}$$

$$\eta_m = \frac{13.8}{T_a\,\omega} - \frac{S_{p(\omega)}\,26.6\,\pi^2\,n_{r(\omega)}\,C_o}{S_{a(\omega)}\,M_s\,T_R\,S_o\,\omega}$$

$$\eta_{Tot} = \frac{13.8}{T_a\,\omega}$$

$$\xi = \frac{\delta}{[4\pi^2 + \delta^2]^{1/2}}$$

$$\xi = \left(\frac{\omega_2 - \omega_1}{\omega_n}\right)\frac{1}{\theta_2 - \theta_1}$$

MECHANICAL AND RADIATION
LOSS FACTOR IN FLANGED CYLINDRICAL
SHELL

$$\eta_{rad} = \frac{13.8}{\omega}\left(\frac{1}{T_a} - \frac{1}{T_v}\right)$$

$$\eta_{Tot} = \frac{13.8}{T_v\,\omega} + \underset{\text{DIRECT}}{\eta_{rad}}\ \text{or}\ \underset{\text{IN-DIRECT}}{\eta_{rad}}$$

$$\eta_{rad} = \left(\frac{S_{a(\omega)}}{S_{p(\omega)}}\right)\left(\frac{13.8}{T_s}\,\frac{M_s}{\omega}\right)\left(\frac{S_o}{C_o^2\,\pi^2\,2\,n_{s(\omega)}}\right)$$

$$\eta_{rad} = \left(\frac{S_{a(\omega)}}{S_{p(\omega)}}\right)\frac{M_s\,S_o}{2\pi^2\,n_{s(\omega)}\,C_o}\left(\frac{\eta_{rad} + \eta_m}{1}\right)$$

$$\eta_{rad} = \left(\frac{S_{p(\omega)}}{S_{a(\omega)}}\right)\left(\frac{26.6\,\pi^2\,n_{r(\omega)}\,C_o}{M_s\,T_R\,S_o\,\omega}\right)$$

FIG 7.7A

Chapter 8.

Radiation Properties of Cylindrical Shells to Narrow Band Acoustic Excitation.

8.1. Introduction.

Acoustical properties of complex structures consisting of flat panels have been studied and some of the most useful papers published are given in references 2, 10 and 11. There are many structures in practical use that consist of curved panels and one would expect that in some frequency ranges the flat panel analysis would be adequate for such structures, but in other frequency ranges modifications of flat panel analysis might be necessary. The nature and extent of this modification has been studied by Manning and Maidanik (2) who found that two distinct modifications are necessary. The first is associated with the geometry of the cylinder and the second, with the effect of curvature on the structural vibration. When the effects of curvature on the vibrational field of the cylinder are neglected, the cylinder's radiative properties can be described in terms of an "equivalent plate". The equivalent plate is a flat panel defined such that it has the same dimensions as the cylindrical shell, the vibrational modes in the circumferential direction of the cylinder are symmetric and the acoustical coupling between the various cells is determined by the cylindrical geometry. Because of the symmetry of the circumferential vibrational modes and the geometry in the circumferential direction, the piston modes and the axial strip modes (Appendix 2) whose strip radiators lie along the axial direction are rendered poor radiators. The waves that lie below the critical frequency radiate only if it is scattered by a discontinuity such as a boundary. Since no discontinuity in the circumferential direction of a cylinder exists, no radiation can arise from a wave that travels in this direction if its wavelength is shorter than the acoustic wavelength in the surrounding medium. Thus the equivalent plate formalism takes account only of the radiation from circumferential strip modes that lie along the circumferential direction of the cylinder.

In this Chapter a brief description of the method used by Manning and Maidanik (2) for the determination of radiation efficiency of cylinders is given. The method is then applied to obtain the radiation efficiency of a flanged cylindrical shell. The computed theoretical results are compared with the experimental results.

8.2. Theoretical Consideration.

Basic consideration of the analysis of radiation properties of cylindrical shells, both theoretically and experimentally are based on the modifications of the flat panel theory. The basis of the flat panel theory is an equation derived by Smith (10) which states that the response of a resonant structure to an incoming sound field is governed by the relationship

$$M\langle V^2\rangle = \left[\frac{2\pi^2 C_o}{\rho_o\,\omega^2}\right]\frac{S_p(\omega)}{1}\;\frac{R_{rad}}{R_{TOT}} \qquad 1$$

Thus the structural energy during vibration is given by a constant times the ratio of the re-radiated power from the structure to the total power loss which is the sum of the re-radiated power and the internal dissipation. By defining a suitable mean square velocity, these powers may be defined in terms of the resistances shown in equation (1), from which it can be seen that if the radiation resistance is very large compared to the internal damping ($R_{rad} \gg R_{mech}$) then the modal energy of the structure will come to equilibrium with the modal energy of the acoustic field. (See Chapter 3.). However, when $R_{rad} \ll R_{mech}$, the modal energy of the structure will assume in the steady state condition, a value, a function $\mu(\omega)$ less than the equilibrium value, where

$$\mu(\omega) = R_{rad} \, (R_{mech} + R_{rad})^{-1} \qquad 2.$$

When the structure is a large complex system as shown in fig. 6.42A where many structural modes are present, even in a fairly narrow frequency band, it is not practical to consider the response of each mode individually. It is rather more sensible to consider quantities such as the acceleration spectra of the structure and how they are related to the acoustic field spectra. With the help of some reasonable assumptions regarding the modal energy and the modal density distribution in the vibration field of the structure, the appropriate extension of Smith's equation is made by Maidanik (9).

If two systems having a given number of modes are coupled together then the number of modes in the combined system will usually be equal to the sum of modes in each system, but the coupling may change the specific motion of the system in the sense that the mode of the combined system may have a motion which is common to both systems, and in a given frequency band where some modes of one system and the other may lie, the modes may combine in such a way that the composite modes lie in another frequency band and vice versa. If the systems and their coupling are rather complex, so that the motion of the structure is a complicated combination of all parts of the composite system, then it is statistically as likely that the modes will combine in such a way that the outgoing modes in a given frequency band will be replaced by the others. Consequently, not only the number of modes merely add but also the modal densities add, and this concept may equally well be applied where more than two systems are coupled. If the structure is complex and the coupling between its various parts is such that it induces energy exchange between them, then equipartition of modal energy may be assumed. This would lead to assigning to each part of the structure energy in proportion to the amount of modal density which they contribute to the total modal energy.

8.21. Radiation Properties of cylindrical shell (experimental).

The total resistance (Rrad + Rmech) is defined by,

$$R_{TOT} = \frac{Pd}{\langle V_s^2 \rangle} = Rrad + Rmech$$

Where Pd is the total power dissipated by the structure including radiation.

The total energy stored in the system (in the steady state condition) is given by,

$$E_{TOT} = M\langle V_s^2\rangle \qquad 4$$

The rate of energy dissipation by the structures given by

$$Ps = \beta_s E_{TOT}, \qquad 5$$

where βs is the energy decay constant of the structure and is given by

$$\beta s = \frac{13.8}{Ts} \qquad 6$$

hence $$R_{TOT} = \left(\frac{13.8}{Ts}\right)M \qquad 7$$

Under the equipartition of energy, the expression for the coupling factor from chapter(3)is,

$$\mu(\omega) = \left(\frac{Sa(\omega)}{Sp(\omega)}\right) \Gamma^{-1}(\omega), \qquad 8$$

With $$\Gamma(\omega) = \left[2\pi^2 \ (n_s(\omega) /M)\right] C_o/\rho_o \qquad 9$$

By combining equations 2, 7, 8 and 9, the expression for the radiation resistance (Rrad) when the structure excited indirectly is given by,

$$Rrad = \left[\frac{Sa(\omega)}{sp(\omega)}\right] \left[\left(\frac{13.8}{Ts}\right) \left(\frac{M^2}{2\pi^2}\right)\right]\left[\frac{1}{ns(\omega)}\right] \frac{\rho_o}{co} \qquad 10$$

In the case of the structure being driven mechanically by external random forced and the acoustic field being generated by the structure only, the relation for the radiation resistance (Rrad) is from chapter(3)and expressed as:

$$Rrad = \frac{Sp(\omega)}{Sa(\omega)} \ 2\pi^2 \ \beta_R \ n_R(\omega) \ Co/\rho_o \qquad 11$$

Where β_R is the energy decay constant of the room and is given by

$$\beta_R = \frac{13.8}{T_R} \qquad 12$$

By combining the equations 11 and 12, the expression for the radiation resistance is as follows:-

$$\text{Rrad} = \left[\frac{Sp(\omega)}{Sa(\omega)}\right] \left[\frac{13.8}{T_R} \quad \frac{2\pi^2 \quad n_R(\omega)}{1}\right] \frac{(Co)}{(\rho_o)} \qquad 13$$

which gives the radiation resistance in terms of the pressure field spectral density, the acceleration spectral density and the room constant.

The radiative properties of a structure consisting of flat or curved panels is described in terms of the radiation efficiency, or, equivalently, in terms of the radiation loss factor (ηrad (Reference 48). These are related by

$$\eta\text{rad} = \frac{\rho_o . C_o \sigma}{\omega \, m_S} = \frac{\text{Rrad}}{\omega \, M} \qquad 14$$

By combining the equations 10 and 14 gives the expression for the radiation efficiency as (Indirect Excitation)

$$\sigma = \left(\frac{Sa(\omega)}{Sp(\omega)} \right) \left(\frac{13.8}{T_S} \right) \left(\frac{Mms}{2\pi^2 Co^2} \right) \left(\frac{1}{n s(\omega)} \right) \qquad 15$$

and by combining the equations 13 and 14 gives the expression for the radiation efficiency as (Direct Excitation).

$$\sigma = \left(\frac{Sp(\omega)}{Sa(\omega)}\right) \left(\frac{13.8}{Tk}\right) \left(\frac{2\pi^2}{\rho_o^2}\right) \left(\frac{m_s}{M}\right) \left(\frac{n_R(\omega)}{1}\right) \qquad 16$$

The total decay time Ts and the mechanical decay time Tv of the structure were measured (see chapter 7).

8.22. Radiation Properties of cylindrical shell (theoretical)

The effects of curvature on the vibrational motion of a cylinder has been analysed by Smith (10), Arnold and Warburton (14) and many other investigators (chapter 2). Smith showed that the curvature tends to increase the flexural-wave speeds, especially for modes of low circumferential mode numbers. This increase in wave speed is most pronouced below the ring frequency and tapers off as the frequency increases above and beyond the ring frequency. This increase causes a corresponding increase in the resonance frequencies of the cylinder since the wavelengths are fixed by the geometry and the boundary conditions only.

The expressions derived by Manning and Maidanik (2) for the vibration field of a cylindrical shell are based on the equivalent plate formalism and that near and above the ring frequency ($f > fr$), the radiation efficiency of the equivalent plate and that of the cylinder it represents are essentially the same. For the equivalent plate the resonance frequencies are governed by the expression

$$\nu^2 = \beta^2 a^4 k^4 \qquad 17$$

while those of the cylindrical shells are governed by the expressions derived by He (13),

$$\nu^2 = \beta^2 a^4 k^4 + (1 - \mu^2) \ k_y / k)^4 \qquad 18$$

Where, $\beta = \dfrac{h}{2\sqrt{3}\, a} = \dfrac{Co^2}{C_L^2} \dfrac{1}{Vg}$, $C_L = f_r \pi 2\, a = \left(\dfrac{E}{\rho_s (1-\mu^2)}\right)^{1/2}$

$Vg = \dfrac{fg}{fr} = \dfrac{Co^2}{C_L^2} \dfrac{2\sqrt{3}\, a}{h} = \dfrac{Co^2}{C_L^2 \beta}$,

$k = (k_x^2 + k_y^2)^{1/2}$, $\quad n = k_x a$,

$m = k_y \left(\dfrac{\ell}{\pi}\right)$, $\quad \gamma = \dfrac{a}{\ell}$, $k_y = \dfrac{\pi m}{}$,

$\nu = \dfrac{f}{fr} = \dfrac{2\pi a f}{C_L} = \dfrac{\omega a}{C_L}$ $\quad k \ \dfrac{n}{a} = \dfrac{n}{L\gamma}$,

$$k^2 = \left(\frac{n}{a}\right)^2 + \left(\frac{\pi m}{L}\right)^2 = \frac{1}{L^2}\left(\frac{n^2}{\gamma^2} + \pi^2 m^2\right),$$

By substituting the above expressions in equation 17, the normalised resonance frequency equation for the equivalent plate is,

$$\left.\begin{aligned} \nu_P &= \left[\beta^2 \gamma^4 \left[\frac{n^2}{\gamma^2} + \pi^2 m^2\right]^2\right]^{1/2} \\ \text{or } &= \left[\frac{Co^4}{C_L^4}\frac{\gamma^4}{\nu_g^2}\left[\frac{n^2}{\gamma^2} + m^2\pi^2\right]^2\right]^{1/2} \end{aligned}\right\} \quad 19$$

and for the cylindrical shell is,

$$\left.\begin{aligned} \nu &\simeq \left[\beta^4\gamma^4\left[\frac{n^2}{\gamma^2} + m^2\pi^2\right]^2 + \left[1-\mu^2\right] m^4\pi^4\left[\frac{n^2}{\gamma^2} + \pi^2 m^2\right]^{-2}\right]^{1/2} \\ \nu &\simeq \left[\frac{C_o^4}{C_L^4}\frac{\gamma^4}{\nu_g^4}\left[\frac{n^2}{\gamma^2} + m^2\pi^2\right]^2 + \left[1-\mu^2\right] m^4\pi^4\left[\frac{n^2}{\gamma^2} + m^2\pi^2\right]^{-2}\right]^{1/2} \end{aligned}\right\} \quad 20$$

The circumferential strip modes that radiate in the equivalent plate formalism satisfy the relations,

$$ak_x \leq \left(\frac{C_L}{Co}\right)\nu \quad 21$$

When the curvature effects are taken into account, equation (20) still represents the condition that must be satisfied by a circumferential strip mode but because of the curvature there may occur modes that satisfy the conditions, $k_o > k$ (where $k_o = \frac{2\pi Co}{f}$) even though $f < fr < fg$ and these modes that satisfy the relation in addition to that stated in equation (20)are AF modes and is given by the expression,

$$ak_x \leq \frac{C_L}{Co}\nu \; R_e\left[\left\{(1-\mu^2)^{1/2} - \nu\left(1-\left(\frac{\nu}{\nu_g}\right)^2\right)^{1/2}\right\}^{1/2}\right] \quad 22$$

For computing the radiative properties, a digital computer program appendix (5) was written for an ICL 1905 computer to solve equations 19 to 22 for the test cylinder parameters given in chapter 6.

The results of this computation are given in a plot of fig. 8.2(A,B) as the normalised circumferential wave number $ak_x(n)$ and as a function of normalised frequency for various values of the axial-mode numbers (m). In the plot of fig. 8.2A, the light dashed lines represent the loci of modes of equal axial-mode numbers in the equivalent plate (equation 12). The triangle gives the locations of some of the modes in the equivalent plate. The light solid lines represent the loci of modes of equal axial-mode numbers in the cylinder (equation 20). The circles give the locations of some of the modes in the cylinder.

The solution of equation (21) with equality sign is plotted in fig. 8.2A. and is represented by the heavy dashed lines. Modes that lie to the right of these lines and to the left of the lines of constant frequency ν_g $\left(\nu_g = \frac{f_g}{f_r} \right)$ are circumferential-strip modes in the equivalent plate. The plot of equation (22) with the equality sign is represented in fig. 8.2A by the heavy, full line. Modes that are enclosed by these curves are A F modes.

The radiation efficiency in the range of frequency where acoustically fast modes occur is given by

$$\sigma = n_f / n_{tot} \qquad 23$$

Where n_f is the number of acoustically fast modes in the frequency band of interest and n_{tot} is the total number of modes in the same frequency band.

The equivalent plate formalism takes account only of the radiation from circumferential strip modes that lie along the circumferential direction of the cylinder and thus the radiation efficiency is given by the expression,

$$\sigma = n_{cs} \cdot \bar{\sigma}_{cs} \; / \; n_{tot} \qquad 24$$

Where n_{cs} is the number of circumferential strip modes and $\bar{\sigma}_{cs}$ is the average modal radiation efficiency of these nodes

Equation (22) is derived on the assumption that the acoustically fast modes have modal-radiation efficiencies equal to unity. The radiation efficiency of the test cylinder was thus calculated using equation (23 and (24) and the result of this computation is shown in fig. 8.3C

8.3. Experimental Techniques used for the Measurement of Radiation Efficiency of the Flanged Cylindrical Shell.

The procedure adopted in these experiments follows closely the procedure that was used in the measurements of $Sa(\omega)/Sp(\omega)$ and $Sp(\omega)/Sa(\omega)$ explained in chapter 7 part (2). The experimental flow diagram and the function of various instruments is given in chapter 4 section 4.7. (iii). The direct determination of the radiation efficiency refers to measurements conducted on the mechanically driven cylinder and the use of equation (16) for the computation. The indirect determination refers to the measurements conducted on the response of the specimen to a reverberant sound field and the use of equation (15) for the computation. The results of the $Sp(\omega)/Sa(\omega)$ and $Sa(\omega)$ are shown in figs. 8.3A and 8.3B and the radiation efficiency computed from the responses are given in fig. 8.3C. The modal densities and the decay times of the room and the structure were determined as explained in previous chapters.

8.4. Discussion of the Results.

The most significant feature of the comparison shown in fig. 8.3C between analytical results obtained from exciting the structure directly and indirectly is the deviation of the latter from the former by 4 dB at the ring frequency, 5.5 dB at the critical frequency and on an average of 6.5 dB between 800 Hz and 3.5 k Hz. The calculation of the ring frequency, $\left[\frac{E}{\rho_o (1-\mu^2)}\right]\left[\frac{2\pi a}{1}\right]^{-1}$, and its accuracy depended on the material constants and the diameter of the cylinder while the accuracy of the critical frequency, $\frac{Co^2 \sqrt{3}}{\pi h}\left[\frac{E}{\rho (1-\mu^2)}\right]^{-1/2}$, depended on the material constants, the square of the speed of sound and the material thickness. A slight change in these parameters could lead to deviation in the calculated values for ring and critical frequencies.

The value obtained for the radiation efficiency from the experimental data and theoretical computation, all show higher values at 3.450 k Hz and 9.250 k Hz. This indicates that the statistical energy approach based on well thumbed assumptions for obtaining the radiation properties of the cylindrical shells are in good agreement with the equivalent plate formalism. The modal density obtained from the theoretical computation in the 50 Hz frequency band showed that maximum number of modes were excited in the frequency range of 3.450 k Hz to 3.550 k Hz. This means that a good coupling between the acoustic field and the structure existed in this region giving rise to modal energy flow from one set of modes to the others. At and near the critical frequency on the other hand, there were not as many structural modes that were excited but the readiation efficiency is quite high showing that many acoustic modes do not necessarily have to couple well with the individual structural modes to render energy flow from fluid to the structure.

To obtain the graph in figs. 8.3 (A,B,C) the cylindrical shell was excited in frequency bandwidths of 50 Hz. If a wider frequency bandwidth (e.g. 200 Hz, 1/3 octave) had been used, the graph would have been much smoother because we would then be averaging over a wider frequency range and so lose resolution. Figs 8.3 (A,B,C) shows that the energy content varies widely over a narrow frequency range and by using a narrow frequency bandwidth we are able to pin point with greater accuracy the point at which the maximum energy content occurs.

The experimental results show a close, (1.5 - 3 dB), agreement with the theoretical results at and near the ring frequency while at the critical frequency the agreement is not so good. Below 1300 Hz, not many radiating modes seem to occur hence poor comparison. No attempt was made to compute the forced radiation efficiency in this region using the approximate theory discussed in reference (2).

Although the results do not show very close agreement, they allow some of the following observations to be made:

a) The measured radiation efficiency falls away sharply from the theoretical values below 1300 Hz.

b) The radiation efficiency measured from the direct excitation of the structure do not agree closely with the theoretical results.

c) The well defined peaks in the radiation efficiency plots reveal much more information that might otherwise have been lost if analysis made in the wider frequency bandwidths.

8.5. Conclusions.

The experimental results obtained with the aid of automatic space and time averaging system and the radiation efficiency computed from this data showed a reasonable agreement with the theoretical results shown in fig. 8.3C. Thus a confidence in the instrument is established. Using this technique, a great deal of analysis time was saved because the major part of the information had been reduced in one frequency sweep rather than having to take point by point measurement of $Sa(\omega)$, and $S_p(\omega)$ and then compiling the results after a lengthy and tedious computation.

The radiation efficiency is high at the ring and critical frequencies showing that a maximum energy flow between the structure and the reverberant sound field took place. Above the critical frequency where theoretically most of the modes suppose to uncouple and one should expect to get the radiation efficiency equal to one but from the experimental and the computed results this does not appear to be so.

The results have shown that it is not necessarily correct to assume that many acoustic modes couple with an individual structural mode even if the modal density in a particular frequency band is high.

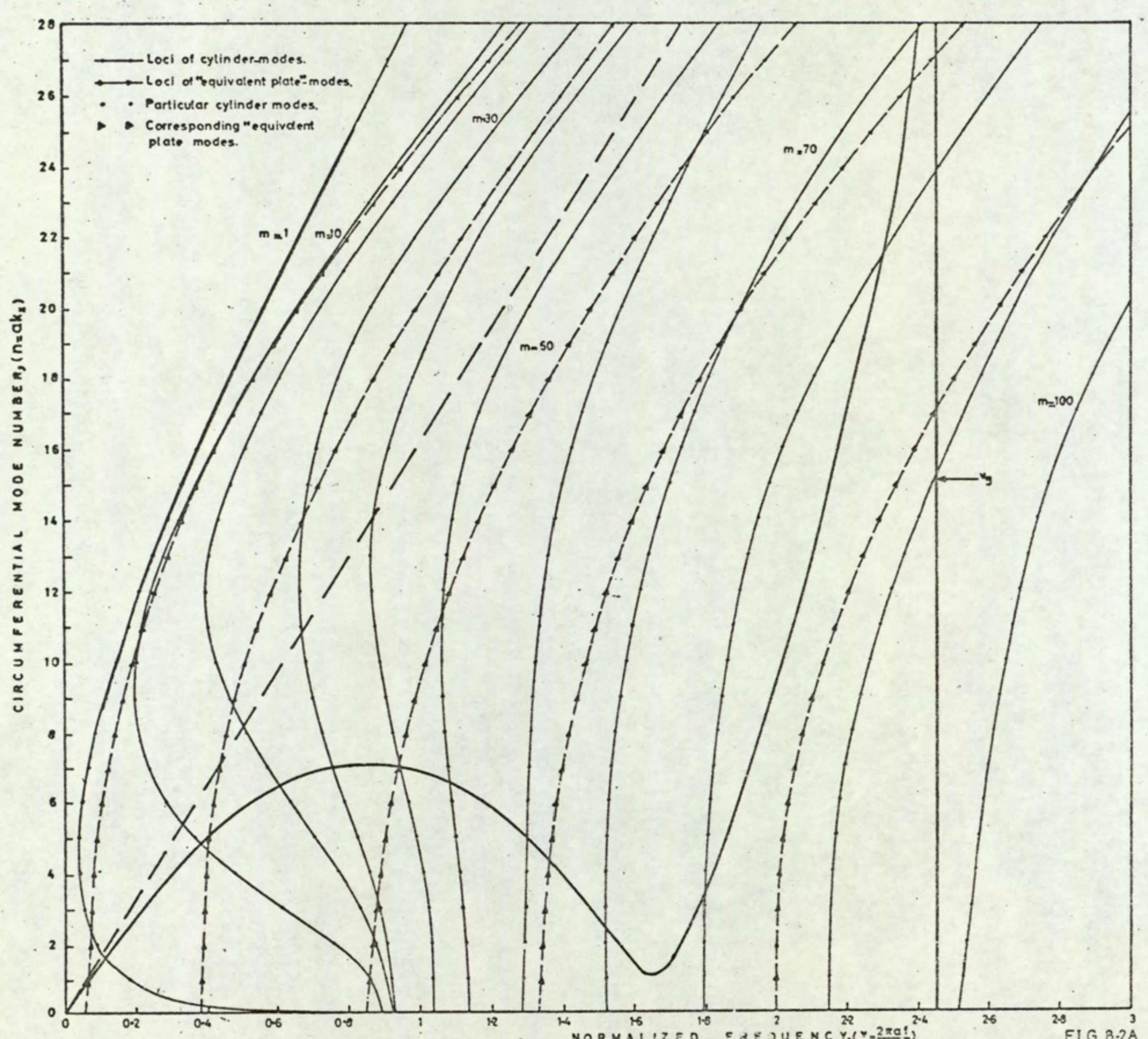

FIG 8-2A

CIRCUMFERENTIAL-MODE NUMBERS AS A FUNCTION OF NORMALIZED FREQUENCY FOR VARIOUS AXIAL-MODE NUMBERS.

LOCI OF CYLINDER MODES FOR A GIVEN AXIAL-MODE NUMBER

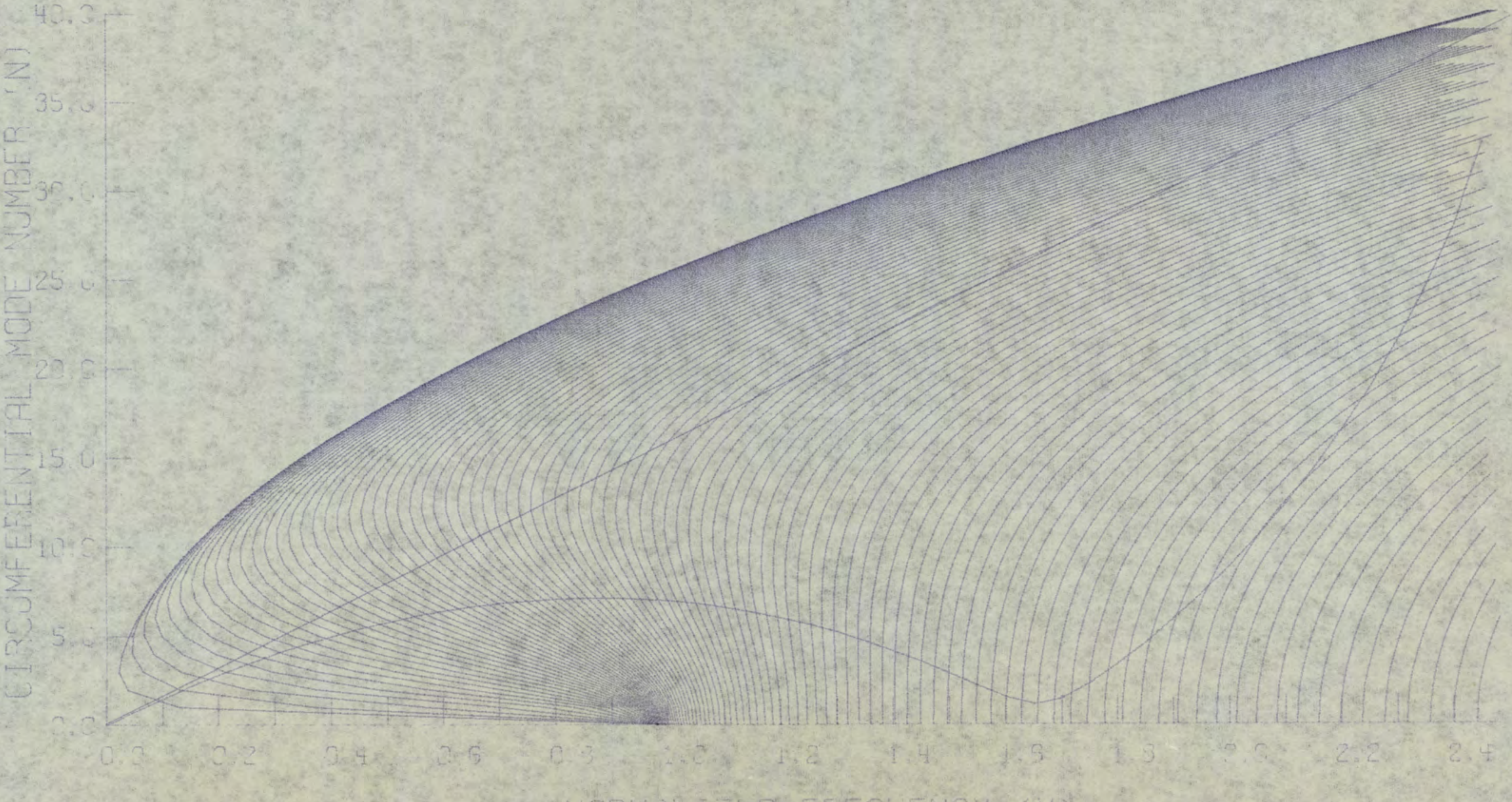

FIG 3.25

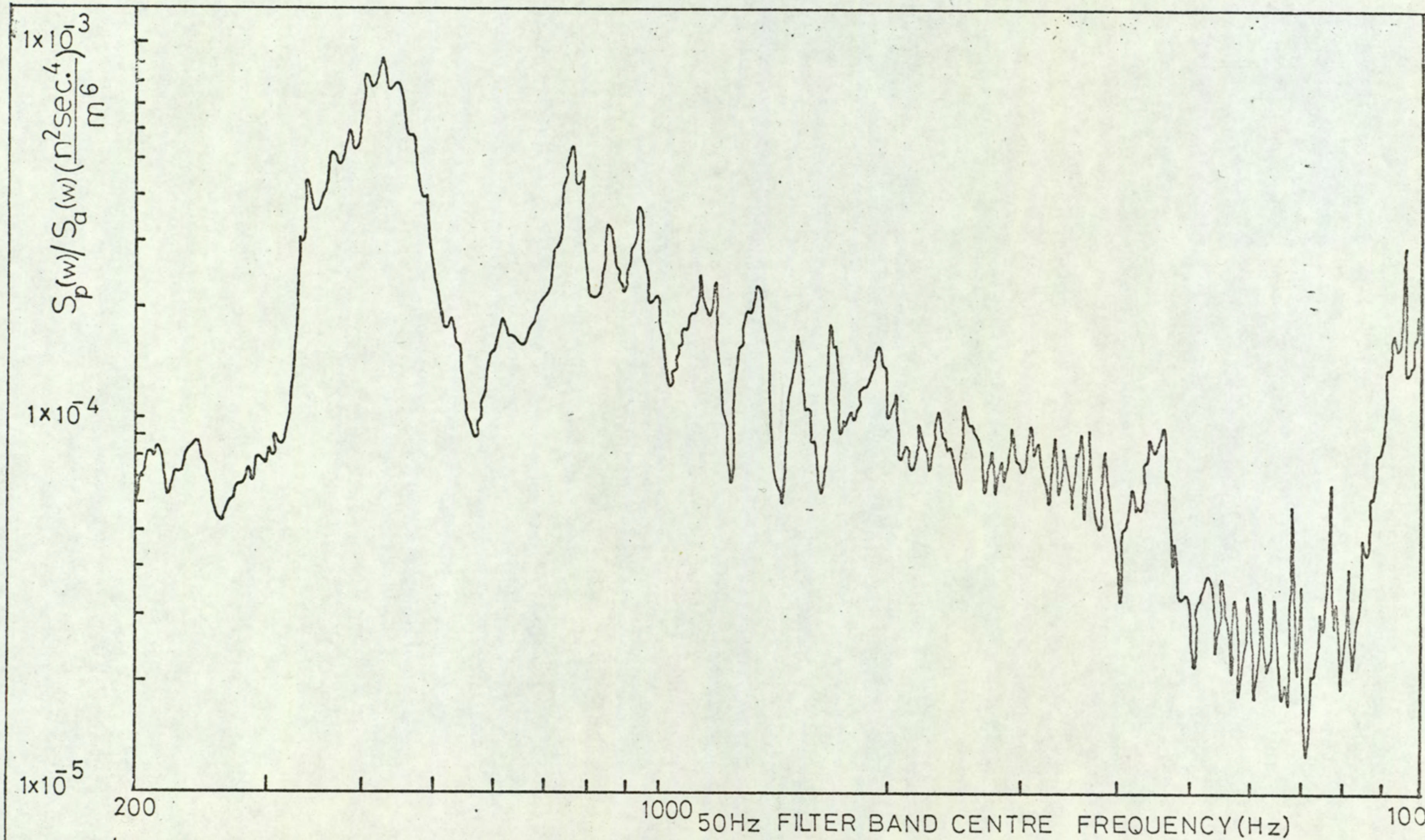

$S_p(w)/S_a(w)$ FOR THE FLANGED CYLIDRICAL SHELL EXCITED DIRECTLY FIG 8·3A

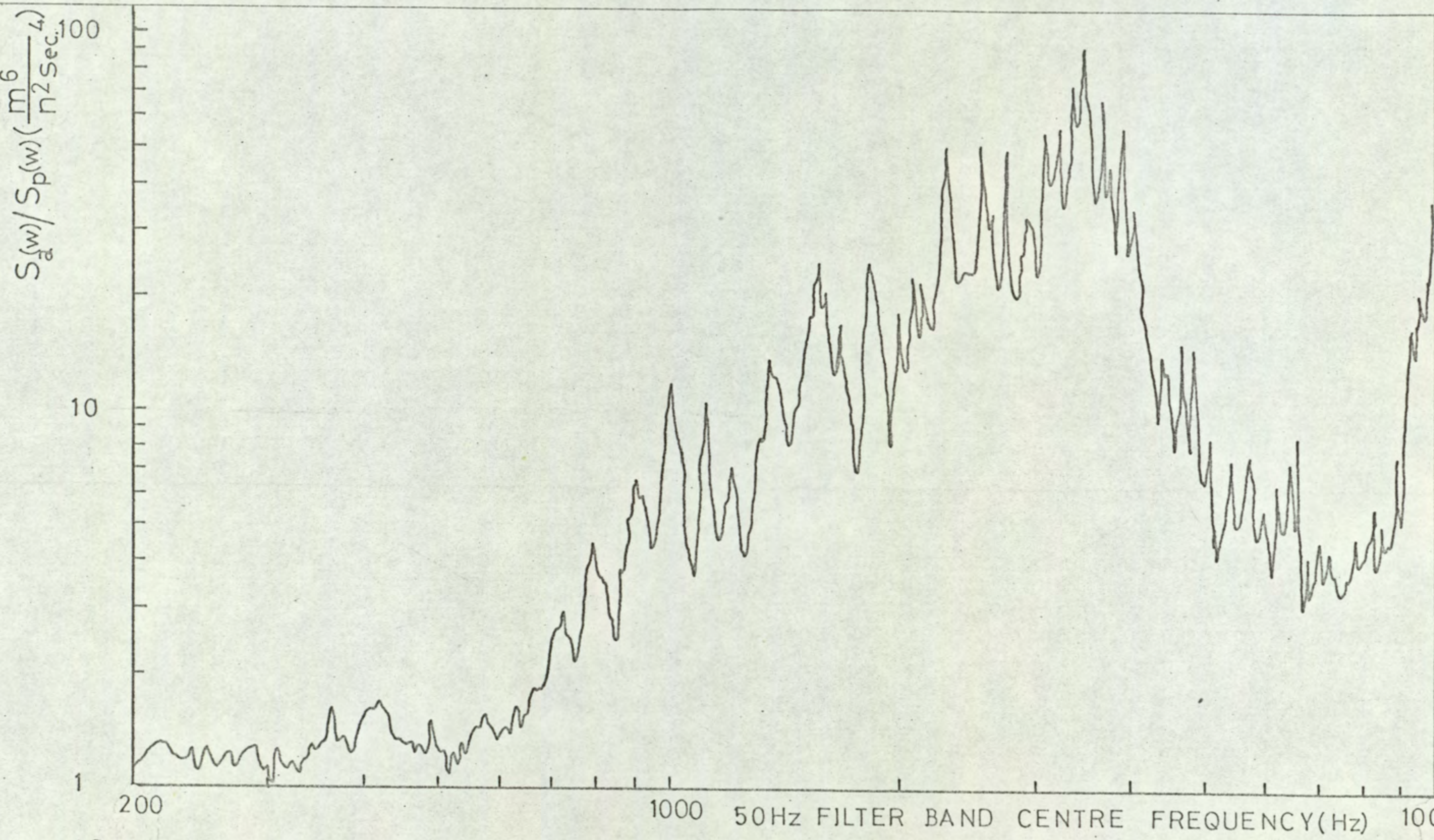

$S_d(w)/S_p(w)$ FOR THE FLANGED CYLINDRICAL SHELL INDIRECTLY EXCITED

FIG 8.3B

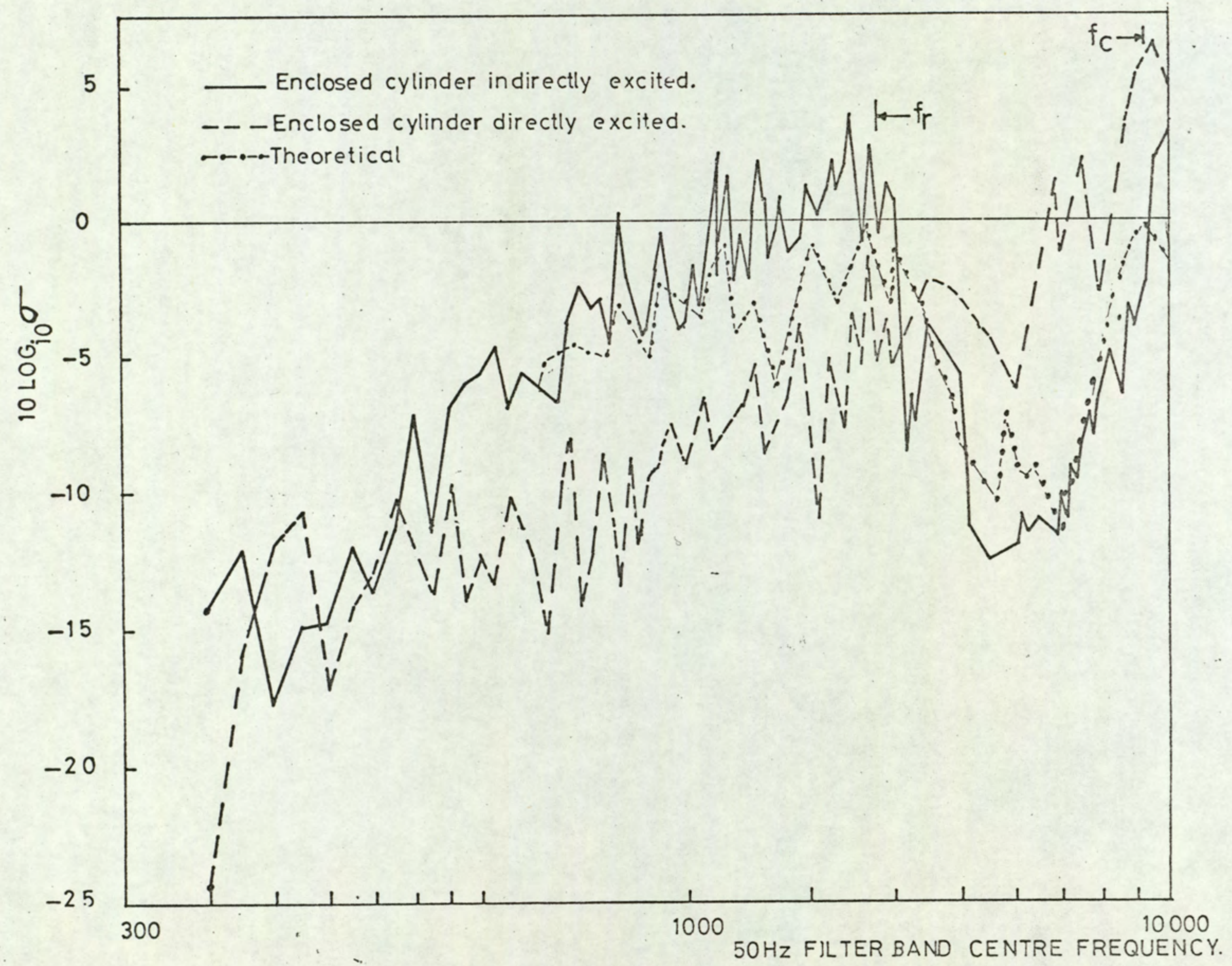

RADIATION EFFICIENCY OF FLANGED CYLINDRICAL SHELL FIG 8·3C

CHAPTER 9.

General Conclusions.

The aim of this work was to provide more accurate basic information than was hitherto available for use in investigation concerning noise transmission in various structures, with particular reference to the aircraft industry.

Attention was confined to plate type-structures formed into cylindrical shells, data regarding the primary factors of which had to be accurately obtained.

The mechanical damping of the cylinder used was obtained from decay measurements taken on it in a vacuum; this was done so that the effect of acoustic damping could be considered to be negligible. From the results shown in the chapter on damping (Chapter 7), it was concluded that the effects of acoustic damping on the structure when placed in the air was so small (1×10^{-4}) at frequencies above 8k Hz that they could be neglected. The technique applied (decay rate) for reducing this data gave an insight into the usefulness of the method and will be used in future investigations. The prime advantage gained from the method employed - the test was performed on a complete practical structure having flanges, welded joints, and enclosed ends - was that only one analysis was needed. This work might be extended to include structures on various geometries and the effects of damping layers thereon, thus providing information which would be most useful as data on the variation of mechanical damping at higher frequencies on scaled models which is not readily available.

The response of structures to acoustic excitation is dependent upon the number of modes being excited but it was possible to identify these only at lower frequencies (<1500 Hz) since at higher frequencies the modes were so close together as to make individual resolution impossible. The only way to estimate the number of modes at higher frequencies was to take the average number which lay within a narrow (1,10,50 etc) frequency band. Some of these were determined experimentally in the lower frequency ranges from frequency against amplitude plots. For the cylindrical shell it was found that the modes were so close together (even in a narrow frequency band) that mode counting was virtually impossible. Techniques were used in separating the modes but in the lower frequencies (<1500 Hz)only.

For determining the modal densities at higher frequencies (up to 20 k Hz) resort had to be made to the theoretical expressions developed by Arnold and Warburton (11). With the aid of an ICL 1905 Computer the equations were solved, the results obtained being shown in figs. 6.32 (A,B). The computed results of modal densities show that above the ring frequency (3778 Hz), the number of modes that lay in a frequency band of 50 Hz were, in this case, approximately constant. This is in close agreement with the result of Heckl(13) who performed similar work. The result that the modal density is almost constant supports the assumption that cylinders vibrate like a flat plate above the ring frequency. A useful bonus obtained from the computations was the table of resonant frequencies given in Appendix 3.

It was most important to obtain accurate information about the acoustic qualities of the room in which the experiments were carried out (i.e. whether or not the room was reverberant and/or diffuse in the frequency range of interest). This was because the theoretical expressions (discussed in chapter 3) relating to the exchange of energy between the structure and acoustic field modes to random excitation were based on the assumption that this field was reverberant. If the field was not completely reverberant, the theory will still be useful but the results obtained would not be so accurate. It was observed during the experiments that the type of acoustic field around the specimen had strong influence on the test results. This information was obtained from the measurement of reverberation and diffusibility, the results of which are given in chapter 5.

The conclusions drawn from these measurements of reverberation and diffusibility were :-

(a) Above 8k Hz the intensity of sound level in some frequency ranges was very small (approaching spurious signal level) that the structure could not be excited effectively.

(b) Although reflectors were used in the room and loud speakers arranged in positions such as to create a reverberant and diffused field condition, it was found that this could not be achieved efficiently when the room was excited in the narrow frequency band (<50 Hz).

An improvement to the acoustics of the test chamber above this frequency could be achieved by replacing the existing wall surface with sound reflective material.

For the experimental work, six loudspeakers were used to excite the test chamber with an input source from a signal generator and a maximum noise level of 114 dB only could be obtained. With the chamber being excited with a pneumatic noise generator - which is now being installed a noise level of up to 160 dB will be achieved, so improving any limitations set by the loudspeakers. An extension of this work - for the general definition of room acoustics - is under progress using a cross-correlation technique, and further insight into the parameters so far determined will be obtained.

The parameter that governs the sound radiation is the radiation efficiency, which describes the power flow linkage between the structural vibration and the transmitted sound pressure. From a reciprocity argument, the radiation efficiency also governs the response of structures to sound fields, however, the transmission of sound through structures is a problem combining response and radiation.

The radiation efficiency was calculated from the ratio of the measured values of the average acceleration and sound pressure spectral densities of the structure. This data was reduced with the aid of the automatic space and time averaging system - an instrument designed and developed especially for this work - so avoiding the necessity of carrying out point by point measurements. A better accuracy was thus obtained from this since errors due to measurement and calculation were much reduced.

The experimental results are in good agreement with the theoretical results (shown in fig. 8.3c) except in the lower frequencies (<1300 Hz). Although the measurements were carefully made, small errors due to instrumentation and analysis were unavoidable even though system calibration was done before each test. The theoretical expressions used for obtaining radiation efficiency, however, were based on certain assumptions (acoustically fast modes have modal radiation efficiency equal to unity) which could not be obtained in practise, and so some disagreement between the theoretical results and the practical results were unavoidable; these differences were, however, small.

In the course of writing this thesis an attempt was made to outline the nature of the research that has been carried out on the response of structures to random acoustic excitation. The knowledge gained from this is valuable, in particular with reference to its application to noise transmission in aircraft structures and to establishing confidence in the methods and an understanding of their limitations.

REFERENCES.

1. P. M. MORSE — Vibration and sound (McGraw-Hill Book Co. (1948.

2. MANNING & MAIDANIK — Radiation properties of Cylindrical Shells. (J. Acoust.Soc.Am.Vol.36, No. 9. (1964).

3. ZENER C — Elasticity and Analasticity of Metals. (University of Chicago (Press.(1948) P.63-65).

4. R. PLUNKETT — Measurement of Damping.

5. B. J. LAZAN — Energy dissipation mechanisms in structures, with particular reference to metal damping.

6. A.L. KIMBALL — Friction and Damping in vibration. (Schenectady, N.Y. Journal of the Applied Mechanics).

7. D. J. MEAD — The practical problems of assessing damping treatments (Journal of Sound & Vibration (1964).

8. G.C. KENNEDY & PANCU — Use of vectors in vibration measurement and analysis. (J.A. Sciences Vol.14, 1947, No.11).

9. G. MAIDANIK — Response of ribbed panels to reverber-and acoustic fields. (J.A.S.A. Vol.34, No. 6 (1962)).

10. P. W. SMITH Jnr — Response and Radiation of structural modes escited by sound. (J.A.S.A. Vol. 34, (1962)).

11. R.H. LYON & G. MAIDANIK — Power flow between linearly coupled oscillator. (J.A.S.A. Vol. 34, No. 5, (1962)).

12. R. H. LYON — Sound radiation from a beam attached to a plate. (J.A.S.A. Vol. 34, No. 9 (1962)).

13. M. HECKL. — Vibration of point driven cylindrical shells. (J.A.S.A. Vol. 34, No.10, 1962)).

14. ARNOLD & WARBURTON — The flexural vibration of thin cylinders. (Vo.167, Part A, P.62-80).

15. WHITE & POWELL — Transmission of random sound and vibration through a rectangular double wall. (A.S.A. 36, 2004(A), (1964)).

16. P. H. WHITE — Tranâduction of boundary-layer noise by a Rectangular Panel. (J.A.S.A.,39, 1254 (A) (1966)).

17. P.H. WHITE — Sound transmission through a finite closed cylindrical shell. (J.A.S.A. 39, 1254 (A) (1965)).

18. MACDUFF & CURRERI — Vibration Control. (McGraw-Hill (1958)).

19. M.H. HECKL — New Methods for understanding and controlling vibration of complex structures. (Bolt Beranck & Newman Report No. 875).

20. L. CREMER — (Acoustics 5, 245-256, (1955).

21. L.G. COPLEY — Integral Equation Method for Radiation from Vibrating Bodies. (J.A.S.A., 11.5, 11.7, 13.7 (1966)).

22. G. CHERTOCK — Sound radiation from Vibrating surfaces (J.A.S.A. Vol. 36, No.7 (1964).

23. E.M. CHRITENSEN — Jet Noise and Shear flow instability seen from an Experimental Viewpoint. (Journal of the applied Mechanics (1967).

24. S.H. CRANDALL — Random Vibrations Vol. 2. (The M.I.T. Press (1958)).

25. G.S. PISARENKO — Dissipation of Energy During Mechanical Vibration. Vol. I and II. (Akademiya Nauk Ukainskoi S.S.R.1962).

26. H. LAMB — The Dynamical Theory of Sound. (Dover Publication).

27. C.M. HARRIS — Handbook of Noise Control. (McGraw-Hill Book Co).

28. E.O. DOEBLIN — Measurement Systems and Applications (McGraw-Hill Book Co).

29. RAYLEIGH, LORD — The Theory of Sound Vol. 142. (Dover Publications).

30. RUIZICKA, J.E. (Editor) Structural damping (1959) (Papers presented at A.S.M.W. Annual Meeting) American Society of Mech.Eng., N.Y.

31. RICHARD E.J. AND D.J. MEAD Noise and Acoustic. Fatigue in Aeronautics. (John Wiley & Sons Ltd.)

32. DEN HARTONG Mechanical Vibrations. McGraw Hill 4th Edition 1956)).

33. CREDE, C.F. Vibration and Shock Isolation. (John Wiley, New York, (1951)).

34. MARVIN, R.S. The dynamic mechanical properties of polyisobutylene,

35. FOSTER, F. Ein Noore.

36. JENSEN, J.W. Damping capacity - It's measurement and significance. U.S. Bureau of Mines, Washington, R.of I.5442 (1959).

37. MYKLSTAD, N.O. Concept of complex damping. Journal of Applied Mech. Vol.19 (1952)

38. ZENER C. Elasticity and Anelasticity of metals. University of Chicago Press (1948).

39. TIMOSHENKO, S The theory of plates and shells.(McGraw-Hill Book Co. (1940) p.439.

40. WARBURTON, G.B. Vibration of cylindrical shells in an acoustic medium. Journal of Mech.Eng. Science (1960).

41. GREENSPON, J.E. Vibration of a thick walled cylindrical shell. J.A.S.A. Vol. 32, No. 5 (1960).

42. CLARKSON AND MERCER Use of cross-correlations in studying the response of lightly damped structures to random forces. A.I.A.A. Journal 3. 2287, (1965).

43. COOK L. AND ASSOCIATES Measurement of correlation coefficients in reverberant sound fields. J.A.S.A. Vol. 27 No. 6 (1965).

44. SCHRODER, M.R. New Method of measuring reverberation time. J.A.S.A. Vol. 37, (1965).

45. BARON, M.L. AND BLEICH, H.H. — J. Appl. Mechanics, 21 (1954) (178-184).

46. FLUGGE, W. — Static amd Dynamic der Schaler (Berlin, Germany) 1934 p.p. 115 and 230.

47. LOVE, A.E.H. — A Treatise on the mathematical Theory of Elasticity (Dover Publications, N.Y. 1944).

48. LYON, R.H. AND MAIDANIK, G. — Statistical Method in Vibration Analysis. A.I.A.A. Journal Vol. 2.No.6, (1964).

49. JOHNSON, R.A. AND BARR, A.D.S. — Acoustic and Internal Damping in Uniform Beams. Journal of Mech. Engineering Science, Vol.11, No. 2. (1969).

50. SABINE, W.C. — Collected papers on Acoustics. Havard University Press (1922). (Also published in 1964 by Dover Publications). Inc. N.Y.

51. MEYER, E. — Beitrage Zue Unstersuchung des Nachalles, E.N.T. (1927).

52. MEYER, E. AND JUST, P. — Zue Messung Von Nachhall-daven und Schallabsorption. E.N.T. (1928).

53. STRUTT, M.J.O. — Uben eine Vollantomatische Nachhall - Messvoruchtung E.N.T. (1930).

54. WENTE, E.C. AND BIDELL, E.H. — Chronographic Method of measuring reverberation time. J.A.S.A. (1930).

55. HUNT, F.V. — Apparatus technique for reverberation measurement. J.A.S.A. Vol. 8. (1936).

56. VAN BRAUNMWHL. H. AND WEBER, N. — E in Vielseitiges registrueremdes Mess-und Steuvgeret fiin Elektroakustische Zwicke E.N.T. (1935).

57. KENARD, E.H. — Journal of Applied Mechanics. 20, 33-40. (1953).

58. JUNGER, M.C. AND ROSATO, F.J. — Journal of Acoustic Soc. of America 26, 709-713 (1954).

59. SMITH, P.W. — Journal of Acoustic Soc. of America 27, 1065-1072 (1955).

60. MIRSKY, I. AND HERRMANN, C.R. Journal of Acoustic Soc. of America 29, 1116-1123 (1957).

61. LIN, T.C. AND MORGAN, G.W. Trans American Soc. Mech. Engineers. 78, 255-261 (1956).

62. YI-YIAN YU. Journal of Aero/Space Sci. 25, 699-715 (1958).

63. COOPER, R.M. AND NAGHDI, M. Journal of Acoustic Soc. of America 28, 56-63. (1956).

64. COOPER, R.M. AND NAGHDI, M. Journal of Acoustic Soc. of America 29, 699-715 (1958).

65. GREENSPON, J.E. J. Aero/Space Science 27, 37-40 (1960).

66. MIRSKY, I. AND HERRMANN Journal of Acoustic Soc. of America. 31, 97-103 (1959).

67. KNUDSEN, V.O. Resonance on small room. J.A.S.A. Vol. 4. 1932.

ACKNOWLEDGEMENTS.

I wish to thank Professor E. Downham, Professor of Mechanical Engineering, for his ready and willing assistance, valuable advice, and encouragement throughout the course of the work.

Dr. L. Yeh of the English Electric Company Limited, Mechanical Engineering Laboratories, Whetstone, went out of his way to provide extensive facilities at Whetstone for work in connection with the measurement of structural damping.

I also extend my thanks to the members of the applied dynamics team of the department for their help and suggestions.

I gratefully acknowledge the financial support given to this project by the Ministry of Technology.

Appendix 1.

1.1. Note on use of decibels (dB)

The numerical levels of sound is usually quoted in 'decibels' because the audible sounds cover a wide range of pressure magnitudes. By measuring the noise pressure on a logarithmic scale to the base of 10, the enormous range of noise pressures can be condensed to numbers which are much more manageable and less susceptible to errors. The human ear also assesses a sound pressure magnitude in terms of its ratio to other sounds. In effect, the ear/brain measuring system has a logarithmic response, and supplies the senses with a signal approximately proportional to the logarithm of the incoming sound pressure.

The decibel scale is ten times the logarithm to base ten of the ratio of two power quantities, or quantities proportional to power and one of which is a standard reference quantity. In decibels (dB) the sound power level (P W L) of the sound source emitting an acoustic power of W_1 relative to another standard reference sound source emitting a power of W ref is

$$P\,W\,L = 10 \log_{10} \frac{W_2}{W_{ref}} \quad \text{dB} \quad \text{re } W_{ref}. \qquad 1.$$

So long as the power of the reference source is quoted alongside the number of dB's obtained from this, any value for W ref. could be chosen. In the generally accepted decibel P W L scale, W ref. is usually taken to be 10^{-13}W and in some countries it is 10^{-12}W.

The acoustic power flow across a unit area is represented by the acoustic intensity (I_1). Being a power quantity, this can be measured on a decibel scale by comparing it with a reference acoustic intensity, I ref.

The intensity level (IL) at a point in the sound field is defined by

$$IL = 10 \log_{10} \frac{I_1}{I\ ref.} \text{ dB} \qquad \text{re I ref.} \quad 2.$$

I ref. is commonly taken to be:

10^{-12} W/M² (10^{-16} W/CM²)

hence,

$$IL = 10 \log_{10} I_1 + 120 \text{ dB re } 10^{-12} \text{ W/M}^2. \qquad 3.$$

The response of a flexible structure depends upon the incident sound pressure rather than on the power emitted by the source or the acoustic intensity. The intensity is a power quantity and in a radiating field is proportional to the square of the pressure amplitude and is shown by

$$\text{Intensity (I)} = \frac{p^2}{\rho_o C_o} \qquad 4.$$

where p is the r.m.s. acoustic pressure, p^2 is therefore proportional to a power quantity and ρ_o, C_o are the ambient density of fluid and speed of sound. The sound pressure level (SPL) in decibel for a sound pressure p^2 is defined in the following way:

$$SPL = 10 \log_{10} \frac{P_1^2}{P^2\ ref}, \qquad 5$$

$$= 20 \log_{10} \frac{P_1}{P\ ref} \text{ dB} \qquad \text{re p ref.} \quad 6$$

The value of p ref is usually taken to be 0.0002 microbar ($= 0.0002\ dyn/cm^2 = 0.00002\ N/M^2$)

and $$S\ P\ L = 20 \log_{10} P_1 + 74\ dB\ re\ 0.000\ 2\ \mu bar \qquad 7$$

Where p_1 must be measured in microbars.

All commercial noise measuring apparatus performs the conversion into microbars and also adds the 74 dB to give us the actual value of SPL in dB's.

The value of Pref. was originally chosen as being the minimum sound pressure perceptible by a good human ear. The value of I ref. in IL ($= 10^{-12}\ W/M^2$) was chosen such that the numerical value of IL should be almost the same as that of SPL for plane or spherical waves under NTP atmospheric conditions. The relationship under these conditions is,

$$S\ P\ L = IL + 0.2\ dB\ re\ 0.0002\ \mu bar \qquad 8$$

0.2dB is usually a negligible quantity and the values of SPL and IL are therefore virtually identical at NTP.

To work back from the measured SPL to find the pressure in Newton $/M^2$ ($p_{1,N}$,) the following relationship may be used

$$SPL = 10 \log_{10} P_{1}, + 94\ dB\ re\ 0.0002\ \mu bar \qquad 9$$

If p_1 is required in Lb/ft^2 ($P_{1,lb.}$)

$$SPL = 10 \log_{10} P_{1,lb.} + 127.6\ dB\ re\ 0.0002\ \mu bar \qquad 10$$

When sound pressures from two independent sound sources add together, it is important to remember that the two SPL values are not added together to get the total SPL value. If the two independent r.m.s. sound pressures adding at a point are p_1 and p_2 then the total mean square sound pressure is

$$p_t^2 = p_1^2 + p_2^2 \qquad 11$$

So that, $SPL \text{ total} = 10 \log_{10} \dfrac{p_1^2 + p_2^2}{p^2_{ref.}} dB \quad \text{re. } p \text{ ref}$ 12

If the two sound pressures are equal, so that $p_1^2 = p^2$

then, $SPL \text{ total} = 10 \log_{10} \dfrac{2p_1^2}{p^2 \text{ ref.}}$ 13

$$\left.\begin{aligned} &= SPL_1 + 3dB \quad \text{re p ref.} \\ \text{or,} \quad &= SPL_2 + 3dB \quad \text{re p ref.} \end{aligned}\right\} \qquad 14$$

The above definition of the dB scales have been applied to the overall sound power and pressure being measured. They can be extended to enable spectrum levels to be quoted in dB's relative to a given reference power or pressure. Suppose the analysis of a random pressure shows that in the frequency band of bandwidth Δf, centred on f_c, the pressure has a mean square component of $p^2 \Delta f$. Then the SPL contributed by that band is

$$SPL_{\Delta f} = 10 \log_{10} \frac{p^2 \Delta f}{p^2 \text{ ref}} \quad db \qquad \text{re p ref.} \qquad 15$$

In practice Δf is likely to be 1/3 octave or constant frequency bandwith (10 Hz, 20 Hz, 50 Hz, etc). The spectral density of the pressure has the average value of $p^2_{\Delta f} / \Delta f$ in the band Δf, this may be converted into the dB scale by writing

$$\text{Spectrum level, } S(f) = 10 \log_{10} \frac{p^2_{\Delta f} / \Delta f}{p^2 \text{ ref.}} \qquad 16$$

$$= SPL_{\Delta f} - 10 \log_{10} \Delta f \text{ dB per unit frequency.} \qquad 17$$

Appendix 2.

TERMINOLOGY.

2.1. Decay Time /60 db.

This is defined as the interval within which the signal power decays by a factor 10^6 (i.e. by 60 db, corresponding to an amplitude decay by a factor of 10^3) and can readily be shown to be related to the loss factor (η) as

$$\eta \simeq 2.2. \left[T_{60\,(sec)}\, f_{Hz} \right]^{-1}$$

where f denotes the centre frequency of the band in which measurements are taken.

2.2. Free Field.

It is a field in which the effect of the boundaries are negligible over the region of interest. The actual pressure impinging on an object placed in an otherwise free field will differ from the pressure which would exist at that point with the object removed, unless the acoustic impedance of the object matches the acoustic impedance of the medium. A free field room is an 'Anechoic' Room.

2.3. Diffuse Sound Field.

It is a sound field such that the sound pressure level is everywhere the same and all directions of energy flux are equally probable.

2.4. Reverberation Room.

It is an enclosure in which all the surfaces have been made as sound reflective as possible.

2.5. Ring Frequency (fr)

It is the frequency at which the longitudinal wavelength in the cylinder material is equal to the circumference and is given by,

$$fr = \frac{C_L}{2\pi a}$$

2.6. Critical Frequency (fg or fc)

The wavelength of the bending wave equation

$$B = \frac{C_B}{f} = \left[\frac{1.8 \times h \times C_L}{f}\right]^{1/2}$$

show that free fluxual waves in a plate have wavelengths which are inversely proportional to the square root of the frequency. When a plate is excited at frequency f, by a plane acoustic whose trace wavelength on the surface of the plate is equal to λ_B, the flexural wavelength for frequency f, there will be complete matching between the free and forcing wave. Such a matching is called 'Coincidence'

When a plate is excited by sound waves, coincidence can occur for a certain combination of frequency and angle of incidence provided that the frequency lies within specified limits. Consider an incident plane sound wave travelling with speed Co, and frequency f, which strikes a plate at an angle of incidence, θ, as shown in fig. 2.6A. The trace waveform over the surface of the plate will then have a frequency f, a wavelength $\lambda/\mathrm{Sin}\theta$ and a trace velocity $a/\mathrm{Sin}\theta$ Coincidence will occur when,

$$C_\beta = \frac{Co}{\mathrm{Sin}\theta}$$

$$\text{i.e. } \lambda_\beta = \frac{C_B}{f} = \frac{Co}{f\ \mathrm{Sin}\theta}$$

Thus the coincidence frequency is given by,

$$f\theta = S^2/1.8 \times h \times C_L \times \mathrm{Sin}^2\theta \quad \mathrm{Hz.}$$

From the above equation it can be seen that the frequency limits within which coincidence can occur are given by the condition $0 \leq \mathrm{Sin}\theta \leq 1$. The upper limit, $f = \infty$ when ($\sin\theta = 0$) is not in fact achieved because the assumptions for the existance of free flexural waves are no longer valid (λB is no longer compared with h) The free upper limit for f_θ is given by the condition for Rayleigh waves. The lower limits for f_θ determines the critical frequency fc.

$$fc = \frac{Co^2}{1.8 x h x C_L} \text{ Hz}$$

This is the coincidence frequency for grazing incidence sound waves.

2.7. Sabine Absorption.

The sabin is a measure of the sound absorption of a surface; it is equivalent of 92.9×10^{-3} M^2 of perfectly absorptive surface.

The sabine absorption in a room is the sound absorption a' defined by the Sabine reverberation-time equation.

$$6_{60} = 0.161 \frac{V}{a'}$$

where V is the volume of enclosure in cubic meters and a is the total Sabine absorption in square meters.

2.8. Classification of Modes.

The class divisions are based on the magnitude relative to the speed of sound Co and the bending-wave speed C_B and the phase speeds in the directions of the panel edges cx and cy. The classes are:

(i) Acoustically fact (AF) modes: $C_B \geq Co$

(ii) Acoustically slow (AS) mode: $C_B < Co$

(a) Strip Modes: either Cx or Cy $>$ Co, $\sigma_s \ll 1$

(b) Piston Modes: both Cx and Cy$<$Co, $\sigma_p \ll \sigma_s$

where σ_f is the radiation efficiency of strip mode

σ_s is the radiation efficiency of piston mode.

σ_p is the radiation efficiency of piston mode.

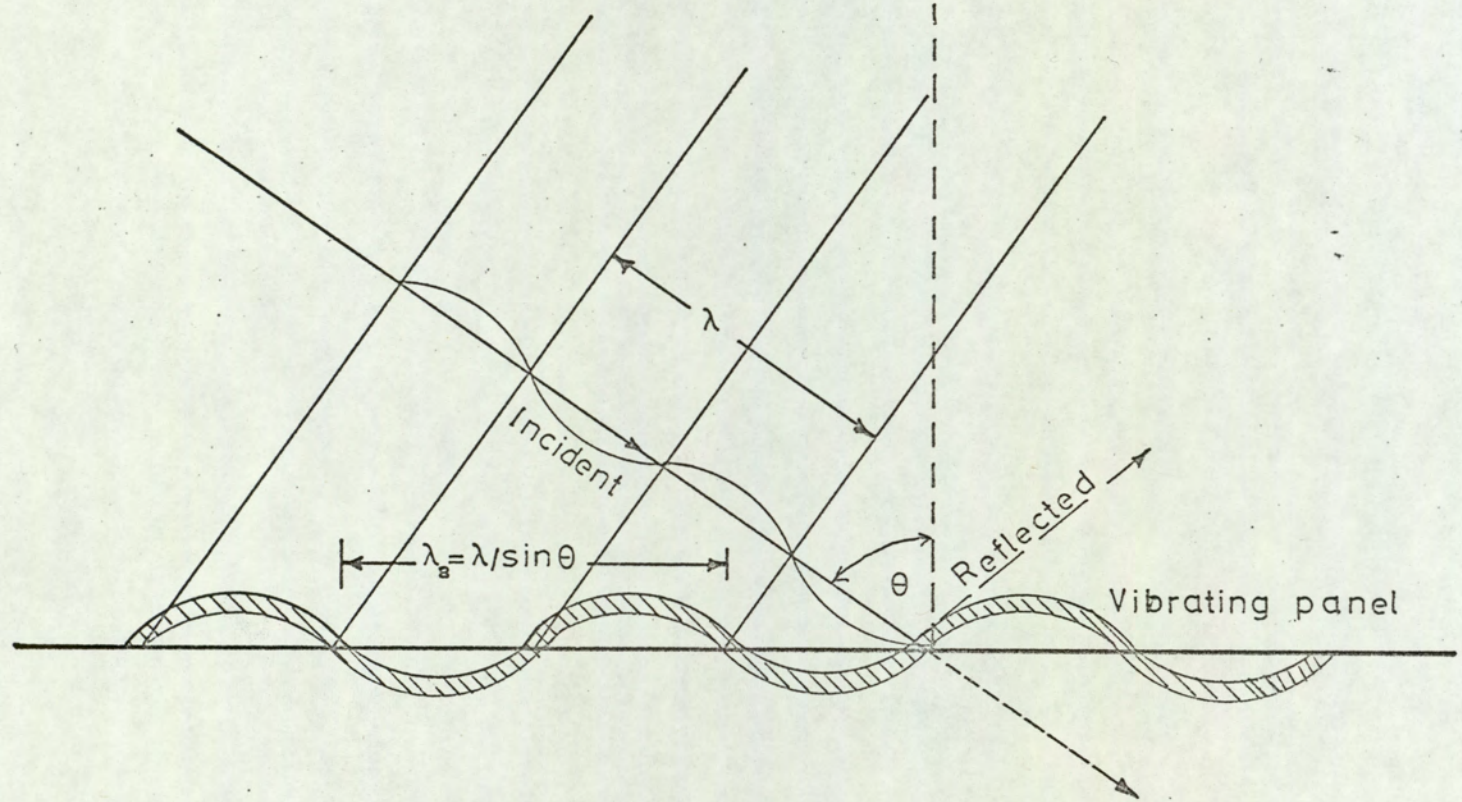

ILLUSTRATION OF WAVE COINCIDENCE

FIG 2.6A

APPENDIX 3

The Computer Program

The Algol program printed here was used in all the computation. The program computes all the roots of the cubic equation for N varying from 2:1:59 and M varying from 1:1:160. The value of the lowest real cubic root is used for the frequency computation. The summary of the procedure is as follows:-

Solve cubic Equation for M x N,
Solve frequency equation and
store in F_i ....F_{mn}.

↓

Sort F's into numerical order

↓

Print F's until one of them
$\geqslant$ 20 kHz

Explanation of the input parameters

PI	=	3.14159263
H	=	Thickness of cylinder material
A	=	Diameter of the cylinder
L	=	Length of the cylinder
F	=	Frequency
G	=	Acceleration due to gravity
SIGMA	=	Poisson's Ratio
E	=	Young's Modulus

RHO = Density of the material

ROOT = Root of the cubic equation

ALPHA = H/A

BETA = (ALPHA * ALPHA)/12

N = Number of circumferential waves

M = Number of axial half waves

ML = Lower number of axial half waves

MH = Higher number of axial half waves

NL = Lower number of circumferential waves

NH = High number of circumferential waves.

```
STATEMENT
    0          'INPUT' 0=CRO  'OUTPUT' 0=LPO
    0          'SPACE' 10000
    0          'BEGIN'
    1              'REAL''PI,H,A,L,F,SIGMA,E,RHO,FREQSTEP,ROOT,ALPHA,BETA,SIGMSQ,G,
    1              LAMBDA,LAMBDA2,LAMBDA4,N2,LF;
    1              'INTEGER' N,I,M,F1,ML,MH,NL,NH;
    2              'REAL' 'ARRAY' K[0:3];
    3
    3
    3              'PROCEDURE' SHELLSORT(A,N);
    5              'VALUE' N;
    6              'INTEGER' 'ARRAY' A;
    7              'INTEGER' N;
    8              'BEGIN'
    8                  'INTEGER' I,J,K,M,W;
    8                  'FOR' I:=1 'STEP' I 'UNTIL' N 'DO' M:=2*I-1;
   11                  'FOR' M:=M '/' 2 'WHILE' M#0 'DO'
   12                  'BEGIN'
   12                      K:=N-M;
   14                      'FOR' J:=1 'STEP' 1 'UNTIL' K 'DO'
   15                      'BEGIN'
   15                          'FOR' I:=J 'STEP' -M 'UNTIL' 1 'DO'
   17                          'BEGIN'
   17                              'IF' A[I+M] 'GE' A[I] 'THEN' 'GOTO' L1;
   19                              W:=A[I];
   20                              A[I]:=A[I+M];
   21                              A[I+M]:=W;
   22                          'END';
   23          L1:                 ;
   24                      'END';
   25                  'END';
   26              'END';
   26
   26
   26              'PROCEDURE' CUBICROOT(P,ROOT);
   28              'REAL' 'ARRAY' P;
   29              'REAL' ROOT;
   30              'BEGIN'
   30                  'REAL' S,T,B,C,D;
   30                  S:=P[1]/3.0;
   32                  T:=S*P[1];
   33                  B:=0.5*(S*(T/1.5-P[2])+P[3]);
   34                  T:=(T-P[2])/3.0;
   35                  C:=T*T*T;
   36                  D:=B*B-C;
   37                  D:='IF' B=0.0 'THEN' ARCTAN(1.0)/1.5 'ELSE' ARCTAN(SQRT(-D)/
   37                                                                 ABS(B))/3.0;
   38                  B:=-SQRT(T)*SIGN(B)*2.0;
   39                  C:=COS(D)*B;
   40                  T:=-SQRT(0.75)*SIN(D)*B-0.5*C-S;
   41                  D:=-T-C-2*S;
   42                  C:=C-S;
   43                  'FOR' C:=C,D 'DO' 'IF' ABS(C) 'LE' ABS(T) 'THEN' T:=C;
   45                  ROOT:=T;
   46              'END';
   46
   46
```

```
        SELECT OUTPUT(0);
        PI:=3.14159263;
        I:=0;
        H:=READ;
        A:=READ;
        L:=READ;
        G:=READ;
        SIGMA:=READ;
        E:=READ;
        RHO:=READ;
        LF:=READ;
        FREQSTEP:=READ;
        ML:=READ;
        MH:=READ;
        NL:=READ;
        NH:=READ;
        'BEGIN'
        'INTEGER' 'ARRAY' FREQ[1:(MH-ML+1)*(NH-NL+1)];
        ROOT:=0.0;
        ALPHA:=H/A;
        BETA:=ALPHA*ALPHA/12;
        SIGMSQ:=SIGMA*SIGMA;
        'FOR' M:=ML 'STEP' 1 'UNTIL' MH 'DO'
        'BEGIN'
              LAMBDA:=M*PI*A/L;
              LAMBDA2:=LAMBDA*LAMBDA;
              LAMBDA4:=LAMBDA2*LAMBDA2;
              'FOR' N:=NL 'STEP' 1 'UNTIL' NH 'DO'
              'BEGIN'
                    N2:=N*N;
                    K[0]:=1.0;
                    K[1]:=1+0.5*(3-SIGMA)*(LAMBDA2+N2)+BETA*((LAMBDA2+N2)
                    '**' 2+2*(1-SIGMA)*LAMBDA2+N2);
                    K[1]:=-K[1];
                    K[2]:=0.5*(1-SIGMA)*(LAMBDA2+N2)'**'2+0.5*(3-SIGMA-2*
                    SIGMSQ)*LAMBDA2+0.5*(1-SIGMA)*N2+BETA*(0.5*(3-SIGMA)*
                    (LAMBDA2+N2)'**'3+2*(1-SIGMA)*LAMBDA4-(2-SIGMSQ)
                    *LAMBDA2*N2-0.5*(3+SIGMA)*N2*N2+2*(1-SIGMA)*LAMBDA2+
                    N2);
                    K[3]:=0.5*(1-SIGMA)*(1-SIGMA)*(1+SIGMA)*LAMBDA4+0.5*
                    (1-SIGMA)*BETA*((LAMBDA2+N2)'**'4-2*(4-SIGMSQ)*LAMBDA4
                    *N2-8*LAMBDA2*N2*N2-2*N2*N2*N2+4*(1-SIGMSQ)*LAMBDA4+4*
                    LAMBDA2*N2+N2*N2);
                    K[3]:=-K[3];
                    CUBICROOT(K,ROOT);
                    F:=SQRT(ROOT*E*G/(RHO*(1-SIGMSQ)))/(2*PI*A);
                    I:=I+1;
                    FREQ[I]:=F;
              'END';
        'END';
        SHELLSORT(FREQ,(MH-ML+1)*(NH-NL+1));
        'FOR' N:=0 'STEP' 10 'UNTIL' I 'DO'
        'BEGIN'
              NEWLINE(1);
              'IF' N '/' 100*100=N 'THEN' NEWLINE(1);
              'IF' N '/' 500*500=N 'THEN' PAPERTHROW;
              'FOR' M:=1 'STEP' 1 'UNTIL' 10 'DO' PRINT(FREQ[N+M],8,0);
              'IF' FREQ[N+10]>20000 'THEN' 'GOTO' L1;
        'END';
L1:     PAPERTHROW;
        'END';
'END';
```

Tables of resonant frequencies of free vibration of Flanged Cylindrical Shell. $\frac{H}{A} = 0.0053$

72	91	119	138	155	162	200	210	221	233
244	274	280	290	297	310	333	347	360	364
374	391	395	405	422	431	453	458	461	468
471	471	482	482	492	505	523	538	549	567
567	570	576	584	586	602	626	629	641	656
656	658	677	679	687	690	696	699	704	709
717	720	728	735	749	759	786	789	795	798
807	816	819	820	822	827	827	830	835	846
860	870	872	873	880	898	904	919	924	924
934	945	946	960	963	966	969	971	978	982
987	1000	1008	1011	1016	1017	1024	1033	1037	1045
1046	1054	1058	1062	1091	1094	1106	1110	1114	1118
1118	1121	1126	1126	1132	1141	1144	1151	1153	1164
1167	1168	1172	1185	1186	1187	1192	1208	1208	1225
1229	1233	1241	1249	1254	1256	1262	1263	1279	1285
1288	1292	1294	1296	1298	1299	1299	1307	1309	1318
1332	1332	1333	1342	1348	1349	1356	1363	1365	1365
1368	1368	1375	1384	1391	1417	1420	1421	1423	1425
1435	1446	1447	1458	1463	1466	1469	1470	1473	1477
1480	1485	1489	1496	1505	1508	1509	1516	1520	1522
1522	1524	1534	1541	1542	1544	1548	1555	1557	1563
1564	1578	1590	1584	1587	1588	1600	1606	1614	1623
1637	1638	1641	1644	1647	1653	1654	1655	1657	1660
1661	1666	1671	1674	1675	1677	1684	1685	1694	1697
1698	1699	1712	1714	1722	1727	1729	1736	1740	1749
1751	1753	1755	1763	1766	1768	1771	1780	1785	1796
1797	1803	1807	1815	1819	1820	1824	1829	1830	1839
1840	1842	1854	1855	1856	1861	1866	1867	1875	1875
1883	1885	1889	1891	1894	1898	1899	1899	1899	1903
1912	1915	1920	1923	1925	1927	1929	1938	1942	1948
1955	1965	1969	1969	1977	1977	1979	1989	1991	1991
1993	1996	2006	2007	2009	2011	2016	2019	2041	2048
2051	2052	2053	2056	2059	2066	2068	2068	2067	2073
2073	2075	2080	2080	2080	2088	2088	2096	2098	2100
2110	2112	2114	2114	2116	2124	2124	2139	2140	2146
2151	2151	2157	2157	2158	2168	2170	2174	2179	2180
2188	2191	2192	2193	2195	2202	2202	2204	2215	2216
2219	2224	2227	2233	2237	2239	2242	2252	2255	2256
2259	2263	2263	2264	2278	2285	2290	2293	2297	2300
2301	2302	2303	2304	2308	2312	2317	2318	2319	2320
2322	2324	2326	2332	2334	2336	2340	2341	2344	2347
2353	2363	2364	2370	2376	2377	2380	2381	2381	2391
2395	2399	2400	2401	2403	2410	2412	2417	2422	2422
2424	2428	2431	2433	2439	2439	2443	2448	2459	2460
2474	2475	2477	2478	2480	2483	2484	2489	2491	2494
2499	2499	2503	2503	2504	2510	2519	2526	2529	2533
2536	2536	2539	2539	2540	2540	2547	2555	2555	2555
2557	2560	2566	2569	2569	2569	2570	2573	2573	2573
2575	2582	2593	2598	2599	2606	2616	2616	2618	2620
2624	2626	2627	2628	2628	2632	2636	2637	2637	2644

Tables of resonant frequencies of free vibration of Flanged Cylindrical Shell. $\frac{H}{A} = 0.0053$

2644	2648	2649	2650	2652	2655	2658	2660	2668	2681
2685	2697	2678	2698	2699	2706	2707	2708	2711	2712
2714	2721	2721	2723	2723	2726	2728	2728	2730	2731
2736	2763	2766	2767	2773	2774	2774	2776	2777	2777
2778	2779	2780	2780	2782	2786	2786	2788	2789	2793
2793	2794	2799	2803	2804	2806	2811	2816	2819	2822
2826	2829	2834	2834	2838	2842	2845	2850	2851	2854
2856	2856	2856	2860	2862	2863	2872	2872	2873	2880
2882	2885	2886	2892	2893	2897	2899	2900	2903	2904
2909	2911	2916	2924	2924	2924	2927	2929	2933	2935
2940	2944	2952	2953	2953	2956	2961	2962	2964	2965
2965	2966	2973	2973	2979	2980	2989	2995	2997	3000
3000	3002	3003	3010	3014	3017	3021	3025	3026	3027
3027	3030	3031	3033	3034	3034	3036	3039	3041	3042
3043	3045	3053	3054	3055	3063	3067	3067	3068	3071
3074	3075	3076	3076	3077	3081	3083	3088	3092	3093
3094	3094	3095	3102	3103	3107	3110	3113	3115	3116
3120	3121	3121	3129	3133	3137	3139	3140	3141	3141
3143	3148	3151	3155	3156	3156	3159	3161	3162	3162
3164	3173	3173	3184	3184	3186	3188	3192	3196	3198
3198	3203	3404	3207	3207	3209	3209	3213	3216	3219
3219	3220	3221	3233	3234	3234	3235	3237	3243	3249
3251	3251	3253	3255	3260	3263	3266	3266	3274	3275
3280	3281	3282	3282	3283	3283	3285	3293	3294	3294
3297	3302	3303	3304	3305	3308	3309	3309	3310	3311
3315	3315	3315	3317	3323	3327	3331	3333	3333	3337
3339	3340	3343	3344	3344	3345	3348	3350	3353	3358
3359	3366	3366	3367	3367	3367	3368	3368	3371	3373
3373	3376	3378	3380	3387	3388	3390	3390	3396	3401
3404	3407	3409	3409	3412	3413	3413	3417	3419	3422
3423	3424	3428	3428	3428	3430	3431	3434	3440	3444
3451	3451	3453	3453	3454	3454	3455	3458	3459	3465
3470	3472	3472	3478	3479	3480	3481	3482	3482	3486
3489	3491	3491	3492	3494	3495	3505	3508	3509	3509
3510	3514	3515	3527	3528	3530	3530	3531	3534	3534
3535	3536	3537	3538	3539	3546	3550	3551	3557	3557
3561	3561	3563	3563	3563	3564	3565	3573	3576	3576
3583	3583	3586	3589	3590	3591	3595	3595	3596	3597
3598	3598	3599	3600	3603	3604	3609	3612	3614	3614
3619	3620	3623	3623	3624	3624	3625	3626	3633	3635
3637	3639	3640	3643	3645	3649	3649	3652	3654	3655
3655	3658	3663	3664	3664	3667	3670	3671	3675	3675
3679	3684	3686	3689	3690	3690	3690	3693	3697	3709
3710	3711	3711	3711	3711	3714	3715	3715	3717	3718
3728	3729	3730	3732	3732	3734	3735	3739	3741	3741
3744	3751	3754	3759	3761	3763	3768	3769	3770	3772
3776	3778	3780	3780	3782	3782	3785	3788	3794	3795
3796	3797	3799	3799	3812	3814	3814	3816	3818	3822
3825	3827	3828	3829	3834	3836	3837	3839	3839	3839
3845	3846	3851	3853	3856	3859	3863	3866	3868	3876

Tables of resonant frequencies of free vibration of Flanged Cylindrical Shell. $\frac{H}{A} = 0.0053$

3877	3879	3880	3883	3883	3884	3887	3888	3889	3889
3889	3893	3893	3893	3897	3897	3900	3907	3907	3907
3909	3910	3911	3912	3914	3919	3928	3929	3930	3932
3932	3932	3936	3937	3942	3943	3947	3947	3949	3955
3958	3964	3964	3966	3972	3972	3975	3977	3978	3979
3981	3983	3983	3986	3986	3987	3988	3995	3996	4000
4002	4002	4004	4005	4016	4020	4022	4027	4027	4028
4029	4030	4031	4041	4041	4044	4046	4051	4051	4054
4057	4058	4062	4063	4064	4069	4070	4070	4073	4078
4078	4081	4085	4086	4090	4091	4097	4097	4098	4106
4109	4110	4112	4115	4120	4126	4127	4131	4132	4133
4133	4135	4136	4143	4143	4146	4151	4154	4156	4160
4161	4162	4162	4165	4168	4169	4178	4181	4183	4183
4183	4186	4188	4190	4194	4197	4197	4202	4202	4203
4210	4211	4212	4212	4212	4214	4214	4217	4219	4220
4223	4224	4224	4228	4232	4235	4236	4239	4243	4252
4254	4256	4256	4257	4261	4266	4269	4270	4275	4276
4277	4279	4279	4283	4284	4287	4287	4290	4291	4295
4297	4302	4302	4306	4307	4308	4314	4315	4317	4317
4323	4324	4331	4339	4339	4343	4346	4348	4350	4355
4357	4360	4362	4363	4364	4369	4370	4371	4372	4372
4378	4380	4381	4381	4381	4390	4393	4394	4395	4402
4404	4404	4410	4410	4410	4425	4426	4435	4437	4437
4440	4442	4444	4446	4450	4451	4454	4454	4455	4458
4460	4465	4466	4467	4470	4471	4472	4476	4478	4484
4487	4491	4492	4496	4498	4499	4504	4505	4505	4506
4510	4511	4515	4518	4519	4527	4529	4531	4532	4538
4539	4539	4540	4541	4542	4543	4545	4548	4548	4551
4552	4554	4554	4559	4562	4563	4564	4568	4570	4579
4579	4582	4582	4584	4588	4600	4601	4602	4603	4607
4611	4612	4613	4614	4619	4621	4623	4623	4624	4629
4638	4638	4640	4643	4643	4645	4646	4651	4652	4654
4658	4660	4661	4667	4671	4672	4674	4678	4685	4687
4691	4691	4695	4697	4697	4698	4701	4705	4708	4710
4710	4713	4717	4725	4733	4736	4737	4738	4740	4742
4748	4749	4750	4755	4755	4759	4759	4767	4768	4771
4772	4773	4774	4775	4775	4780	4783	4784	4787	4796
4798	4799	4807	4813	4820	4824	4825	4827	4828	4831
4831	4831	4834	4836	4837	4837	4840	4845	4848	4849
4851	4852	4852	4852	4855	4855	4856	4857	4858	4859
4862	4862	4866	4870	4874	4877	4880	4890	4890	4894
4895	4896	4899	4911	4912	4914	4915	4918	4927	4927
4931	4931	4932	4932	4933	4933	4936	4938	4942	4945
4949	4949	4951	4951	4951	4953	4954	4958	4959	4961
4974	4974	4975	4982	4994	4997	4998	5001	5008	5010
5011	5011	5012	5013	5015	5018	5019	5022	5022	5023
5024	5025	5033	5041	5043	5044	5050	5051	5052	5052
5056	5063	5064	5065	5075	5076	5076	5082	5087	5088
5092	5093	5096	5098	5100	5101	5110	5110	5110	5110
5113	5118	5123	5124	5125	5135	5144	5145	5147	5149

Tables of resonant frequencies of free vibration of Flanged Cylindrical Shell. $\frac{H}{A} = 0.0053$

5153	5155	5155	5156	5159	5160	5163	5166	5168	5170
5171	5175	5176	5176	5177	5178	5178	5181	5182	5184
5186	5189	5194	5200	5203	5205	5209	5211	5212	5215
5216	5219	5220	5225	5228	5230	5234	5238	5245	5249
5250	5251	5254	5255	5256	5256	5259	5260	5260	5264
5264	5268	5269	5269	5270	5273	5279	5282	5290	5292
5300	5301	5308	5309	5310	5312	5314	5315	5316	5319
5326	5326	5331	5335	5336	5337	5343	5348	5353	5357
5359	5360	5360	5361	5361	5363	5366	5369	5371	5375
5376	5380	5381	5386	5388	5388	5390	5407	5411	5415
5415	5419	5420	5420	5421	5423	5430	5434	5434	5435
5439	5444	5450	5452	5453	5453	5455	5463	5465	5465
5466	5469	5470	5474	5483	5484	5485	5488	5495	5495
5504	5505	5510	5513	5515	5516	5517	5520	5520	5520
5522	5523	5527	5528	5531	5532	5535	5535	5535	5535
5538	5544	5548	5550	5556	5557	5558	5562	5569	5570
5573	5573	5575	5579	5581	5583	5584	5587	5590	5593
5597	5598	5601	5602	5604	5606	5612	5620	5620	5621
5622	5623	5627	5632	5634	5636	5638	5638	5640	5641
5642	5646	5648	5661	5663	5667	5677	5678	5678	5680
5682	5682	5686	5687	5688	5690	5694	5694	5696	5698
5709	5709	5713	5715	5725	5725	5725	5726	5727	5733
5741	5742	5743	5744	5745	5746	5746	5748	5756	5756
5763	5768	5770	5772	5778	5785	5785	5787	5791	5792
5798	5802	5803	5806	5814	5817	5820	5821	5822	5825
5827	5827	5828	5832	5834	5835	5837	5847	5848	5850
5854	5857	5858	5859	5864	5866	5870	5871	5875	5878
5879	5882	5888	5889	5890	5894	5897	5898	5899	5901
5903	5906	5907	5912	5917	5918	5920	5921	5923	5927
5931	5933	5935	5937	5940	5940	5943	5946	5946	5948
5948	5951	5952	5957	5959	5963	5968	5968	5971	5972
5972	5977	5982	5983	5986	5987	5998	6002	6005	6009
6011	6016	6025	6028	6029	6030	6032	6032	6033	6036
6040	6040	6043	6047	6048	6049	6049	6050	6052	6056
6059	6061	6067	6070	6074	6075	6076	6080	6080	6083
6086	6086	6091	6102	6107	6118	6120	6126	6126	6130
6131	6132	6140	6141	6144	6145	6146	6148	6149	6151
6151	6152	6153	6157	6160	6163	6167	6168	6169	6173
6176	6183	6188	6191	6193	6196	6199	6203	6205	6213
6218	6219	6219	6224	6231	6233	6239	6242	6243	6246
6249	6250	6251	6255	6256	6258	6262	6262	6264	6264
6268	6268	6270	6271	6272	6273	6276	6280	6280	6285
6286	6291	6291	6291	6291	6292	6298	6303	6305	6307
6308	6317	6319	6320	6322	6325	6328	6333	6337	6342
6342	6348	6350	6355	6362	6362	6363	6366	6369	6369
6370	6372	6375	6376	6380	6384	6387	6388	6390	6392
6393	6396	6398	6405	6409	6411	6412	6415	6415	6418
6418	6422	6425	6435	6436	6438	6442	6443	6443	6448
6449	6454	6469	6475	6476	6478	6481	6481	6481	6482
6482	6488	6490	6497	6502	6503	6505	6506	6509	6510

Tables of resonant frequencies of free vibration of Flanged Cylindrical Shell. $\frac{H}{A} = 0.0053$

6510	6512	6514	6522	6526	6529	6532	6534	6535	6535
6536	6540	6543	6546	6549	6557	6559	6564	6568	6569
6579	6590	6593	6593	6595	6602	6603	6604	6604	6605
6608	6608	6611	6612	6619	6622	6622	6628	6629	6629
6630	6633	6634	6636	6638	6641	6641	6647	6649	6651
6654	6655	6655	6656	6658	6662	6665	6676	6679	6680
6684	6685	6687	6688	6688	6689	6697	6700	6705	6705
6711	6713	6713	6713	6719	6720	6720	6721	6724	6727
6729	6730	6737	6740	6740	6748	6754	6754	6757	6758
6760	6763	6763	6769	6774	6774	6776	6779	6779	6783
6783	6783	6797	6797	6803	6807	6807	6811	6811	6814
6816	6820	6823	6828	6832	6833	6834	6837	6847	6850
6852	6853	6854	6855	6856	6856	6857	6860	6865	6871
6881	6884	6890	6890	6894	6896	6900	6900	6901	6904
6905	6905	6905	6910	6917	6920	6921	6929	6932	6936
6936	6941	6943	6945	6947	6951	6954	6958	6964	6966
6972	6974	6975	6979	6980	6980	6983	6989	6997	6997
6999	7002	7010	7012	7014	7019	7026	7026	7026	7027
7029	7030	7032	7033	7033	7033	7037	7040	7041	7043
7045	7051	7053	7056	7056	7059	7061	7063	7064	7068
7071	7073	7084	7086	7086	7093	7097	7098	7098	7100
7101	7101	7102	7105	7108	7111	7112	7112	7117	7118
7124	7125	7134	7136	7140	7142	7147	7149	7154	7155
7157	7157	7162	7164	7168	7170	7172	7175	7179	7180
7184	7185	7189	7191	7193	7195	7195	7199	7202	7203
7204	7213	7218	7224	7226	7226	7227	7229	7230	7237
7239	7244	7244	7251	7254	7257	7271	7272	7273	7275
7282	7282	7285	7285	7286	7287	7288	7293	7293	7293
7296	7296	7303	7310	7313	7313	7313	7315	7317	7323
7324	7334	7335	7344	7350	7351	7352	7355	7356	7357
7357	7361	7391	7371	7378	7385	7385	7386	7397	7398
7405	7406	7409	7411	7412	7415	7415	7416	7418	7418
7420	7422	7427	7429	7430	7438	7438	7438	7439	7440
7441	7445	7447	7451	7452	7458	7459	7460	7467	7469
7470	7473	7477	7480	7481	7482	7487	7492	7494	7494
7494	7500	7502	7506	7508	7509	7513	7520	7526	7526
7527	7533	7539	7540	7541	7541	7543	7544	7545	7547
7550	7551	7551	7551	7552	7554	7563	7564	7565	7566
7574	7580	7592	7587	7587	7593	7607	7608	7608	7609
7610	7611	7612	7613	7619	7620	7629	7630	7630	7632
7637	7638	7639	7642	7651	7655	7656	7664	7664	7666
7670	7673	7677	7677	7680	7689	7689	7690	7692	7693
7694	7698	7700	7702	7704	7710	7712	7712	7715	7715
7725	7729	7731	7733	7736	7740	7746	7749	7750	7754
7758	7766	7768	7768	7779	7781	7781	7787	7790	7791
7792	7793	7794	7795	7797	7806	7814	7815	7815	7816
7822	7824	7827	7828	7829	7829	7834	7834	7840	7841
7844	7852	7852	7857	7860	7863	7864	7865	7868	7871
7871	7873	7879	7880	7885	7886	7888	7889	7889	7890
7900	7905	7908	7908	7908	7909	7913	7919	7919	7919

Tables of resonant frequencies of free vibration of Flanged Cylindrical Shell. $\frac{H}{A} = 0.0053$

7922	7928	7931	7931	7934	7935	7935	7935	7941	7945
7946	7950	7954	7955	7956	7964	7966	7967	7969	7970
7979	7980	7982	7984	7986	7990	7993	7994	7998	8001
8004	8006	8007	8013	8026	8027	8029	8030	8031	8032
8034	8035	8040	8047	8050	8050	8051	8055	8055	8056
8065	8065	8073	8074	8075	8078	8078	8079	8084	8087
8087	8097	8098	8098	8107	8112	8113	8113	8126	8127
8130	8130	8135	8136	8137	8139	8142	8144	8146	8147
8157	8159	8160	8161	8162	8166	8173	8173	8175	8177
8178	8181	8188	8191	8195	8196	8210	8212	8216	8217
8219	8221	8222	8223	8238	8240	8241	8242	8244	8246
8247	8248	8250	8257	8257	8259	8272	8272	8273	8276
8277	8280	8282	8287	8287	8288	8291	8291	8295	8295
8299	8302	8302	8304	8307	8310	8315	8319	8319	8322
8325	8327	8331	8332	8333	8338	8342	8343	8344	8351
8352	8356	8357	8357	8358	8359	8366	8369	8370	8374
8376	8378	8385	8388	8394	8395	8395	8395	8403	8407
8411	8413	8415	8415	8416	8418	8420	8422	8423	8424
8428	8428	8430	8437	8450	8450	8452	8458	8459	8459
8461	8461	8466	8467	8470	8471	8472	8477	8487	8491
8492	8495	8497	8506	8506	8512	8514	8514	8515	8519
8525	8532	8533	8536	8540	8540	8542	8544	8546	8551
8555	8555	8557	8557	8559	8560	8570	8570	8574	8575
8579	8582	8585	8586	8587	8594	8597	8603	8604	8606
8608	8615	8617	8621	8625	8626	8634	8635	8641	8642
8643	8645	8658	8659	8663	8666	8671	8678	8679	8680
8682	8685	8685	8687	8689	8692	8692	8698	8701	8701
8705	8707	8709	8711	8712	8714	8717	8722	8724	8726
8726	8730	8731	8731	8733	8738	8740	8744	8752	8755
8757	8758	8762	8769	8770	8770	8773	8774	8776	8785
8786	8793	8795	8796	8796	8797	8799	8800	8801	8802
8811	8812	8815	8818	8819	8824	8824	8829	8829	8829
8830	8836	8837	8837	8838	8843	8845	8851	8853	8855
8857	8863	8864	8871	8876	8880	8880	8881	8882	8887
8889	8889	8890	8890	8903	8907	8910	8911	8918	8922
8929	8929	8932	8933	8934	8936	8944	8945	8948	8948
8950	8951	8951	8957	8966	8967	8967	8974	8980	8982
8982	8985	8986	8988	8989	8990	8990	9006	9006	9007
9007	9015	9017	9018	9019	9019	9020	9028	9032	9035
9036	9036	9037	9040	9050	9063	9067	9067	9076	9078
9080	9081	9082	9085	9085	9086	9089	9090	9096	9098
9104	9107	9107	9107	9121	9124	9130	9133	9134	9136
9137	9138	9140	9143	9144	9147	9148	9148	9149	9157
9160	9165	9171	9175	9177	9185	9187	9187	9190	9191
9192	9192	9193	9193	9193	9198	9200	9200	9206	9208
9216	9217	9217	9224	9225	9227	9230	9231	9236	9240
9242	9245	9248	9249	9255	9255	9258	9259	9264	9266
9267	9268	9268	9272	9281	9283	9285	9286	9288	9289
9291	9291	9293	9295	9298	9298	9300	9311	9311	9317
9319	9320	9331	9333	9337	9338	9340	9350	9352	9353

Tables of resonant frequencies of free vibration of Flanged Cylindrical Shell. $\frac{H}{A} = 0.0053$

9355	9356	9357	9361	9364	9365	9365	9367	9370	9373
9378	9381	9381	9383	9386	9390	9393	9395	9395	9404
9407	9411	9422	9427	9427	9429	9436	9437	9440	9440
9444	9444	9444	9448	9449	9451	9458	9460	9466	9466
9468	9471	9478	9479	9483	9484	9494	9494	9500	9501
9504	9505	9506	9507	9510	9512	9512	9512	9513	9514
9514	9527	9531	9535	9538	9539	9549	9556	9561	9570
9570	9573	9575	9577	9585	9588	9589	9590	9591	9592
9595	9598	9604	9607	9608	9609	9611	9613	9618	9621
9623	9624	9634	9638	9640	9640	9642	9646	9650	9650
9650	9653	9653	9656	9657	9658	9661	9663	9664	9671
9672	9674	9674	9676	9678	9681	9685	9685	9690	9692
9695	9700	9704	9706	9714	9715	9717	9719	9721	9727
9733	9736	9738	9738	9739	9742	9754	9755	9756	9757
9758	9760	9767	9768	9769	9773	9776	9776	9777	9777
9777	9780	9780	9782	9784	9790	9790	9795	9797	9799
9803	9808	9809	9822	9823	9831	9832	9833	9834	9837
9837	9838	9842	9843	9846	9846	9848	9850	9857	9865
9869	9876	9881	9881	9884	9885	9888	9889	9896	9898
9903	9905	9918	9921	9921	9923	9926	9930	9931	9931
9935	9936	9941	9941	9942	9942	9942	9943	9951	9954
9958	9959	9961	9963	9964	9967	9968	9969	9971	9976
9983	9984	9997	9999	10004	10004	10004	10010	10010	10011
10018	10020	10027	10039	10040	10042	10050	10051	10055	10060
10061	10063	10066	10073	10074	10076	10078	10078	10087	10090
10091	10094	10095	10095	10096	10100	10100	10103	10105	10107
10109	10109	10110	10110	10118	10119	10127	10128	10128	10129
10134	10134	10135	10140	10148	10153	10158	10158	10159	10160
10160	10164	10169	10169	10170	10171	10180	10181	10182	10183
10191	10196	10197	10198	10200	10204	10205	10213	10214	10214
10214	10215	10220	10221	10222	10231	10232	10233	10242	10244
10245	10249	10253	10259	10259	10261	10261	10265	10268	10268
10275	10276	10276	10277	10277	10280	10282	10284	10288	10291
10294	10297	10300	10300	10302	10305	10316	10325	10325	10326
10337	10338	10341	10342	10346	10350	10351	10351	10353	10353
10353	10357	10361	10363	10363	10374	10379	10382	10382	10384
10386	10391	10394	10394	10396	10404	10413	10419	10425	10429
10430	10433	10434	10436	10438	10438	10442	10443	10445	10446
10449	10452	10453	10453	10455	10455	10460	10465	10471	10473
10475	10475	10481	10490	10496	10497	10498	10502	10503	10511
10512	10513	10517	10517	10524	10525	10527	10527	10537	10540
10540	10547	10555	10560	10562	10563	10567	10569	10571	10571
10573	10581	10594	10595	10595	10597	10599	10600	10602	10608
10610	10610	10615	10616	10618	10618	10618	10618	10621	10622
10622	10626	10628	10630	10631	10636	10637	10645	10646	10647
10647	10651	10655	10658	10665	10667	10671	10671	10673	10678
10678	10681	10683	10685	10686	10687	10691	10694	10699	10701
10703	10703	10703	10705	10707	10711	10712	10721	10725	10726
10738	10739	10742	10746	10757	10758	10760	10764	10764	10766
10770	10771	10773	10773	10775	10784	10787	10788	10789	10790

Tables of resonant frequencies of free vibration of Flanged Cylindrical Shell. $\frac{H}{A} = 0.0053$

10790	10795	10796	10798	10801	10803	10805	10808	10812	10813
10814	10814	10817	10819	10822	10822	10830	10832	10834	10841
10841	10845	10848	10860	10860	10866	10868	10870	10872	10873
10876	10878	10879	10880	10898	10901	10902	10903	10912	10914
10919	10924	10925	10925	10934	10935	10937	10937	10942	10943
10944	10944	10950	10953	10958	10959	10960	10963	10963	10967
10969	10975	10976	10979	10979	10980	10984	10988	10990	10990
10992	10994	10996	11000	11004	11005	11010	11011	11019	11034
11036	11037	11045	11043	11053	11055	11057	11060	11062	11073
11074	11075	11079	11080	11083	11090	11092	11092	11094	11095
11100	11104	11105	11106	11111	11115	11115	11115	11118	11119
11122	11125	11125	11128	11131	11132	11135	11135	11136	11139
11143	11146	11147	11150	11154	11157	11157	11159	11159	11160
11161	11169	11169	11171	11172	11179	11184	11186	11189	11192
11201	11201	11202	11203	11203	11206	11214	11215	11216	11221
11221	11236	11236	11242	11242	11242	11242	11244	11244	11248
11252	11255	11258	11260	11261	11264	11272	11279	11281	11286
11288	11289	11289	11291	11296	11298	11304	11305	11310	11311
11313	11318	11318	11319	11324	11326	11326	11327	11329	11333
11340	11340	11340	11341	11341	11343	11344	11351	11353	11360
11361	11370	11374	11375	11377	11391	11397	11401	11402	11406
11409	11410	11411	11413	11418	11418	11419	11421	11424	11426
11428	11429	11434	11438	11448	11449	11452	11454	11455	11464
11465	11468	11469	11471	11474	11475	11476	11479	11480	11480
11495	11498	11505	11505	11505	11506	11508	11510	11517	11523
11524	11529	11532	11535	11537	11538	11538	11538	11543	11546
11550	11558	11559	11563	11576	11576	11577	11578	11579	11581
11582	11585	11599	11601	11601	11604	11607	11612	11614	11615
11617	11620	11623	11625	11626	11626	11629	11633	11638	11640
11640	11642	11643	11643	11648	11654	11655	11656	11657	11661
11665	11668	11669	11670	11675	11679	11682	11682	11693	11695
11696	11697	11697	11703	11705	11705	11709	11713	11714	11714
11715	11716	11716	11717	11720	11724	11725	11729	11733	11737
11738	11743	11745	11752	11753	11753	11761	11764	11765	11766
11772	11772	11773	11775	11779	11791	11791	11792	11796	11799
11800	11810	11819	11823	11824	11824	11825	11832	11835	11835
11837	11837	11838	11848	11849	11849	11850	11850	11851	11852
11859	11861	11863	11869	11876	11881	11881	11882	11883	11884
11889	11892	11894	11896	11896	11899	11901	11901	11907	11912
11913	11914	11915	11915	11930	11942	11944	11945	11947	11950
11955	11963	11965	11967	11967	11967	11971	11976.	11979	11980
11986	11988	11989	11989	12005	12007	12007	12010	12012	12012
12013	12015	12016	12022	12023	12027	12036	12037	12037	12038
12038	12041	12048	12054	12064	12064	12065	12065	12074	12074
12075	12079	12081	12085	12087	12087	12090	12094	12095	12100
12101	12104	12106	12110	12112	12113	12123	12127	12134	12136
12136	12138	12141	12149	12152	12156	12158	12162	12170	12170
12174	12177	12179	12180	12180	12180	12181	12181	12184	12185
12187	12188	12192	12192	12193	12193	12197	12197	12200	12201
12202	12205	12208	12218	12219	12220	12225	12231	12234	12235

Tables of resonant frequencies of free vibration of Flanged Cylindrical Shell. $\frac{H}{A} = 0.0053$

12236	12237	12237	12254	12254	12255	12260	12261	12261	12263
12266	12266	12267	12268	12269	12272	12276	12276	12276	12281
12287	12294	12298	12298	12299	12301	12317	12321	12322	12327
12328	12329	12331	12338	12347	12348	12350	12351	12351	12356
12362	12362	12364	12367	12372	12373	12373	12374	12374	12374
12375	12378	12381	12388	12392	12395	12398	12399	12401	12402
12404	12405	12410	12414	12417	12424	12425	12429	12435	12435
12436	12438	12446	12451	12452	12460	12465	12466	12467	12468
12469	12475	12478	12481	12490	12494	12499	12501	12503	12511
12511	12513	12514	12516	12517	12520	12524	12525	12529	12530
12534	12537	12538	12539	12541	12552	12555	12556	12560	12561
12567	12567	12567	12568	12570	12570	12577	12582	12585	12586
12586	12592	12609	12613	12616	12617	12618	12624	12624	12625
12626	12632	12634	12636	12647	12652	12654	12655	12656	12659
12659	12663	12663	12663	12667	12672	12676	12683	12683	12686
12686	12687	12688	12690	12691	12697	12698	12699	12701	12702
12705	12713	12714	12714	12721	12722	12723	12726	12728	12736
12739	12739	12748	12749	12753	12754	12754	12754	12754	12757
12759	12760	12767	12769	12771	12772	12773	12775	12776	12777
12779	12781	12790	12792	12795	12797	12799	12803	12809	12810
12812	12824	12826	12832	12835	12837	12842	12842	12842	12844
12846	12847	12849	12850	12853	12854	12856	12860	12863	12867
12868	12875	12877	12878	12882	12888	12890	12894	12903	12908
12909	12909	12912	12912	12912	12916	12923	12925	12928	12932
12938	12940	12941	12941	12944	12947	12949	12951	12960	12966
12966	12969	12970	12970	12973	12975	12975	12977	12978	12989
12997	12998	12998	13000	13001	13002	13003	13008	13010	13025
13025	13026	13031	13036	13037	13039	13047	13048	13049	13053
13053	13056	13057	13058	13065	13071	13073	13080	13083	13083
13086	13087	13087	13087	13090	13091	13107	13111	13115	13119
13120	13122	13126	13129	13132	13134	13142	13149	13150	13151
13151	13153	13155	13165	13165	13166	13168	13171	13172	13174
13177	13177	13180	13185	13193	13194	13196	13196	13198	13200
13202	13203	13212	13214	13218	13227	13229	13232	13234	13235
13236	13236	13237	13237	13239	13242	13247	13249	13250	13252
13255	13259	13260	13263	13269	13269	13272	13272	13282	13285
13294	13294	13299	13300	13302	13306	13311	13312	13317	13324
13324	13326	13327	13329	13330	13332	13335	13335	13336	13337
13338	13339	13340	13340	13341	13341	13347	13351	13352	13356
13358	13362	13364	13367	13371	13376	13377	13378	13378	13378
13384	13387	13398	13398	13402	13407	13411	13420	13426	13427
13428	13428	13431	13431	13432	13441	13446	13447	13449	13455
13457	13458	13459	13461	13464	13471	13474	13481	13484	13486
13499	13499	13500	13503	13504	13507	13507	13508	13512	13513
13515	13521	13522	13522	13523	13525	13525	13534	13535	13535
13536	13536	13544	13548	13556	13557	13559	13559	13560	13563
13570	13571	13576	13580	13582	13583	13591	13591	13597	13598
13604	13607	13609	13613	13615	13617	13619	13621	13634	13638
13639	13642	13648	13648	13649	13657	13664	13664	13665	13671
13671	13675	13676	13682	13686	13689	13696	13697	13697	13700

Tables of resonant frequencies of free vibration of Flanged Cylindrical Shell. $\frac{H}{A} = 0.0053$

13705	13708	13708	13710	13712	13713	13716	13718	13719	13720
13720	13729	13734	13739	13742	13744	13747	13751	13753	13761
13762	13762	13770	13772	13772	13782	13783	13783	13784	13785
13785	13786	13789	13789	13790	13790	13792	13794	13800	13800
13802	13808	13810	13817	13825	13826	13828	13829	13833	13839
13842	13842	13843	13847	13849	13850	13852	13852	13857	13869
13871	13871	13874	13875	13876	13881	13882	13888	13892	13893
13897	13898	13900	13902	13907	13907	13909	13913	13914	13915
13916	13918	13919	13922	13923	13926	13931	13934	13934	13935
13935	13941	13948	13948	13954	13955	13959	13963	13965	13969
13974	13978	13983	13985	13985	13991	13992	14000	14000	14004
14010	14012	14013	14017	14021	14025	14026	14030	14030	14032
14032	14033	14033	14042	14044	14044	14045	14047	14055	14057
14057	14067	14073	14079	14080	14081	14087	14087	14093	14093
14103	14103	14104	14105	14112	14113	14116	14121	14122	14124
14124	14126	14129	14137	14137	14138	14140	14145	14156	14158
14158	14166	14167	14167	14170	14174	14176	14176	14179	14179
14183	14187	14191	14194	14194	14197	14199	14201	14202	14209
14212	14214	14214	14217	14220	14222	14226	14235	14242	14249
14254	14254	14255	14256	14257	14264	14269	14270	14284	14286
14286	14286	14289	14291	14296	14315	14317	14318	14318	14319
14320	14324	14324	14324	14324	14325	14330	14337	14339	14342
14343	14344	14345	14355	14356	14357	14358	14359	14362	14362
14363	14369	14372	14373	14376	14376	14378	14379	14380	14380
14383	14385	14385	14386	14390	14398	14398	14403	14409	14411
14415	14416	14416	14417	14418	14421	14422	14426	14426	14432
14432	14443	14443	14445	14461	14462	14466	14468	14472	14473
14479	14480	14481	14482	14482	14483	14492	14498	14500	14502
14504	14504	14504	14510	14519	14521	14526	14528	14529	14531
14533	14536	14539	14541	14542	14545	14545	14547	14549	14551
14552	14553	14554	14554	14556	14559	14560	14563	14575	14579
14581	14581	14584	14588	14595	14600	14603	14610	14610	14617
14619	14621	14621	14622	14626	14630	14631	14631	14637	14638
14641	14642	14643	14646	14648	14649	14653	14653	14658	14674
14676	14681	14683	14694	14699	14709	14712	14714	14716	14717
14719	14721	14725	14726	14726	14730	14731	14735	14735	14742
14742	14743	14745	14747	14747	14750	14751	14753	14756	14757
14757	14758	14767	14767	14768	14772	14776	14776	14783	14785
14791	14795	14808	14809	14811	14813	14816	14817	14818	14819
14823	14830	14833	14835	14837	14840	14846	14847	14860	14865
14865	14870	14872	14874	14878	14882	14888	14889	14896	14898
14898	14903	14905	14908	14914	14917	14921	14926	14927	14927
14929	14933	14935	14935	14936	14936	14938	14939	14941	14943
14943	14944	14948	14949	14951	14953	14953	14957	14966	14967
14967	14967	14969	14972	14974	14978	14979	14986	14989	14991
14995	14996	14999	15000	15000	15002	15006	15020	15020	15023
15025	15027	15032	15035	15037	15040	15041	15042	15049	15050
15051	15051	15053	15058	15062	15064	15067	15067	15074	15074
15076	15079	15080	15084	15087	15091	15099	15100	15108	15108
15110	15111	15115	15118	15120	15127	15134	15135	15137	15141

Tables of resonant frequencies of free vibration of Flanged Cylindrical Shell. $\frac{H}{A} = 0.0053$

15142	15143	15143	15143	15146	15152	15153	15154	15154	15157
15161	15161	15162	15179	15181	15183	15183	15191	15191	15191
15204	15204	15206	15206	15206	15206	15215	15217	15222	15222
15223	15229	15232	15232	15239	15243	15247	15248	15251	15254
15254	15254	15262	15264	15265	15268	15273	15276	15276	15276
15276	15278	15285	15288	15289	15289	15298	15301	15313	15316
15320	15325	15327	15341	15351	15351	15352	15352	15353	15354
15357	15359	15361	15362	15363	15365	15365	15366	15372	15373
15373	15374	15374	15380	15390	15390	15391	15392	15401	15403
15414	15420	15423	15425	15427	15427	15428	15430	15430	15431
15440	15441	15445	15448	15449	15450	15452	15462	15472	15475
15477	15479	15481	15485	15485	15487	15488	15488	15500	15504
15504	15505	15507	15508	15511	15513	15518	15524	15527	15530
15534	15534	15540	15541	15542	15543	15543	15545	15549	15550
15558	15563	15563	15565	15569	15570	15571	15573	15574	15580
15581	15583	15583	15584	15586	15597	15598	15598	15607	15610
15611	15614	15615	15617	15618	15621	15621	15625	15627	15629
15632	15634	15634	15635	15637	15637	15639	15647	15651	15651
15654	15659	15663	15665	15665	15667	15676	15676	15678	15680
15683	15684	15698	15700	15700	15702	15703	15704	15709	15711
15712	15712	15725	15726	15731	15737	15737	15739	15747	15747
15748	15750	15753	15765	15772	15774	15776	15780	15780	15782
15784	15785	15787	15792	15796	15796	15800	15804	15804	15807
15808	15809	15811	15813	15815	15821	15821	15823	15825	15825
15826	15832	15834	15842	15842	15843	15846	15846	15846	15866
15866	15869	15870	15870	15875	15877	15881	15884	15886	15891
15892	15900	15909	15911	15912	15917	15918	15918	15920	15920
15922	15929	15932	15933	15952	15952	15955	15957	15959	15960
15960	15976	15977	15985	15985	15987	15987	15989	15991	15994
15994	15995	15995	15996	15998	16000	16007	16012	16013	16014
16016	16017	16019	16021	16026	16028	16034	16035	16037	16040
16044	16047	16047	16053	16058	16064	16065	16073	16080	16084
16087	16095	16097	16099	16104	16104	16111	16114	16115	16118
16120	16121	16123	16125	16130	16131	16133	16133	16135	16138
16142	16144	16147	16147	16148	16149	16152	16152	16157	16158
16159	16161	16162	16167	16172	16173	16176	16184	16186	16187
16188	16191	16201	16206	16207	16207	16209	16210	16213	16213
16215	16215	16215	16218	16220	16221	16232	16232	16233	16233
16233	16237	16247	16257	16260	16260	16263	16264	16264	16265
16268	16268	16272	16273	16275	16279	16282	16282	16284	16291
16295	16303	16309	16309	16310	16316	16318	16324	16324	16326
16329	16329	16329	16329	16334	16350	16351	16352	16354	16356
16366	16367	16368	16371	16375	16376	16377	16377	16378	16383
16386	16389	16390	16400	16403	16405	16410	16414	16417	16417
16418	16425	16426	16430	16430	16431	16433	16433	16434	16436
16437	16439	16444	16447	16449	16454	16457	16469	16473	16474
16475	16478	16484	16487	16487	16489	16492	16496	16500	16505
16508	16514	16518	16520	16521	16524	16530	16533	16537	16538
16539	16543	16546	16551	16554	16558	16558	16559	16561	16565
16573	16574	16575	16575	16578	16582	16585	16589	16592	16594

Tables of resonant frequencies of free vibration of Flanged Cylindrical Shell. $\frac{H}{A} = 0.0053$

16598	16599	16606	16612	16613	16619	16622	16622	16640	16640
16641	16642	16644	16645	16645	16648	16648	16648	16653	16654
16657	16663	16664	16665	16670	16674	16676	16677	16679	16683
16683	16693	16712	16718	16719	16724	16729	16729	16730	16731
16732	16732	16733	16735	16735	16736	16738	16740	16745	16746
16748	16752	16754	16756	16757	16759	16759	16759	16766	16766
16767	16770	16776	16776	16776	16776	16788	16790	16793	16796
16798	16800	16801	16807	16810	16813	16816	16819	16820	16821
16824	16825	16827	16833	16838	16843	16850	16851	16857	16858
16859	16866	16068	16872	16873	16875	16875	16877	16879	16880
16883	16889	16891	16892	16892	16894	16895	16897	16901	16905
16910	16912	16914	16915	16918	16922	16922	16922	16924	16927
16937	16938	16940	16944	16945	16946	16950	16951	16951	16952
16964	16969	16970	16971	16977	16980	16981	16981	16986	16987
16988	16996	17000	17000	17004	17018	17028	17029	17031	17034
17035	17037	17042	17046	17046	17049	17051	17053	17056	17060
17064	17066	17066	17067	17071	17072	17075	17089	17090	17090
17091	17093	17094	17095	17099	17102	17103	17104	17105	17111
17114	17114	17117	17123	17128	17129	17135	17137	17141	17142
17143	17148	17151	17153	17154	17154	17161	17166	17167	17168
17172	17173	17181	17185	17191	17197	17201	17203	17204	17205
17210	17213	17216	17217	17217	17218	17220	17223	17241	17244
17244	17244	17244	17255	17258	17262	17265	17268	17270	17279
17280	17285	17294	17296	17297	17298	17299	17301	17308	17309
17313	17314	17315	17315	17323	17323	17325	17327	17329	17332
17333	17336	17343	17343	17343	17344	17347	17350	17351	17351
17356	17356	17303	17363	17364	17371	17373	17374	17379	17380
17382	17385	17387	17390	17393	17396	17400	17402	17404	17410
17411	17414	17421	17423	17427	17428	17428	17428	17429	17432
17438	17439	17439	17442	17443	17444	17448	17448	17456	17459
17466	17471	17476	17478	17478	17487	17490	17492	17492	17498
17501	17502	17508	17509	17510	17511	17513	17520	17524	17525
17529	17535	17539	17542	17542	17543	17544	17545	17545	17548
17548	17548	17549	17549	17554	17558	17560	17561	17561	17570
17570	17571	17572	17572	17578	17586	17589	17590	17590	17596
17597	17600	17604	17604	17608	17621	17621	17621	17622	17627
17627	17652	17657	17657	17658	17658	17660	17662	17668	17679
17679	17680	17680	17681	17682	17684	17687	17688	17688	17690
17692	17694	17700	17710	17710	17710	17714	17715	17717	17719
17720	17725	17734	17745	17748	17750	17750	17751	17761	17766
17769	17769	17770	17771	17771	17772	17774	17775	17777	17779
17783	17784	17786	17788	17794	17796	17799	17811	17814	17818
17821	17827	17827	17830	17831	17831	17835	17839	17843	17846
17847	17852	17053	17858	17861	17863	17868	17878	17879	17881
17883	17883	17886	17887	17889	17891	17893	17898	17899	17912
17916	17918	17918	17921	17922	17923	17923	17924	17926	17927
17939	17949	17956	17958	17963	17969	17971	17972	17984	17985
17992	17994	17995	17996	17996	18001	18002	18007	18008	18009
18012	18012	18016	18016	18019	18019	18020	18020	18021	18021
18022	18022	18042	18024	18025	18025	18027	18030	18039	18040

Tables of resonant frequencies of free vibration of Flanged Cylindrical Shell. $\frac{H}{A} = 0.0053$

18052	18052	18055	18059	18059	18065	18065	18065	18069	18073
18075	18080	18084	18086	18090	18093	18096	18097	18099	18100
18101	18102	18103	18107	18111	18111	18115	18115	18115	18116
18126	18133	18136	18139	18141	18145	18153	18157	18158	18158
18160	18162	18163	18165	18167	18168	18171	18174	18182	18182
18188	18200	18208	18212	18221	18222	18222	18223	18226	18227
18229	18232	18232	18233	18234	18235	18235	18236	18237	18240
18241	18242	18250	18254	18260	18264	18264	18267	18268	18270
18273	18278	18278	18281	18287	18287	18288	18295	18302	18305
18305	18305	18309	18311	18313	18317	18318	18320	18326	18328
18333	18336	18336	18342	18344	18346	18348	18350	18353	18358
18363	18370	18371	18375	18382	18383	18383	18384	18392	18395
18398	18399	18400	18406	18408	18410	18412	18413	18416	18437
18437	18438	18440	18454	18456	18459	18461	18462	18463	18463
18466	18468	18473	18475	18477	18479	18483	18486	18487	18490
18490	18495	18502	18503	18507	18507	18509	18513	18514	18514
18519	18519	18525	18526	18527	18527	18528	18530	18530	18531
18534	18537	18541	18547	18552	18552	18562	18564	18572	18575
18581	18584	18585	18588	18588	18592	18601	18607	18608	18618
18621	18623	18627	18632	18634	18643	18645	18651	18654	18654
18657	18658	18658	18661	18661	18665	18666	18669	18671	18672
18672	18673	18675	18677	18680	18689	18689	18689	18690	18693
18695	18695	18701	18703	18704	18704	18704	18705	18711	18712
18714	18718	18719	18724	18725	18727	18729	18731	18735	18737
18739	18740	18745	18746	18753	18753	18759	18760	18764	18764
18764	18765	18779	18780	18785	18785	18788	18789	18791	18791
18792	18802	18806	18806	18807	18813	18813	18815	18819	18831
18831	18832	18834	18837	18841	18849	18851	18853	18854	18857
18860	18861	18869	18872	18874	18875	18875	18878	18879	18884
18886	18889	18894	18902	18902	18905	18911	18913	18914	18916
18918	18925	18925	18926	18929	18930	18935	18941	18942	18944
18944	18945	18945	18949	18963	18963	18965	18967	18968	18969
18970	18973	18977	18981	18982	18988	18998	19000	19005	19006
19008	19010	19010	19010	19012	19013	19014	19016	19033	19036
19039	19045	19048	19050	19052	19052	19054	19055	19056	19062
19063	19063	19070	19074	19076	19083	19084	19085	19086	19087
19094	19094	19102	19110	19113	19116	19119	19119	19123	19126
19128	19128	19136	19144	19155	19156	19157	19160	19162	19165
19166	19166	19166	19167	19167	19168	19173	19178	19181	19183
19187	19195	19200	19203	19207	19208	19208	19211	19215	19221
19221	19222	19225	19227	19233	19235	19237	19242	19242	19247
19247	19248	19256	19259	19269	19271	19277	19280	19284	19284
19288	19290	19291	19293	19300	19300	19303	19304	19307	19309
19312	19315	19319	19320	19322	19326	19326	19330	19332	19332
19336	19338	19340	19340	19350	19352	19353	19356	19357	19357
19358	19362	19362	19362	19365	19368	19370	19373	19375	19385
19390	19397	19403	19405	19405	19407	19407	19407	19414	19415
19416	19416	19416	19416	19423	19425	19425	19427	19429	19434
19434	19438	19438	19442	19446	19451	19455	19468	19475	19481
19482	19485	19487	19492	19492	19492	19497	19498	19498	19499

Tables of resonant frequencies of free vibration of Flanged Cylindrical Shell. $\frac{H}{A} = 0.0053$

19499	19500	19504	19507	19508	19509	19511	19511	19515	19517
19524	19524	19524	19525	19528	19529	19532	19533	19539	19543
19543	19545	19546	19548	19562	19565	19568	19572	19574	19581
19585	19587	19598	19599	19605	19607	19611	19612	19622	19625
19626	19628	19628	19629	19635	19636	19638	19645	19648	19649
19653	19655	19657	19661	19661	19663	19666	19671	19672	19672
19673	19675	19678	19682	19682	19686	19689	19689	19692	19692
19696	19707	19708	19709	19710	19718	19725	19730	19738	19739
19742	19743	19744	19746	19746	19747	19752	19752	19754	19757
19758	19765	19766	19768	19770	19770	19781	19783	19784	19787
19794	19800	19802	19803	19804	19806	19814	19819	19819	19824
19828	19835	19843	19854	19857	19857	19862	19863	19868	19871
19872	19875	19877	19880	19881	19882	19885	19886	19888	19892
19893	19894	19894	19898	19898	19899	19906	19909	19911	19914
19917	19917	19917	19920	19928	19936	19937	19940	19942	19942
19943	19947	19958	19961	19964	19967	19968	19969	19970	19981
19986	19991	19993	19994	19995	19998	19999	19999	20005	20006

TOTAL MILL TIME 143 secs.

APPENDIX 4

The Computer Program for the Determination of Radiation Efficiency.

Explanation of some of the input parameters.

M = Axial - mode numbers = I : I : 100.

N = Circumferential - mode numbers = 0 : I : 39.

MU = Poissons ratio = 0.29.

E = Youngs modulus = 30,000000. ($2.092 \times 10^6 \times kg/M^2$)

RHO = 0.000735 a constant.

CA = Speed of sound = 13050 in/sec. (331.46M/sec.)

L = Length of the sylinder = 72 ins. (I.8288 M)

H = Thickness of the material = 0.048. ($I.2192 \times 10^{-3}$ M)

A = Radius = 9 ins. (0.2286 M)

PI = 3.14159236.

V1,V2.,V3 = Normalized frequency steps.

CL = Longitudival wave speed.

VP = Equivalent plate resonant frequencies.

V = Cylinder resonant frequencies.

AK X I = Relation that satisfy circumferential strip modes.

AK X 2 = Relation that satisfy acoustically fast modes.

```
11/34/23        06/02/70        COMPILED BY XALT MK. 1E
STATEMENT
     0      'LIBRARY' (ED,SUBGROUPSRF7)
     0      'BEGIN'
     1          'INTEGER' NN,M,N;
     1          'REAL' MU,E,RHO,CA,L,H,A,V1,V2,V3,P,PI,CL,C,C2,VG,NUC,GAMMA,Q,NUU,
     2                                                  G,VP,AKX1,AKX2,L2,V;
     2          'REAL' FREQSTEP,F,FF,F1,RATIO,LOGRATIO;
     3          'INTEGER' 'ARRAY' COUNT1,COUNT2[1:1000];
     4
     4
     4          'PROCEDURE' ON(N);
     6          'VALUE' N;
     7          'INTEGER' N;
     8          'EXTERNAL';
     8
     8
     8          'REAL' 'PROCEDURE' ALOG10(X);
    10          'VALUE' X;
    11          'REAL' X;
    12          'EXTERNAL';
    12
    12
    12          ON(9);
    14          SELECT INPUT(0);
    15          SELECT OUTPUT(0);
    16          MU:=READ;
    17          E:=READ;
    18          RHO:=READ;
    19          CA:=READ;
    20          L:=READ;
    21          H:=READ;
    22          A:=READ;
    23          V1:=READ;
    24          V2:=READ;
    25          V3:=READ;
    26          FREQSTEP:=READ;
    27          P:=1-MU*MU;
    28          CL:=SQRT(E/(RHO*P));
    29          PI:=3.14159263;
    30          P:=SQRT(P);
    31          C:=CA/CL;
    32          C2:=C*C;
    33          VG:=C2*SQRT(12)*A/H;
    34          NUC:=C2*A*3.464/H;
    35          GAMMA:=A/L;
    36          Q:=(C*GAMMA) '**' 4/(NUC*NUC);
    37          'FOR' V:=V1 'STEP' V2 'UNTIL' V3 'DO'
    38          'BEGIN'
    38                NEWLINE(1);
    40                L2:=V/VG;
    41                'IF' L2>1 'THEN' 'GOTO' ENDLOOP;
    42                AKX1:=V/C;
    43                AKX2:=P-V*SQRT(1-L2);
    44                'IF' AKX2<0.0 'THEN'
    44                'BEGIN'
    44                      AKX2:=0.0;
    46                      'GOTO' OUT;
    47                'END';
```

```
                    AKX2:=AKX1*SQRT(AKX2);
    OUT:            PRINT(V,5,3);
                    PRINT(AKX1,8,6);
                    PRINT(AKX2,8,6);
    ENDLOOP:        ;
            'END';
            NN:=100;
            'FOR' M:=1 'STEP' 1 'UNTIL' 1000 'DO' COUNT1[M]:=COUNT2[M]:=0;
            'FOR' M:=1 'STEP' 1 'UNTIL' 100 'DO'
            'BEGIN'
                    PAPERTHROW;
                    NUU:=M*M*9.8775;
                    'FOR' N:=0 'STEP' 1 'UNTIL' NN 'DO'
                    'BEGIN'
                            G:=N*N/(GAMMA*GAMMA)+NUU;
                            G:=G*G;
                            VP:=SQRT(Q*G);
                            V:=SQRT((Q*G)+P*NUU*NUU/G);
                            NEWLINE(1);
                            'IF' V>VG 'THEN'
                            'BEGIN'
                                    NN:=N-1;
                                    'GOTO' TOOBIG;
                            'END';
                            PRINT(M,3,0);
                            PRINT(N,8,0);
                            PRINT(VP,8,6);
                            PRINT(V,8,6);
                            F:=V*CL/(2*PI*A);
                            FF:=F '/' FREQSTEP+1;
                            AKX1:=V/C;
                            'IF' N<AKX1 'THEN' COUNT1[FF]:=COUNT1[FF]+1;
                            AKX2:=P-V*SQRT(1-V/VG);
                            AKX2:='IF' AKX2<0.0 'THEN' 0.0 'ELSE' AKX1*SQRT(AKX2);
                            'IF' N<AKX2 'THEN' COUNT2[FF]:=COUNT2[FF]+1;
                    'END';
    TOOBIG:         'IF' NN<0 'THEN' 'GOTO' NOMORE;
            'END';
    NOMORE:PAPERTHROW;
            F1:=0;
            F:=VG*CL/(2*PI*A);
            'FOR' N:=0 'STEP' FREQSTEP 'UNTIL' F 'DO'
            'BEGIN'
                    NEWLINE(1);
                    PRINT(N,6,0);
                    PRINTCH(29);
                    PRINT(N+FREQSTEP,6,0);
                    SPACE(5);
                    F1:=F1+1;
                    WRITE(0,FORMAT('('-NNNDSSS')'),COUNT1[F1]);
                    WRITE(0,FORMAT('('-NNNDSSS')'),COUNT2[F1]);
                    RATIO:='IF' COUNT1[F1]=0 'THEN' 0.0 'ELSE' COUNT2[F1]/
                                                                        COUNT1[F1];
                    PRINT(RATIO,1,5);
                    LOGRATIO:='IF' COUNT1[F1]=0.0 'THEN' -99999.99999 'ELSE'
                                                            10.0*ALOG10(RATIO);
                    PRINT(LOGRATIO,5,5);
            'END';
            PAPERTHROW;
    'END;
```